Faculté de génie
Département de génie civil et de génie du bâtiment

Effet couplé des caractéristiques des granulats-fibres et de la rhéologie du mortier sur les performances hétérogènes du béton autoplaçant renforcé de fibres (FR-SCC)

Coupled Effect of Fiber-Aggregate Characteristics and Mortar Rheology on Heterogeneous Performance of Fiber Reinforced Self Consolidating Concrete (FR-SCC)

Thèse de doctorat

Spécialité : Génie civil

Naimeh Nouri

Thèse présentée au département de génie civil et de génie du bâtiment en vue de l'obtention du grade Docteur en philosophie en génie

(A dissertation submitted in fulfillment of the requirements for the degree of Doctor of Philosophy in Civil Engineering)

Jury: Ammar Yahia   Directeur

               Kamal Henri Khayat   Co-directeur

               Brahim Benmokrane   Rapporteur

               Fodhil Kassimi   Examinateur

               Hamdy Mohamed   Examinateur

Sherbrooke (Québec), Canada   July 2022

To my Family

RÉSUMÉ (en français)

L'utilisation des suspensions cimentaires très fluides, telles que le béton autoplaçant (BAP), dans l'industrie du béton, notamment pour la réparation, vise à faciliter la coulée des éléments densément renforcés. Ceci grâce aux divers avantages que présentent les BAP à l'état frais et durci. Cependant, les matériaux cimentaires sont généralement considérés comme fragiles, avec de faibles résistances à la traction et à la flexion et ayant une faible capacité de déformation. Par conséquent, le béton est renforcé par des barres d'armature et des fibres pour améliorer la résistance à la traction et à la flexion ainsi que la ductilité des structures en béton. D'autre part, si l'ajout de fibres aux matériaux cimentaires améliore leurs performances mécaniques, cela peut avoir un impact négatif sur leur maniabilité. Cette étude traite les performances d'écoulement homogène (capacité de passage, blocage et stabilité dynamique) du béton autoplaçant renforcé de fibres (BAP-F) comme l'un des matériaux les plus prometteurs pour les applications de réparation. Les performances du BAP-F, en tant que suspension diphasique, dépendent des caractéristiques de la phase granulaire fibrée (squelette solide en suspension) et celles de mortier (phase suspendante).

Le squelette solide joue un rôle clé dans la performance globale du béton. Ainsi, l'optimisation de la combinaison fibre-gros granulats (F-A) est nécessaire pour améliorer la maniabilité des BAP-F. Dans la première phase de ce projet, une étude approfondie a été entreprise pour identifier l'effet couplé des caractéristiques des fibres et des gros granulats sur la compacité granulaire (PD) de la combinaison F-A. Le squelette F-A peut-être caractérisé en termes de distribution granulométrique (PSD), de teneur volumétrique et morphologie des gros granulats, ainsi que de la taille, de la rigidité et de la teneur en fibres. Dans cette phase, différents types de fibres avec des dimensions et des rigidités différentes, incluant les fibres métalliques, de polypropylène et de polyoléfine, ont été étudiées. De plus, quatre combinaisons de trois classes différentes de granulats grossiers ont été utilisées pour proportionner les mélanges F-A. Les résultats ont montré que des fibres de longueur plus courte, de diamètre plus petit et plus flexibles peuvent conduire à une PD plus élevée des systèmes F-A. Par ailleurs, le squelette de gros granulats avec des vides interparticulaires plus grands conduit à plus d'espace disponible permettant la déformation des fibres, améliorant ainsi la PD des mélanges F-A. Afin de simuler l'état de compactage du squelette F-A dans la matrice du béton lors des écoulements à faible débit, le système de F-A faiblement compacté (LPD) a été considéré. D'autre part, pour décrire l'état de compacité du squelette F-A dans le cas du béton projeté et du pompage à haute pression, où un niveau très élevé de compactage est appliqué sur le système F-A, une PD du système fortement compacté (DPD) a été définie. Il a été constaté que le LPD des systèmes F-A est principalement affecté par la teneur volumétrique et la taille des fibres, alors que le DPD était davantage contrôlé par la rigidité des fibres. De nouveaux modèles empiriques ont été proposés pour prédire le LPD et le DPD des combinaisons F-A en fonction des caractéristiques des gros granulats et des fibres, ainsi que du taux de compactage. Les modèles établis ont été utilisés pour proposer une nouvelle approche d'optimisation des mélanges de BAP-F afin d'atteindre l'ouvrabilité désirée.

Dans la deuxième phase de cette étude, le BAP-F a été considéré comme une suspension diphasique de squelette solide composé de fibres et de gros granulats (F-A $\geq$ 5 mm) dans une suspension de mortier avec des particules solides inférieures à 5 mm. En conséquence, l'effet couplé de la teneur volumétrique des fibres et de la distribution granulométrique des gros granulats, ainsi que les propriétés rhéologiques du mortier sur la capacité de passage et la stabilité dynamique de divers mélanges BAP-F ont été étudiés. Au total, 19 mélanges BAP-F destinés à des travaux de réparation

conventionnelle et à haute résistance ont été formulés avec des rapports eau/liant (W/B) respectifs de 0,42 et 0,35 et des microfibres Métalliques de 0,1 % à 0,5 % de teneur volumétrique. Les performances d'écoulement des mélanges étudiés ont été évaluées en termes de fluidité (essai d'affaissement), de capacité de passage (essais J-Ring et L-Box) et de stabilité dynamique (essai T-Box). Selon les corrélations établies, les principaux paramètres influençant les performances d'homogénéité des BAP-F sont le W/B, le volume de pâte (V_p), la densité volumétrique le ratio teneur volumétrique sur la compacité granulaire des F-A (φ/φ_{max}), le dosage en superplastifiant (HRWR), la teneur en fibres, la rhéologie du mortier et le volume de mortier en excès. Aussi, les résultats de l'analyse de robustesse ont révélé que les performances d'écoulement homogène du BAP-F sont plus sensibles aux variations du φ/φ_{max} et du volume de pâte plutôt qu'aux variations de la rhéologie du mortier, du W/B ou du dosage de HRWR. De nouveaux indices de blocage (BI) et de ségrégation dynamique (DSI) ont été proposés dans cette phase. Les indices BI et DSI proposés peuvent être utilisés pour évaluer la variation de φ/φ_{max} de la portion de F-A s'écoulant dans des zones d'écoulement restreintes et non restreintes. Les indices BI et DSI proposés peuvent permettre une évaluation plus adaptée des changements induits par le blocage et le cisaillement dans le volume relatif et la distribution granulométrique des gros granulats et la teneur en fibres. Une nouvelle classification des BAP-F basée sur la maniabilité est proposée reposant sur des compromis établis entre les performances d'écoulement dans des conditions restreintes et non restreintes, y compris la capacité de passage, la résistance au blocage et la stabilité dynamique. Les caractéristiques des constituants du mélange permettant d'obtenir les mélanges BAP-F avec des niveaux de résistance conventionnels et élevés, tout en ayant des performances d'écoulement homogène acceptables, ont ensuite été recommandées.

Cependant, les essais empiriques susmentionnés tels que J-Ring, L-Box et T-Box ne peuvent pas être correctement appliqués pour évaluer les performances d'écoulement du BAP-F dans des conditions d'écoulement restreintes (applications de réparation). Par conséquent, dans cette étude, un nouveau dispositif d'essai empirique, Square-Box a été utilisé pour évaluer les performances d'écoulement homogène des mélanges BAP-F pour les applications de réparation (écoulement confiné). Le dispositif est composé d'un circuit fermé de quatre canaux rectangulaires à surface fermée mesurant 200 mm de hauteur, 700 mm de longueur et 100 mm de largeur, donnant une boîte avec des dimensions extérieures de 700 × 700 mm, de dimensions intérieures de 500 × 500 mm et une hauteur de 200 mm. Il a été révélé que contrairement aux essais L-Box et T-Box conventionnels, le Square-Box proposé pouvait simuler avec succès les conditions d'écoulement lors de la coulée des mélanges BAP-F, y compris la distance d'écoulement et le confinement, l'effet de paroi et la présence de barres d'armature encombrées. Les performances des mélanges BAP-F ont été évaluées en termes de stabilité dynamique et de capacité de passage dans des éléments non renforcés et renforcés.

Selon les résultats expérimentaux, les indices de ségrégation dynamique et de blocage des mélanges BAP-F étudiés concordent bien avec les caractéristiques du système F-A et les propriétés rhéologiques du mortier. Selon les corrélations établies, la teneur en fibres et le ratio φ/φ_{max} de F-A ont montré un effet plus significatif sur les performances d'écoulement homogène du BAP-F que sur la rhéologie du mortier. Les mélanges étudiés ont montré des indices de blocage significativement plus élevés avec le dispositif proposé par rapport à ceux obtenus à l'aide du test L-Box conventionnel. En outre, l'effet négatif de la performance d'un écoulement hétérogène sur les propriétés mécaniques des mélanges BAP-F étudiés a été évalué. Les résultats expérimentaux ont montré qu'une ségrégation dynamique plus élevée conduit à des valeurs très variables de

résistance à la compression à différentes distances d'écoulement (p. ex. application de réparation). Une nouvelle classification de capacité de remplissage a été établie pour les mélanges BAP-F. Les spécifications des mélanges FR-SCC avec une stabilité dynamique élevée et des propriétés de capacité de passage ont été recommandées. Celles-ci incluent les plages appropriées de teneur volumétrique et de rhéologie de la pâte de ciment, la PSD de granulats, la teneur en macrofibres d'acier et le ratio φ/φ_{max} de la combinaison fibres-gros granulats pour les conditions d'écoulement confiné et restreint (par exemple, applications de réparation).

Dans la dernière phase de cette étude, les mélanges BAP-F étudiés dans la phase 3 ont été coulés dans le dispositif d'essai développé pour évaluer l'effet combiné des caractéristiques des constituants du mélange, de la distance du point de la coulée, de l'effet de paroi et de la présence de barres de renforcement sur la distribution et l'orientation des fibres. En utilisant la méthode d'analyse d'image en 3D, la distribution verticale et horizontale ainsi que l'orientation des fibres ont été évaluées. Les résultats ont indiqué que la présence et la disposition des barres provoquaient une hétérogénéité de la distribution et de l'orientation des fibres dans la région avoisinante des barres. De plus, les résultats ont indiqué que le nombre de fibres diminuait sur une distance d'écoulement plus longue, indiquant la ségrégation dynamique et le blocage des fibres à travers le dispositif d'écoulement. Cependant, l'augmentation de la distance d'écoulement affecte positivement l'orientation des fibres (parallèle à la direction d'écoulement) sur toute la longueur de du dispositif. Selon les modèles empiriques établis, de bonnes corrélations ont été trouvées entre les caractéristiques du F-A (en termes de ratio φ/φ_{max} et le volume de fibre (Vf)) et la rhéologie du mortier avec les performances d'écoulement homogène des mélanges BAP-F. Selon les résultats expérimentaux, le φ/φ_{max} des gros granulats et la viscosité plastique du mortier ont montré un effet plus remarquable sur l'Orientation et la Distribution des Fibres (FOD) que sur Vf et le seuil de cisaillement du mortier (τ0). Par conséquent, l'optimisation des mélanges BAP-F en termes d'effet couplé du ratio φ/φ_{max} et de la viscosité plastique, en plus de prendre en compte l'effet de paroi et de barre d'armature ainsi que la distance d'écoulement est une approche prometteuse pour obtenir une distribution et une orientation appropriées des fibres, dans des conditions d'écoulement en zone confinée (c.-à-d., la réparation).

Mots-clés : Blocage, Réparation du béton, Distance du point de coulée, Stabilité dynamique, Mélange fibres-gros granulats, Distribution et orientation des fibres, Béton autoplaçant fibré, Squelette granulaire, Compacité granulaire, Distribution granulométrique, Capacité de passage, Rhéologie, Effet de paroi.

ABSTRACT

The use of highly-flowable cementitious mixtures, such as self-consolidating concrete (SCC), in concrete industry including repair application aims to facilitate the casting of highly congested reinforced elements. This is based on the various advantages of SCC mixtures in both fresh and hardened states. However, cementitious materials are generally considered as brittle, with low tensile and flexural strengths and weak strain capacity. Therefore, concrete is reinforced by rebar and fibers to improve strength-strain capacity and ductility of concrete structures. On the other hand, the addition of fiber to cementitious materials enhances their mechanical performance but can negatively impact their workability. This study deals with the homogenous performance of fiber-reinforced self-consolidating concrete (FR-SCC) as one of the most promising materials for repair applications. The performance of FR-SCC, as a diphasic suspension, depends on the characteristics of both fiber-coarse aggregate (suspended-solid skeleton) and mortar (suspending liquid) phases.

The solid components play a key role in the overall performance of the concrete produced. Then, the optimization of the fiber-coarse aggregate (F-A) combination is necessary to enhance the workability design of FR-SCCs. In the first phase of this study, a comprehensive investigation was undertaken to identify the coupled effect of the characteristics of fibers and coarse aggregate on the packing density (PD) of F-A combination used without any cement paste/mortar. The F-A skeleton can be characterized in terms of particle-size distribution (PSD), volumetric content, and morphology of the coarse aggregate, as well as size, rigidity, and content of fibers. Various types of steel, polypropylene, and polyolefin fibers having different sizes and rigidities are investigated in this phase. Moreover, four combinations of three different classes of coarse aggregate were used to proportion F-A mixtures. Test results showed that shorter length, smaller diameter, and more flexible fibers can lead to higher PD of F-A systems. Moreover, the coarser aggregate skeleton with larger interparticle voids led to more available space for fibers to be deformed, hence improving the PD of F-A mixtures. To simulate the packing state of F-A skeleton in concrete matrix through the mixing process and low casting rates, the loosely-packed system (LPD) of F-A was considered without any compaction. On the other hand, to describe the packing state of F-A skeleton in the case of shotcrete and highly-pressure pumping, where a higher level of compaction applies on the F-A system, the densely-packed system (DPD) were defined. It was found that the LPD of F-A mixtures is mostly affected by the volumetric content and size of the fibers, however, the DPD was more controlled by the rigidity of fibers. New empirical models were proposed to predict the LPD and DPD of F-A combinations given the characteristics of coarse aggregate and fibers, as well as the level of compaction. The established models were employed to propose a new proportioning approach for FR-SCC mixtures to achieve the targeted workability.

In the second phase, FR-SCC considered as a diphasic suspension of fiber and coarse aggregate (F-A ≥ 5 mm) skeleton in mortar suspension with solid particles finer than 5 mm. Accordingly, the coupled effect of the volumetric content of fibers and particle-size distribution of coarse aggregate, as well rheological properties of the mortar on the passing ability and dynamic stability of various FR-SCC mixtures were investigated. In total, 19 FR-SCC mixtures for conventional and high strength repair application were proportioned with water-to-binder ratios (W/B) of 0.42 and 0.35,

respectively, and macro steel fibers of 0.1% to 0.5% volumetric contents. Flow performance of the investigated mixtures were evaluated in terms of flowability (slump-flow test), passing ability (J-Ring and L-Box set-ups), and dynamic stability (T-Box test). According to the established correlations, the main influencing parameters on homogeneous performance of FR-SCC include W/B, paste volume (V_p), volumetric content-to-packing density of F-A (φ/φ_{max}), HRWR dosage, fiber content, mortar rheology, and volume of excess mortar. The robustness analysis results revealed that homogeneous flow performance of FR-SCC is more sensitive due to variations of the φ/φ_{max} and paste volume rather than mortar rheology, W/B, and HRWR dosage. New blocking (BI) and dynamic segregation (DSI) indices were proposed in this phase. The proposed BI and DSI indices can be employed to evaluate the variation of φ/φ_{max} of F-A portion flowing through restricted and non-restricted flow conditions, respectively. The proposed BI and DSI indices can enable proper assessment of the blocking- and shear-induced changes in the relative volume and particle-size distribution of coarse aggregate and fiber contents. A new workability-based classification is proposed based on the established trade-offs between flow performance under restricted and non-restricted conditions, including passing ability, blocking resistance, and dynamic stability. Characteristics of mixture constituents for FR-SCC mixtures with conventional- and high-strength levels were then recommended to ensure an acceptable homogeneous flow performance.

However, the aforementioned empirical tests such as J-Ring, L-Box, and T-Box cannot be properly applied to evaluate the flow performance of FR-SCC under restricted flow conditions (repair applications). Therefore, in this study, a new empirical Square-Box test set-up was employed to evaluate the homogeneous flow performance of FR-SCC mixtures for repair applications (confined flow). The set-up consists of a close-circuit of four close-surface rectangular channels measuring 200 mm in height, 700 mm in length, and 100 mm in width, yielding a box with 700 × 700 mm outer dimensions, 500 × 500 mm inner dimensions, and a height of 200 mm. It was revealed that unlike the conventional L-Box and T-Box tests, the proposed Square-Box test could successfully simulate the flow conditions during casting of FR-SCC mixtures, including the flow distance and confinement, wall effect, and presence of highly congested reinforcing bars. The performance of FR-SCC mixtures was assessed in terms of dynamic stability and passing ability in non-reinforced and reinforced elements, respectively.

According to the experimental results, the dynamic segregation and blocking indices of the investigated FR-SCC mixtures were found in good agreements with characteristics of F-A combination and rheological properties of mortar. According to the established correlations, fiber content and φ/φ_{max} of F-A showed more significant effect on homogenous performance of the FR-SCC rather than the mortar rheology. The investigated mixtures exhibited significantly higher blocking indices through the proposed set-up compared to those obtained using the conventional L-Box test. Furthermore, the negative effect of the heterogeneous flow performance on mechanical properties of the investigated FR-SCC mixtures was assessed. The experimental results reflected that higher dynamic segregation led to more dissimilar compressive strength values at different flow distances. A new filling ability classification was established for FR-SCC mixtures. The specifications of the FR-SCC mixtures with high dynamic stability and passing ability properties were recommended. These include the appropriate ranges of volumetric content and rheology of

cement paste, PSD of aggregate, macro-steel fiber content, and φ/φ_{max} of fiber-coarse aggregate combination for confined and restricted flow conditions (e.g., repair application).

In the last phase of this study, the FR-SCC mixtures investigated in Phase 3 were cast in the developed test set-up to evaluate the combined effect of mixture component characteristics, distance from casting point, wall effect, and the presence of reinforcement bars on fiber distribution and orientation. Using Image analysis method, the vertical and horizontal fiber distribution, as well as 3D fiber orientation was assessed. The results indicated that the presence and arrangement of bars caused fiber distribution and orientation heterogeneity in the region close to the bars. Moreover, the results indicated that the number of fibers decreased in longer flow distance, referring to dynamic segregation and blocking of fibers across the set-up. However, increasing flow distance positively affected fiber orientation (parallel to the flow direction) through the length of the set-up. According to the established empirical models, good correlations were found between characteristics of fiber-coarse aggregate (in terms of relative volumetric content to packing density of fiber-coarse aggregate (φ/φ_{max}) and volume of fiber (V_f)) and mortar rheology with homogeneous performance of FR-SCC mixtures. According to the experimental results, the φ/φ_{max} of coarse aggregates and plastic viscosity of mortar exhibited more remarkable effect on FOD than V_f and mortar yield stress (τ_0). Therefore, optimizing the FR-SCC mixtures in terms of coupled effect of φ/φ_{max}, and plastic viscosity, in addition to considering wall and rebar effect as well as the flow distance is a promising approach to achieve proper fiber distribution and orientation, for confined flow conditions (i.e., repair).

Keywords: Blocking, Concrete repair, Distance from casting point, Dynamic stability, Fiber-coarse aggregate mixture, Fiber distribution and orientation, Fiber-reinforced self-consolidating concrete, Granular skeleton, Packing density, Particle-size distribution, Passing ability, Rheology, Wall effect.

ACKNOWLEDGEMENT

CONTENTS

List of Figures

List of Tables

List of symbols

V_{air}	Air content
AEA	Air Entraining Agent
D_A	Average diameter of aggregate
AVG_{PD}	Average of PD values
BI	Blocking Index
F_b	Buoyancy force
CS	Coarser portion of sand
COV_{PD}	Coefficient of Variation (COV_{PD}) of the PD
CPM	Compressible Packing Model
f'_c	Compressive strength
CSHI	Compressive-strength heterogeneity index
JRF	Concrete flow in J-Ring
CSR	Conventional Strength Repair
COD	Crack Opening Displacement
γ_c	Critical deformation
DPD	Densely-packed PD
ρ_b	Densities of binder
ρ_{CA}	Densities of coarse aggregate
ρ_f	Densities of fiber
ρ_{sand}	Densities of sand
ρ_w	Densities of water
D_f	Diameter of fiber
ΔJ-ring	Difference between slump and J-Ring flow
ΔN_f	Difference between the number of fibers
FD	Drag force
DSI	Dynamic Segregation Index
DSI_{set-up}	Dynamic segregation index in the Square-Box set-up
DSI_{TB}	Dynamic segregation indices obtained from the T-Box set-up
HB_{FO}	Effect of horizontal bar on fiber orientation
HB_{FD}	Effect of horizontal reinforcing bars on vertical distribution of fibers
LB_{FO}	Effect of longitudinal bar on in-plane orientation of fibers
VB_{FO}	Effect of the vertical bar on out-of-plane orientation of fibers
VB_{FD}	Effect of vertical bar on horizontal fiber distribution
WE_{FO}	Effect on in-plane orientation of fibers
FDSI	Fiber Dynamic Segregation Index
FOD	Fiber Orientation and Distribution
FSSI	Fiber Static Segregation Index
F-A	Fiber-Coarse Aggregate
FRC	Fiber-Reinforced Concrete
FRSCCM	Fiber-Reinforced Self-Consolidating Cement-based Material
FR-SCC	Fiber-Reinforced Self-Consolidating Concrete
FCAR	Fluid Concrete with Adapted Rheology
WE_{FD}	Formwork-wall effect on fiber distribution
GF	Glass fibers
BI_{LB}	Granular blocking through the L-Box set-up
F_g	Gravity force
HI	Heterogeneity Index
HSR	High Strength Repair
HRWR	High-Range Water-Reducer

Φ	In-plane orientation angle
ICT	Intensive Compaction Tester
L_f	Length of fiber
LPD	loosely-packed PD
D_{max}	Maximum diameter
$PD_{maximum}$	Maximum packing density of fiber-aggregate
MSA	Maximum-Size Aggregate
PD_{medium}	Medium packing density of fiber-aggregate
D_{min}	Minimum diameter
$PD_{minimum}$	Minimum packing density of fiber-aggregate
E	Modulus of elasticity
N_f	Number of fibers
θ	Out of plane orientation angle
PD	Packing Density
PD_A	Packing density of aggregate
PD_{F-A}	Packing density of fiber-aggregate combination
PD_{Ref}	Packing density of reference mixture
PSD	Particle Size Distribution
μ_p	Plastic viscosity
μ_{p-FM}	Plastic viscosity of fine mortar
μ_{p-M}	Plastic viscosity of mortar
τ_{0-P}	Plastic viscosity of paste
PP	Polypropylene
PVA	Polyvinyl Alcohol
GU	Portland cement
AV_i	Ratio of 3D surface area-to-volume of each coarse aggregate
φ/φ_{max}	Ratio of the volumetric content (φ)-to-packing density (φmax) of fiber-aggregate combination
$\varphi_{CS}/\varphi_{max-CS}$	Relative-solid packing fraction of fine sand
Fresis	Resistance force
Re	Reynolds number
RMSE	Root-mean-square error
S/A	Sand to total aggregate ratio
I	Second moment of area of fiber's cross section
SCC	Self-Consolidating Concrete
CD	Shape-dependent drag coefficient
SF	Slump Flow value
SDPD	Standard Deviation of PD values
ρ	Suspending fluid density
$TerC^3$	Ternary blended cement
TD	Tilt-down
TU	Tilt-up
T_c^{shear}	Time of gravity induced particle migration
$T_c^{gravity}$	Time of shear
AVA	Total surface area-to-unit volume
UBI_{LB}	Ultimate blocking index in the L-Box test
UHPC	Ultra High-Performance Concrete
VSI	Visual Stability Index
VCA	Volume of coarse aggregate
V_f	Volume of Fiber

V_p	Volume of paste
V_{sand}	Volume of sand
	Volumetric content of coarse aggregate
	Volumetric content of fiber
W/B	Water-to-Binder ratio
τ_0	yield stress
τ_{0-FM}	Yield stress of fine mortar
τ_{0-M}	Yield stress of mortar
μ_{p-P}	Yield stress of paste

CHAPTER 1 INTRODUCTION

1.1. Research Background

A large volume of self-consolidating concrete (SCC) has been used over the last decades, dating back to 1986. SCC has some important benefits because of its ease of placement (high fluidity) to cast congested reinforcement elements [1,2]. This high fluidity is provided by using the new generations of chemical and mineral admixtures. However, due to high fluidity of SCC, it can show some heterogeneity during transportation, placement, compaction and/or finishing [3]. This can be explained by increasing the fluidity of the fluid phase (i.e., cement paste or mortar matrix), which can increase the risk of segregation (static and dynamic).

Dynamic segregation is defined as separation of solid particles from mortar and can lead to heterogeneous flow of the mixture in the formwork [4]. Static segregation occurs when the concrete is at rest and coarse aggregate settle down given their higher density compared to the paste/mortar suspending fluid [5,6]. On the other hand, dynamic segregation occurs during flow when the fluid phase is not able to carry the solid particles and keep the homogeneity. These heterogeneous phenomena can lead to blockage of the flow. Local aggregate separation and segregation may occur and the concrete flowing across the obstacles can be blocked [7]. Therefore, high fluidity is not the only important parameter that should be considered for SCC, stability of fresh concrete is also another effective parameter that should be achieve [6,7].

Accordingly, SCC should satisfy the three basic characteristics of workability including: filling ability, passing ability, and stability [1,2]. Stability can be divided in two different types: a) static stability: the resistance of mixture to segregation after casting, b) dynamic segregation: resistance to separation of coarse aggregate from mortar during flow [4,8].

Cementitious materials are typically characterized as brittle, with a low tensile strength and strain capacity [9]. Therefore, the use of fibers is preferred to obtain enhanced ductile performance. The addition of fiber mainly influences tensile strength, flexural strength, and all mechanical properties of concrete in the hardened state [10]. However, due to the presence of more solid particles (i.e., fibers) in addition to coarse aggregate, fiber-reinforced self-consolidating concrete (FR-SCC) can be considered a more heterogeneous mixture comparing to normal SCC [11]. Indeed, the incorporation of fibers as additional solid inclusions can reduce the workability of the mixture. Therefore, a higher dosage of superplasticizer is required to obtain a given level of flowability of SCC. Therefore, the mortar matrix of the FR-SCC mixture can have less viscosity values comparing to normal SCC [11,12]. This can increase the risk of blocking of fibers and aggregate through the narrow gaps between the reinforcing bars [10]. Therefore, the mixture proportioning should be adjusted to obtain proper fluidity and high stability of FR-SCC to allow adequate flow properties through congested bars without any heterogeneity or blockage.

In order to ensure adequate flow performance of FR-SCC for casting reinforced sections, it is necessary to optimize the physical and rheological characteristics of its different phases, including cement paste and mortar matrices [11], which are the homogeneous portions of the mixture in this study. Furthermore, the grading and packing density of aggregate, fiber characteristics (type, content, and aspect ratio), the arrangement of reinforcing bars (e.g., diameter, spacing, and distribution) should also be considered in the optimization process, because these factors affect the

passing ability and dynamic segregation of FR-SCC. Moreover, heterogeneous behavior of FR-SCC can also include the uneven distribution and orientation of fibers in the cast element [13]. In the case of FR-SCC, proper orientation and distribution of fibers can also significantly influence their mechanical performance [10,13]. Uniform distribution (vertical and horizontal) of fibers in structural elements and number of perpendicular oriented fibers can result in higher flexural and tensile strength values [10,13].

Different set-ups are proposed in literature to investigate the effect of mixture proportions and rheological properties of concrete, fiber characteristics, bar arrangement, and distance from the casting point on passing ability of FR-SCC [11,14]. However, these studies were carried out without considering the coupled effect of aggregate-fiber-reinforcing bars on heterogeneity of FR-SCC. Indeed, the combined effects of aggregate-fiber-reinforcing bars are found as the main gap in the literature regarding the heterogeneous behavior of FR-SCC.

1.2. Research needs

The studies presented earlier [1-11] have investigated the effect of different individual parameters on heterogeneous performance of FR-SCC. They have shown the effects of mixture proportions and rheological properties of concrete, fiber characteristics, bar arrangement, and distance from the casting point on passing ability of the FR-SCC and fiber distribution and orientation. Fibers can arrange themselves in different orientations in concrete due to geometrical restrictions (i.e., effects of formwork wall or reinforcing bars). The investigations carried on the effect of fiber orientation on mechanical performance of FR-SCC were also presented. As explained earlier, the orientation of fibers can significantly affect the mechanical properties of cast elements. There are also few papers discussing the variation of fiber orientations and distribution at different distances from the casting point.

The characteristics of coarse aggregate can affect the rheological properties of the mixtures. On the other hand, as a solid portion of the concrete mixture, they can influence the orientation and dispersion of fibers. The packing density, grading, and volumetric content of aggregate can considerably affect the variation of orientation and distribution of fibers during casting process. These effects can be more critical in presence of obstacles (i.e., reinforcing bars) and formwork walls, due to blocking and wall effect phenomenon, respectively. The placement configuration, diameter, and spacing of reinforcing bars can significantly affect the passing ability of any type of fluid concrete, especially in the case of FR-SCC mixtures having high solid contents (i.e., fibers and aggregate).

Therefore, in order to fundamentally evaluate the heterogeneous performance of FR-SCC during casting of structural elements, it is highly necessary to consider the combined effects of aggregate-fiber-reinforcing bars on dynamic stability and passing ability of fiber-aggregate system, as well as distribution and orientation of fibers at different distances from the casting point. These combined effects were not studied yet in any research, and they are still unknown. Accordingly, the combined effects of aggregate-fiber-reinforcing bars were found as the main gap in the literature carried on heterogeneous behavior of FR-SCC, and consequently, this is the research to be concluded in this study.

According to the previous section, the main input effective parameters of this study are presented as follow:

- Rheology of mortar: This includes the mortar matrices containing different volume of cement paste with a given rheology (i.e., given water-to-binder ratio (W/B)) and a constant sand to total aggregate ratio (S/A).
- Characteristics of coarse aggregate: These consist of different combinations of different classes of coarse aggregate and different nominal sizes, morphology, and grading. These different combinations lead to different packing density values.
- Characteristics of fibers: These consist of volumetric content, size, and rigidity (type) of fibers.
- Characteristics of fiber-aggregate system: Using different combinations of coarse aggregate (different packing density) and fibers can allow to characterize the fiber-aggregate system (F-A) by measuring the packing density of F-A.
- Arrangement of reinforcing bars: The selected arrangement of bars in this study includes three different vertical and horizontal configurations of steel bars and different spacing conditions of non-reinforced, narrowly, highly, and moderately spaced. An extra arrangement without any reinforcing bars will also be included to evaluate dynamic segregation. These arrangements of bars are selected based on repair applications.
- Distance from the casting point: In this study, the heterogeneous performance of FR-SCC mixtures is evaluated at different distances from the casting points.
- Different applications: All the effective parameters that are mentioned (fiber and aggregate characteristics, arrangement of bars, etc.) are usually encountered in repair applications. This application can be related to confined flow conditions in the presence of reinforcing bars.

Accordingly, the effect of these main effective parameters on the heterogeneous performance of the FR-SCC can be presented, as follow:

- Dynamic stability and passing ability of fibers, aggregate, and F-A combinations: These include the horizontal and vertical distributions of fiber and aggregate through the proposed set-up. Accordingly, the volumetric content of fibers and coarse aggregate, as well as packing density of fiber-aggregate system are measured in different distances from the casting point. These measurements are carried out on fresh samples taken from the non-reinforced and reinforced set-ups to evaluate pure dynamic segregation and blockage, respectively. These results will be compared with the results of the empirical tests of SCC, such as the J-Ring, L-Box, and T-Box set-ups.
- Vertical distribution and 3D orientation of fibers: These properties will be evaluated from the hardened samples, which are taken in different distances from the casting points, behind and after the reinforcing bars. Accordingly, image analysis technics are employed to evaluate the vertical distribution and orientation of fibers in different cross-section samples. These measurements will be applied to evaluate the effect of reinforcing bars and formwork walls.
- Mechanical performance: This includes the compressive values of the samples, taken from different distances from the casting point.

Based on these parameters, the new set-up is proposed to evaluate the heterogeneous performance of FR-SCC for repair applications. The main influencing parameters to be studied in this research:

- Characteristics of coarse aggregate: (Particle size distribution, packing density, and content).
- Characteristics of fibers: (size, rigidity, and content).
- Rheological properties of suspending mortar.
- Reinforcing bars distribution, spacing, and arrangement.

References

[1] K.H. Khayat, Workability, testing, and performance of self-consolidating concrete, ACI Materials Journal, 96 (3) (1999) 346-353, https://dx.doi.org/10.14359/632.

[2] K. H. Khayat, C. Hu, H. Monty, Stability of self-consolidating concrete, advantages, and potential applications, in: A. Skarendahl, O. Petersson (Eds.), Proceedings of the first International RILEM Symposium on Self Compacting Concrete, Stockholm, Sweden, (1999), 143-152.

[3] A. Yahia, P.C. Aïtcin, Self-consolidating concrete, in: Science and Technology of Concrete Admixtures, Woodhead Publishing, (2016), 491-502, https://doi.org/10.1016/B978-0-08-100693-1.00026-6.

[4] B.I.O. Koura, M. Hosseinpoor, A. Yahia, Coupled effect of fine mortar and granular skeleton characteristics on dynamic stability of self-consolidating concrete as a diphasic material, Construction and Building Materials, 263 (2020) 120131, https://doi.org/10.1016/j.conbuildmat.2020.120131.

[5] M. Hosseinpoor, B.I.O. Koura, A. Yahia, Rheo-morphological investigation of static and dynamic stability of self-consolidating concrete: A biphasic approach, Cement and Concrete Composites, (2021) 104072, https://doi.org/10.1016/j.cemconcomp.2021.104072.

[6] M. Hosseinpoor, B.I.O. Koura, A. Yahia, New diphasic insight into the restricted flowability and granular blocking of self-consolidating concrete: Effect of morphological characteristics of coarse aggregate on passing ability of SCC, Construction and Building Materials, 308 (2021) 125001, https://doi.org/10.1016/j.conbuildmat.2021.125001.

[7] N. Roussel, A theoretical frame to study stability of fresh concrete, Materials and Structures, 39 (1) (2006) 81-91, https://doi.org/10.1617/s11527-005-9036-1.

[8] B. Esmaeilkhanian, D. Feys, K.H. Khayat, A. Yahia, New test method to evaluate dynamic stability of self-consolidating concrete, ACI Materials Journal, 111 (3) (2014) 299-308, https://doi.org/10.14359/51686573.

[9] R. Zerbino, J.M. Tobes, M.E. Bossio, G. Giaccio, On the orientation of fibres in structural members fabricated with self-compacting fibre reinforced concrete, Cement and Concrete Composites, 34 (2) (2012) 191-200, https://doi.org/10.1016/j.cemconcomp.2011.09.005.

[10] G. Žirgulis, O. Švec, E.V. Sarmiento, M.R. Geiker, A. Cwirzen, T. Kanstad, Importance of quantification of steel fibre orientation for residual flexural tensile strength in FRC, Materials and Structures, 49 (2016) 3861-3877, https://doi.org/10.1617/s11527-015-0759-3.

[11] K.H. Khayat, F. Kassimi, P. Ghoddousi, Mixture design and testing of fiber-reinforced self-consolidating concrete, ACI Materials Journal, 111 (2) (2014) 143-152, https://doi.org/10.14359/51686722.

[12] S.-D. Hwang, K.H. Khayat, Effect of mixture composition on restrained shrinkage cracking of self-consolidating concrete used in repair, ACI Materials journal, 105 (5) (2008) 499-509, https://dx.doi.org/10.14359/19980.

[13] E. Jasiūnienė, V. Cicėnas, P. Grigaliūnas, Ž. Rudžionis, A.A. Navickas, Influence of the rheological properties on the steel fibre distribution and orientation in self-compacting concrete, Materials and Structures, 51 (2018) 103, https://doi.org/10.1617/s11527-018-1231-y.

[14] L. Ferrara, P. Bamonte, A. Caverzan, A. Musa, I. Sanal, A comprehensive methodology to test the performance of Steel Fibre Reinforced Self-Compacting Concrete (SFR-SCC), Construction and Building Materials, 37 (2012) 406-424, https://doi.org/10.1016/j.conbuildmat.2012.07.057.

CHAPITER 2 Objectives and phases of research

2.1 Objectives

According to the literature review and the selected parameters in the previous sections, the main objectives of this study are:

- Studying the coupled effect of packing density of coarse aggregate and fiber-aggregate system, arrangement of reinforcing bars, and rheology of the mortar matrix on dynamic stability and passing ability of FR-SCC.
- Evaluating the coupled effect of fiber-aggregate-bars characteristics and rheological properties of mortar, as well as the formwork walls on 3D orientation of fibers.
- Determining the effect of dynamic segregation and blocking of both fibers and coarse aggregate on mechanical performance of FR-SCC.
- Evaluating the effect of formwork walls on distribution and orientation of fibers during casting process.
- Proposing new indices to evaluate dynamic stability and passing ability of FR-SCC. The effect of arrangement of the reinforcing bars and distance from the casting point is considered.
- Proposing new packing density-based DSI/BI indices based on the variation of volumetric-content-to-packing density ratio of fiber-aggregate combination, determined at different distances from the casting point.

2.2 Principle Phases of Research

For achieving the targeted objectives, the study will be carried out with the following complementary phases:

- Phase 0: Literature Review.

- Phase 1: Investigating the coupled effect of fibers and aggregate characteristics on packing density of fiber-aggregate combination.

- Phase 2: Evaluating the coupled effect of fiber-aggregate characteristics and mortar rheology on flowability, passing ability, and dynamic segregation of FR-SCC mixtures using T-Box and L-Box set-ups.

- Phase 3: Determining the effect of fiber-aggregate-mortar characteristics, bar arrangements, and different distances from casting point on dynamic segregation and blocking of fiber-coarse aggregates and mechanical performance, using new developed set-up for repair applications.

- Phase 4: Investigation the coupled effect of fibers-aggregate-bar characteristics, rheology of mortar, and formwork walls on distribution and 3D orientation of fibers at different distances from casting point, using Image analysis and new developed set-up for repair applications.

2.2.1   Phase 0: Literature Review

This phase addresses the state of art for this research given the targeted objectives of this study. in parallel to the targeted phases. The state of art starts with highlighting the importance of the selection of fiber-aggregate characteristics, paste volume, W/B in accordance with workability and rheology behavior required for repair applications. This phase introduced the different types of heterogeneous performance of FR-SCC mixtures in terms of dynamic segregation and blocking of fiber-coarse aggregate, as well as uneven fiber distribution and orientation. This literature review also provides a background on the different empirical test methods used to evaluate the homogeneous performance of FR-SCC mixtures. Based on this literature review, a new test set-up was developed to evaluate the effect of presence and arrangement of bars, as well as distance from casting point on both fresh and hardened properties of FR-SCCs.

2.2.2   Phase 1: Investigating the coupled effect of fibers and aggregate characteristics on packing density of fiber-aggregate combination.

The incorporation of steel fibers in fluid concrete with adapted rheology (FCAR) can improve its mechanical performance and cracking resistance. However, the presence of fibers can increase the risk of heterogeneity of FR-SCC mixtures, especially in presence of reinforcing bars. This can therefore increase the risk of blocking of fibers and aggregate through the narrow gaps between the reinforcing bars as well as segregation during flow (i.e., dynamic segregation) or thereafter at rest (i.e., static segregation). In order to ensure adequate flow performance of FR-SCC for casting reinforced sections, it is necessary to optimize the physical and rheological characteristics of its different phases, including cement paste and mortar matrices, as well as the grading and packing density of aggregate and fibers (type, content, and aspect ratio). It is worth mentioning that the negative effect of fibers on workability of FR-SCC can be due to the negative effect of fibers on packing density (PD) of the fiber-coarse aggregate (F-A) combination. The PD can reflect the voids within the F-A skeleton to be filled with mortar. An adequate optimization of the characteristics of the F-A skeleton can enhance the performance of FR-SCC in fresh and hardened states. Therefore, in this phase the effect of different types of steel and synthetic fibers as well as various particle size distribution of coarse aggregates on PD of F-A are evaluated. Test results showed that large (long and thick) fibers have more negative effect on PD than small (short and thin) fibers. Moreover, the F-A mixtures proportioned with more flexible fibers experienced higher PD comparing to the rigid fibers due to their higher deformation through the interparticle voids. It was found that the effect of PSD of aggregate on PD of fiber-aggregate combination is related to the mean diameter of voids between aggregate: Increasing space between aggregate led to more effective space for fiber to be deformed and, consequently, higher packing density can be achieved. In this phase, the optimum fiber contents were obtained for different types of fibers and particle size distributions of aggregate to achieve the minimum, medium and maximum packing density of fiber-aggregate combinations for repair application. The selected F-A mixtures with minimum, medium and maximum packing density are considered as mixture proportioning of FR-SCC mixtures in the next phase (Phase 2).

2.2.3   Phase 2: Evaluating the coupled effect of fiber-aggregate characteristics and mortar rheology on flowability, passing ability, and dynamic segregation of FR-SCC mixtures using T-Box and L-Box set-ups.

In this phase, FR-SCC was considered as a diphasic suspension of fiber and coarse aggregate (F-A ≥ 5 mm) skeleton in mortar suspension with solid particles finer than 5 mm. The coupled effect of the volumetric content of fibers, coarse aggregate particle-size distribution, and rheological properties of the mortar on the passing ability and dynamic stability of various FR-SCC mixtures was investigated. Two different classes of FR-SCC mixtures for conventional strength repair (CSR) and high strength repair (HSR) applications are of concern in this phase. For each minimum, medium, and maximum fiber-coarse aggregate packing densities (Phase 1), different volumes of paste of 0.27, 0.30, 0.33 for CSR as well as 0.33, 0.35, 0.37 for HSR applications were considered, respectively. The workability of FR-SCC mixtures is investigated using J-Ring, L-Box (passing ability) and T-Box (dynamic stability) tests. According to the workability results, a new workability classification is proposed to identify the mixtures with high passing ability and dynamic stability to be used in the next phase.

2.2.4   Phase 3: Determining the effect of fiber-aggregate-mortar characteristics, bar arrangements, and different distances from casting point on dynamic segregation and blocking of fiber-coarse aggregates and mechanical performance, using new developed set-up for repair applications.

In link with the previous phase, the big part of the research lies in this phase. This phase includes two parts, including developing a new empirical test set-up to evaluate the homogeneous flow performance of FR-SCC mixtures under confined flow conditions. The performance was evaluated in terms of dynamic stability and passing ability in non-reinforced and reinforced elements, respectively, using sampling method in fresh state. According to the results of this phase, the multiphasic specifications of the high filling ability FR-SCC mixtures for repair application were finally recommended. The same heterogenous performance of FR-SCC mixtures during distance from casting point was found for the mechanical performance of the investigated FR-SCC mixtures. This once again confirms the synergy between fresh and hardened properties of cementitious mixtures that must be considered to design a repair section. As a conclusion, this phase contributes in developing ways to fundamental understanding the homogeneous performance of FR-SCC as a diphasic mixture through restricted flow conditions (i.e., repair application).

2.2.5   Phase 4: Investigation the coupled effect of fibers-aggregate-bar characteristics, rheology of mortar, and formwork walls on distribution and 3D orientation of fibers at different distances from casting point, using Image analysis and new developed set-up for repair applications.

The optimized selected FR-SCC mixtures from phase 3 are used in this phase to evaluate the distribution and orientation of fibers (FOD) during different distances from casting point, using the developed test set-up (in hardened state). FOD affect the mechanical and/or fresh performance of FR-SCC. Optimum mixture proportion is necessary to ensure proper FOD which is a function of internal and external effective parameters. This phase discusses the combined effect of fiber dosage, aggregate particle size distribution (packing density), rheological properties of mortar, as internal parameters, as well as distance from casting point, wall effect and the presence of reinforcement bars (external parameters) on distribution and orientation of fibers.

2.3 Thesis structure and original contributions

The thesis is divided into 9 chapters that are summarized as follows (Figure 2-1):

Chapter 1 provides an overview of the research background and significance, as well as the research gaps.

Chapter 2 follows the objectives and different phases of the study, some of them are treated as scientific articles.

Chapter 3 provides the detailed literature review and the research gaps which are of concern in this dissertation.

Chapter 4 discusses the methodology employed for each phase of this study to accomplish the targeted objectives. The materials, testing procedures according to standards and methods carried in literature are discussed.

Chapter 5 discusses and investigates the effect of different types of fibers and aggregate characteristics on packing density of fiber-aggregate combinations as one of the most important parameters on performance of fiber-reinforced cementitious mixtures.

Chapter 6 investigates the coupled effect of fiber-aggregate-mortar rheology on heterogenous performance of FR-SCC in terms of dynamic segregation, passing ability and granular blocking.

Chapter 7 discusses on the new developed test set-up used to evaluate the effect of presence and arrangement of bars, fiber-aggregate characteristics and mortar rheology on fiber-aggregate distribution in different distances from casting point, by sampling method at fresh state.

Chapter 8 discusses and investigates the formwork wall, distance from casting point, concrete characteristics, and reinforcement bars on horizontal and vertical fiber distribution as well as 3D orientation of fibers using Image analysis, at hardened state.

Chapter 9 provides a summary of the most important findings of this study. On the other hand, recommendations for future work are also presented.

It worth mentioning that Chapters 5-8 correspond to either published or submitted articles, as follows:

Chapter 5: Naimeh Nouri, Masoud Hosseinpoor, Ammar Yahia, Kamal H. Khayat. Coupled effect of fiber and granular skeleton characteristics on packing density of fiber-aggregate mixtures, 342 (2022) 127932, Construction and Building Materials (2022). https://doi.org/10.1016/j.conbuildmat.2022.127932.

Chapter 6: Naimeh Nouri, Masoud Hosseinpoor, Ammar Yahia, Kamal H. Khayat, Homogeneous flow performance of steel-fiber reinforced self-consolidating concrete for repair application: A biphasic approach, Submitted June 5th, Cement and Concrete Composites (2022).

Chapter 7: Naimeh Nouri, Masoud Hosseinpoor, Ammar Yahia, Kamal H. Khayat, Homogenous flow performance of steel fiber-reinforced self-consolidating concrete for repair applications: Developing a new empirical set-up, Submitted June 14th, Cement and Concrete Composites (2022).

Chapter 8: Naimeh Nouri, Masoud Hosseinpoor, Ammar Yahia, Kamal H. Khayat, Fibers' orientation and distribution of steel fiber-reinforced self-consolidating concrete in reinforced and confined elements, to be submitted in June 2022.
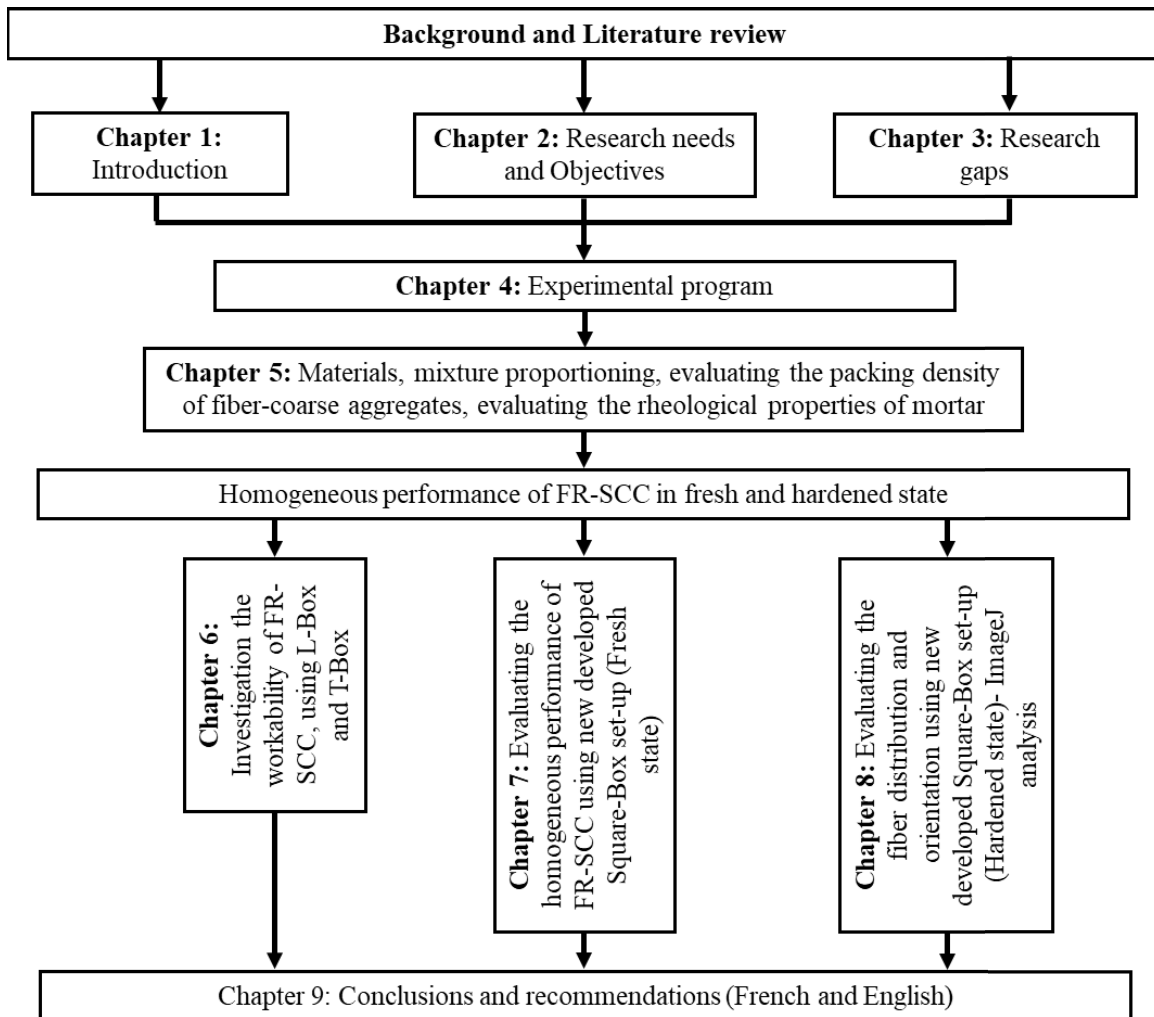
Figure 2-1 Diagram of the thesis organization.

CHAPITER 3 LITERATURE REVIEW

The design and use of fiber-reinforced self-consolidating concrete (FR-SCC) has increased recently in construction and repair applications. The presence of fibers in FR-SCC can increase the risk of separation of fibers and aggregate (F-A) from the paste/mortar during the flow of the material into place (dynamic segregation) and, thereafter, at rest (static segregation). Moreover, the presence of reinforcing bars can increase the risk of blocking of fiber-reinforced concrete (FRC) through narrow obstacles, which can lead to improper orientation of fibers that can impair mechanical properties. This paper presents an overview of the mechanisms, evaluation methods, and parameters that can influence the heterogeneous flow performance of FR-SCC and FRC. This paper addresses a critical review on key parameters affecting the heterogeneous performance of fiber-reinforced cementitious mixtures (uniform distribution of fibers and workability of FRC and FR-SCCs), including rheological properties of the suspending phase, fiber type, volume of fiber (V_f), and aspect ratio of fibers, as well as the particle-size distribution and packing density (PD) of the coarse aggregate and fiber-coarse aggregate (F-A) skeleton. The flow behavior of FRC is discussed as a bi-phasic material, including a suspending phase (paste or mortar) and suspended F-A materials. Moreover, the paper discusses various empirical methods to evaluate the homogenous flow behavior of FRC. It was found that characteristics of the solid skeleton have dominant effects on heterogeneous performance of FRC and FR-SCC mixtures comparing to rheological properties of suspending phase. The coupled effect of F-A characteristics in terms of packing density of F-A combination should be considered to optimise workable FR-SCC mixtures.

3.1 Introduction

Cement-based materials are brittle in nature with limited tensile strength and strain capacity in the hardened state. The addition of fiber can enhance the tensile and flexural strengths and ductility of fiber-reinforced concrete (FRC) [1-3]. Fibers transfer loads and bridge across micro and macro cracks and lead to strain hardening behavior of FRC. Generally, macro fiber transfer loads through macro-cracks after the peak in stress-strain curve, while micro fibers prevent the opening of tiny ones [4]. Fiber-reinforced SCC (FR-SCC) has greatly facilitated the casting of densely reinforced and complex structural elements [5-7]. However, the presence of fibers induces more heterogeneity compared to normal SCC [8]. Indeed, the incorporation of additional solid inclusions can reduce the workability of the mixture and, consequently, a higher dosage of superplasticizer is required to achieve a given level of flowability of FR-SCC. Therefore, the mortar matrix of the FR-SCC can have less viscosity compared to normal SCC [9,10]. This can increase the risk of blocking of fibers and aggregate through narrow gaps among reinforcing bars [11]. Hence, the optimization of the physical and rheological characteristics of cement paste and mortar [10-12] should be adjusted to obtain proper fluidity, high filling, and passing ability to allow adequate flow properties in the presence of reinforcement bars without segregation or blockage.

Moreover, due to their influence on workability of FR-SCC, the grading and packing density of aggregate, fiber characteristics (type, content, and aspect ratio), the arrangement of reinforcing bars (e.g., diameter, spacing, and distribution) [11,13] should be considered in the optimization process. High fluidity is not the only important parameter that should be considered, its stability is also another effective parameter that should be achieved [14,15]. Segregation of solid particles is defined as the separation of solid particles from the mortar matrix [16] that can lead to

heterogeneous flow of the mixture in the formwork [17]. Static segregation occurs when the concrete is at rest and coarse aggregate settle down given their higher density compared to the paste/mortar suspending fluid [18,19]. On the other hand, dynamic segregation occurs during flow when the fluid phase is not able to carry the solid particles and ensure homogeneous suspension [20]. These heterogeneous phenomena can lead to blockage of the flow. Local aggregate separation and segregation can occur, and the concrete flowing across the obstacles can be blocked [21]. The heterogeneous behavior of FRC and FR-SCC can include the uneven distribution and orientation of fibers in the cast element [13]. Proper orientation and distribution of fibers can significantly influence mechanical performance [12,22]. Uniform distribution (vertical and horizontal) of fibers in structural elements and number of perpendicular oriented fibers to applied forces can result in higher flexural and tensile strength values [23]. Accordingly, FR-SCC should satisfy the three basic characteristics of workability including: flowability, passing ability, and stability [12].

This study aims to discuss the main influencing parameters on the heterogeneous flow behavior of FRC and FR-SCC, in terms of static and dynamic stability, passing ability, as well as orientation and distribution of fibers. The effect of fiber-aggregate distribution as well as fiber orientation on mechanical performance of FRC is also discussed. Empirical test methods that can be used to evaluate static and dynamic segregation resistance of the fiber and aggregate as well as fiber orientation are presented.

3.2 Heterogeneous flow behavior of cement-based suspensions: Effective parameters related to mixture constituents

The heterogeneous flow behavior of FRC and FR-SCC can be classified into two main categories, including poor passing ability and instability (distribution) of fibers and aggregate, as well as improper orientation of fibers in different zones of the formwork. The main parameters related to mixture constituents that affect passing ability and stability are discussed below.

3.2.1   Fiber-aggregate characteristics

The presence of fibers can reduce the workability of FRC and increase the required energy for placement, consolidation, and finishing processes. This is due to the interaction of fibers and aggregate that leads to higher internal flow resistance. In the case of low fiber content, the hydrodynamic interaction between the suspending fluid and solid particles may not significantly alter the workability of the mixture. In this case, the fibers are far from each other and can easily displace and randomly orient towards the flow direction (Figure 3-1a) [24]. When the fiber and aggregate move through a viscous suspending fluid (paste/mortar), a flow field can be created around them, which causes their translations (distribution) and rotations (orientation). The shear flow leads the fibers to reorient parallelly to its direction (flow velocity).
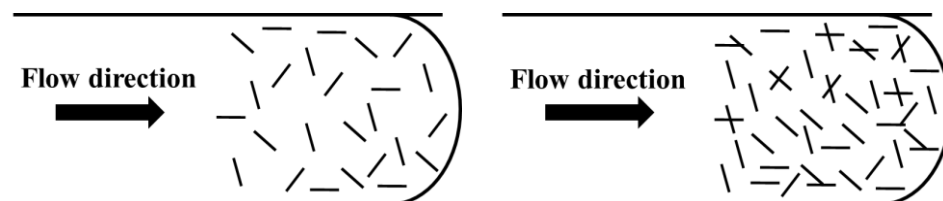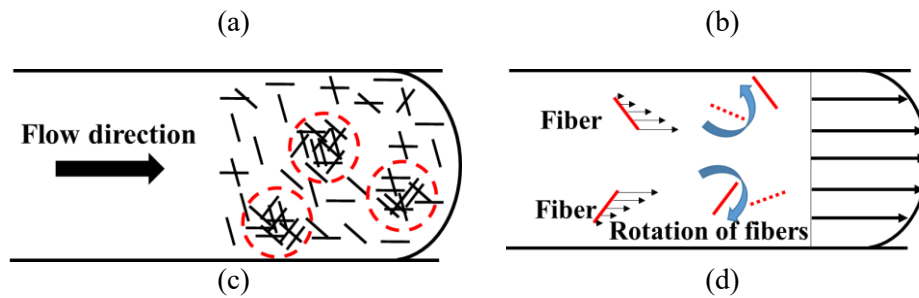
Figure 3-1 Fiber distribution and orientation patterns of (a) low (b) moderate, and (c) high dosages of fibers under shear flow and wall effects, and (d) flow velocity profile [24].

Increasing the fiber content can increase the interaction between the fibers (Figure 3-1b) [24], hence altering workability of fresh concrete. In the case of high fiber dosages (such as higher than 0.5%) (Figure 3-1c), the fiber interactions can lead to disorder their orientation. The use of fiber beyond a certain content can lead to fiber clamping and improper distribution and orientation of the fibers (Figure 3-1c) [24]. On the other hand, the use of high volume of fibers and coarse aggregate can increase the concentration of aggregate at the center of the slump flow and J-Ring spread. This is attributed to considerable interactions between fibers and aggregate.

The effect of fiber content on the performance of FRC in the fresh and hardened states was evaluated [25-27]. Khayat and Roussel [28] studied the workability and rheology of FR-SCC mixtures made with 38-mm steel fibers. High flowability was obtained when the fiber volume is limited to 0.5%. El-Dieb et al. [29] evaluated the effect of steel and polypropylene (PP) fibers on flowability of FR-SCC. The authors reported an optimum PP fiber content between 1.3 and 1.4 kg/m3, depending on the cement content, beyond which the flowability of FR-SCC mixtures decreased. Mehdipour and Libre [30] defined a fiber factor reflecting the coupled effect of size and content of fibers on flow performance of fiber-reinforced self-consolidating cement-based material (FRSCCM). The bleeding and visual stability index (VSI = 0 to 3) were employed to assess the stability and fiber homogeneity in slump flow test. The mixtures with fiber factor less than 150 showed a VSI of 0 (stable), while fiber flocs were observed in the mortar mixtures with fiber factor higher than 150. The fiber factor of 150 was thus reported as a critical value, beyond which there is a negative effect on flow and mechanical performance of fiber-reinforced mortars due to inadequate fiber orientation and distribution (FOD). On the other hand, El-Dieb et al. [29] recommended fiber factors between 70 and 110 to achieve appropriate flow characteristics.

Increasing fiber content can lead to promote fiber balling which prevent their movement (lack of workability) and act as obstacles. To achieve proper self-consolidating performance, the fiber content should be optimized given the mixture compositions, including water-to-binder ratio (W/B), superplasticizer dosages, cement content, volume and grading of aggregate, etc. Increasing the volume of paste can improve the homogeneous distribution of fibers while keeping proper flowability and stability of the mixture [31-33]. For a given workability level, higher fiber content can thus be incorporated in presence of higher paste content and, consequently, higher mechanical performance can be achieved.

The fiber stiffness has a negative effect on flowability of FRC due to the higher interaction between rigid fibers than flexible ones [30]. This can therefore disturb the motion of the fibers and promote clumping. Schmid and Klingenberg [34] showed that in the case of viscous suspension with high fiber content, the fiber-fiber interactions (Figure 3-2) are more dominant on fiber clumping than the hydrodynamic contacts. The fiber interactions can result in mechanical linking (Figure 3-2a) and elastic interlocking (Figure 3-2b) of fibers. The mechanical linking force depends on surface texture and shape of fibers, while the elastic interlocking mechanism is related to the normal and frictional forces. The elastic interlocking forces influence the flocs formation [34, 35]. Schmid and Klingenberg [34] reported that fiber flocs are formed due to the frictional and repulsive inter-fiber forces, as shown in Figure 3-2c.

(a) Mechanical linking   **(b)** Elastic force   **(c)** Inter-fiber forces
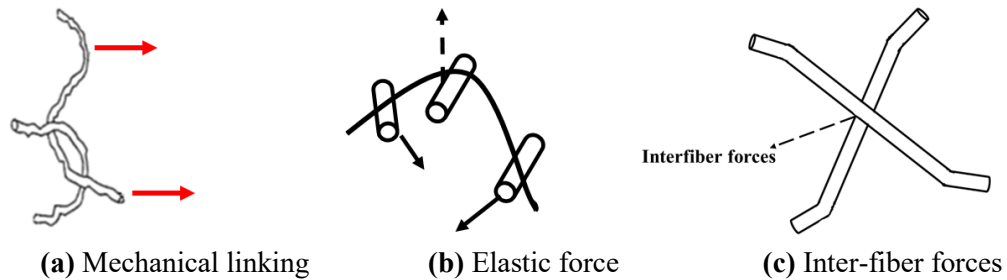
Figure 3-2 Forces responsible of fiber's clumping [34].

The presence of repulsive forces among rigid fibers contributes to their uniform distribution (Figure 3-3a). However, increasing the inter-fibers friction beyond a critical value leads to formation of flocs, which has negative effect on the fresh and hardened performance of FRC (Figure 3-3b).

(a)   (b)

Figure 3-3 Flocculation of fibers: (a) homogeneously dispersed fibers and (b) fiber flocculation [34].

Shanwan et al. [35] considered the mesoscopic and microscopic frictions between the fiber. As shown in Figure 3-4, different types of contacts and frictions, including longitudinal-to-longitudinal (Figure 3-4a), longitudinal-to-transversal (Figure 3-4b) and transversal-to-transversal (Figures 3-4c and 3-4d) contacts were considered depending on fiber rigidity. These inter-fiber interactions cause the formation of a fiber network. Increasing the fiber volume fraction and/or fiber rigidity can increase the contact points and, hence leading to stronger network forces between the fibers and rise the risk of agglomeration [34] with direct effect on workability of FRC mixtures.

(a) longitudinal-to- longitudinal   (b) longitudinal-to-transversal

(c) transversal to- transversal   (d) transversal to- transversal
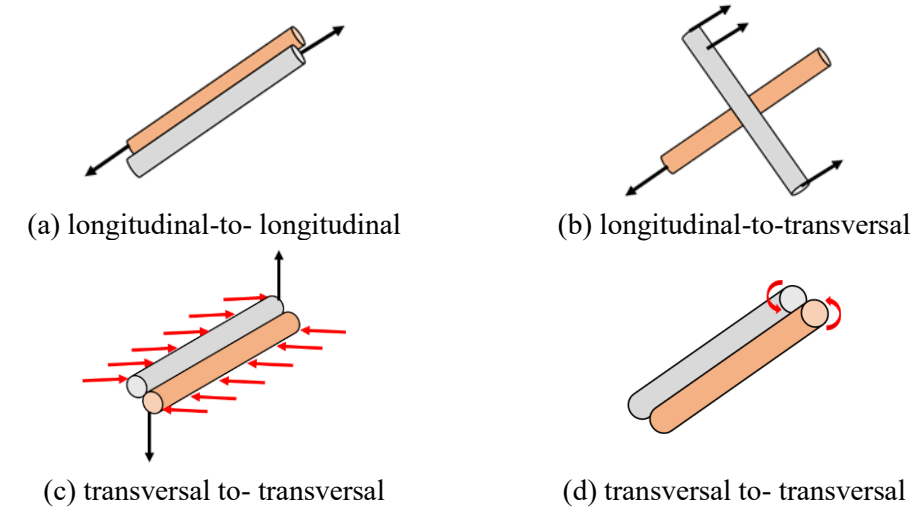
Figure 3-4 Different fiber frictions based on directions of fibers and forces [35].

Mehdipour and Libre [30] investigated the effect of flexible and rigid fibers on flow characteristics of FRSCCM mixtures. For a given volume of fibers, the use of rigid fibers led to 8% to 50% reduction in slump flow of the investigated mixtures compared to flexible polypropylene (PP) ones. On the other hand, Ahmad and Umarb [36] assessed the effect of content and rigidity of glass and polyvinyl alcohol (PVA) fiber types on workability of FR-SCC. The slump flow decreased by 20 mm as a result of adding 0.2% and 0.3% of glass and PVA fibers. Moreover, the use of flexible PVA fibers resulted in higher passing ability than that observed for the mixtures containing glass fibers. This is attributed to their less rigidity.

Furthermore, in a given aggregate system, the use of smaller fibers (microfibers of low diameter and length) can lead to higher number of fibers compared to those macro fibers. Higher specific surface area of smaller fibers can lead to more negative effects on workability of FRC mixtures, which is attributed to the lower volume of paste available to lubricate the aggregate-fiber system. In this case, higher amount of cement paste is required to cover the relatively high surface of fibers and achieve adequate workability.

Emdadi et al. [37] studied the effects of aspect ratio (i.e., length-to-diameter ratio of 300, 600, 1400) and volumetric fraction (0.01% to 0.7%) of PP fibers on fluidity of FRC mixtures. For a given fiber content, the mixtures incorporating shorter fibers (6 mm) showed lower fluidity than those containing longer ones (28 mm). Nehdi and Ladanchuk [26] also reported lower slump flow values for the FRC mixtures proportioned with short (12-mm length) steel fibers compared to those made with the longer ones (30- to 50-mm length). However, the longest fibers (50 mm) led to form more fiber clusters, hence inducing more blockage behind the reinforcing bars in the L-Box set-up (h_2/h_1 of 0.06) than the 30-mm ones (h_2/h_1 of 0.21). Moreover, the authors reported that the slump flow and L-Box h_2/h_1 ratios obtained for the FRC mixtures made with a combination of short and long fibers were higher than those made by the mono-sized fibers. This positive effect is due to improving the packing density of the hybrid system. Indeed, fiber's content, size and rigidity, affect the packing density of aggregate and consequently workability of FRC mixtures.

Aggregate characteristics, including morphological characteristics, particle-size distribution, and packing density can also significantly influence the workability of concrete [38-40]. Farokhzad et al. [41] evaluated the effect of aggregate grading on the performance of SCC. They reported that increasing the size of fine aggregate can reduce their ability to fill the gaps within the coarser particles and, therefore, lower the packing density. Lower amount of cement paste was thus available to lubricate the granular system, hence increasing the V-funnel time. The particle-size distribution of the granular skeleton is a key parameter that should be considered when proportioning concrete. Hafid et al. [42] reported a significant effect of morphological characteristics of fine aggregate on their packing density and rheological behavior of mortar mixtures. Ostrowski et al. [40] studied the effect of coarse aggregate morphology on fresh and hardened properties of self-consolidating FRC (SCFRC) mixtures. Lower slump flow values for the mixtures containing higher contents of irregular-coarse aggregate. On the other hand, higher plastic viscosity values were obtained for the mixtures containing both regular and irregular coarse aggregate.

Furthermore, one of the most effective parameters on workability of FRC mixtures is their particle-size distribution (PSD). Accordingly, a granular dispersion of fine and coarse aggregate can be described in three different PSD conditions, as shown in Figure 3-5.
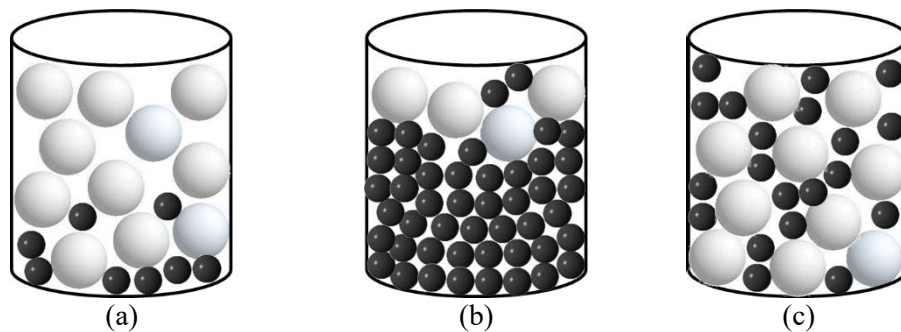
Figure 3-5 Different gradations of coarse and fine aggregate, including a) coarse particles are dominant (loosening effect), b) fine particles are dominant (wall effect), and c) continuously grading [43].

In the case of higher volume of coarse aggregate (Figure 3-5a), the fine and coarse particles can easily separate from each other due to the high tendency of fine aggregate to immerge among the coarser ones, hence increasing the risk of segregation. In contrast, in the case of higher volume of fine aggregate, coarse aggregates move to the top layers of the mixture (Figure 3-5b). In the case of a continuous granular skeleton (Figure 3-5c), solid particles can interlock and decrease the risk of segregation. Esmaeilkhanian et al. [44] reported that using an optimum PSD of solid skeleton can result in suspensions with higher fluidity and minimum risk of segregation. Therefore, the selection of an optimized PSD to enhance the flow performance, leading to a granular skeleton of high packing density.

3.2.2   Packing density – empirical and theoretical models

Several empirical and theoretical models were proposed to evaluate the packing density of granular dispersion as a function of their PSD [45-50]. De larrard [45] introduced a linear model to predict the packing density of aggregate. The interaction between the particles was considered using the wall and loosening effects, as follows:

$$\alpha_t = min_{i=1}^{n} \left[\frac{\alpha_i}{1-(1-\alpha_i)\sum_{j=1}^{i-1} a_{ij}\cdot\varphi_j - \sum_{j=i+1}^{n} b_{ij}\cdot\varphi_j} \right] \qquad \text{Equation 3-1}$$

where α_t is the theoretical packing density of polydisperse mix of the n aggregate subclasses, α_i and φ_j are the packing density and volumetric content of aggregate classes 'i' and 'j', respectively, and n is the total number of aggregate classes. The loosening (a_{ij}) and wall effect (b_{ij}) were considered using the following Equations. 3-2 and 3-3:

$$a_{ij} = \begin{cases} \sqrt{1-(1-\frac{d_j}{d_i})^{1.02}} & ,d_i > d_j \\ 0, & d_i \leq d_j \end{cases} \qquad \text{Equation 3-2}$$

$$b_{ij} = \begin{cases} 1-(1-\frac{d_i}{d_j})^{1.50} & ,d_j > d_i \\ 0, & d_j \leq d_i \end{cases} \qquad \text{Equation 3-3}$$

de Larrard [45] also developed the compressible packing model (CPM) to predict the virtual packing density of binary granular dispersions of two different size-subclasses of particles under compaction, as follows:

$$\alpha = Min\left(\alpha_1 = \frac{\beta_1}{1-(1-\frac{\beta_1}{\beta_2}a_{12})y_2}, \alpha_2 = \frac{\beta_2}{1-(1-\beta_2+b_{21}\beta_2(1-\frac{1}{\beta_1}))y_1} \right) \qquad \text{Equation 3-4}$$

where α is virtual packing density obtained by CPM model, α_1 and α_2 are the virtual packing densities of the binary mixture when coarse and fine particles are dominant, respectively; β_1 and β_2 as well as y_1 and y_2 are the virtual packing densities and volumetric fractions of the coarse particles related to classes 1 and 2 with respect to the total solid volume, respectively.

The packing density (φ_{max}) can be calculated using the compaction index K that is related to the packing process to fill and compact the particles inside the container:

$$K = \frac{\frac{y_1}{\beta_1}}{\frac{1}{\varphi_{max}}-\frac{1}{\alpha_1}} + \frac{\frac{y_2}{\beta_2}}{\frac{1}{\varphi_{max}}-\frac{1}{\alpha_2}} \qquad \text{Equation 3-5}$$

Roquier [50] proposed a new 4-parameter CPM model to predict the packing density of spherical particles. This model consists of the wall and loosening effects, the compaction index, and the critical cavity size ratio (x_0). Below the x_0 value, the fine particles do not disturb the packing density of coarser ones, otherwise, small particles can change the configuration of coarser ones. To visualize the effect of size ratio (x) on packing density of solid particles, the perturbed region due to interface of fine and coarse particles is shown in Figure 3-6.
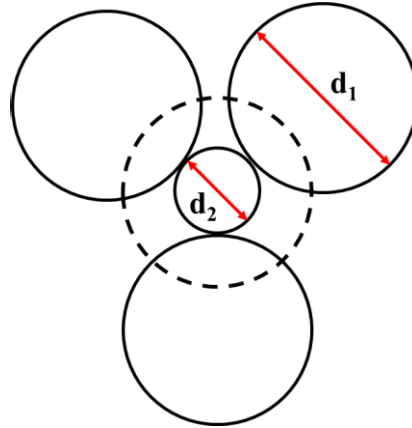
Figure 3-6 Definition of the spherical reference cell for studying the loosening effect [50].

Accordingly, the diameter of disturbed volume by the loosening effect is:

$$D_{disturbed} = d_2 \sqrt{1 + \frac{2\,k_{p1}}{x}} \qquad \text{Equation 3-6}$$

where, $x = d_2/d_1$ and k_{p1} can be calculated based on boundary conditions for spherical particles. Therefore, the virtual packing density of fine aggregate (β_2) is equal to:

$$\beta_2 = \alpha_2 \frac{1+K}{K} \qquad \text{Equation 3-7}$$

where α_2 is the real packing density of fine particles and K is compaction index. Up to now, only packing density of aggregate skeleton has been considered. However, during casting elements, the concrete flow may be restricted by the reinforcing bars and formwork walls. Incorporating fibers in this restricted flow condition can significantly affect the workability of FRC mixtures. This is due to the interaction of fibers and aggregate which has direct effect on packing density of fiber-aggregate combination. Therefore, the optimization of the packing density of fiber-aggregate is an effective alternative to ensure adequate stability and flow performance.

The packing density of fiber-aggregate mixtures is not sufficiently investigated. De Larrard [45] evaluated the effect of steel fibers' characteristics on packing density of coarse and fine particles using the CPM model. Accordingly, the ratio between the distance of propagation and the size of the particles (k_f) was considered. It was reported that increasing the content and length of fibers can negatively influence the packing density of aggregate. As can be observed in Figure 3-7, for a

given fiber content and PSD of aggregate, increasing the length and diameter of the fibers can result in lower fiber-aggregate packing density.

<div align="center">(a)   (b)</div>
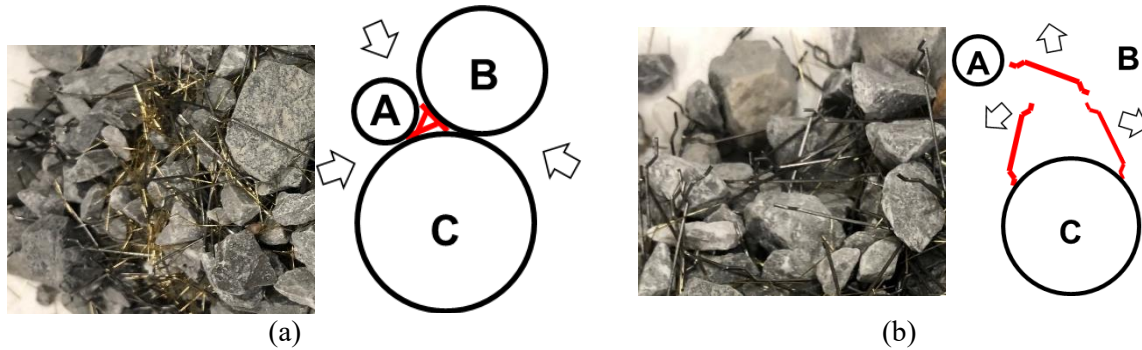
Figure 3-7 Effect of different fiber sizes, including the (a) micro and (b) macro steel fibers on packing density of fiber-aggregate combination.

Indeed, the shorter and thinner fibers can properly fill the voids between the aggregate particles (Figure 3-7a) and, therefore, increase the packing density of fiber-aggregate mixture. However, the longer and thicker fibers push away the aggregate and increase the inter-particle distances (voids), hence lowering the fiber-aggregate packing density (Figure 3-7b). It is worthy to mention that the whole length of fibers can not disturb the packing density of aggregate skeleton. Indeed, it is dead ends of fibers that should be considered for the perturbed region (υ_p). The length of this zone can be determined as fiber length-aggregate diameter/2 (Figure 3-8). Therefore, the mean packing density fiber-aggregate system ($\bar{\alpha}$) can be evaluated, as follows:

$$\bar{\alpha} = (1\text{-}V_f\text{-}N_f \times \upsilon_p)\, \alpha \qquad\qquad \text{Equation 3-8}$$

where V_f is fiber volume, N_f is number of fibers, α is actual packing density of a monodisperse mix.

<div align="center">(a)   (b)</div>
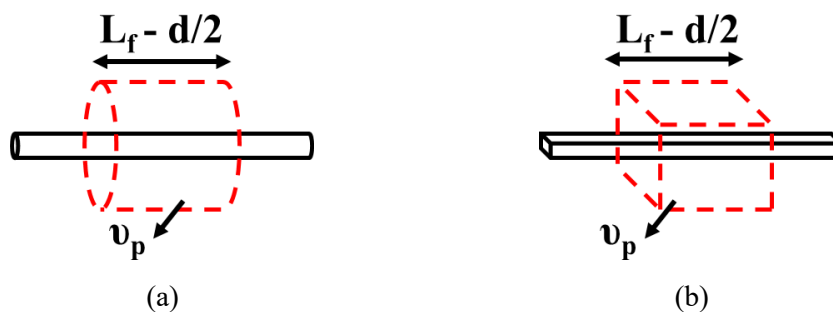
Figure 3-8 Perturbed volumes for (a) cylindrical and (b) prismatic fibres [45].

However, this model is not applied in the case of flexible fibers. According to de Larrard [45], flexible fibers can be deformed between aggregate under pressure (Figure 3-9a), therefore, their effect on disturbed zone is less than the rigid fibers. More specifically, the deformed flexible fibers can contribute to properly fill the voids within the aggregate particles, hence increasing the packing density of the system. On the contrary, the rigid undeformed fibers do not allow the aggregate to

be more compacted which consequently decreases the packing density of fiber-aggregate mixture (Figure 3-9b).
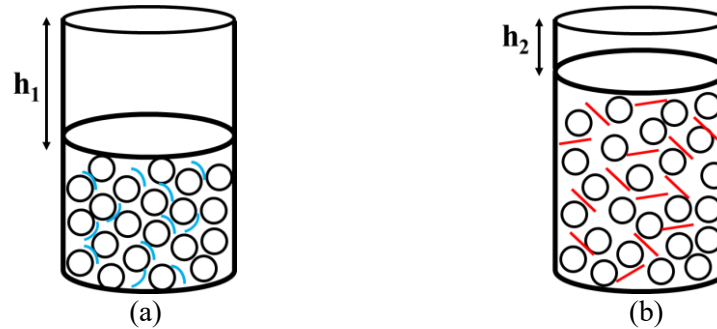
Figure 3-9 Packing density of combination of aggregate with (a) flexible and (b) rigid fibers ($h_1 > h_2$).

As an example, a given aggregate mixture of packing density of 0.603 is mixed with different volumetric contents (0.4% to 0.9%) of two different fiber types. These include a rigid-macro-steel fiber of 30-mm length, aspect ratio 55, and elastic modulus of 200 GPa, as well as a flexible propylene fiber of 19-mm length and aspect ratio 156. The packing density values of the fiber-aggregate mixtures were measured using the intensive compaction tester (ICT) device [51] and presented in Figure 3-10. In general, the ICT is employed for testing compaction of granular materials, such as soil and aggregate of concrete [52, 53]. The test consists in applying a normal pressure of 20 kPa to perform the packing density measurements. This pressure is usually recommended to prevent crushing of aggregate during testing. In total, 150 gyratory cycles were then applied. As can be observed in Figure 3-10, for a given fiber dosage of 0.4% to 0.9%, the packing density (PD) of fiber-aggregate mixtures containing flexible polypropylene fibers are higher (0.597 - 0.603) than those obtained for rigid-macro-steel ones (0.588 - 0.590). This is due to higher deformation of flexible fibers through the interparticle voids, hence increasing the packing density of the system.
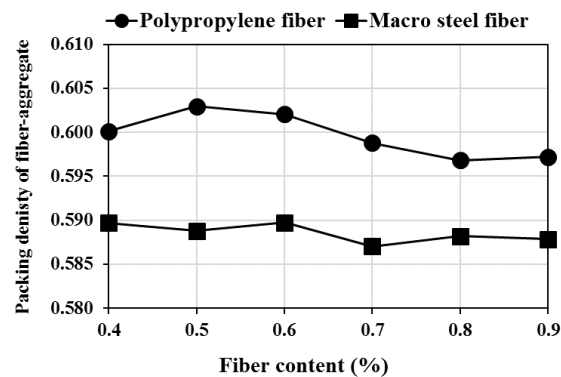
Figure 3-10 Effect of rigidity of fibers on packing density of fiber-aggregate combination.

Moreover, it is reported that the negative effect of rigid and long fibers is more highlighted in the case of coarse particles comparing to fine aggregate [45]. Therefore, the packing density of F-A combination is also function of aggregate characteristics. As illustrated in Figure 3-11, adding fiber to fine and coarse aggregate systems can have dual effects on packing density of F-A combination.

When aggregate size increases, fibers cannot fill the space between aggregate and, consequently, decreases the packing density of F-A system.
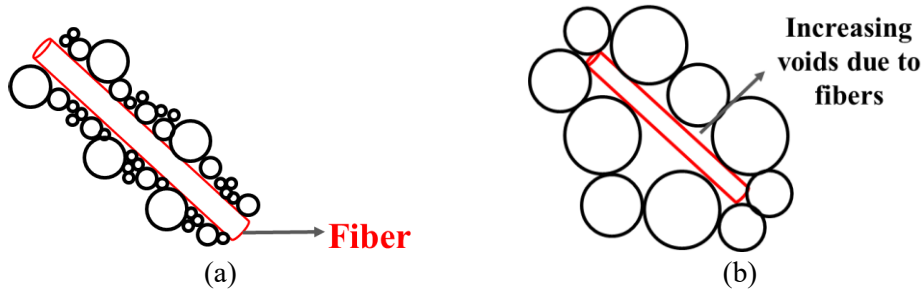
Figure 3-11 Dual effect of incorporating fibers on packing density of (a) fine and (b) coarse aggregate systems.

Lam [54] developed two models to predict packing density of fiber-sphere particles combination, considering the replacing and filling regimes. In the replacing regime, packing density can be altered by replacing a given volume of fine particles and voids by an equal volume of mid-sized particles and fibers. Therefore, based on characteristics of fibers (i.e., dosage, size, and rigidity), packing density can be increased by filling the space among the particles with fibers or decreased by pushing them apart in the case of high fiber content and/or long-rigid fibers.

This can be related to the particle-to-fiber size ratio S (particles diameter-to-fiber size ratio) forming extra void volume [54]. This extra void can be created in the vicinity of disturbed zone (Figure 3-8) at the interface region between the fibers and particles. The packing density in a replacement regime can then be calculated, as follows:

$$\rho_c = \frac{\rho_{fi,o}}{1 - F_f\left[1 - \rho_{fi,o}\left(1 + K_f\right)\right] - F_m\left[1 - \rho_{fi,o}(1 + K_m)\right]} \qquad \text{Equation 3-9}$$

where $\rho_{fi,o}$ is the bulk packing density of fine particles without any extra void, F_f and F_m are the volumetric fractions of fibers and mid-sized particles, respectively. Moreover, K_f and K_m are defined, as follow:

$$K_f = \alpha_f \beta_f Z_{fib} \qquad \text{Equation 3-10}$$

$$K_m = \alpha_m \beta_m Z_{fim} \qquad \text{Equation 3-11}$$

where $Z_{fim} = r/R_m$, the ratio of the radius of fine particle-to-mid-sized particle, Z_{fib} is the ratio of the fine particles' radius-to-fiber size. Moreover, α_f and α_m are shape factors, defined as $\alpha_f = 2$ for fibers and $\alpha_m = 3$ for spheres, respectively. Similarly, in a filling regime, the packing density of fiber-particles combination can be evaluated, as follows:

$$\rho_c = \frac{\rho'_m \left(1 - F_f\right)}{F_m - F_f \left[F_m - \rho'_m \left(1 - F_f\right)\right]} \qquad \text{Equation 3-12}$$

where ρ'_m is the maximum packing density of the mid-sized particles within a fiber network without fine particles. The effect of interaction between fibers and mid-sized particles, and the mid-sized with fine particles is investigated by considering two systems of 1/10/100 (mid-sized ratio/fiber size = 10) and 1/5/25 (mid-sized ratio/fiber size = 5). It is reported that decreasing the ratio of fine-to-mid-sized particles exhibit more significant effect on packing density than reduction of the ratio of mid-sized particles-to-fiber size. Moreover, the study revealed that changing the size of the mid-sized particles toward the fiber size can increase the size of pore space (voids) which should be filled by the fine particles. This can increase the packing density of fiber-sphere particles combination. This can be due to lower negative effect of fine/mid-sized particles ratio, i.e. loosening and wall effect [52]. On the other word, increasing the mean diameter of voids between aggregate leads to more space for fibers to be deformed and increases the packing density of the system. As an example, 0.6% and 0.9% dosages of a macro steel fiber of 30 mm length and aspect ratio 55, and elastic modulus of 200 GPa were mixed with 2 different coarse aggregate mixtures of PSD-1 and PSD-2. It is worthy to mention that the PSD-1 mixtures exhibited higher packing density than the PSD-2 mixture. Having the specific surface of the aggregate mixtures, the mean diameter of void calculated by the ratio of void volume (i.e. 1 - packing density of aggregate)-to-the surface area of coarse aggregate in unit volume of fiber-aggregate combination. Deformation of the fibers after packing density measurements were evaluated using image analysis of the deformed fibers (Figures 3-12a and 3-12b). This was estimated by the mean values of the ratio of the fiber deflections-to-the total fiber length (in %).

(a)   (b)
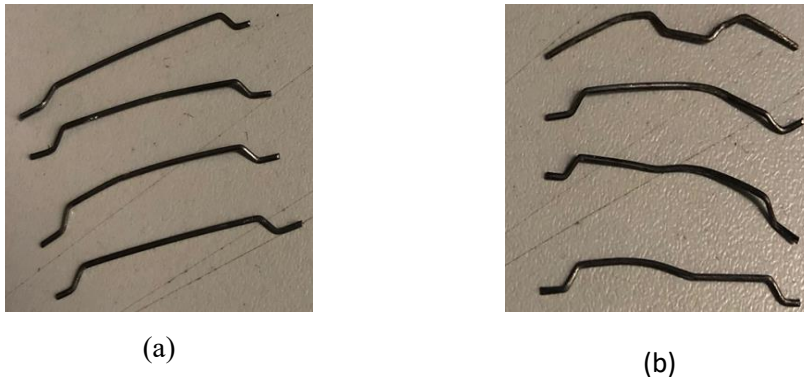
Figure 3-12 Deformed fibers after packing density measurements of fiber-aggregate mixtures made with (a) PSD-1 and (b) PSD-2 aggregate mixtures.

As shown in Figure 3-13a, increasing the mean diameter of voids can lead to higher deformation of fibers after packing density measurements. Higher deformation of fibers consequently led to higher packing density of fiber-aggregate combination (Figure 3-13b).

(a)   (b)
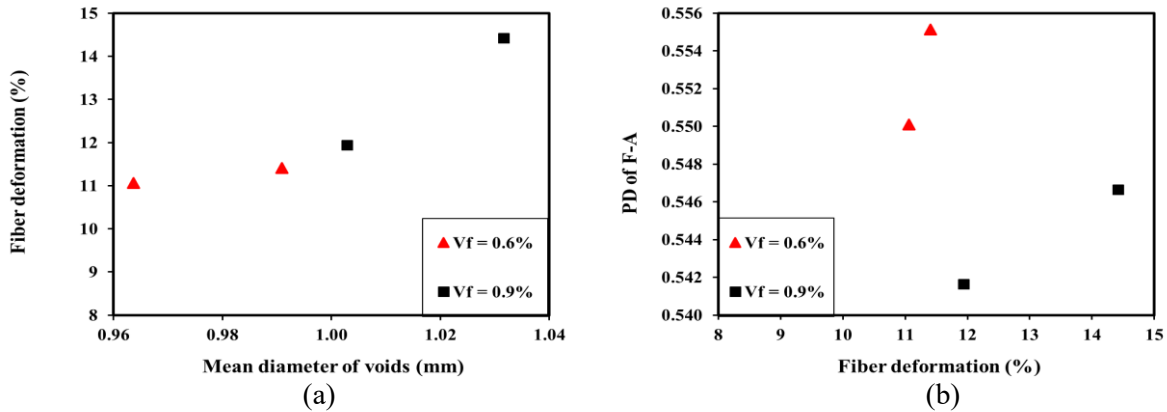
Figure 3-13 (a) Effect of mean diameter of voids on fiber deformation and (b) effect of fiber deformation on PD of fiber-aggregate systems.

Chu et al. [55] investigated the effect of rigid fibres on PD of fiber-aggregate combinations of different contents (0 - 2%) of rigid steel fibers of 30- and 60-mm length, as well as various classes of aggregate (0.6 - 20 mm). The authors reported that increasing fiber size and content decreased packing density of fiber-aggregate combination, specially in the case of the coarser aggregate (20 mm). The rate of changing packing density of fiber-aggregate was reported as a function of fiber size and aggregate characteristics. They reported that increasing fiber size and aggregate diameter leads to more negative effect on packing density of F-A. The effect of fiber size and content on packing density of F-A system was evaluated using a parameter K, as follows:

$$K = -0.00512 \ (G/D)0.5(L/D)1.5 \qquad\qquad \text{Equation 3-13}$$

where G is mean diameter of aggregate, and L and D are fiber's length and diameter, respectively. According to the establish equation, increasing fiber length has negative effect on packing density of F-A combination. It is worthy to mention that Equation 3-13 was proposed for rigid fibers (e.g., steel fibers). However, it is still unknown how flexible synthetic fibers, such as polypropylene fibers, affect the packing density of fiber-aggregate combination and consequently workability of FRC. Indeed, evaluation of the packing density of the flexible fiber-aggregate system is complicated because the synthetic fibers stick to each other.

It can be concluded that optimizing the packing density of fiber-aggregate combination is a useful tool to reach FRC mixture with high workability and adequate mechanical performance due to minimizing the void among solid particles that should be filled by paste or mortar (the required extra volume of paste to lubricate solid particles).

Accordingly, to evaluate the effect of optimization of fiber-aggregate packing density on homogeneous performance of FR-SCC, two different classes of crushed limestone coarse aggregates of 5-10 mm (CA1), and 5-14 mm (CA2) are considered. Four different combinations of coarse aggregate: N1(100%-CA1), N2 (80%-CA1 and 20%-CA2), N3 (60%-CA1 and 40% CA2), and N4 (40%-CA1 and 60%-CA2) are considered to evaluate the effect of PSD of granular skeleton. Also, the SCC mixtures are reinforced by macro steel fibers (30 mm length and aspect

ratio 55, and elastic modulus of 200 GPa). The packing density of fiber-aggregate skeleton can be achieved using mentioned empirical methods or experimentally.

The dynamic segregation of five FR-SCC mixtures with different values of PD of fiber-aggregate is investigated using J-Ring test. The variation of the difference between slump and J-Ring flow ($\Delta_{\text{J-ring}}$) versus the variation of the ratio of the volumetric content (φ)-to-packing density (φ_{max}) of fiber-aggregate combination is plotted in Figure 3-14.
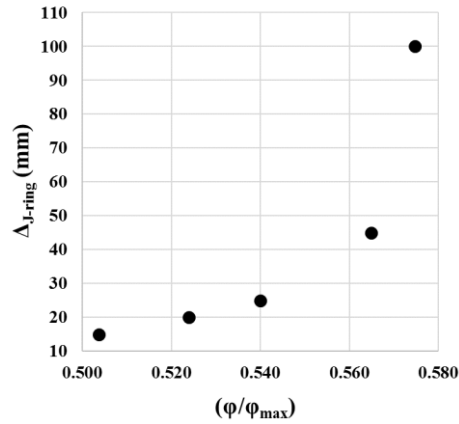
Figure 3-14 Effect of packing density of fiber-aggregate combination on heterogeneous performance of FR-SCC.

As can be observed in Figure 3-14, the blocking of FR-SCC mixtures is influenced by the φ/φ_{max} of fiber-aggregate skeleton. A granular skeleton with higher φ/φ_{max} results in more interaction between fibers and aggregate which limits their movement. This can significantly increase the risk of blockage of fibers and aggregate behind the bars. This can lead to higher heterogeneous behavior of FR-SCC. It can be concluded that optimizing the packing density of fiber-aggregate skeleton is a useful tool for enhancing homogeneous performance of fiber reinforced cementitious materials.

3.2.3   Rheology of suspending paste/mortar matrix

The rheological behavior of SCC can be characterized by its yield stress (τ_0) and plastic viscosity (μ_P) parameters [56]. SCC mixtures are designed with low yield stress to enhance their deformability and filling ability, as well as adequate viscosity to maintain homogeneous suspension during flow in the formworks. However, low yield stress mixtures can undergo higher risk of segregation of solid particles from suspending paste/mortar. Cement paste and solid particles tend to separate vertically before setting, which is referred to static segregation in the absence of flow (Figure 3-15a). During flow, this separation can occur horizontally and vertically and is referred to dynamic segregation (Figure 3-15b).

(a) Static segregation   (b) Dynamic segregation
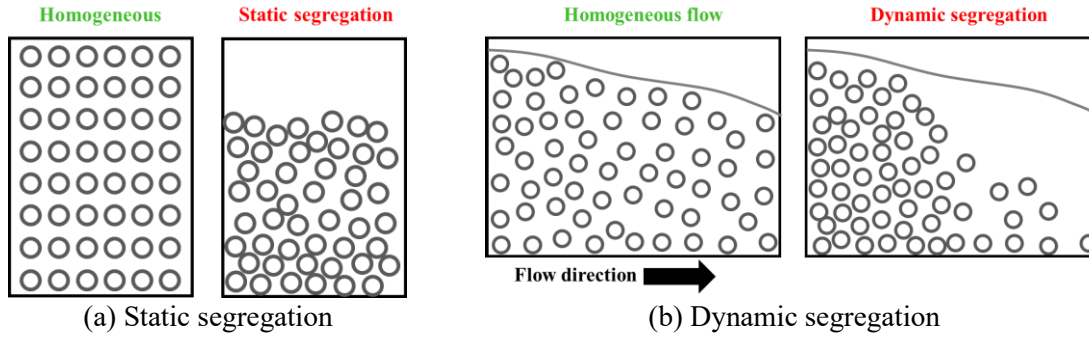
Figure 3-15 Static and dynamic segregation [57].

In the absence of reinforcing bars, the gravity-induced and shear-induced particle migrations are responsible for static and dynamic segregations, respectively [19, 58]. It is reported that [19] in the case of industrial casting of concrete, gravity induced particle migration dominates all other sources of heterogeneity induced by flow.

<u>Static segregation</u>: When concrete is still plastic, coarse solid particles settle down while paste/mortar move upward (static segregation) [59]. Indeed, in the case of highly flowable FRC mixtures, any difference between the densities of the suspended particles (fiber and aggregate) and suspending phase (paste/mortar) can lead to gravity-induced segregation of suspended solids. Furthermore, the rheological properties of suspending fluid play a vital role on their settlement. In the absence of external forces, the forces acting on a single aggregate in the paste/mortar are buoyancy (F_b), gravity (F_g), and resistance force generated by the yield stress of cement paste/mortar. If the resistance force (F_{resis}) is higher than difference between buoyancy and gravity (F_g-F_b), aggregate remains stable. Under static condition, $F_{resis} = \tau\, A_s$, in which τ is the yield stress of the suspending fluid, and A_s is the cross-sectional area of the particle. On the other hand, unstable state occurs when stress generated by the buoyancy and gravity is enough to overcome the yield stress of suspending paste/mortar [18], the restoring force (F_{resis}, exerted by the cement paste) can be replaced by drag force (F_D). The drag force exerted on solid particles by the suspending fluid can be calculated, as follows:

$$F_D = \frac{1}{2} \times \rho \times C_D \times A \times V^2 \qquad\qquad \text{Equation 3-14}$$

where, ρ is suspending fluid density, C_D is the shape-dependent drag coefficient, A is the surface area of particles' projections perpendicular to the flow direction, and V is the relative velocity of particle and suspending fluid. The flow regime is determined using the Reynolds number as the ratio of the inertia-to-drag forces, as follows:

$$\text{Re} = \frac{\rho \times V \times d}{\eta} \qquad\qquad \text{Equation 3-15}$$

where d is particle diameter and η is the apparent viscosity of the suspending fluid. The drag coefficient C_D is a function of the particle shape and flow regime. In a stokes flow regime (i.e., Re << 1), CD is equal to 24/Re. However, in the case of the creeping motion of a sphere in a yield stress fluid, in addition to Reynolds number, Tabuteau et al. [60] recommended two other

dimensionless numbers of Bingham and Yield numbers to be considered to calculate the drag coefficient, as follow:

$$\text{The Bingham number: } Bi = \frac{\tau_0}{K(V/d)^n} \qquad\qquad \text{Equation 3-16}$$

$$\text{Yield number: } Y = \frac{3\tau_0}{gd\Delta\rho} \qquad\qquad \text{Equation 3-17}$$

$$CD = \frac{4Bi}{Y\,Re} \qquad\qquad \text{Equation 3-18}$$

It was reported in literature that the drag coefficient is also dependent on the morphology of particles, including their elongation and surface roughness [61,62]. It can be thus concluded that in order to enhance the stability of the highly flowable concrete mixtures, both the rheological properties of the suspending mortar and shape characteristics of the solid dispersions, as well as controlling the casting rate (flow velocity) must be taken into consideration.

Roussel [63] proposed two criteria to ensure the static stability of suspended solid particles in a Bingham suspending fluid, as follow:

$$\text{Static stability criteria : } \begin{cases} d < d_c, \text{ Regardless of solid fraction } \varphi & \text{Equation 3-19} \\[2mm] \varphi > \varphi_c, \text{ if } d > d_c & \text{Equation 3-20} \end{cases}$$

where

$$d_c = \frac{K.\tau_0}{|\rho_s - \rho_f|g} \qquad\qquad \text{Equation 3-21}$$

$$\varphi_c = \frac{\varphi_{max}}{\sqrt[3]{\dfrac{6M.\tau_0}{\pi|\rho_s - \rho_f|.d.g} + 1}} \qquad\qquad \text{Equation 3-22}$$

where d is particle diameter, dc is a critical particle size which its beyond the suspension is not stable, ρ_s and ρ_f are the densities of the suspended particles and suspending fluid, respectively, τ_0 is the yield stress of the suspending fluid, and g is the gravitational acceleration. Moreover, φ_c is the critical volumetric content of the particles beyond which the suspension is stable at rest, and φ_{max} is the maximum packing density of the suspended particles. Furthermore, K and M are the shape-dependent parameters equal 18 and $3\pi/4$ for identical spheres, respectively. Stability of the highly flowable suspensions at rest can therefore be achieved by adequate optimization of the characteristics of both suspending fluid (rheological properties), and suspended particles (morphology, PSD, volumetric content, and packing density).

In the case of FRC mixture, the packing density of F-A combination can be considered instead of only aggregate for adequate stability. Also, to study the effect of particles morphology (d in the case of plain concrete), as already mentioned, the parameter of L_f-d/2 can be considered instead of d. It is reported that for particles with diameter higher than dc, segregation occurs and the velocity moving of sphere particles in a Bingham fluid (suspending phase) can be calculated as:

$$V_s = \frac{d}{\mu_p} \left(\frac{d}{18} \left(\rho_s - \rho_f \right) g - \tau_0 \right) \qquad \text{Equation 3-23}$$

where ρ_s and ρ_f are sphere and fluid density, respectively, and μ_p and τ_0 are plastic viscosity and yield stress of fluid (Bingham). Based on this equation, all particles move at the same speed and the average distance among them remain constant, which is a function of initial solid fraction. However, during casting, particles stop moving because of the boundary conditions of wall effect (e.g. bottom of the mold). The hydrodynamic interactions between particles are negligible. However, as already mentioned, in the case of fiber-aggregate skeleton, especially in the case of high fiber content (Figure 3-1), the interaction between fibers and aggregate and, consequently, hydrodynamic interactions become more important. Moreover, since fibers can act like obstacles, their presence can be considered as a boundary condition which changes the distance among aggregate by being placed among them and prevent their movement (especially rigid fibers).

In the case of dynamic segregation, the shear induced particle migrations is responsible for the heterogeneous behavior of concrete during flow [58]. This migration can occur due to the velocity gradient between solid particles (fibers and aggregate) and suspending fluid (paste/mortar). Shear stress decreases from maximum value in the bottom of the formwork to zero (flow surface). In the vicinity of free surface, there is a layer in which materials are not sheared and plug flow can occur ($\tau < \tau_0$) (Figure 3-16). In the middle layer, materials are sheared. Finally, in the bottom layer, particles settle under gravity.
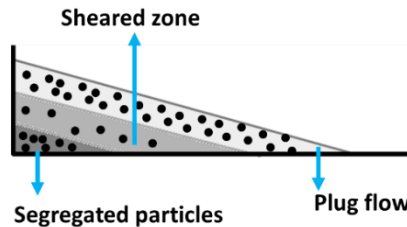
Figure 3-16 Multilayer structure in a flow regime [58].

Indeed, due to shear-induced particle migration, solid particles migrate from high-shear rate zones towards the lower shear-rate zones. The shear-induced particle migration under shear stress can be defined by the equation bellow:

$$\frac{\partial \varphi}{\partial t} + \frac{\partial (u_z \varphi)}{\partial z} = \nabla . \left\{ a^2 K_c \varphi \, \nabla (\varphi \frac{\partial u_z}{\partial r}) + K_\eta \varphi^2 a^2 \frac{\partial u_z}{\partial r} \frac{\nabla \eta}{\eta} \right\} \qquad \text{Equation 3-24}$$

where φ is particles concentration, t represents the time, u_z shows the velocity component in the flow direction, z is the flow direction, a is the particle radius, r is the radial direction, η is the apparent viscosity of the concrete mixture, and K_c and K_g are dimensionless constant coefficients.

As the shear rate is a ratio of particle falling rate-to-particle size, the first term of the right side in Equation 3-23, i.e. stress gradient, cause particles to move [64, 65]. Indeed, in highly sheared or highly concentrated zones, particles collisions force particles to migrate from the zones where particles are migrating to. This effect is balanced by the local increase in the suspension viscosity due to this migration [19] (described in the second term of the right side in Equation (23)).

It can be concluded that heterogeneous performance of cementitious mixtures can be due to the shear and gravity induced particle migration. When the local volume fraction of particle reaches the so-called random loose packing, both shear and gravity induced particle migration stop. It is important to kept in mind that the characteristic time of two types particle migrations is different, which are expressed by:

$$T_c^{shear} = \frac{H^2}{10 \, a^2 \, \varphi^2 \, \gamma} \qquad \text{Equation 3-25}$$

$$T_c^{gravity} = \frac{18\eta H}{g\Delta\rho a^2} \qquad \text{Equation 3-26}$$

where T_c^{shear}, $T_c^{gravity}$ are representative of time of shear and gravity induced particle migration, respectively. H is the thickness of the smallest dimension of the flow element [19]. In the case of characteristics time related to the shear induced particle migration, the profile of particle volume fraction shows a steady state when the suspension reaches a critical deformation (γ_c). This critical deformation is less in the case of high concentrated mixture due to local shear thickening. For characteristics time related to gravity induced particle migration, it can be found that coarse particles most tend to migrate due to the power two of their diameter in Equation 3-25. However, non-of these equations consider the effect of fibers and their interaction with solid particles, on shear and gravity induced particle migration. This interaction can change the particle collision frequency and gradients in viscosity of the suspension.

Ferrara et al. [12] investigated the flow behavior of FR-SCC mixtures proportioned with different contents of water, cement, and superplasticizer by ±5%, ±2%, and ±3% variations, respectively. Correlations between the fresh properties, fiber distribution, and mechanical properties were established. Static segregation of FR-SCC mixtures was evaluated using a cylinder of 250-mm height and 80-mm diameter. The cylinder was cast and cut after hardening into three equal sections, corresponding to top, middle, and bottom layers. The highest difference in fiber concentration from top to bottom layers (static segregation) was reported for higher water content mixtures compared to superplasticizer dosage and cement contents. For example, increasing by 5% of water led to increasing the fiber content from 31 kg/m3 in top and middle sections to 77 kg/m^3 in bottom one. On the other hand, increasing cement content and HRWR dosage resulted in variation of fiber content in top to bottom layers from 47 to 53 and 39 to 59 kg/m3, respectively. It can be concluded that lower water content and superplasticizer dosage, as well as higher cement content can lead to higher yield stress or plastic viscosity values and, consequently, lower segregation of fibers and aggregate.

Jasiuniene et al. [13] investigated the effect of rheological properties of concrete on fibers' orientation and distribution (FOD). Three rheological values were investigated by variation of content of zeolite powder from 0 to 20%, by mass of cement. A 1200-mm beam was cast from one corner to evaluate FOD (no vibration was applied). The hardened beam was then cut into 10 equal longitudinal cross sections (at each 120 mm). The results showed that the zeolite dosage has remarkable effect on both fiber distribution and orientation. This is due to its effect on rheological properties of concrete (yield stress and viscosity). The highest vertical scattering and horizontal inhomogeneity in fiber distribution were observed for the SCC mixtures with the lowest plastic viscosity (t_{500} = 1.06 s). Also, a high orientation factor, corresponding to more fiber orientation parallel to the flow direction, was found for the mixtures with a high value of slump flow (655 mm) and low t_{500} of 1.06 s. It is worth remarking that although low value of viscosity has positive effect on proper fiber orientation (parallel to flow direction), but negatively affects the homogeneous distribution of fibers. The authors reported that the FOD is influenced by rheological properties of concrete, due to their effect on concrete flow velocity profile. Increasing water-to-binder ratios or superplasticizer content was reported to be a very effective way to increase the fluidity of FRC, but shows negative effect on its stability [13, 66, 67]. Koura et al. [68] evaluated the coupled effect of characteristics of coarse aggregate (> 1.25 mm) and rheological properties of suspending fine mortar (< 1.25 mm) on dynamic stability of SCC. The coarse aggregate was characterized in terms of the ratio of its volumetric content (φ)-to-packing density (φ_{max}). The rheological properties of the suspending fine mortar portion, consisted of cement paste and finer portion of aggregate (< 1.25 mm), were characterized in terms of yield stress, plastic viscosity, critical strain, shear storage, and loss moduli. The authors reported that φ/φ_{max} of coarse aggregate shows a dominant effect on dynamic stability of SCC. The optimization of the paste volume and ratio of φ/φ_{max} are effective parameters on dynamic stability of SCC rather than the water-to-binder ratio and high-range water reducer (HRWR) dosages. However, a similar approach can be employed for flowable FRC mixtures to evaluate the coupled effect of mortar/past rheology, characteristics of aggregate and fibers on their homogenous flow performance and fibers' orientation and distribution. In order to obtain a proper mixture proportioning of FRC and FR-SCC, the influence of various effective parameters should be considered simultaneously. In the case of low yield stress and plastic viscosity of paste/mortar, the drag force exerted on solid objects is low and suspending paste/mortar can not carry aggregates and fiber in their initial place.

3.3 Casting-related parameters

3.3.1 Distance from casting point

The distance travelled by FRC can affect the distribution of aggregate and FOD [13], as well as its mechanical performance [9]. Accordingly, the variation of fibers and coarse aggregate concentration obtained at different distances from the casting point with respect to the reference mixture can represent the horizontal dynamic stability and passing ability of FRC. Spangenberg et al. [19] reported a decrease in the volumetric fraction of solid particles with the horizontal flow distances. The maximum concentration of solid particles was therefore found in the vicinity of the casting point. Ferrara et al. [12] reported that increasing the distance from casting point led to decreasing fiber content from 80 to 29 kg/m^3 through a 1500-mm length beam (dynamic

segregation of fibers). The authors reported that this uneven distribution of fibers negatively affects the mechanical performance of FRC mixtures. However, as shown in Figure 3-17, in the case of FRC, fibers located in longer distances to the casting point were found to be oriented more parallel to the flow direction and perpendicular to the cross section of cast element [13]. This can consequently improve the mechanical performance of concrete located at longer distances from the casting point. More perpendicularly oriented fibers to the cross section can be more effective in resisting against the stresses induced by the flexural charges. As already mentioned, rheological properties of suspending matrix can also affect FOD. Therefore, for in-depth evaluation of FOD, the coupled effect of rheological properties of suspending as well as distance from casting point should be considered.
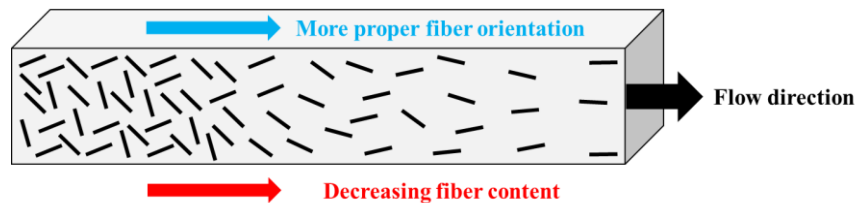
Figure 3-17 Effect of distance from the casting point on distribution and orientation of fibers [13].

Ferrara et al. [12] investigated two mixtures of low and high viscosity using 1500-mm long beam. The cement content varied from +2% (mixture-1) to -2% (mixture-2) compared to a reference mixture. The V-Funnel time values of 12 and 6 s were obtained for the mixtures-1 and -2, respectively, representing higher plastic viscosity for the mixture-1. The effect of FOD on mechanical performance was then investigated using 4-point bending tests on 500-mm beams cut from 1500-mm long beams (specimen-1 closest to casting point, specimen-3 the furthest from casting point). The crack opening displacement (COD) was also measured representing toughness of the element. The variation of COD versus the distance from the casing point is shown in Figure 3-18.

(a)   (b)
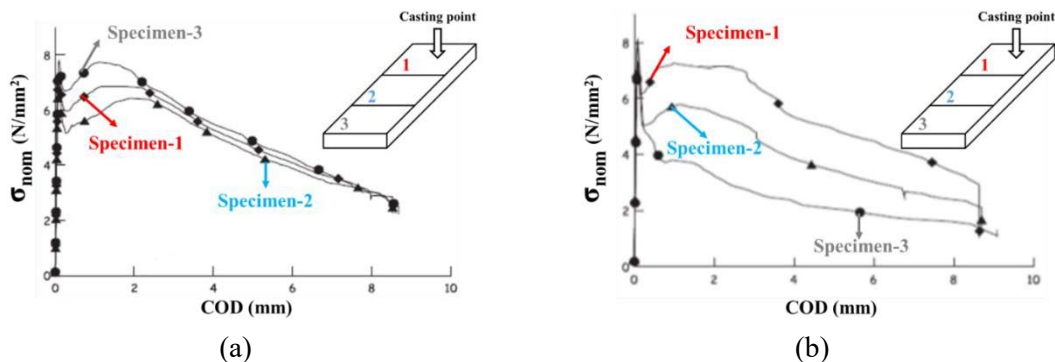
Figure 3-18 Effect of rheological properties of mixture on mechanical performance of FRC based on variation of cement content by (a) +2% and (b) -2% values [12].

In the case of higher viscous mixture-1 (Figure 3-18), a dominant positive effect of increasing distance from casting point on fiber orientation was found comparing to its negative effect on the number of fibers through the length. Accordingly, the maximum flexural strength values of 7.5 and 6 MPa were obtained for the CODs in the ranges of 0-2 mm for the samples 3 and 1, respectively. On the other hand, in the case of low viscous mixture-2 (Figure 3-18b), a dominant negative effect distance from casting point on decreasing number of fibers (direct negative effect on mechanical performance) was observed by increasing distance from casting point comparing to its positive effect on more proper fiber orientation. Less value of flexural strength was obtained for sample 3 (proper fiber orientation) than the sample-1 containing higher fiber content.

It can be concluded that optimizing the flow performance of FRC in fresh state can lead to achieve comparable mechanical performance using a lower fiber dosage, but more desire fiber orientation instead of increasing fiber content on mechanical performance.

3.3.2   Reinforcing bars

In order to study the heterogeneous flow performance of FRC in reinforced elements, the effect of characteristics of reinforcing bars on passing ability of FRC mixtures should be investigated [3, 69-72]. Fibers can act as an internal reinforcement to enhance the tensile and flexural strength of concrete matrix. However, incorporation of fibers without installing any reinforcing bars is not an economical solution to improve the mechanical performance of concrete under flexural and tensile loads. Indeed, a high volume of fibers is required to achieve the equivalent structural enhancements of the reinforcing bars. FRC can then be used for structural applications in combination with conventional reinforcements [73, 74].

A highly flowable FRC (e.g., FR-SCC), the reference concrete mixtures (without fibers) should exhibit low plastic viscosity and yield stress values compared to plain SCC. As explained earlier, this can lead to higher risk of dynamic segregation for FR-SCC mixtures which can be intensified in presence of reinforcing bars (Figure 3-19).
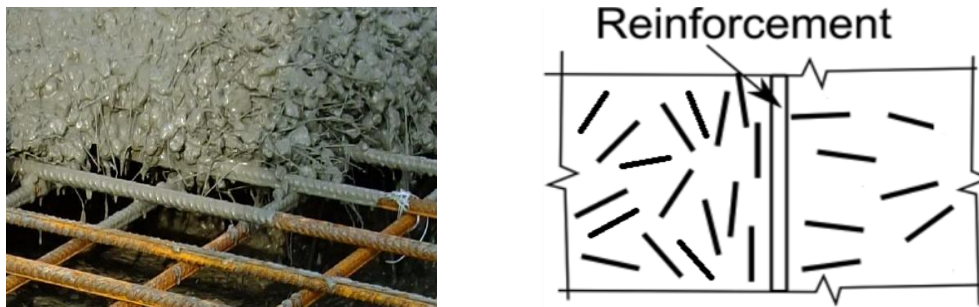
Figure 3-19 Blocking of fibers and aggregate behind the rebars [75, 76].

Indeed, as already mentioned, particles migrate from high shear rate zones to lower one [19]. The presence of bars can increase this heterogeneity by increasing the shear rate gradients (more shear induced particles migration). Although, in the mixtures with high risk of segregation, there is higher risk of blockage of solid particles behind the bars, even in the case of stable mixtures there is still risk of blockage. This is a function of solid particles fraction, size (diameter) of particles, and free space between bars [77]. To minimize the risk of this uneven phenomenon, reducing size of

particles, increasing distance between bars and reduction of volume fraction of solid particles are recommended.

On the other hand, it was proved that particles can block between obstacles even if their size is significantly less than the space between bars. This can be due to formation of particle arches between the reinforcement bars [78]. Indeed, particles disperse in a fluid randomly, therefore, several particles can reach to a gap among obstacles, at the same time which leads to arc formation. Roussel et al. [78] investigated this phenomenon using 5-mm sieve for evaluation of the passing ability of 3-mm dry grains (Figure 3-20a).

(a)   (b)   (c)
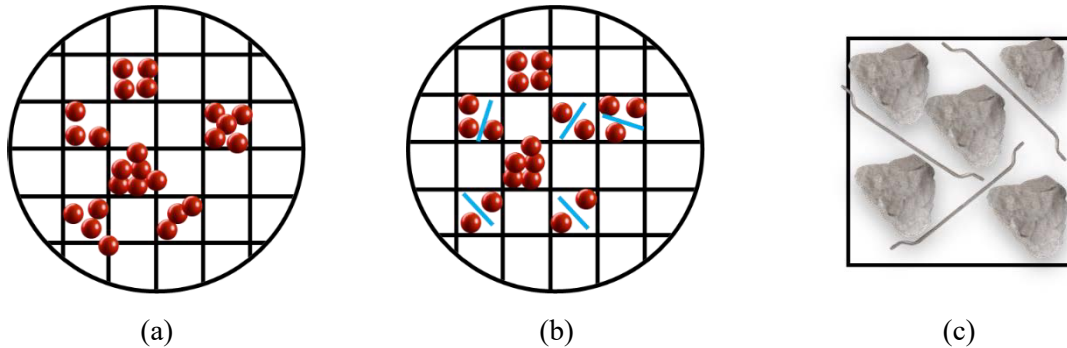
Figure 3-20 Blocking of a) sphere particles and b) fibers-sphere particles combinations through a mesh, c) blocking of fiber-aggregate in one hole of mesh [78].

As shown in Figure 3-20, although the diameter of particles is less than the size of mesh, the blocking phenomenon occurred. Actually, the movement of some particles have been stopped by the bridge formed ahead. In the case of fiber-reinforced concrete, the situation is harsher, and presence of fibers as additional solid particles can increase the risk of arches formation behind bars and, consequently, more blockage of fibers and aggregate can occur (Figure 3-20b and c). The passing ability of FR-SCC mixtures under restricted flow conditions were evaluated in literature [72, 75]. Sahmaran et al. [32] investigated the effect of different types of steel fibers on workability of FR-SCC using the slump flow (horizontal free flowability) and J-ring (restricted flowability) test methods. The authors reported that the incorporation of macro fibers (30-mm length, aspect ratio 55) can increase the risk of dynamic segregation and blocking in the reinforced elements. Grunewald [66] reported that the particle-size distribution and content of aggregate, as well as the volumetric content and aspect ratio of fibers are the main factors that affect the allowed clear spacing between the reinforcing bars to avoid rids of blockage. Ding et al. [79] reported that incorporation of steel fibers can increase the shear strength and change the failure mode from brittle behavior to a ductile flexural performance. Accordingly, increasing steel fiber content by 25 kg/m3 allowed to increase the distance between stirrups from 150 to 250 mm to achieve comparable structural performance under shear stresses. Kassimi et al. [69] proposed a modified J-Ring set-up to evaluate passing ability of FRC mixtures by reducing the number of bars from 16 (the standard one [80]) to 8. They reported that there is no clear relationship between the J-Ring spread values, obtained using the standard-16 bars J-Ring set-up, and the fiber factor ($V_f L_f/d_f$). Therefore, lower number of bars in the modified set-up led to adequate space between the bars (at least 2.5 times larger than the fiber length).

As can be observed in Figure 3-21, interaction between the fibers and reinforcing bars can lead to uneven orientation of fibers around the reinforcing bars which has direct effect on mechanical performance.
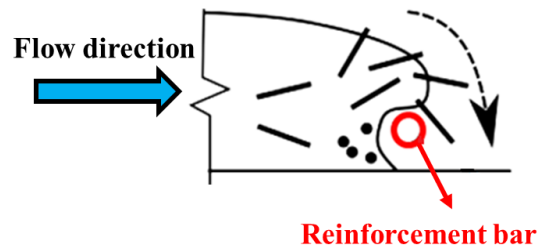
Figure 3-21 Changing orientation pattern of fibers around bars [75].

Indeed, the presence and arrangement of bars affect both in-plain and out-plain orientation angles λ and θ, respectively. In the case of restricted flow conditions (repair application), the presence of bars in addition to four wall flow condition have significant effect on fibers orientation. For illustration of this phenomenon, different cut section for evaluation of variation of in plain and out of plain fiber orientation is shown in Figure 3-22.
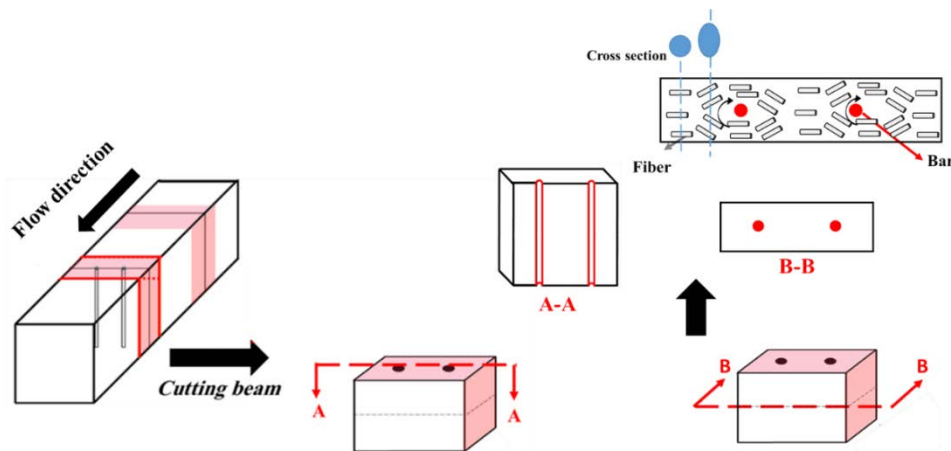
Figure 3-22 The effect of bars and formwork walls on out of plain and in plain orientation of fibers.

Using image analysis, the number, vertical, and horizontal positions, surface area, form (i.e., circular or elliptic shapes), dimensions, and angle of cut fibers in each section plane in neighbor of the reinforcing bars and formwork walls can be determined. For example, Žirgulis et al. [75] investigated the effect of presence and arrangement of bars on fiber orientation in longitudinal and transverse directions in addition to fiber distribution. They cast different FR-SCC slabs, reinforced with different layers of unidirectional (U) and grid (G) type reinforcing bars as well as the non-reinforced slabs (N) (Figure 3-23). The dash lines in Figure 3-23b represents the positions of reinforcement bars. The results show that in the bottom section, fibers orient parallel to the bars (X direction), before reaching to the vicinity of bars. On the other hand, a perpendicular orientation was observed behind the bars. This can be related to fiber blockage next to the bars.
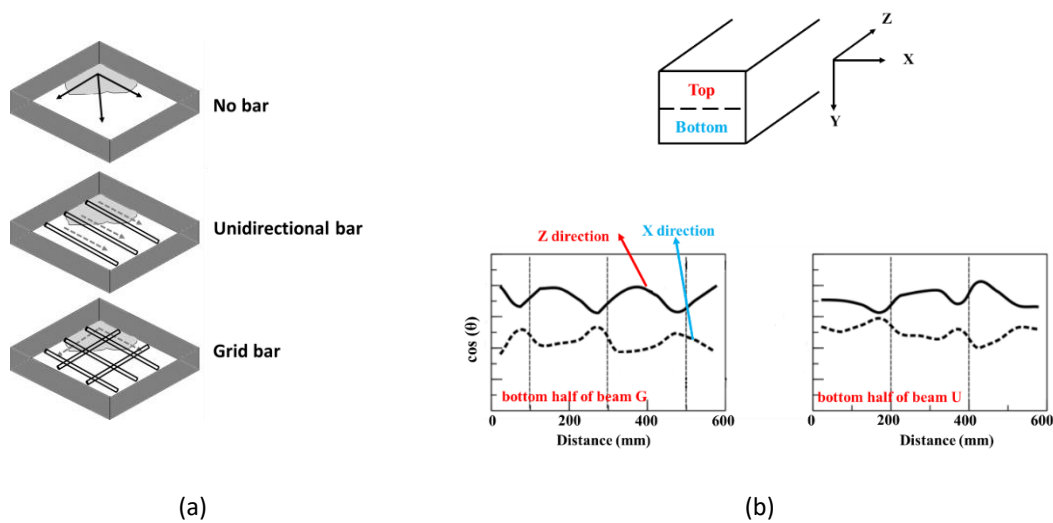
Figure 3-23 Effect of a) presence and arrangement of reinforcing bars on b) orientation of fibers [75].

In the case of fiber distribution, Žirgulis et al. [75] reported that for the beams sampled from non-reinforced slabs, lower normalized number of fibers to the total number of fibers in the beam were found in the top (0.24) and middle layers (0.36), respectively, compared to those found in the bottom layer (0.39) (Figure 3-24). This corresponds to the free gravitational settlement of fibers toward the bottom layers of the non-reinforced slabs. On the other hand, the beams cut from unidirectional reinforced slabs showed an equal normalized number of fibers 0.38 in the middle and bottom layers. However, the cut beams from the grid-reinforced slabs showed a higher number of fibers in the middle layer (0.41) rather than the bottom one (0.34) which corresponds to blocking of fibers between the reinforcing-bar grids.
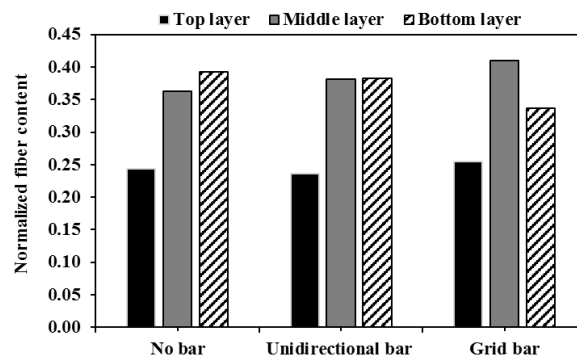
Figure 3-24 Effect of presence and arrangement of reinforcing bars on distribution of fibers [75].

Various investigations were carried out to evaluate the effect of fibers on mechanical performance of reinforced elements, such as pull out of fibers and bonding to the matrix [81-83]. However, the coupled effect of orientation and distribution of fibers, as well as reinforcing bars on mechanical

properties of reinforced FRC elements must be also considered, because the presence of reinforcing bars and their arrangement that can affect FOD [11,72].

Therefore, in order to better understanding the heterogeneous flow behavior of flowable FRC mixtures, the presence and arrangement of reinforcing bars must be considered in addition to the effect of characteristics of the FRC mixtures' constituents.

3.4 Methods to assess flow homogeneity of cement-based suspensions

3.4.1 Methods to determine fiber and aggregate distribution

The heterogeneous flow behavior of highly flowable concrete mixtures (with and without fibers) were evaluated through different empirical set-ups, such as slump flow [84], J-Ring [85], U-Box, L-Box, and Filling Box [86] set-ups. As shown in Table 3-1, Tregger et al. [20] divided the final spread after the slump flow test to three different radial zones A, B, and C. The variation of coarse aggregate content in each radial zone, evaluated using the wet-sieving of the concrete in each zone, can reflect the dynamic segregation of SCC. Using the same methodology, Ferrara et al. [12] proposed a fiber dynamic segregation index (FDSI) based on the variation of fiber content in the inner (200 mm) and outer (500 mm) circular zones of the slump-flow spread. This FDSI index is normalised to the average value of fiber concentration. Furthermore, the static segregation of fibers was evaluated by identification of variation of fiber contents in three different vertical layers of a cut hardened cylindrical specimen. The fiber static segregation index (FSSI) was calculated as the ratio of variation of fiber content in the bottom and top sections to the total fiber content. However, it must be noted that the flow distance may not representative of those traveled by concrete during casting process.

Stahli et al. [87] used a U-shaped formwork to evaluate the effect of orientation and distribution of fibers on mechanical performance of FRC. As shown in Table 3-1, the set-up consists of one horizontal and two vertical sections. Concrete initially starts to flow downward through the section A, then continues to flow in the horizontal direction (section B) before it goes up (section C) towards the end of the formwork. This set-up can be used to simulate the confined and closed surface flow conditions, such as the case of flow conditions for repair applications. After hardening, the fiber content in each section was evaluated using CT-scanning of the hardened-cut sections.
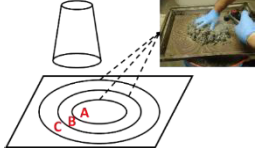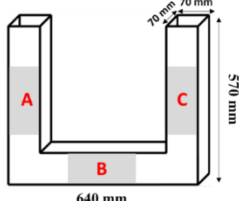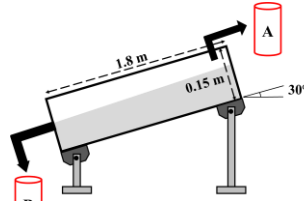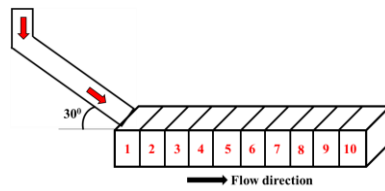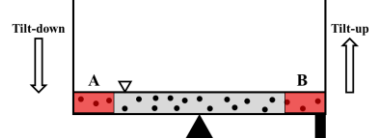
It is worthy to mention that the short flow distance through the conventional empirical tests, such as slump flow, J-Ring, U-Box, L-Box, and filling box, are not representative to those traveled by concrete during casting process in formworks. New empirical set-ups were then proposed to evaluate dynamic stability of the investigated mixtures under more reasonable flow distances (Table 3-1). Shen et al. [16,88] evaluated the changes in the volumetric fraction of coarse aggregate of SCC flowing through an inclined channel of 1.8-m length (Table 3-1). Jasiuniene et al. [11] proposed a similar set-up to investigate the effect of casting distances on dynamic segregation of steel fiber reinforced-SCC (SFR-SCC) mixtures (Table 3-1). Accordingly, the orientation and distribution of fibers in ten hardened-cut cross sections along an inclined beam were determined using image analysis.

Esmaeilkhanian et al. [44] proposed the T-Box set-up to evaluate the dynamic stability of SCC (Table 3-1) under a given number (60) of tilting cycles of 2-s period. The number and duration of the tilting cycles can simulate distance and velocity of concrete flow in the formworks. Due to the applied tilting cycles, the coarse aggregate gradually accumulates in the tilt-down zone and higher content of cement paste and mortar is obtained in the tilt-up zone. The dynamic segregation in T-Box set-up can then be calculated, as follows:

$$\text{DSI (\%)} = \frac{V_{tilt-down} - V_{tilt-up}}{average\ (V_{tilt-down}, V_{tilt-up})} \times 100\% \qquad \qquad \text{Equation 3-27}$$

where $V_{tilt-down}$ and $V_{tilt-up}$ are the volumetric content of coarse aggregate (> 4.75 mm) obtained in the cylindrical samples (100-mm diameter and 200-mm height) taken from the tilt-down and tilt-up sections, respectively.

Table 3-1 Different set-ups to evaluate dynamic segregation of SCC and FRC mixtures

References	Set-up	Configuration of set-up	DSI*
1)	Tregger et al. [20] and Ferrara et all. [12]	Slump flow	Standard deviation of the aggregate contents
2)	Stahli et al. [87]	U-Shaped Set-up	Variation of fiber content
3)	Shen et al [16, 88]	Flow channel	$\dfrac{\varphi A_A - \varphi A_B}{\varphi A_A}$
4)	Jasiuniene et al. [13]	Cast beam	Variation of fibre volumetric content
5)	Esmaeilkhanian et al. [44] and Koura et al. [68]	T-Box	[44]: $\dfrac{V_{tilt-down}-V_{tilt-up}}{average\,(V_{tilt-down},V_{tilt-up})}\times100\%$ [68]: $\dfrac{(\frac{\varphi}{\varphi_{max}})_{tilt-down}-(\frac{\varphi}{\varphi_{max}})_{tilt-up}}{(\frac{\varphi}{\varphi_{max}})_{Reference}}\times100\%$

*DSI: Dynamic segregation index

The dynamic segregation indices proposed by Esmaeilkhanian et al. [44] and Shen et al. [16,88] can only consider the variation of volumetric content of coarse aggregate in different flow zones, while the changes in their PSD and packing density were neglected. However, it was revealed by various theoretical models that the rheological properties of suspensions (plastic viscosity $\mu_p(\varphi)$ and yield stress $\tau_0(\varphi)$) depend not only on the ratio of the volumetric content (φ)-to-packing density (φ_{max}) of suspended particles and rheological properties of the suspending fluid (plastic viscosity $\mu_p(0)$ and yield stress $\tau_0(0)$). The most well-known examples of rheological models of suspensions include those proposed by Krieger and Dougherty [89] for viscosity (Equation 3-27) and Chateau et al. [90] for yield stress (Equation 3-28), as follow:

$$\frac{\mu(\varphi)}{\mu(0)} = (1 - \frac{\varphi}{\varphi_{max}})^{-\eta\varphi_{max}} \qquad \text{Equation 3-28}$$

$$\frac{\tau(\varphi)}{\tau(0)} = \sqrt{(1-\varphi) \times (1-\frac{\varphi}{\varphi_{max}})^{-\eta\varphi_{max}}}$$

Equation 3-29

where η is the shape-dependent intrinsic viscosity which equals 2.5 for spheres.

Koura et al. [91] investigated the coupled effect of particles characteristics (>1.25 mm) and rheological properties of fine mortar (<1.25 mm) on dynamic segregation of SCC. They reported that the relative-solid packing fraction (φ/φ_{max}) of coarse aggregate exhibited a significant effect on performance of SCC in fresh and hardened states, in terms of flowability, passing ability, and compressive strength [91]. The authors evaluated the dynamic segregation of SCC by variation of relative-solid packing fraction (φ/φ_{max}) of coarse aggregate (> 1.25 mm) in the samples taken from the tilt-down and tilt-up sections of the T-Box set-up to that of the reference mixture, as follows [77]:

$$\text{DSI (\%)} = \frac{(\frac{\varphi}{\varphi_{max}})_{tilt-down}-(\frac{\varphi}{\varphi_{max}})_{tilt-up}}{(\frac{\varphi}{\varphi_{max}})_{Reference}} \times 100\%$$

Equation 3-30

The authors reported that increasing φ/φ_{max} of coarse aggregate can significantly enhance the dynamic stability of SCC mixtures. Similarly, considering the variation of relative-solid packing fraction of fiber-aggregate combination through the empirical set-ups can be recommended as a more realistic index to evaluate the heterogeneous flow performance of highly-flowable FRC mixtures, as follows:

$$DSI_{f-a_i}(\%) = \frac{\frac{\Phi_{f_i} + \Phi_{a_i}}{\Phi_{max_{f-a_i}}} - \frac{\Phi_{f_{Reference}} + \Phi_{a_{Reference}}}{\Phi_{max_{f-a_{Reference}}}}}{\frac{\Phi_{f_{Reference}} + \Phi_{a_{Reference}}}{\Phi_{max_{f-a_{Reference}}}}} \times 100\%$$

Equation 3-31

where Φ_{f_i}, Φ_{a_i}, $\Phi_{max_{f-a_i}}$, and $\Phi_{max_{f-a_{Reference}}}$ are the volumetric content of fiber and coarse aggregate, as well as the packing density of fiber-aggregate combinations, obtained in different sampling sections i = 1 to n, located at different distances to the casting point, and reference mixture, respectively. The DSI_{f-a_i} index can exhibit the scattering of volumetric content-to-packing density ratio of fiber-aggregate combination in each sampling section of (i = 1 to n) with respect to the reference mixture. Koura et al. [68] explained that the positive effect of increasing φ/φ_{max} on dynamic stability of mixture can be related to strong lattice structure of aggregates. This can remarkably prevent the movement of aggregate and, therefore, reduce the shear-induced particle migrations (higher dynamic stability of mixture). Moreover, the authors [68,91] reported that the φ/φ_{max} of coarse aggregate exhibits more dominant effect on flowability, passing ability, and dynamic stability of SCC comparing to the rheological properties of suspending mortars.

The effect of mixture compositions on homogeneity of cementitious mixtures (with and without fibers) during flow can be more critical in presence of reinforcing bars due to blocking and wall

effect phenomena. The placement configuration, diameter, and spacing of reinforcing bars can significantly affect the passing ability of concrete, especially in the case of FRC and FR-SCC mixtures containing additional solid dispersions (i.e., fibers) in addition to aggregate. In order to evaluate the heterogeneous performance of FRC and FR-SCC during casting of structural elements, it is essential to consider the effect of reinforcing bars on heterogeneous distribution of fiber-aggregate system, as well as fibers' orientation at different distances from the casting point. Due to the absence of reinforcing bars, the empirical set-ups shown in Table 3-1 are not able to evaluate the passing ability of flowable FRC mixtures in reinforced elements. Proposing new set-ups involving the presence of reinforcing bars can lead to a more realistic evaluation of the heterogeneous flow behavior of highly flowable FRC mixtures during casting process.

The interest in repair and strengthening (rehabilitation) of structures has increased in the last decades. Indeed, repairing the existing damaged concrete structures is more cost-effective solution compared to the demolition and the reconstruction of structures. Moreover, most of the repair works are done in relatively small zones of the structural elements, with and without any reinforcement, where it is difficult to vibrate. The use of high allowable cementitious mixtures, such as SCC, can be beneficial solution for this type of application.

However, SCC has a higher volume of paste and fine particles than conventional concrete, which increases the risk of shrinkage and cracking [18,19]. To combat this frequent incidence, the use of fiber-reinforced cementitious mixtures for repair application is of particular interest due to their mechanical advantages and lower shrinkage, hence leading to better durability of repaired elements. However, casting of FR-SCC in small spaces to be repaired can enface some sorts of instabilities (e.g., F-A blockage), due to altering their homogeneous flow performance passing through the restricted zones.

3.4.2   Methods to assess fiber orientation

Considering fiber as a rigid slender object, its 3D orientation can be represented by the unit vector "P" directed toward the fiber's axis, as shown in Figure 3-25.
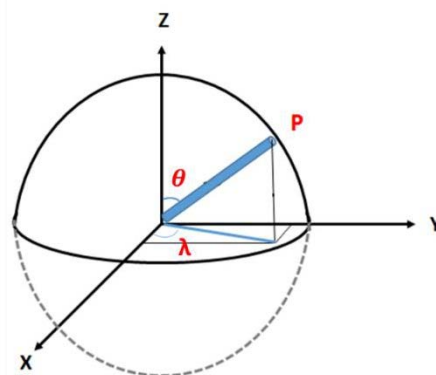
Figure 3-25 Coordinate system employed for representing fiber orientation [92].

As illustrated in Figure 3-25, λ is the orientation angle in the cross-section plane X-Y. Moreover, θ is the orientation angle out of the cross-section plane X-Y, measured between the fiber vector (P)

and the X-Y plane's normal vector (i.e., Z axis: perpendicular to the cut section plane X-Y). In order to determine the orientation angles λ and θ, each cut fiber (with circular cross section) can be considered as an ellipse in the cross-sectional samples (Figure 3-26).
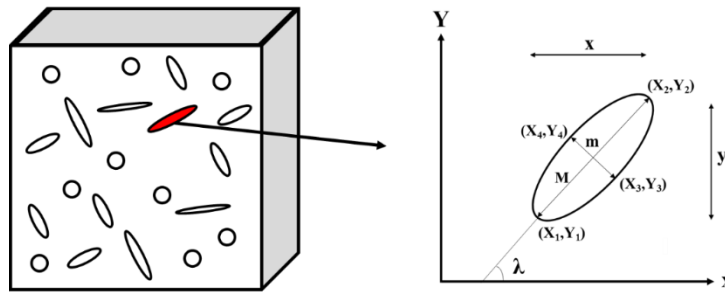
Figure 3-26 Schematic illustration of the cut fibers in a cross section.

According to the geometrical definitions in Figure 3-25, the in-plane and out-of-plane orientation angles λ and θ can be calculated, as follow:

$$0° \leq \lambda \leq 180° = \sin^{-1}\left(\frac{Y}{M}\right) = \cos^{-1}\left(\frac{X}{M}\right) \qquad \text{Equation 3-32}$$

$$0° \leq \theta \leq 90° = \cos^{-1}\left(\frac{m}{M}\right) \qquad \text{Equation 3-33}$$

where $X = |X_2 - X_1|$ and $Y = |Y_2 - Y_1|$ are the projected fiber lengths on X and Y axes, and $m = \sqrt{(X_4 - X_3)^2 + (Y_4 - Y_3)^2}$ and $M = \sqrt{(X_2 - X_1)^2 + (Y_2 - Y_1)^2}$ are the minor and major diameters of the fiber's cut section, respectively. The coordinates of the center-point of each fiber's cut section can also be determined to evaluate the distribution of fibers in a cross section. High-resolution images of the hardened FRC cut sections are required to evaluate the content, FOD using image processing tools.

The effect of fiber orientation on mechanical performance of FRC is related to the geometry of the fiber' cut section [92,93]. The perpendicular oriented fibers to the cross section (i.e., θ = 0°), corresponding to a perfect circle (i.e., m = M in Figure 3-26), leads to the highest flexural and tensile performances [92]. Different possibilities of cut fibers in a given cross section are shown in Figure 3-27.
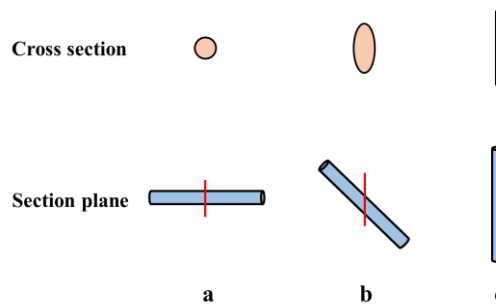
Figure 3-27 Different cross-sections of a cut fiber: (a) circle (plane is perpendicular to the fibre), (b) ellipse (plane is inclined to the fiber), and (c) rectangle (fiber lies in the plane) [92].

Investigating the relation between FOD and mechanical behavior of FRC is of particular interest [93]. Song et al. [24] reported that FOD are influenced by the distance from the casting point, wall effect, casting method, and rheological properties of the mixture. Meng and Khayat [94] evaluated the fiber orientation and distribution on 76 × 76 mm slices cut from rectangular beams after a flexural test, using image analysis. Images taken from each cross section are divided into 21 × 21 units, then the number of fibers per each unit was counted. Distribution of fibers were then evaluated using parameter α (fiber dispersion coefficient), defined as a function of the position and number of cut fibers in a given cross section, as follows:

$$\alpha = \exp[- \frac{1}{x_0} \sqrt{\frac{\sum_{i=1}^{n}(x_i - x_0)^2}{n}}] \qquad \text{Equation 3-34}$$

where n is the number of the units, xi represents the fiber number in the i-th unit, and x_0 represents the average number of fibers in a given unit. The α values of 0 and 1 correspond to segregation and uniform distribution of fibers, respectively. Moreover, a fiber orientation coefficient η was defined to evaluate the effect of fiber orientation on mechanical performance of UHPC as function of out of plane orientation angles (θ) of the fibers in each slice, as follows:

$$\eta = \int_{\theta_{min}}^{\theta_{max}} g(\theta)cos\theta^2 \ d\theta \qquad \text{Equation 3-35}$$

where η varies between 0 and 1, corresponding to orientation of all fibers parallel and perpendicular to the cross section, respectively. Moreover, g(θ) is a probability function of distribution of fibers' orientation, as follows:

$$g(\theta) = \frac{(\sin\theta)^{2p-1} \times (\cos\theta)^{2q-1}}{\int_{\theta_{min}}^{\theta_{max}}(\sin\theta)^{2p-1} \times (\cos\theta)^{2q-1} \ d\theta} \qquad \text{Equation 3-36}$$

where p and q are the shape parameters that should be selected more than 0.5 [94]. The authors reported that there is a significant relationship between the rheological properties, FOD, and flexural performance of UHPC. They evaluated the distribution of fibers through a cross section based on visual observation which is not accurate enough. A statistical analysis is thus needed to precisely evaluate the 3D orientation (θ and λ in Figure 3-25 and 3-26), as well as horizontal and vertical distributions of fibers. As an example, a FR-SCC mixture consists of 0.25% volumetric content of macro steel fiber (30-mm length and aspect ratio of 55) was cast in a prism of 100 mm × 100 mm × 400 mm. The hardened sample was then cut in the middle (i.e., 100 mm × 100 mm cross section). The section is painted using black ink and then polished for better identification of the cut fiber sections. An image was taken from the cross section and then converted to a binary format using the ImageJ software (Figure 3-28). ImageJ was also employed to determine the vertical and horizontal distribution of fibers across the investigated cross section.
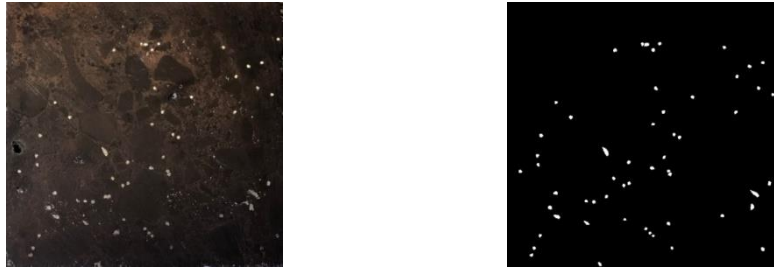
Figure 3-28 The image of the treated cross section and its binary format to highlight FOD.

According to the carried-out image analysis, a total of 57 fibers were detected and analyzed. These fibers occupy a total surface area of 78746498 µm2, which corresponds to approximately 0.82% of the concrete cross-section (100 × 96.047 mm). The statistical distribution of the vertical and horizontal positions of the fiber cut section are presented in Figures. 3-29a and 3-29b, respectively.

(a)   (b)
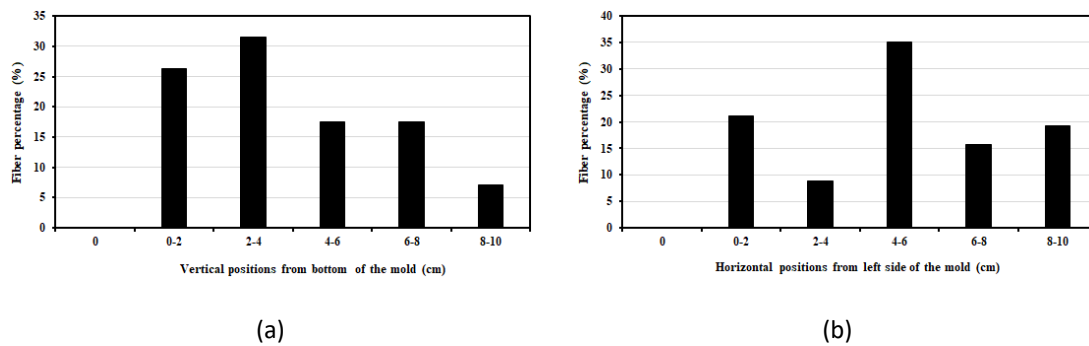
Figure 3-29 Vertical and (b) horizontal distributions of cut fibers with respect to the bottom and left side of the mold, respectively.

As can be observed in Figure 3-29a, the fibers are more concentrated at 0-2 and 2-4 cm distances from the bottom of the mold, corresponding to 26.3% and 31.6% of total 57 number of fibers, respectively. However, the minimum vertical concentration of 7% is obtained at the top 2-cm layer of the mold. This refers to the static segregation of the fibers towards the bottom layers. As shown in Figure 3-29b, the maximum horizontal concentration of 35.1% is obtained at the center of the mold (i.e., 5±1 cm from the left side of the mold). This corresponds to the effect of side walls of the formwork on distribution of fibers.

Song et al. [24] investigated the effect of different casting methods, content, and distribution of fibers on flexural performance of fiber reinforced UHPC mixtures. Two casting methods, including a) continuous casting from one side of the mould and b) the randomly casting without any continuous flow were investigated [24]. The reported results showed that in the case of continuous casting, increasing fiber content from 0 to 2.5% increased the flexural strength from 9 to 30 MPa. In the case of randomly casting and 2.5% steel fiber content, the flexural strength ranged from 9 to 24 MPa. The continuous casting method can thus ensure proper orientation of fibers, hence resulting in higher flexural strength, rather than the non-continuous and randomly casting. Žirgulis et al. [75] employed X-ray tomography and image analysis to evaluate the effect of fiber orientation

on flexural strength of FR-SCC, cast in 1200 mm × 1200 mm × 150 mm slabs. Different standard beams of 150 mm × 150 mm × 550 mm were then sawn from the cast slabs to carry out the flexural strength measurements. Different slices were then taken from the crack locations of the specimens to evaluate fibers' orientation using an orientation factor β, as follows:

$$\beta = \frac{N_f A_f}{A_c V_f}$$ Equation 3-37

where A_c and A_f are the surface area of the concrete cross section and a single cut fiber, respectively, V_f is volumetric content of fiber in the reference mixture, and N_f is the number of cut fibers in a cross section, identified using image analysis and CT scanning [11]. If β equals unity, it means that all the fibers are oriented perpendicularly to the cross section (i.e., ideal orientation). On the other hand, the zero value of β corresponds to the parallel orientation of all the fibers to the cross section (i.e., inappropriate orientation). It is worthy to mention that although the orientation factor β in Equation 3-36 can reflect two extreme conditions of parallel or perpendicular orientations of all the fibers (β = 0 or 1), this index cannot represent the realistic 3D orientation of fibers for its median values 0 < β < 1. According to Equation 3-36, $\beta = \frac{A_r}{V_f}$ corresponds to the ratio of the relative surface area of all the fibers in a cross section, with respect to that cross section area $(A_r = \frac{N_f A_f}{A_c})$, to the relative volume of the fibers to the concrete mixture (i.e., volumetric content of fibers V_f). As shown in Figure 3-30, an out-of-plane orientation angle θ (Figure 3-25) between 0 and 90° (excluding the 0 and 90° values) leads to higher surface area of a given number of cut fibers in a cross section compared to an ideal orientation θ = 0° of those fibers, hence resulting in higher β values, obtained using Equation 3-36. On the other word, regardless of the orientation of the fibers in a cross section, higher surface area of the cut fibers, induced either by higher content of fibers or non-perpendicular orientation of fibers to the cross section, can lead to higher β values which is controversial to the definition of the orientation factor β. Therefore, β cannot be perfectly representative to evaluate the orientation of fibers. Furthermore, the β values cannot evaluate the in-plane orientation (λ in Figure 3-25) of fibers, representing the wall effect on fiber orientations in a mold.
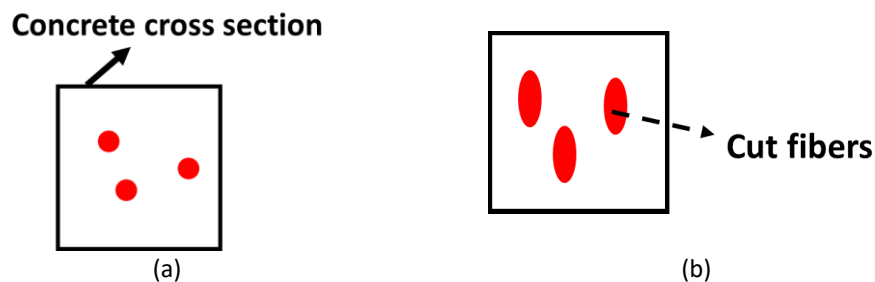
Figure 3-30 Different type of cut fiber shape in a given cross section, including (a) perpendicular and (b) inclined to the cut section plane.

Kang et al. [95] and Yoo et al. [96] investigated the effect of casting method on fiber distribution and, consequently, the flexural strength of UHPFRC using image analysis. FOD were determined in different specimens fabricated using two different casting methods, including the random and parallel castings with respect to the longitudinal direction of the formwork (Figure 3-31). Based on

the geometry of cut fibers in a cross section, the fiber orientation coefficient (η) was calculated using Equation 3-34. The flexural strength measurements revealed that the parallel casting to the formwork length resulted in higher resistance against the first-cracking load and flexural strength rather than the randomly casting direction. As explained earlier, this is attributed to better FOD in the case of parallel casting.
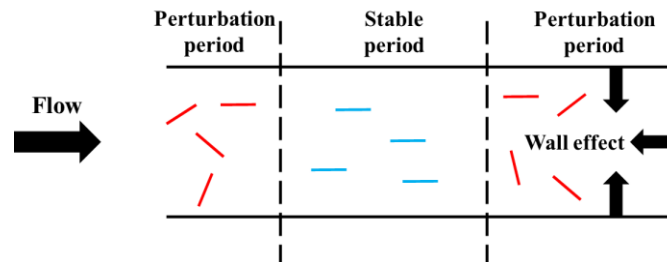
Figure 3-31 Dynamic mechanism of the fiber orientation in a flowing fiber-reinforced mixture [24].

In order to understand the mechanisms governing the orientation of fibers during casting, Song et al. [24] considered three flowing zones of being cast element, including disturbance, stability, and re-disturbance zones. As can be observed in Figure 3-31, the fibers are randomly oriented at the casting point. Then, due to the walls effect and viscous forces, the fibers are aligned parallelly to the flow direction in the middle zone (stability zone). Finally, when the concrete reaches the end of the formwork, the fiber orientation is disturbed. This is attributed to wall effect at higher flow distances. This phenomenon was also reported by Jasiuniene et al. [13]. Accordingly, the most appropriate fiber orientation (parallel to the casting direction) corresponds to the middle section of the formwork (the stable period in Figure 3-31). Wang et al. [97] studied the effect of rheological properties on steel-fiber reinforced UHPC mixtures proportioned with fiber contents between 1% and 3%. Rheological properties were controlled by means of changing the water-to-cement ratio (w/c) and superplasticizer dosage. Cube specimens measuring 70.7 mm length, height, and width were cast. Distribution of fibers were then evaluated using images taken from different cross sections at different casting distances. After the image processing, the fiber distribution coefficient (α) is calculated using Equation 3-33. It was revealed that the parameter α decreased with superplasticizer dosage in the case of mixtures made with water-to-cement (w/c) ratios of 0.22 and 0.24. However, increasing the fiber content showed a negative effect on fiber distribution coefficient. This can be due to the higher risk of segregation in the case of higher w/c required to achieve a given workability for higher fiber dosages. Higher interlocking between a big number of fibers can therefore result in more heterogeneous behavior of UHPC. A significant relationship between the rheological properties, distribution, and content of fibers was reported. Accordingly, increasing the yield stress and viscosity of the mixture up to their optimum values led to higher segregation resistance and increased the α values. However, these resulted in opposite effect on fiber distribution coefficient, due to the fact that fibers cannot move easily in the case of more viscous matrices. Therefore, it can be concluded that there are moderate rheological properties which ensure optimum fiber distribution factor ($\alpha = 0.91$) and, consequently, an appropriate mechanical performance.

As reported by Martinie and Roussel [8], the preferred orientation of fibers depends on their size and geometry of the cast element. Fibers in vicinity of the formwork walls showed more parallel patterns to flow direction (i.e. proper orientation) (Figure 3-32). This is due to the fact that it is impossible to find a fiber perpendicular to a wall at a distance lower than half of the fiber length (L_f / 2). This was also reported by other researchers [98, 99] using image analysis techniques.
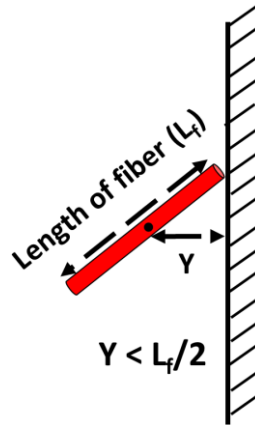
Figure 3-32 Orientation of fibers due to wall effect [8].

In order to achieve appropriate mechanical performances, especially flexural strength, a proper FOD is essential. However, the above review revealed that the optimization of the FOD is a challenging process. The physical characteristics of fibers, including type, volumetric content, length, and aspect ratio are the main influencing parameters to achieve adequate filling ability (i.e., flowability and passing ability) and ensure appropriate distribution and orientation of fibers in the cast elements. For example, inadequate aspect ratio and volumetric fraction of fibers can cause poor fiber dispersion and formation of fiber balling during casting [98]. These characteristics should therefore be considered for mixture proportioning and rheological/workability design of highly flowable FRC mixtures [27,76]. In addition to the image analysis techniques, which was discussed earlier, FOD can also be evaluated using different experimental methods, including X-ray tomography [100,101], electric conductivity [102,103], infrared thermography [104], the electromagnetic induction [105], and active microwave thermography methods [106, 107].

Ozyurt et al. [108] evaluated segregation of fibers using the electrical conductivity measurements. However, these results are dependent on the concrete age. Moreover, this method is only applicable for the conductive fibers, such as carbon and steel fibers. Torrents et al. [109] proposed an inductive method to limit the effect of the concrete age for steel fiber-reinforced mixtures. This includes measuring the produced inductance change when a magnetic field is applied (Figure 3-33). An analyser generates an electric flow that produces a magnetic field inside the spire (with a square cross section). Based on ferromagnetic properties of the fibers, the magnetic permeability can be changed and, consequently, the inductance variation is measured. Therefore, the fiber content and orientation can be determined.
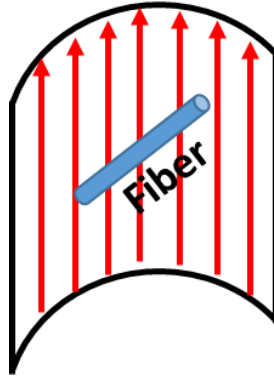
Figure 3-33 A single fiber inside a spire using decomposition of the
magnetic flux through the fiber [109,110].

Mehdipour et al. [111] evaluated the distribution of steel fibers in fiber-reinforced cement-based mortar (FRCM) using near-field microwave reflectometry. Since only the dielectric materials reflect microwave signals, their signal properties can show the homogeneity of FRCM. The value of reflection coefficient |Γ| measured in different zones corresponding to the bottom, middle, and top zones of the specimen. The results indicated that at 3 GHz frequency, increasing fiber content from 0% to 1% and 2% increased the |Γ| values up to an optimum value of 2% and then decreases. This can be explained by an improper FOD induced by the fiber balling in the case of high fiber contents. The authors reported that both microwave and image analysis methods can successfully evaluate FOD. Among all these methods, image analysis is generally recommended as an accurate method with low cost. Other methods, including manual counting, are not reliable due to operator errors.

3.5 Conclusions

In this chapter, a comprehensive review of the heterogeneous flow behavior of FRC was presented. Based on the critical review, the following concluding remarks can be drawn:

- The heterogeneous flow behavior FRC can be classified in two categories: 1) non-uniform distribution (segregation) of fibers and aggregate; and 2) undesired orientation of fibers. Heterogeneous flow behavior of FRC can impair mechanical performance.

- Higher rigidity, size, and content of fibers can increase the risk of segregation by pushing apart coarse aggregate from each other, thus and negatively influencing the packing density of the fiber and aggregate system. However, this depends on the PSD and characteristics of the fibers and aggregate.

- Interaction between fiber and coarse aggregate affects packing density of solid skeleton and, consequently, the stability of FRC. The packing density of fiber-aggregate combination should be considered instead of that of the aggregate only in proportioning FR-SCC. There is a lack of a theoretical model considering the coupled effect of fibers (content, size, and rigidity) and coarse aggregate (morphology, PSD, and content) to predict the packing density of fiber-aggregate combination.

- Workable FRC and FR-SCC mixtures in reinforced formworks can be achieved by considering the coupled effect of the characteristics of different constituent phases of the mixture and casting conditions. This includes the rheological properties of the suspending mortar, particle-size distribution and morphological properties of aggregate, fiber characteristics (type, content, and aspect ratio), packing density of fiber-aggregate combination, as well as the casting distance and the arrangement of reinforcing bars (diameter, spacing, and distribution).

- The interaction between the solid particles showed a significant effect on dynamic stability and passing ability of cementitious mixtures compared to rheological properties of the suspending matrix (i.e., paste or mortar).

- Majority of the existing empirical models can evaluate the stability and passing ability of FRC mixtures by variation of the volumetric content (φ) of the fiber and coarse aggregate under flow. A more realistic evaluation of heterogeneous flow behavior of FRC can be achieved by considering the ratio of the volumetric content-to-packing density (φ/φ_{max}) of fiber and coarse aggregate combination at different distances from the casting point or passing through the reinforcing bars.

- Higher distance from the casting point can change the distribution and orientation pattern of fibers. Designing an appropriate casting plan (consisting of adequate rheological properties of the suspending fluid) is needed to avoid negative effect of casting distance on dynamic segregation of fibers.

- Rheological properties of the suspending matrix can have positive and negative effect on fiber orientation and distribution, respectively. Accordingly, lower viscosity can lead to better fiber orientation while increases the risk of dynamic. Optimizing the rheological properties of the suspending matrix is recommended to achieve proper fiber orientation and distribution and mechanical performance. Uniform distribution (vertical and horizontal) of fibers in structural elements and number of perpendicular oriented fibers can result in higher flexural and tensile strengths of FRC mixtures.

- Image analysis techniques are recommended as the most accurate and cost-effective methodology to evaluate the distribution and orientation of fibers in cast elements.

References

[1] A. Emdadi, I, Mehdipour, N. A. Libre, M. Shekarchi, Optimized workability and mechanical properties of FRCM by using fiber factor approach: theoretical and experimental study, Materials and Structures, 48 (4) (2015) 1149–1161, https://doi.org/10.1617/s11527-013-0221-3.

[2] Y. Lu, Z. Liu, S. Li, W. Li, Behavior of steel fibers reinforced self-stressing and self-compacting concrete-filled steel tube subjected to bending, Construction and Building Materials, 156 (2017) 639–651, http://dx.doi.org/10.1016/j.conbuildmat.2017.09.019.

[3] X. Ning, Y. Ding, F. Zhang, Y. Zhang, Experimental study and prediction model for flexural behavior of reinforced SCC beam containing steel fibers, Construction and Building Materials, 93 (2015) 644–653, http://dx.doi.org/10.1016/j.conbuildmat.2015.06.024.

[4] B. Chun, D. Y. Yoo, Hybrid effect of macro and micro steel fibers on the pullout and tensile behaviors of ultra-high-performance concrete, Composites 162 (2019) 344–360, https://doi.org/10.1016/j.compositesb.2018.11.026.

[5] T. K. Erdem, K. H. Khayat, A. Yahia, Correlating Rheology of Self-Consolidating Concrete to Corresponding Concrete-Equivalent Mortar, ACI Materials Journal, 106 (2) (2009) 154-164.

[6] K. H. Khayat, Workability, Testing, and Performance of Self-Consolidating Concrete, ACI Materials Journal, 96 (3) (1999) 346-353.

[7] N. Roussel, Understanding the Rheology of Concrete, first ed., Woodhead Publishing, Sawston, Cambridge, United Kingdom, 2011, 9780857090287.

[8] L. Martinie, N. Roussel, Simple tools for fiber orientation prediction in industrial practice, Cement and Concrete research, 41 (10) (2011) 993-1000, https://doi.org/10.1016/j.cemconres.2011.05.008.

[9] E.V. Sarmiento, G. Zirgulis, S. Sandbakk, M.R. Geiker, T. Kanstad, Influence of concrete flow on fibre distribution, orientation and mechanical properties of fibre reinforced concrete, 8th RILEM International Symposium on Fiber Reinforced Concrete: challenges and opportunities, BEFIB, (2012), pp. 418 – 430.

[10] K. M. A. Hossain, M. Lachemi, M. Sammour, M. Sonebi, Influence of Polyvinyl Alcohol, Steel, and Hybrid Fibers on Fresh and Rheological Properties of Self-Consolidating Concrete, materials in civil engineering, 24 (9) (2012) 1211-1220. https://doi.org/10.1061/(ASCE)MT.1943-5533.0000490.

[11] G. Zirgulis, O. Svec, E. V. Sarmiento, M. R. Geiker. A. Cwirzen. T. Kanstad, Importance of quantification of steel fibre orientation for residual flexural tensile strength in FRC, Materials and Structures, 49 (9) (2016) 3861–3877, https://doi.org/10.1617/s11527-015-0759-3.

[12] L. Ferrara, P. Bamonte, A. Caverzan, A. Musa, I. Sanal, A comprehensive methodology to test the performance of Steel Fibre Reinforced Self-Compacting Concrete (SFR-SCC), Construction and Building Materials, 37 (2012) 406–424, https://doi.org/10.1016/j.conbuildmat.2012.07.057.

[13] E. Jasiuniene, V. Cicenas, P. Grigaliunas, Z. Rudzionis, A. A. Navickas, Influence of the rheological properties on the steel fibre distribution and orientation in self-compacting concrete, Materials and Structures, 51 (4) (2018) 1-14, https://doi.org/10.1617/s11527-018-1231-y.

[14] M Sonebi, S Gru¨newald, J Walraven, Filling ability and passing ability of self-consolidating concrete, ACI Materials Journal, 104 (2) (2007) 162–170.

[15] EFNARC (2002) Specification and guidelines for self-compacting concrete. EFNARC, Norfolk. ISBN 0-9539733-4-4.).

[16] L. Shen, Role of Aggregate Packing in Segregation Resistance and Flow Behavior of Self-Consolidating Concrete, Ph.D. thesis, University of Illinois at Urbana-Champaign (2007).

[17] (ACI Committee 237 (2007) Self-consolidating concrete, ACI 237R-07. American Concrete Institute, Farmington Hills.).

[18] W. Yan, W. Cui, L. Qi, Effect of aggregate gradation and mortar rheology on static segregation of self-compacting concrete, Construction and Building Materials, 259 (2020) 119816, https://doi.org/10.1016/j.conbuildmat.2020.119816.

[19] J. Spangenberg, N. Roussel, J.H. Hattel, H. Stang, J. Skocek, M.R. Geiker, Flow induced particle migration in fresh concrete: theoretical frame, numerical simulations and experimental results on model fluids, Cement and Concrete Research, 42 (4) (2012) 633–641, https://doi.org/10.1016/j.cemconres.2012.01.007.

[20] N. Tregger, A. Gregori, L. Ferrara, S. Shah, Correlating dynamic segregation of self-consolidating concrete to the slump-flow test, Construction and Building Materials, 28 (1) (2012) 499–505, https://doi.org/10.1016/j.conbuildmat.2011.08.052.

[21] M. Hosseinpoor, K. H. Khayat, A. Yahia, Numerical simulation of self-consolidating concrete flow as a heterogeneous material in L-Box set-up: coupled effect of reinforcing bars and aggregate content on

flow characteristics, Materials and Structures, 50 (2) (2017) 1-15, https://doi.org/10.1617/s11527-017-1032-8.

[22] S.T. Kang, B. Y. Lee, J. Kim, Y. Y. Kim, The effect of fibre distribution characteristics on the flexural strength of steel fibre-reinforced ultra high strength concrete, Construction and Building Materials, 25 (5) (2011) 2450–2457, https://doi.org/10.1016/j.conbuildmat.2010.11.057.

[23] B. Boulekbache, M. Hamrat, M. Chemrouk, S. Amziane, Flowability of fibre-reinforced concrete and its effect on the mechanical properties of the material, Construction and Building Materials, 24 (9) (2010) 1664–1671.

[24] Q. Song, R. Yu, Z. Shui, X. Wanga, S. Rao, Z. Lin, Optimization of fibre orientation and distribution for a sustainable Ultra-High Performance Fibre Reinforced Concrete (UHPFRC): Experiments and mechanism analysis, Construction and Building Materials, 169 (2018) 8–19, https://doi.org/10.1016/j.conbuildmat.2018.02.130.

[25] L. Ferrara, Y. Park, S. P. Shah, A method for mix-design of fiber-reinforced self-compacting concrete, Cement and Concrete Research, 37 (6) (2007) 957–971, doi:10.1016/j.cemconres.2007.03.014.

[26] M. Nehdi, J. D. Ladanchuk, Fiber Synergy in Fiber-Reinforced Self-Consolidating Concrete, ACI Materials Journal, 101 (6) (2004) 508-517.

[27] I. Mehdipour, N. A. Libre, M. Shekarchi, M. Khanjani, Effect of workability characteristics on the hardened performance of FRSCCMs, Construction and Building Materials, 40 (2013) 611–621, https://doi.org/10.1016/j.conbuildmat.2012.11.051.

[28] K. H. Khayat, Y. Roussel, Testing and performance of fiber-reinforced, self-consolidating concrete, Materials and Structures, 33 (6) (2000) 391-397, https://doi.org/10.1007/BF02479648.

[29] A.S. El-Dieb, M.M. Reda Taha, Flow characteristics and acceptance criteria of fiber-reinforced self-compacted concrete (FR-SCC), Construction and Building Materials, 27 (1) (2012) 585–596, https://doi.org/10.1016/j.conbuildmat.2011.07.004.

[30] I. Mehdipour, N. A. Libre, Linking Fiber Factor to Material Performance of Fiber Reinforced Self-Consolidating Cement-Based Materials, ACI Materials Journal, 114 (1) (2017) 77-91.

[31] AC. Aydin, Self compactability of high-volume hybrid fiber reinforced concrete, Construction and Building Materials, 21 (6) (2007) 1149-1154, https://doi.org/10.1016/j.conbuildmat.2006.11.017.

[32] M. Sahmaran, A. Yurtseven, I. O. Yaman, Workability of hybrid fiber reinforced self-compacting concrete, Building and Environment, 40 (12) (2005) 1672–1677, https://doi.org/10.1016/j.buildenv.2004.12.014.

[33] B. Felekoglu, S. Turkel, Y. Altuntas, Effects of steel fiber reinforcement on surface wear resistance of self-compacting repair mortars, Cement and Concrete Composites, 29 (5) (2007) 391–396, https://doi.org/10.1016/j.cemconcomp.2006.12.010.

[34] C.F. Schmid, D.J. Klingenberg, Properties of Fiber Flocs with Frictional and Attractive Inter fiber Forces. Journal of Colloid and Interface Science, 226 (1) (2000) 136-144, https://doi.org/10.1006/jcis.2000.6803.

[35] A Shanwan, H-E Gassara, G Barbier and A Sinoimeri, New experimental device for measuring the inter-fiber transversal friction, In IOP Conference Series: Materials Science and Engineering, 254 (14) (2017) 142020, doi:10.1088/1757-899X/254/14/142020.

[36] S. Ahmad, A. Umarb, Rheological and mechanical properties of self-compacting concrete with glass and polyvinyl alcohol fibres, Journal of Building Engineering, 17 (2018) 65–74, https://doi.org/10.1016/j.jobe.2018.02.002.

[37] A. Emdadi, I, Mehdipour, N. A. Libre, M. Shekarchi, Optimized workability and mechanical properties of FRCM by using fiber factor approach: theoretical and experimental study, Materials and Structures, 48 (4) (2015) 1149–1161, https://doi.org/10.1617/s11527-013-0221-3.

[38] G. Sokhansefat, M.T. Ley, M.D. Cook, R. Alturki, M. Moradian, Investigation of concrete workability through characterization of aggregate gradation in hardened concrete using X-ray computed tomography, Cement and Concrete Composites, 98 (2019) 150–161, https://doi.org/10.1016/j.cemconcomp.2019.02.008.

[39] K. Molugaram, J.S. Shanker, A. Ramesh, A study on influence of shape of aggregate on strength and quality of concrete for buildings and pavements, In Advanced materials research, 941 (2014) 776-779, https://doi.org/10.4028/www.scientific.net/AMR.94 1-944.776.

[40] K. Ostrowski, L. Sadowski, D. Stefaniuk, D. Walach, T. Gawenda, K. Oleksik, I. Usydus, The effect of the morphology of coarse aggregate on the properties of self-compacting high-performance fiber-reinforced concrete, Materials, 11 (8) (2018) 1–16, https://doi.org/10.3390/ma11081372, 1372.

[41] R. Farokhzad, M. Mahdikhani, A. Bagheri, J. Baghdadi, Representing a logical grading zone for self-consolidating concrete, Construction and Building Materials, 115 (2016) 735–745, https://doi.org/10.1016/j.conbuildmat.2016.04.006.

[42] H. Hafid, G. Ovarlez, F. Toussaint, P.H. Jezequel, N. Roussel, Effect of particle morphological parameters on sand grains packing properties and rheology of model mortars, Cement and Concrete Research, 80 (2016) 44-51, https://doi.org/10.1016/j.cemconres.2015.11.002.

[43] T. Stovall, F. De Larrard, M. Buil, Linear packing density model of grain mixtures, Powder Technol. 48 (1) (1986) 1–12, https://doi.org/10.1016/0032-5910(86)80058-4.

[44] B. Esmaeilkhanian, D. Feys, K. H. Khayat, A. Yahia, New Test Method to Evaluate Dynamic Stability of Self-Consolidating Concrete, ACI Materials Journal, 111 (3) (2014) 299-307.

[45] F. F. de Larrard, Concrete mixture proportioning — a scientific approach, in: S. Mindess, A. Bentur (Eds.), Modern Concrete Technology Series No. 7, E&FN SPON, London (1999) ISBN 9780419235002.

[46] A.B. Yu, R.P. Zou, N. Standish, Modifying the linear packing model for predicting the porosity of nonspherical particle mixtures, Industrial & engineering chemistry research 35 (10) (1996) 3730-3741.

[47] P. Goltermann, V. Johansen, L. Palbøl, Packing of aggregates: an alternative tool to determine the optimal aggregate mix, ACI Materials Journal, 94 (5) (1997) 435–443.

[48] A.K.H. Kwan, K.W. Chan, V. Wong, A 3-parameter particle packing model incorporating the wedging effect, Powder technology, 237 (2013) 172–179, https://doi.org/10.1016/j.powtec.2013.01.043.

[49] A.K.H. Kwan, V. Wong, W.W.S. Fung, A 3-parameter packing density model for angular rock aggregate particles, Powder Technology, 274 (2015) 154–162, https://doi.org/10.1016/j.powtec.2014.12.054.

[50] G. Roquier, The 4-parameter compressible packing model (CPM) including a new theory about wall effect and loosening effect for spheres, Powder Technology. 302 (2016) 247–253, https://doi.org/10.1016/j.powtec.2016.08.031.

[51] Nordtest, Method (NT BUILD 427) for Fresh Concrete: Compactibility with IC-tester (Intensive Compaction Tester) Proj. 1005-91, Nord. Scand. Inst. (1994) 1-4, ISSN 0283-7153 www.nordtest.org.

[52] B.M. Aïssoun, Study of the influence of aggregate characteristics on the rheology of fluid concrete with adapted rheology (in French), M.Sc. thesis, Université de Sherbrooke (2011), http://savoirs.usherbrooke.ca/handle/11143/1590.

[53] B.M. Aïssoun, S-D. Hwang, K.H. Khayat, Influence of aggregate characteristics on workability of superworkable concrete, Materials and Structures, 49 (1) (2016) 597-609. https://doi.org/10.1617/s11527-015-0522-9.

[54] D. C.C. Lam, Packing model for bimodal particle packing with aligned fibers, Journal of Materials Processing Technology, 79 (1-3) (1998) 170–176, https://doi.org/10.1016/S0924-0136(98)00007-7.

[55] S.H. Chu, Y. Jiang, A.K.H. Kwan, Effect of rigid fibres on aggregate packing, Construction and Building Materials, 224 (2019) 326–335, https://doi.org/10.1016/j.conbuildmat.2019.07.072.

[56] G.H. Tattersall, P. Banfill, The rheology of fresh concrete, Pitman Adv. Pub Prog, 759 (1983).

[57] M. Hosseinpoor, Numerical simulation of fresh SCC flow in wall and beam elements using flow dynamics models, PhD thesis, UNIVERSITÉ DE SHERBROOKE (2016).

[58] J. Spangenberg, N. Roussel, J.H. Hattel, E.V. Sarmiento, G. Zirgulis, M.R. Geiker, Patterns of gravity induced aggregate migration during casting of fluid concretes, Cement and Concrete Research, 42 (12) (2012) 1571–1578, https://doi.org/ 10.1016/j.cemconres.2012.08.007.

[59] M. F. Petroua, K. A. Harriesa, F. G.Mariab, V. G. Kollib, A unique experimental method for monitoring aggregate settlement in concrete, Cement and Concrete Research, 30 (5) (2000) 809-816, https://doi.org/10.1016/S0008-8846(00)00223-4.

[60] H. Tabuteau, P. Coussot, J.R. de Bruyn, Drag force on a sphere in steady motion through a yield-stress fluid, Journal of Rheology, 51 (1) (2007) 125-137, https://doi.org/10.1122/1.2401614.

[61] G. Bagheri, C. Bonadonna, On the drag of freely falling non-spherical particles, Powder Technology, 301 (2016) 526-544, https://doi.org/10.1016/j.powtec.2016.06.015.

[62] O, Merkak, L. Jossic, A. Magnin, Spheres and interactions between spheres moving at very low velocities in a yield stress fluid, Journal of non-newtonian fluid mechanics, 133 (2-3) (2006) 99-108, https://doi.org/10.1016/j.jnnfm.2005.10.012.

[63] N. N. Roussel, A theoretical frame to study stability of fresh concrete, Materials and Structures, 39 (1) (2006) 81–91, https://doi.org/10.1617/s11527-005-9036-1.

[64] Z. Zhang, J. Xiao, Q. Zhang, K. Han, J. Wang, X. Hu, A state-of-the-art review on the stability of self-consolidating concrete, Construction and Building Materials, 268 (2021) 121099, https://doi.org/10.1016/j.conbuildmat.2020.121099.

[65] M. S. Choi, Y. J. Kim, S. H. Kwon, Prediction on pipe flow of pumped concrete based on shear-induced particle migration, Cement and Concrete Research, 52 (2013) 216–224, http://dx.doi.org/10.1016/j.cemconres.2013.07.004.

[66] S. Grunewald, J. Walraven, Rheological Study on the Workability of Fiber-Reinforced Mortar, K. Ozawa and M. Ouchi Proceedings of the Second International Symposium on Self-Compacting Concrete, Japan University of Tokyo, 2001, 127-136.

[67] L. Ferrara1, Y. Park. S. P. Shah, Correlation among Fresh State Behavior, Fiber Dispersion, and Toughness Properties of SFRCs, materials in civil engineering, 20 (7) (2008) 493-501.

[68] B. Koura, M. Hosseinpoor, A. Yahia, Coupled effect of fine mortar and granular skeleton characteristics on dynamic stability of self-consolidating concrete as a diphasic material, Construction and Building Materials, 263 (2020) 120131, https://doi.org/10.1016/j.conbuildmat.2020.120131.

[69] F.Kassimi, A. K. El-Sayed, K. H. Khayat, Performance of Fiber-Reinforced Self-Consolidating Concrete for Repair of Reinforced Concrete Beams, ACI Structural Journal, 111 (6) (2014) 1277-1286.

[70] B. Mobasher, X. Destrée, Design and construction aspects of steel fiber-reinforced concrete elevated slabs, ACI Convention, New Orleans, LA, United States, 2010, 95-107.

[71] A. Maria, L. Ferrara, Fiber reinforced Self Consolidating concrete: research and application, American Concrete Institute, SP 274 (2010) 95–107.

[72] G. Zirgulis, O. Svec, M. R. Geiker, A. Cwirzen, T. Kanstad, Variation in fibre volume and orientation in walls: experimental and numerical investigations, Structural Concrete, 17 (4) (2016) 576-587, https://doi.org/10.1002/suco.201500060.

[73] H. Salehi, J. A.O. Barros, Assessment of the performance of steel fibre reinforced self-compacting concrete in elevated slabs, Cement and Concrete Composites, 55 (2015) 268–280, https://doi.org/10.1016/j.cemconcomp.2014.09.016.

[74] M. Mahmod, A. N. Hanoon, H. J. Abed, Flexural behavior of self-compacting concrete beams strengthened with steel fiber reinforcement, Journal of Building Engineering, 16 (2018) 228–237, https://doi.org/10.1016/j.jobe.2018.01.006.

[75] G. Žirgulis, O. Švec, M. R. Geiker, A. Cwirzen, T. Kanstad, Influence of reinforcing bar layout on fibre orientation and distribution in slabs cast from fibre-reinforced self-compacting concrete (FRSCC), Structural Concrete, 17 (2) (2016) 245-256, https://doi.org/10.1002/suco.201500064.

[76] Danish Technological Institute, Concrete Centre, Guideline for execution of steel fibre reinforced SCC (2013).

[77] N. Roussel, T.L.H. Nguyen, O. Yazoghli, P. Coussot, Passing ability of fresh concrete: A probabilistic approach, Cement and Concrete Research, 39 (3) (2009) 227–232, doi:10.1016/j.cemconres.2008.11.009.

[78] N. Roussel, T. L. H. Nguyen, P. Coussot, General Probabilistic Approach to the Filtration Process, Physical review letters, 98 (11) (2007) 114502.

[79] Y. Ding, Z. Youb, S. Jalali, The composite effect of steel fibres and stirrups on the shear behaviour of beams using self consolidating concrete, Engineering Structures, 33 (1) (2011) 107–117, https://doi.org/10.1016/j.engstruct.2010.09.023.

[80] ASTM C1621/C1621M-17, Standard Test Method for Passing Ability of Self-Consolidating Concrete by J-Ring, West Conshohocken, PA; ASTM International (2017), https://doi.org/10.1520/C1621_C1621M-17.

[81] C. Frazão, J. Barros, A. Camões, A. C. Alves, L. Rocha, Corrosion effects on pullout behavior of hooked steel fibers in self-compacting concrete, Cement and Concrete Research, 79 (2016) 112–122, http://dx.doi.org/10.1016/j.cemconres.2015.09.005.

[82] M. Xu, B. Hallinan, K. Wille, Effect of loading rates on pullout behavior of high strength steel fibers embedded in ultra-high performance concrete, Cement and Concrete Composites, 70 (2016) 98-109, http://dx.doi.org/10.1016/j.cemconcomp.2016.03.014.

[83] J. Won, J. Lee, S. Lee, Predicting pull-out behaviour based on the bond mechanism of arch-type steel fibre in cementitious composite, Composite Structures 134 (2015) 633–644, http://dx.doi.org/10.1016/j.compstruct.2015.08.127.

[84] ASTM C1611/C1611M-09be-1. Standard test method for slump flow of self-consolidating concrete, ASTM International, West Conshohocken, PA, 2014.

[85] ASTM C1621/C1621M-17, Standard Test Method for Passing Ability of Self-Consolidating Concrete by J-Ring, West Conshohocken, PA; ASTM International (2017), https://doi.org/10.1520/C1621_C1621M-17.

[86] EFNARC, European Project Group, The European Guidelines for Self-Compacting Concrete: Specification, Production and Use, 2005.

[87] P. Stahli, R. Custer, Jan G. M. van Mier, On flow properties, fibre distribution, fibre orientation and flexural behaviour of FRC, Materials and Structures, 41 (1) (2008) 189–196.

[88] L. Shen, L. Struble, D. Lange, Modeling Dynamic Segregation of Self-Consolidating Concrete, ACI Materials Journal, 106 (4) (2009) 375-380.

[89] I.M. Krieger, T.J. Dougherty, A mechanism for non-Newtonian flow in suspensions of rigid spheres, Trans. Soc. Rheol. 3 (1) (1959) 137–152, https://doi.org/10.1122/1.548848.

[90] X. Chateau, G. Ovarlez, K.L. Trung, Homogenization approach to the behavior of suspensions of noncolloidal particles in yield stress fluids, J. Rheol. 52 (2) (2008) 489–506, https://doi.org/10.1122/1.2838254.

[91] B.I.O. Koura, M. Hosseinpoor, A. Yahia, E.H. Kadri, A. Kaci, A new proportioning approach of low and normal binder self-consolidating concrete based on the characteristics of fine mortar and granular skeleton, Construction and Building Materials, 239 (2020) 117892, https://doi.org/10.1016/j.conbuildmat.2019.117892.

[92] R. Deeb, B.L. Karihaloo, S. Kulasegaram, Reorientation of short steel fibres during the flow of self-compacting concrete mix and determination of the fibre orientation factor, Cement and Concrete Research, 56 (2014) 112–120, https://doi.org/10.1016/j.cemconres.2013.10.002.

[93] B. Boulekbache, M. Hamrat, M. Chemrouk, S. Amziane, Flexural behaviour of steel fibre-reinforced concrete under cyclic loading, Construction and Building Materials, 126 (2016) 253–262, https://doi.org/10.1016/j.conbuildmat.2016.09.035.

[94] W. Meng, K. H. Khayat, Improving flexural performance of ultra-high-performance concrete by rheology control of suspending mortar, Composites Part B, 117 (2017) 26-34, http://dx.doi.org/10.1016/j.compositesb.2017.02.019.

[95] S. T. Kang, J.K. Kim, The relation between fiber orientation and tensile behavior in an Ultra High Performance Fiber Reinforced Cementitious Composites (UHPFRCC), Cement and Concrete Research, 41 (10) (2011) 1001–1014, https://doi.org/10.1016/j.cemconres.2011.05.009.

[96] D. Yoo, G. Zi, S. T. Kang, Y. Yoon, Biaxial flexural behavior of ultra-high-performance fiber-reinforced concrete with different fiber lengths and placement methods, Cement and Concrete Composites, 63 (2015) 51-66, http://dx.doi.org/10.1016/j.cemconcomp.2015.07.011.

[97] R.Wang, X. Gao, H. Huang, G. Han, Influence of rheological properties of cement mortar on steel fiber distribution in UHPC, Construction and Building Materials, 144 (2017) 65–73, https://doi.org/10.1016/j.conbuildmat.2017.03.173.

[98] B. Akcay, MA. Tasdemir, Mechanical behaviour and fibre dispersion of hybrid steel fibre reinforced self-compacting concrete, Construction and Building Materials, 28 (1) (2012) 287–293, https://doi.org/10.1016/j.conbuildmat.2011.08.044.

[99] I. Sanal, N. O. Zihnioglu, To what extent does the fiber orientation affect mechanical performance?, Construction and Building Materials, 44 (2013) 671–681, https://doi.org/10.1016/j.conbuildmat.2013.03.079.

[100] J. Suuronen. P. Kallonen, A., Eik, M., Puttonen, J., Serimaa, R., H. Herrmann, Analysis of short fibres orientation in steel fibre-reinforced concrete (SFRC) by X-ray tomography, Journal of Materials Science, 48 (3) (2013) 1358-1367.

[101] T. Ponikiewski, J. Katzer, X-ray computed tomography of fibre reinforced self-compacting concrete as a tool of assessing its flexural behavior, Materials and Structures, 49 (6) (2016) 2131-2140.

[102] J. F. Lataste, M. Behloul, D. Breysse, Characterisation of fibres distribution in a steel fibre reinforced concrete with electrical resistivity measurements. NDT & E International, 41 (8) (2008) 638-647.

[103] S. J. Barnett, J. F. Lataste, T. Parry, S.G. Millard, M.N. Soutsos, Assessment of fibre orientation in ultra high performance fibre reinforced concrete and its effect on flexural strength, Materials and Structures, 43 (7) (2010) 1009-1023.

[104] S. A. Keo, F. Brachelet, F. Breaban, D. Defer, Steel detection in reinforced concrete wall by microwave infrared thermography, Ndt & E International 62 (2014) 172-177.

[105] L. Ferrara, M. Faifer, S. Toscani, A magnetic method for non destructive monitoring of fiber dispersion and orientation in steel fiber reinforced cementitious composites, Materials and structures, 45 (4) (2012) 575-589.

[106] A. Foudazi, M. T. Ghasr, K. M. Donnell, Application of active microwave thermography to inspection of carbon fiber reinforced composites, IEEE AUTOTEST, (2014) 318-322.

[107] A. Foudazi, I. Mehdipour, K. M. Donnell, K. H. Khayat, Evaluation of steel fiber distribution in cement-based mortars using active microwave thermography, Materials and Structures, 49 (12) (2016) 5051-5065.

[108] N. Ozyurt, LY. Woo, TO. Mason, SP. Shah, Monitoring fiber dispersion in fiber reinforced cementitious materials: comparison of AC impedance spectroscopy and image analysis, ACI Materials Journal, 103 (5) (2006) 340–347.

[109]   JM. Torrents, A. Blanco, P. Pujadas, A. Aguado, P. Juan-Garcia, M.A. Sa´nchez-Moragues, Inductive method for assessing the amount and orientation of steel fibers in concrete, Materials and structures, 45 (10) (2012), 1577-1592.

[110]   SHP Cavalaro, R López, JM Torrents, A Aguado, Improved assessment of fibre content and orientation with inductive method in SFRC, Materials and structures, 48 (6) (2015): 1859-1873.

[111]   I. Mehdipour, M. Horst, R. Zoughi, K. H. Khayat, Use of Near-Field Microwave Reflectometry to Evaluate Steel Fiber Distribution in Cement-Based Mortars, Journal of Materials in Civil Engineering, 29 (7) (2017), 04017029, https://doi.org/10.1061/(ASCE)MT.1943-5533.0001

CHAPITER 4 METHODOLOGY

4.1 Experimental program

To achieve the aforementioned objectives of this study, a comprehensive experimental program with four distinct phases was conducted and summarized in Figure 4-1.
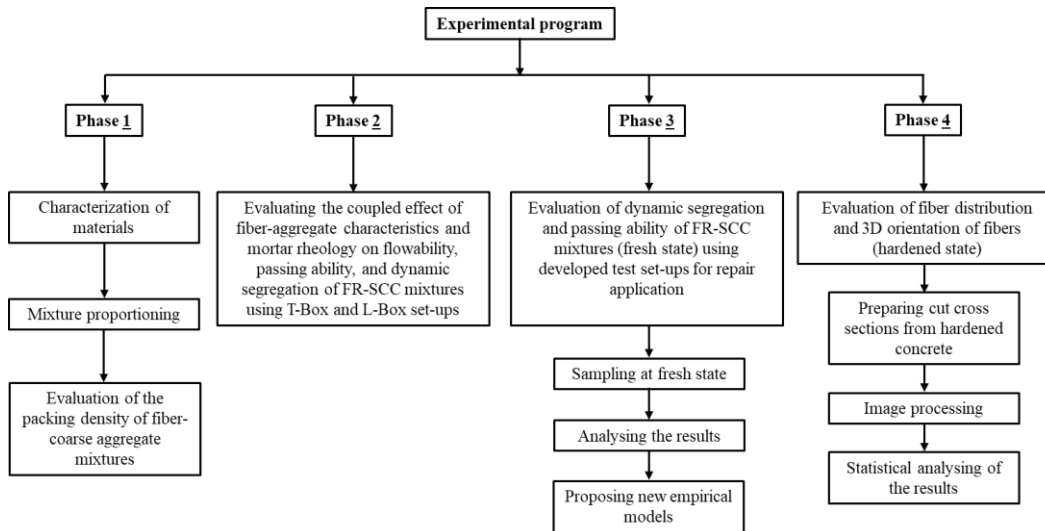
Figure 4-1 Different Phases of the experimental program.

4.2 Phase 1: Investigating the coupled effect of fibers and aggregate characteristics on packing density of fiber-aggregate combination.

This phase consists of evaluating the packing density of fiber-coarse aggregate (F-A) combination. To evaluate the effect of fiber-coarse aggregate combination on packing density of F-A mixtures, three different classes of crushed limestone coarse aggregate of 5–10 mm (CA1), 5–14 mm (CA2), and 5–20 mm (CA3) were used. Two different groups of F-A mixtures were proportioned with the maximum-size aggregate (MSA) of 20 mm (MSA20) and 14 mm (MSA14) for precast and repair applications, respectively. Moreover, two types of steel fibers were mixed with both MSA20 and MSA14 coarse aggregate mixtures. Different types of synthetic fibers were also mixed with the MSA14 mixtures, corresponding to concrete repair applications. The experimental program was divided into two parts. The first phase was undertaken to evaluate the effect of fiber size, rigidity, and volume as well as coarse aggregate characteristics on packing density of the F-A combination. Then, in the second part, the empirical models are established to predict the packing density of F-A mixtures as a function of fiber-coarse aggregate characteristics. The different parts of this phase are summarised in Figure 4-2.
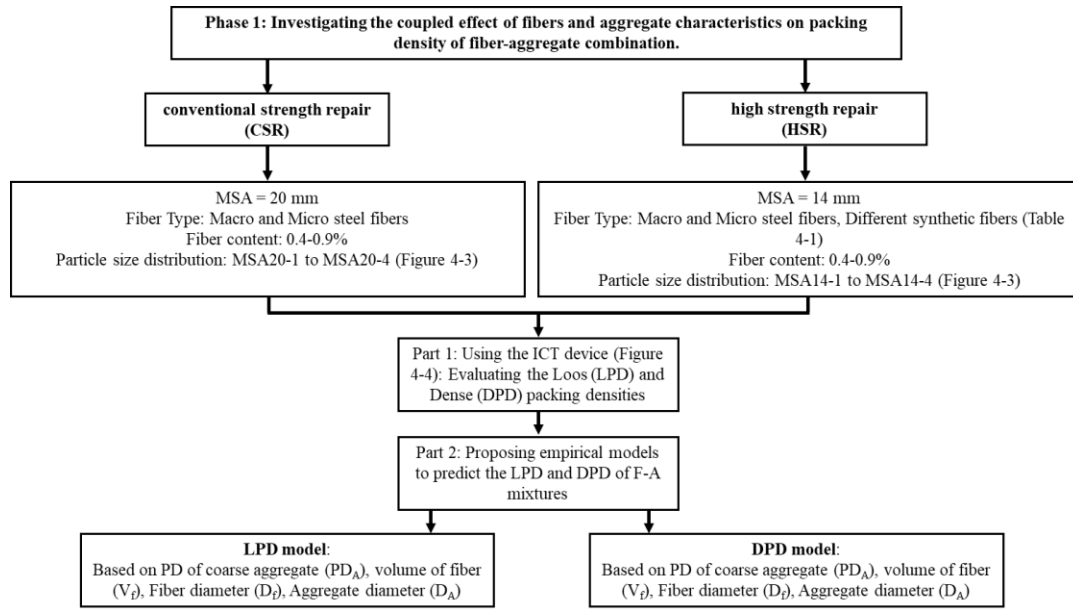
Figure 4-2 Chart of Phase 1.

<div align="center">(a)   (b)</div>
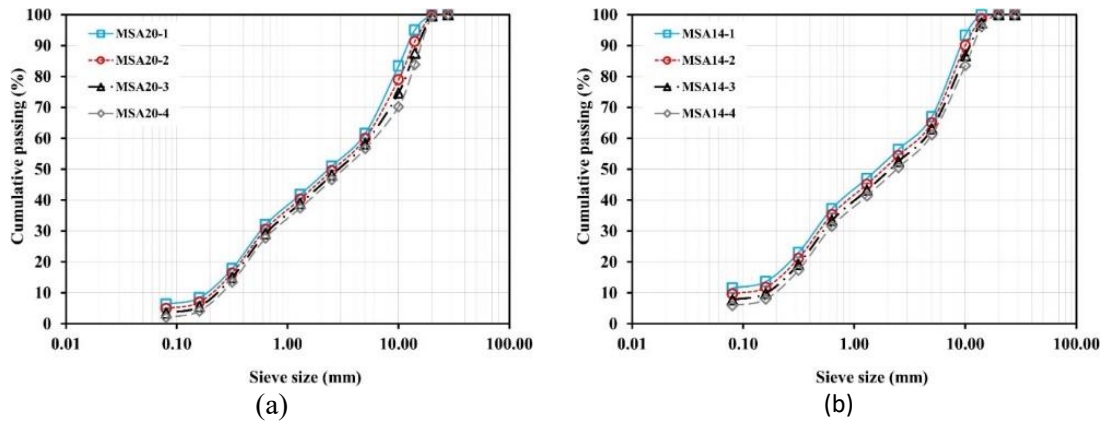
Figure 4-3 Particle-size distributions of investigated coarse aggregate mixtures for (a) precast (MSA20) and (b) repair (MSA14) applications.

Figure 4-4 the Intensive Compaction Tester (ICT) device.

4.3 Phase 2: Evaluating the coupled effect of fiber-aggregate characteristics and mortar rheology on flowability, passing ability, and dynamic segregation of FR-SCC mixtures using T-Box and L-Box set-ups.

In this phase, two different sets of FR-SCC mixtures for repair applications were proportioned with a macro steel fiber, MSA of 14-20 mm, W/B of 0.35-0.42, and V_P of 27%-37% corresponding to conventional (CSR) and high (HSR) strength levels (Table 4-1). The workability of the investigated FR-SCC mixtures was evaluated using the slump flow (flowability), spread in modified J-Ring set-up (with 8 bars), and L-Box blocking ratio (h2/h1 in presence of 2 bars [1]) (passing ability). The homogeneous performance of the investigated mixtures was evaluated in terms of granular blocking in the L-Box set-up (BI index) and dynamic segregation through the T-Box set-up (DSI index), as a diphasic suspension of F-A combination in mortar matrix. This process is shown in Figure 4-5.

Evaluating the coupled effect of fiber-aggregate characteristics and mortar rheology on flowability, passing ability, and dynamic segregation of FR-SCC mixtures using T-Box and L-Box set-ups.

FR-SCC for conventional strength repair (CSR)

Volume of paste = 0.27, 0.30, 0.33
W/B = 0.42
Max size of aggregate = 14 mm
Fiber content = 0.11%-0.5%
sand-to-total aggregate (S/A) = 0.55

FR-SCC for high strength repair (HSR)

Volume of paste = 0.30, 0.33, 0.35
W/B = 0.35
Max size of aggregate = 20 mm
Fiber content = 0.10%-0.19%
sand-to-total aggregate (S/A) = 0.55

Workability measurement

Dynamic stability (T-Box)

Dynamic segregation index (DSI) based on sampling method in fresh state

Passing ability (L-Box and J-Ring)

J-Ring:
$$\Delta JR\ (\%) = \frac{SF - JRF}{SF} \times 100\%$$
SF: Slump flow
JRF: J-Ring flow

L-Box:
blocking ratio = (h_2/h_1)

+

L-Box:
blocking index (BI) based on sampling method in fresh state

Figure 4-5 Chart of Phase 2.

Table 4-1 Proportioning, slump flow, and compressive strength of the investigated FR-SCC mixtures (HRWR and AEA dosages are in mL/100 kg of binder).

Series	Mix	V_P (%)	PSD	V_f in concrete (%)	φ_{max}-of F-A mixture	φ/φ_{max} of F-A	Slump flow (mm)	f'_{c-28d} (MPa)	ΔJR (%)	h_2/h_1	BI (%)	DSI (%)
	CSR1	27	MSA14-1	0.28	0.536	0.571	667	30.2	15.2	0.002	79.7	0.4
	CSR2	27	MSA14-2	0.22	0.544	0.563	665	31.6	9.2	0.636	47.3	17.7
	CSR3	27	MSA14-3	0.11	0.554	0.552	662	33.2	3.0	0.789	11.9	12.2
	CSR4	30	MSA14-1	0.25	0.536	0.546	700	38.9	4.4	0.696	19.5	20.4
CSR	CSR5	30	MSA14-2	0.20	0.544	0.538	673	39.9	3.8	0.800	14.3	18.4
	CSR6	30	MSA14-3	0.11	0.554	0.528	656	47.8	2.2	0.808	18.1	40.3
	CSR7	33	MSA14-1	0.25	0.536	0.521	678	42.9	2.9	0.800	14.6	49.6
	CSR8	33	MSA14-2	0.19	0.544	0.513	685	44.7	0.7	0.909	16.7	71.4
	CSR9	33	MSA14-3	0.11	0.554	0.503	694	46.0	2.1	0.750	9.8	54.8
	CSR10	33	MSA14-3	0.50	0.534	0.523	675	49.4	2.2	0.727	11.4	40.6
	HSR1	33	MSA20-3	0.11	0.533	0.524	683	65.0	3.7	0.808	34.0	35.7
	HSR2	33	MSA20-1	0.19	0.550	0.508	678	62.6	2.9	0.900	25.7	45.1
	HSR3	33	MSA20-2	0.14	0.562	0.496	694	60.4	0.7	1.000	19.1	62.3
	HSR4	35	MSA20-3	0.10	0.533	0.507	678	66.9	4.4	0.750	28.7	32.6
HSR	HSR5	35	MSA20-1	0.19	0.550	0.491	695	66.1	3.7	0.800	22.4	43.1
	HSR6	35	MSA20-2	0.14	0.562	0.480	697	65.3	1.4	0.878	13.5	57.7
	HSR7	37	MSA20-3	0.10	0.533	0.490	694	74.6	7.4	0.682	27.7	27.6
	HSR8	37	MSA20-1	0.18	0.550	0.475	690	71.0	5.1	0.762	21.3	30.4
	HSR9	37	MSA20-2	0.13	0.562	0.464	695	67.7	4.3	0.800	10.4	46.4

The rheological properties of the investigated mortar mixtures (containing aggregate finer than 5 mm) corresponding to the CSR and HSR FR-SCC mixtures were also evaluated. The investigated mortars were considered as diphasic suspensions of coarser portion of sand particles greater than 1.25 in fine mortar, containing aggregate finer than 1.25 mm, to allow precise rheological measurements. On the other hand, the fine mortar itself is considered as a diphasic suspension of fine sand (< 1.25 mm) in cement paste. This process is shown in Figure 4-6.

Step-1: Evaluation of rheological properties of fine mortar (FM)	Step-2: Evaluation of rheological properties of mortar (M)
Assume: Fine mortar = fine sand (FS < 1.25 mm) + cement paste	Assume: Mortar = Coarse sand (CS >1.25 mm) + fine mortar (< 1.25 mm)
Evaluate plastic viscosity (μ_{p-P}) and yield stress (τ_{0-P}) of cement paste	Consider plastic viscosity (μ_{p-FM}) and yield stress (τ_{0-FM}) of fine mortar (step 1)
+	+
Evaluate volumetric content and relative-solid packing fraction of fine sand	Evaluate volumetric content and relative-solid packing fraction of coarse sand
Use empirical models [2,3] to calculate plastic viscosity (μ_{p-FM}) and yield stress (τ_{0-FM}) of fine mortar	Use empirical models [4-7] to calculate plastic viscosity (μ_{p-FM}) and yield stress (τ_{0-FM}) of fine mortar
(a)	(b)

Figure 4-6 Evaluation of the rheological properties of a) fine mortar and b) mortar mixtures.

In total, 13 cement paste mixtures, including 10 for CSR and 3 for HSR series, were prepared and their rheological properties were evaluated (Table 4-2). It is worthy to mention that in order to reproduce the suspending phases exist in the investigated concrete suspensions, the cement paste mixtures were proportioned using the same dosages of HRWR and AEA of their corresponding FR-SCC mixtures.

Table 4-2 Rheological properties of the investigated cement paste mixtures.

Application	Cement paste No.	Corresponding FR-SCC mixture	τ_{0-P} (Pa)	μ_{p-P} (Pa.s)
CSR	P-CSR1	R1	0.61	0.029
	P-CSR2	R2	0.76	0.0287
	P-CSR3	R3	0.95	0.032
	P-CSR4	R4	1.01	0.040
	P-CSR5	R5	1.09	0.040
	P-CSR6	R6	1.22	0.040
	P-CSR7	R7	1.27	0.043
	P-CSR8	R8	1.69	0.047
	P-CSR9	R9	2.85	0.053
	P-CSR10	R10	1.58	0.045
HSR	P-HSR1-3	P1-3	2.16	0.104
	P-HSR4-6	P4-6	4.39	0.122
	P-HSR7-9	P7-9	7.71	0.141

As presented in Table 4-2, the rheological properties of the investigated mortars corresponding to the investigated FR-SCC mixtures were then evaluated using the rheological properties of their corresponding cement paste mixtures (Table 4-3).

Table 4-3 Rheological properties of the investigated mortar mixtures (sand < 5 mm).

Application	Mortar No.	Corresponding FR-SCC mixture	Corresponding cement paste mixture	V_P in mortar	$\tau_{0\text{-M}}$ (Pa)	$\mu_{p\text{-M}}$ (Pa.s)
CSR	M-CSR1	CSR1	P-CSR1	0.39	8.75	2.83
	M-CSR2	CSR2	P-CSR2	0.39	10.91	2.80
	M-CSR3	CSR3	P-CSR3	0.39	13.49	3.07
	M-CSR4	CSR4	P-CSR4	0.42	6.58	3.55
	M-CSR5	CSR5	P-CSR5	0.42	7.05	3.54
	M-CSR6	CSR6	P-CSR6	0.42	7.96	3.55
	M-CSR7	CSR7	P-CSR7	0.46	4.61	3.24
	M-CSR8	CSR8	P-CSR8	0.46	6.12	3.55
	M-CSR9	CSR9	P-CSR9	0.46	10.33	4.02
	M-CSR10	CSR10	P-CSR10	0.46	5.78	3.39
HSR	M-HSR1-3	HSR1-3	P-HSR1-3	0.46	8.49	8.03
	M-HSR4-6	HSR4-6	P-HSR4-6	0.48	12.54	8.20
	M-HSR7-9	HSR7-9	P-HSR7-9	0.50	17.68	8.27

4.4 Phase 3: Determining the effect of fiber-aggregate-mortar characteristics, bar arrangements, and different distances from casting point on dynamic segregation and blocking of fiber-coarse aggregates and mechanical performance, using new developed set-up for repair applications.

In this phase, according to the workability results of Phase 2 (Table 4-1), six CSR mixtures (out of 10 FR-SCC mixtures) exhibiting high passing ability and medium to high dynamic stability, corresponding to the BI values less than 27% and DSI values less than 50%, respectively, were selected for further analyses, using developed test set-ups.

As discussed earlier in literature review, the conventional workability tests, such as L-Box and T-Box set-ups, cannot simulate the confined flow conditions corresponding to the repair application. Accordingly, a new test set-up was proposed to simulate the homogeneous performance of FR-SCC for repair applications in fresh state, including dynamic stability and passing ability. As shown in Figure 4-7, the set-up consisted in a close-circuit of 4 close-surface rectangular channels of 200-mm height, 700-mm length, and 100-mm width (i.e., 700 × 700 mm outer box and 500 × 500 mm inner box with 200-mm height). In order to evaluate the passing ability of the investigated mixtures, the set-up was equipped with four rows of 10-mm diameter reinforcing bar grids positioned in horizontal and vertical configurations, in addition to one longitudinal rebar through the whole length of the set-up (Figure 4-7). Moreover, to evaluate the dynamic stability of the investigated mixtures, the test was also repeated without presence of any reinforcing bars.
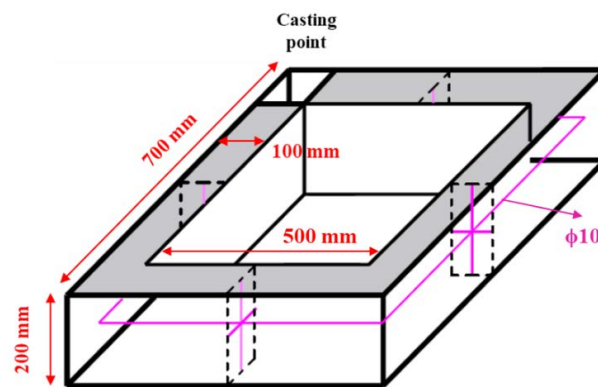
Figure 4-7 Schematics of the proposed Square-Box test to evaluate the passing ability and dynamic stability of the FR-SCC mixtures.

As shown in Figure 4-8a, immediately after casting, the cast beam was divided in 5 different sections (i = 1 to 5) using separators inserted just behind the reinforcing grids at middle of the channels. Then, 5 cylindrical samples measuring 100 mm in diameter and 200 mm in height were taken from each section i = 1 to 5 to evaluate the variation of concentration and distribution of coarse aggregate and steel fibers at different distances from the casting point. The sampling method in the fresh state to evaluate the dynamic stability and passing ability of FR-SCC mixtures is shown in Figure 4-9.

(a)   (b)
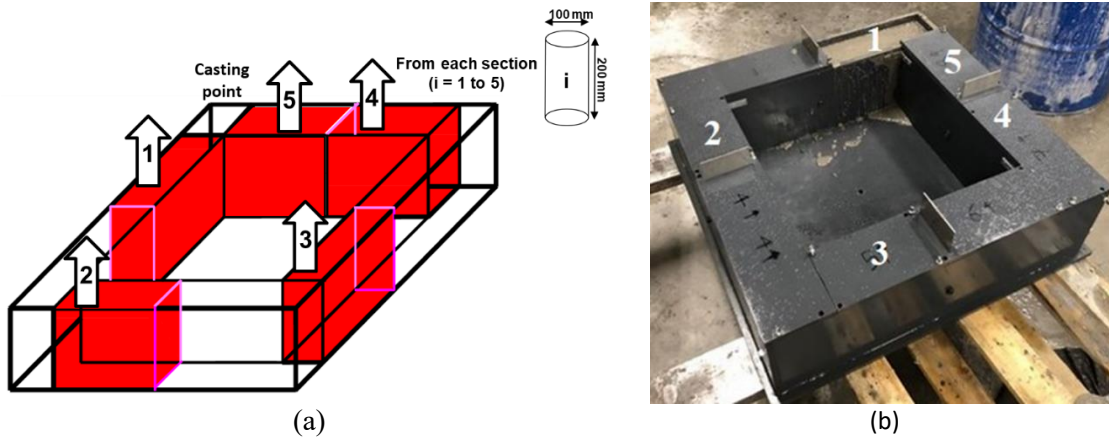
Figure 4-8 Sampling method from each section (i= 1 - 5) of the developed set-up.
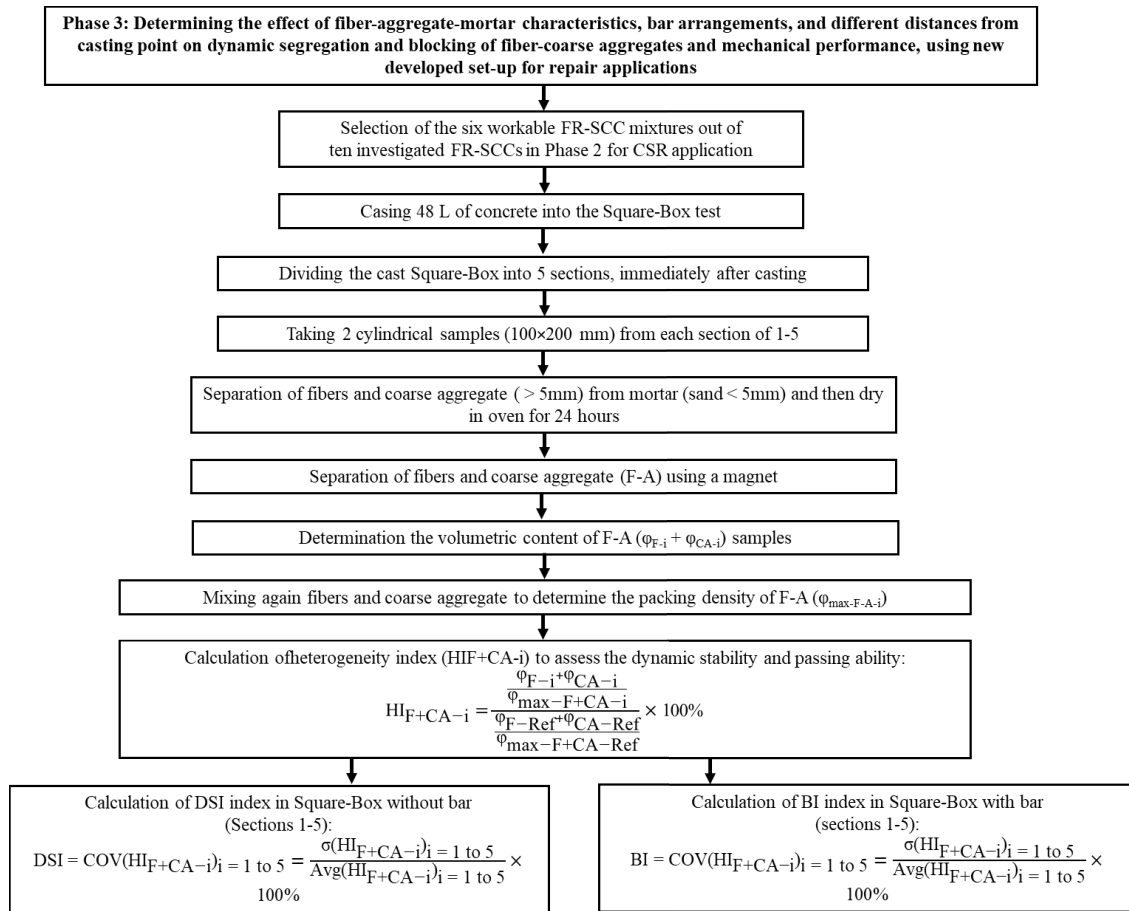
Figure 4-9 Chart of Phase 3.

4.5 Phase 4: Investigation the coupled effect of fibers-aggregate-bar characteristics, rheology of mortar, and formwork walls on distribution and 3D orientation of fibers at different distances from casting point, using Image analysis and new developed set-up for repair applications.

In this phase, the same six FR-SCC mixtures of the phase-3 were cast in the developed channel set-up and left to be hardened. In total, 48 l of each six FR-SCC mixtures was cast into the channels directly from mixer from one corner during almost 18 s. The concrete left to be hardened for 24 hours after mould filling. Then the channel samples were cut perpendicularly to the flow direction, at two sections: one in the beginning (in the middle of first beam: section1) and another one almost at the end of the set-up (in the middle of third beam: section2). The two cut cross sections correspond to two different distances from the casting point. The cutting process and sampling for each kind of bar's arrangement is shown in Figure 4-10.
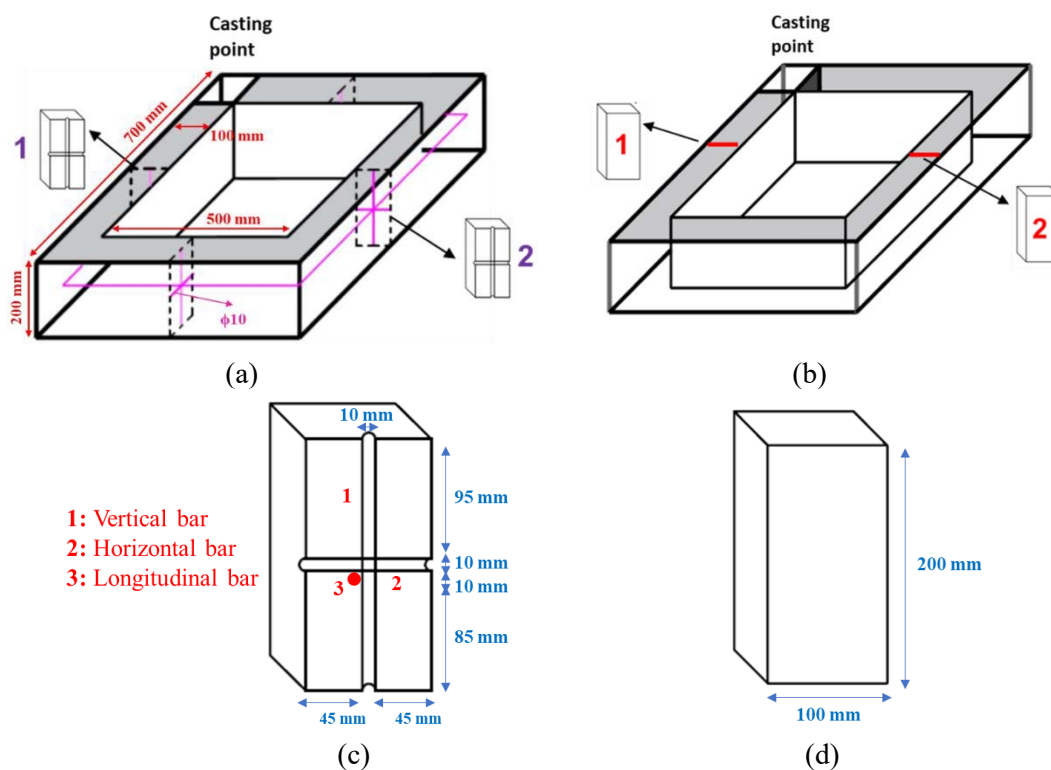
Figure 4-10 The developed set-ups for evaluation of FOD a) reinforced b) non-reinforced channels, and the details of each cross sections of c) with and d) without bar.

After cutting, the surface of each cut cross section was well polished to enhance the contrast between the fibers and the concrete matrix, and then pictured using a high-resolution camera. As shown in Figure 4-11, the image is then converted to a binary format where the white and black pixels represent the cut fibers and concrete matrix, respectively.

<center>(a)   (b)</center>
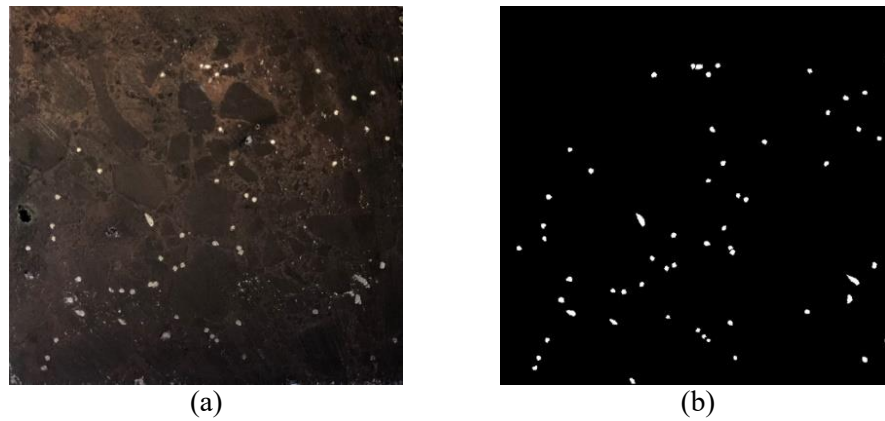
<center>Figure 4-11 a) RGB and b) binary images of a concrete section.</center>

ImageJ software, which is an open-source image processing software code, and Shape Filter plugin is then employed to determine the number, vertical and horizontal positions, surface area, form (i.e., circular or elliptic shapes), dimensions, and angle of cut fibers in each section plane, in neighbor of the reinforcing bars and formwork walls. The evaluation process of fiber distribution and orientation is shown in Figure 4-12.

To compute the horizontal and vertical variation of fiber concentration in both horizontal and vertical directions, the 100×200 mm image corresponding to the total cross-sectional area was divided into 7(horizontal)× 7(vertical) units and illustrated in Figure 4-13. Then, the number of fibers per unit was counted, using the frequency polygon which is a visual representation of fiber distribution.
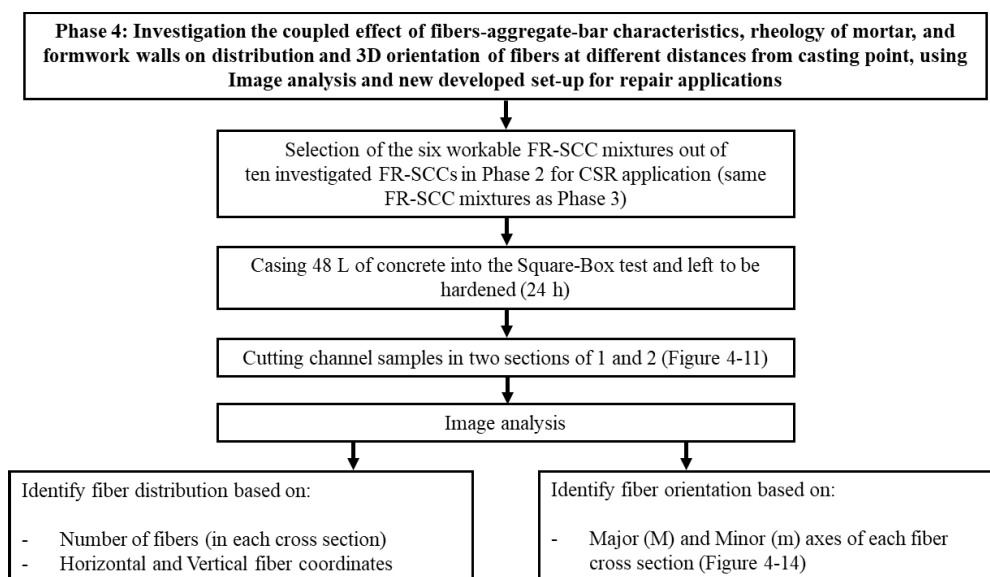
<center>Figure 4-12 Chart of Phase 4.</center>
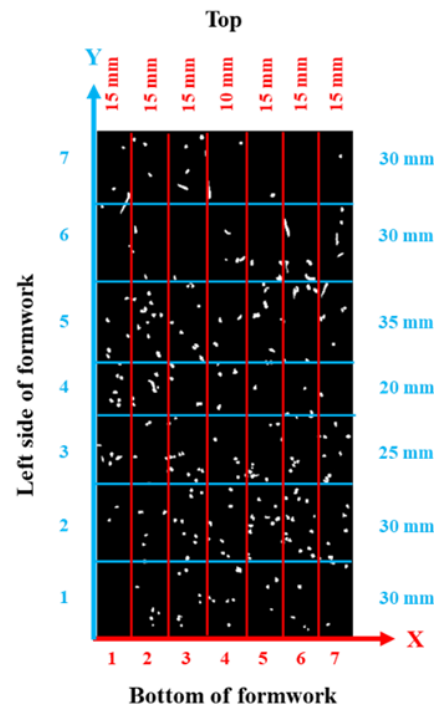
Figure 4-13 Horizontal and vertical unites of a concrete cross section.
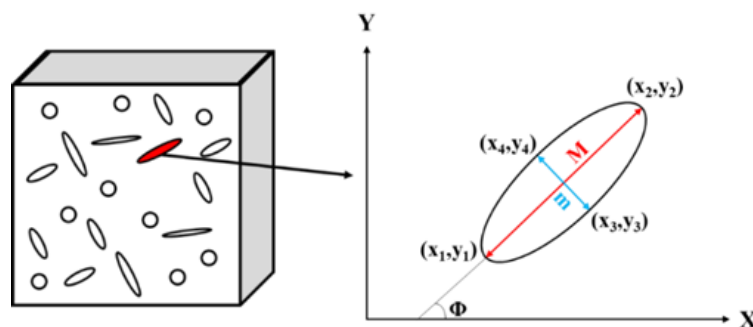
Figure 4-14 Schematic illustration of the fiber orientation in cross section i (an example
for two highly spaced horizontal bars arrangement).

References

[1]   F. Kassimi, A.K. El-Sayed, K.H. Khayat, Performance of fiber-reinforced self-consolidating
      concrete for repair of reinforced concrete beams, ACI Structural Journal, 111 (6) (2014) 1277-1286,
      https://dx.doi.org/10.14359/51687031.

[2]   M. Hosseinpoor, B.I.O. Koura, A. Yahia, E.H. Kadri, Diphasic investigation of the visco-
      elastoplastic characteristics of highly flowable fine mortars, Construction and Building Materials,
      270 (2021) 121425, https://doi.org/10.1016/j.conbuildmat.2020.121425.

[3]   M. Hosseinpoor, B.I.O. Koura, A. Yahia, Rheo-morphological investigation of Reynolds dilatancy
      and its effect on pumpability of self-consolidating concrete, Cement and Concrete Composites, 117
      (2021) 103912, https://doi.org/10.1016/j.cemconcomp.2020.103912.

[4]   C.F. Ferraris, L.E. Brower, Comparison of concrete rheometers: international tests at MB
      (Cleveland OH, USA) in 2003. National Institute of Standards and Technology Interagency Report,
      NISTIR 7145.

[5] X. Chateau, G. Ovarlez, K.L. Trung, Homogenization approach to the behavior of suspensions of noncolloidal particles in yield stress fluids, Journal of Rheology, 52 (2) (2008) 489-506, https://doi.org/10.1122/1.2838254.

[6] H. Hafid, G. Ovarlez, F. Toussaint, P.H. Jezequel, N. Roussel, Estimating measurement artifacts in concrete rheometers from MRI measurement on model materials, In: Khayat, K., Feys, D. (eds) Proceedings of SCC2010: Design, Production and Placement of Self-Consolidating Concrete, Montreal, Canada (2010), RILEM Bookseries, vol 1. Springer, Dordrecht, 127-137, https://doi.org/10.1007/978-90-481-9664-7_11.

[7] S.D. Jo, C.K. Park, J.H. Jeong, S.H. Lee, S.H. Kwon, A computational approach to estimating a lubricating layer in concrete pumping, Computers Materials and Continua, 27 (3) (2012) 189-210, https://doi.org/10.3970/CMC.2011.027.189.

[8] R. Farokhzad, M. Mahdikhani, A. Bagheri, J. Baghdadi, Representing a logical grading zone for self-consolidating concrete, Construction and Building Materials, 115 (2016) 735-745, https://doi.org/10.1016/j.conbuildmat.2016.04.006.

[9] H. Hafid, G. Ovarlez, F. Toussaint, P.H. Jezequel, N. Roussel, Effect of particle morphological parameters on sand grains packing properties and rheology of model mortars, Cement and Concrete Research, 80 (2016) 44-51, https://doi.org/10.1016/j.cemconres.2015.11.002.

[10] K. Ostrowski, K. Oleksik, Comparative analysis of the coarse aggregate shapes used to manufacturing high performance self-compacting concrete, Technical Transaction, 7 (2018) 75-86, https://doi.org/10.4467/2353737XCT.18.101.8796.

[11] L. Struble, R. Szecsy, W.-G. Lei, G.-K. Sun, Rheology of cement paste and concrete, Cement, Concrete and Aggregates, 20 (2) (1998) 269-277, https://dx.doi.org/10.1520/CCA10421J.

[12] ASTM C1611/C1611M-21 Standard Test Method for Slump Flow of Self-Consolidating Concrete, West Conshohocken, PA; ASTM International (2021), https://dx.doi.org/10.1520/C1611_C1611M-21.

[13] ASTM C1621/C1621M-17, Standard Test Method for Passing Ability of Self-Consolidating Concrete by J-Ring, West Conshohocken, PA; ASTM International (2017), https://dx.doi.org/10.1520/C1621_C1621M-17.

[14] K.H. Khayat, F. Kassimi, P. Ghoddousi, Mixture design and testing of fiber-reinforced self-consolidating concrete, ACI Materials Journal, 111 (2) (2014) 143-152, https://doi.org/10.14359/51686722.

[15] B. Esmaeilkhanian, D. Feys, K.H. Khayat, A. Yahia, B.I.O. Koura, M. Hosseinpoor, A. Yahia, Coupled effect of fine mortar and granular skeleton characteristics on dynamic stability of self-consolidating concrete as a diphasic material, Construction and Building Materials, 263 (2020) 120131, https://doi.org/10.1016/j.conbuildmat.2020.120131.

[16] dynamic stability of self-consolidating concrete, ACI Materials Journal, 111 (3) (2014) 299-308, https://doi.org/10.14359/51686573.

[17] M. Hosseinpoor, B.I.O. Koura, A. Yahia, New diphasic insight into the restricted flowability and granular blocking of self-consolidating concrete: Effect of morphological characteristics of coarse aggregate on passing ability of SCC, Construction and Building Materials, 308 (2021) 125001, https://doi.org/10.1016/j.conbuildmat.2021.125001.

CHAPITER 5 Coupled effect of fiber and granular skeleton characteristics on packing density of fiber-aggregate mixtures

Authors and affiliations

Naimeh Nouri : Ph.D. candidate, Cement and Concrete Research Group, Department of Civil and Building Engineering, Université de Sherbrooke, Sherbrooke, Québec, Canada, J1K 2R1.

Masoud Hosseinpoor: Research Associate, Cement and Concrete Research Group, Department of Civil and Building Engineering, Université de Sherbrooke, Sherbrooke, Québec, Canada, J1K 2R1.

Ammar Yahia: Professor, Cement and Concrete Research Group, Department of Civil and Building Engineering, Université de Sherbrooke, Sherbrooke, Québec, Canada, J1K 2R1.

Kamal H. Khayat: Professor, Missouri University of Science and Technology, Center for Infrastructure Engineering Studies, Department of Civil, Architectural and Environmental Engineering, Rolla, MO 65409.

Titre en français: Effet couplé des caractéristiques des fibres et du squelette granulaire sur la densité de tassement des mélanges fibres-granulats.

Coupled effect of fiber and granular skeleton characteristics on packing density of fiber-aggregate mixtures

Naimeh Nouria, Masoud Hosseinpoora,*, Ammar Yahiaa, and Kamal H. Khayatb

aUniversité de Sherbrooke, Department of Civil and Building Engineering, Sherbrooke, Québec, Canada

bMissouri University of Science and Technology, Center for Infrastructure Engineering Studies, Department of Civil, Architectural and Environmental Engineering, Rolla, MO, USA

*Corresponding author: masoud.hosseinpoor@usherbrooke.ca

Abstract

The addition of fiber to cementitious materials enhances mechanical performance but can reduce workability of the fiber-reinforced concrete (FRC) mixtures. This can be due to the negative effect of fibers on packing density (PD) of the fiber-coarse aggregate (F-A) combination. The performance of FRC, as a diphasic suspension, is dependent on the characteristics of both F-A (suspended-solid skeleton) and mortar (suspending liquid) phases. PD can reflect the voids within the F-A skeleton to be filled with mortar. An adequate optimization of the characteristics of the F-A skeleton can modify the performance of FRC in fresh and hardened states. The F-A skeleton can be characterized in terms of particle-size distribution, volumetric content, and morphology of the coarse aggregate, as well as size, rigidity, and content of fibers. In this study, a comprehensive investigation was undertaken to identify the coupled effect of the characteristics of fibers and coarse aggregate on the PD of F-A combination used without any cement paste/mortar. The solid components play a key role in the overall performance of the concrete produced. This study was carried out to optimize the F-A combination and enhance the workability design of FRC. Various types of steel, polypropylene, and polyolefin fibers having different sizes and rigidities were investigated. Moreover, four combinations of three different classes of coarse aggregate were used to proportion F-A mixtures. Test results showed that shorter length, smaller diameter, and more flexible fibers can lead to higher PD of F-A systems. Moreover, the coarser aggregate skeleton with larger interparticle voids led to more available length for fibers to be deformed, hence improving the PD of F-A mixtures. New empirical models were proposed to predict the packing density of F-A combinations given the characteristics of coarse aggregate and fibers, as well as the level of compaction. The established models were employed to propose a new proportioning approach for fiber-reinforced self-consolidating concrete mixtures to achieve the targeted workability.

Keywords: Fiber-coarse aggregate mixture; Fiber-reinforced concrete; Granular skeleton; Packing density; Particle-size distribution; Rigidity.

5.1 Introduction

Hardened cement-based materials are brittle because of their low tensile strength and strain capacity. The addition of fibers can enhance the tensile, flexural, and ductility properties of fiber-reinforced concrete (FRC) [1-3]. However, adding fibers can negatively affect the workability of FRC. This can be due to fiber-aggregate interaction, hence forming blocking

arches in vicinity of obstacles. The negative effect of fibers on workability of FRC depends on content, size (length and diameter), type, and rigidity of fibers [4-6]. From workability point of view, there is a critical content of fibers above which concrete is not flowable anymore and fiber clumping can occur [6-9]. This critical content decreases for larger and rigid fibers. Khayat et al. [10] investigated the effect of fiber characteristics on workability of fiber-reinforced self-consolidating concrete (FR-SCC). The authors optimized FR-SCC mixtures by keeping the average mortar thickness constant to achieve a given workability. This average thickness is function of surface area of aggregate and fibers, as well as the interparticle voids. The packing density (PD) of solid skeleton can reflect the amount of cement paste required to fill the interparticle voids. Higher packing density leads to more excess paste available to cover fibers and aggregate, hence increasing the workability of FR-SCC.

In order to design FR-SCC with adequate properties, the influence of various effective parameters should be considered simultaneously. Hosseinpoor et al. [11, 12] evaluated the coupled effect of characteristics of aggregate, coarser than 1.25-mm diameter, and rheological properties of suspending fine mortar (< 1.25 mm) on stability and passing ability of self-consolidating concrete (SCC). The authors reported that the ratio of the volumetric content-to-packing density (φ/PD) of coarse aggregate shows a dominant effect on homogeneous performance of SCC during flow, and thereafter at rest. Koura et al. [13] showed that the optimization of the paste volume and φ/PD ratio are effective parameters on dynamic stability of SCC rather than the rheology of paste (i.e., water-to-binder ratio and high-range water-reducer (HRWR) dosage). On the other hand, Mehdipour and Libre [6] evaluated the effect of volumetric content and rigidity of polypropylene (PP) and glass fibers (GF) on PD of FR-SCC. They reported that increasing fiber content, especially rigid GF, up to a certain point slightly decreased the PD, beyond which PD of fibers and solid particles drastically decreases. Kwan et al. [14] reported that when fiber content is greater than the one required to fill the interparticle voids, leading to lower PD, the probability of fiber agglomeration can increase.

Although, various studies were carried out to evaluate the effect of fiber characteristics on workability and mechanical properties of concrete [15], limited information exists regarding the correlation between the fiber characteristics, packing density of solid skeleton, and workability of FRC. Aggregate characteristics, including particle-size distribution (PSD) and morphology, can also significantly affect the packing density of solid skeleton (i.e., fiber and aggregate combination) [16-22]. It was revealed that the use of a wide range of PSD shows positive effect on packing density of granular skeleton where the finer particles, up to an optimum content, can fill the voids between the coarser ones, hence increasing the PD [15]. Hafid et al. [22] reported the significant effect of fine particles' morphology (e.g., aspect ratio) on packing density of solid skeleton. The authors employed two different methods, including loose- and random dense-packing methods. It was revealed that vibration and external compaction can significantly change the arrangement of aggregate, hence affecting the PD values. Martinie et al. [23] reported the effect of duration and intensity of vibration on loose- and dense-PDs of fibers. Chu et al. [24] showed that without adequate compaction where the fibers are not yet deformed, the PD of F-A skeleton depends only on the size and rigidity of fibers.

Few studies were carried out to predict the coupled effect of different contents and types of fibers, as well as PSD of aggregate on PD of F-A. Chu et al. [24] investigated the effect of rigid fibres on PD of F-A mixtures for different contents (0-2%) and types of rigid-steel fibers of 30-

and 60-mm length, as well as various classes of aggregate (0.6 to 20 mm). The authors reported that increasing the content and size of fibers led to lower PD of F-A combination, especially in presence of coarse aggregate with higher maximum size (i.e., 20 mm). Using the compressible packing model (CPM), de Larrard [25] reported similar conclusions for mixtures containing rigid-steel fibers and fine and coarse aggregate. However, the proposed CPM model was not validated for flexible fibers. On the other hand, the CPM model was not established to predict the loosely-packed PD (LPD) of F-A, which can more accurately describe the packing state of F-A skeleton in concrete matrix through the mixing process and low casting rates. Actually, during the mixing process, where there is no adequate compaction, fibers are not deformed yet. Therefore, the F-A system is in loose state and the LPD should be taken into consideration. However, in the case of transportation and casting processes, such as shotcrete and highly-pressure pumping, where a higher level of compaction applies on the F-A system, fibres can deform [26, 27]. Therefore, the densely-packed PD (DPD) can more properly simulate the packing state of the F-A skeleton.

In this study, the coupled effect of fiber and coarse aggregate characteristics, including the volumetric content, length, diameter, and rigidity of different flexible and rigid fibers, as well as the PD and size of coarse aggregate on LPD and DPD of F-A combinations were evaluated. Accordingly, three classes of coarse aggregate with different PSDs were mixed with various volumetric fractions of rigid and flexible fibers. The LPD and DPD of the investigated F-A mixtures were evaluated without any compaction and under a given gyratory compaction, respectively. New empirical models were then established to predict the packing density of F-A mixtures under different levels of compaction. A new workability-design approach for fiber-reinforced self-consolidating concrete (FR-SCC) mixtures was then proposed based on the established LPD and DPD models.

5.2 Experimental study

Three different classes of crushed limestone coarse aggregate of 5-10 mm (CA1), 5-14 mm (CA2), and 5-20 mm (CA3) were used. The specific gravity values of the CA1-3 coarse aggregate are 2.72, 2.73, and 2.76, respectively. Two different groups of F-A mixtures were proportioned with the maximum-size aggregate (MSA) of 20 mm (MSA20) and 14 mm (MSA14). Each MSA20 and MSA14 series were proportioned using four different combinations (MSA20-1 to MSA20-4 and MSA14-1 to MSA14-4) of CA1-3 coarse aggregate to achieve wide ranges of PSD. It is worthy to mention that the MSA20 and MSA14 mixtures correspond to those used in precast and repair applications, respectively. The volumetric proportioning, packing density (PD_A), PSD, average diameter (D_A), and the total surface area-to-unit volume (AV_A) of the investigated coarse aggregate mixtures are summarized in Table 5-1 and Figure 5-1. It is worthy to mention that D_A and AV_A of each coarse aggregate mixture were evaluated using the three-dimensional morphological analyses and PSD of different classes of coarse aggregate. As reported by Hosseinpoor et al. [11,12,28,29], several samples of different subclasses of coarse aggregate, corresponding to different successive standard sieves, were scanned using a 3D laser scanner. The larger and smaller sides of the minimum bounding rectangles of the 2D projections of the 3D scanned particles, corresponding to their maximum (D_{max}) and minimum (D_{min}) diameters, respectively, were determined for each subclass of coarse aggregate. The mean diameter of each coarse aggregate subclass ($\overline{D}_i$) was calculated using the average of D_{max} and D_{min} values. Furthermore, the ratio of 3D surface area-to-volume of each coarse aggregate subclasses (AV_i) were determined using 3DSmax software.

Considering the PSD of the investigated coarse aggregate mixtures, the D_A and AV_A values were evaluated using the arithmetic average of mean diameter $\overline{D}_i$ and AV_i values, respectively.

Table 5-1 Proportioning of investigated coarse aggregate mixtures.

Application	Coarse aggregate mixtures	CA1 (%)	CA2 (%)	CA3 (%)	PD_A	D_A (mm)	AV_A (m²/m³)
Precast	MSA20-1	45	50	5	0.560	12.748	737.656
	MSA20-2	30	55	15	0.555	13.139	682.292
	MSA20-3	15	60	25	0.547	13.516	626.929
	MSA20-4	-	65	35	0.545	13.880	571.565
Repair	MSA14-1	100	-	-	0.558	12.595	860.295
	MSA14-2	80	20	-	0.560	12.596	820.313
	MSA14-3	60	40	-	0.561	12.598	780.332
	MSA14-4	40	60	-	0.562	12.599	740.350

Different types of steel fibers were mixed with both MSA20 and MSA14 coarse aggregate mixtures. Different types of synthetic fibers were also mixed with the MSA14 mixtures, corresponding to concrete repair applications. Two different macro- and micro- rigid fibers with different sizes, including the hooked-end macro and straight-micro steel fibers, were investigated. Moreover, the flexible-synthetic fibers included three types of polypropylene fibers, including PPF, TUF, and PSI fibers, as well as two types of polyolefin fibers, including macro-IT and micro-ST fibers. The physical characteristics of the investigated fibers are summarized in Table 5-2.

The experimental program was divided into two phases. The first phase was undertaken to evaluate the effect of fiber size, rigidity, and volume as well as coarse aggregate characteristics on packing density of the F-A combination (sections 3.1 to 3.4). In total, 216 F-A mixtures were proportioned with six fiber volumes (V_f) of 0.4%, 0.5%, 0.6%, 0.7%, 0.8%, and 0.9% mixed with eight coarse aggregate mixtures of MSA-14 and MSA-20 (Table 5-1).

First, the required coarse aggregate (Table 5-1) and fiber volumes to achieve a total solid volume ($V_f + V_{CA}$) of 0.6 L were weighted. The coarse aggregate samples (Figure 5-2a) were manually mixed for 5 min to ensure a homogeneous mixture (Figure 5-2b). The fibers were separated manually and then added to the coarse aggregate (Figure 5-2c). The F-A mixtures were then manually mixed for 5 min to ensure homogeneous dispersions (Figure 5-2d). The PD of the investigated coarse aggregate (PD_A) (Table 5-1) and F-A mixtures were then measured using the intensive compaction tester (ICT) (Figure 5-2e) [30-32]. The testing sample consisted of a cylindrical specimen measuring 100-mm diameter and 200-mm height. The F-A mixtures were poured in the cylindrical container in three equal layers (Figure 5-2f) to ensure vertical homogeneity of the samples. The top surface of the samples was then leveled (Figure 5-2g) before subjecting them to the compaction load. A constant normal pressure of 20 kPa was exerted on the top of the cylindrical specimen and a gyratory motion is applied to induce shear stress [30-32]. The applied normal pressure was selected low enough to avoid aggregate crushing. In total, 50 gyratory cycles with a gyration angle of 40 mrad were applied, and the tests were repeated three times for each sample. It is worth mentioning that the LPD and DPD values were evaluated after 4 and 50 gyratory cycles, respectively.

The PD was calculated as the ratio of the bulk density of the investigated F-A samples after a given number of cycles to their corresponding density value (ρ_{FA}). The ρ_{FA} values were calculated by the volumetric-weighted arithmetic mean of densities of the fiber and coarse aggregate in each mixture. The volume of fiber and coarse aggregate were calculated by

dividing their mass weighted for each sample to their corresponding density values. The reported PD values correspond to the average determined on three different measurements. It is worth mentioning that in the case of LPD, no deformation was observed in the fibers, due to low level of compaction. The LPD values were thus dependent only on the size (i.e., diameter and length) and fiber volume and coarse aggregate characteristics. However, after applying 50 gyratory cycles, the fibers were deformed. Therefore, the difference between the DPD and LPD values can reflect the effect of fibers' rigidity. Accordingly, the effect of volume and size of fibers, as well as coarse aggregate characteristics were evaluated using the LPD values. Moreover, the relative DPD-to-LPD values were investigated to evaluate the effect of fiber rigidity on DPD of F-A mixtures.

The empirical models are then established to predict the packing density of F-A mixtures as function of fiber-coarse aggregate characteristics in the second phase. In the case of the LPD model (further discussed in the section 3.5.1), 126 F-A mixtures were randomly selected and investigated. Furthermore, additional 34 mixtures were proportioned with PPF, TUF, ST, and IT fiber volumes ranging from 0.4% to 1.77% and different PSDs of MSA 14-1, MSA14-2, MSA 14-3, and MSA 14-4 to validate the established model (section 3.5). Moreover, the DPD model (section 3.5.2) was established based on randomly selected 127 mixtures, proportioned with 0.4% to 1.77% volumetric contents of rigid (macro and micro steel) and semi-rigid (IT and ST polyolefin) fibers, as well as eight different PSDs of coarse aggregate mixtures, presented in Table 5-1. The established DPD model is then validated using 100 additional F-A mixtures. These include 29 remaining reference F-A mixtures in addition to 71 F-A mixtures extracted from some empirical tests on 18 FR-SCC mixtures made with a ternary cement (TerC^3), volumetric sand (0-5 mm)-to-total aggregate ratio of 55%, and macro steel fibers.

In the case of mixtures that can be used for repair applications, 9 FR-SCC mixtures were made with MSA14 coarse aggregate mixtures and paste volumes of 0.27, 0.30, and 0.33 and water-to-binder ration (w/b) of 0.42. On the other hand, 9 FR-SCC mixtures for precast application made with MSA20, paste volumes of 0.33, 0.35, and 0.37, and w/b of 0.35 were investigated. The FR-SCC mixtures were prepared with a polycarboxylate-based HRWR to achieve a slump flow of 680 ± 20 mm (Table 5-3). The FR-SCC mixtures were tested using the L-Box [10] and T-Box [13] tests to evaluate their passing ability and dynamic stability, respectively. Various cylindrical samples measuring 100 mm ×200 mm were taken from two lateral sections of the investigated L-Box and T-Box set-ups. These included samples from behind the rebars in the vertical compartment of the L-Box and at the end of the L-Box channel, as well as the tilt-up and tilt-down zones of the T-Box test, using the method described in references [11-13]. In total, 71 concrete samples mixtures were wet-sieved on 5-mm sieve and dried to extract their F-A portions. The volumetric content of macro steel fibers and coarse aggregate in the extracted F-A samples were measured by separating the fibers using a magnet. The LPD and DPD values of the extracted F-A samples were then determined.
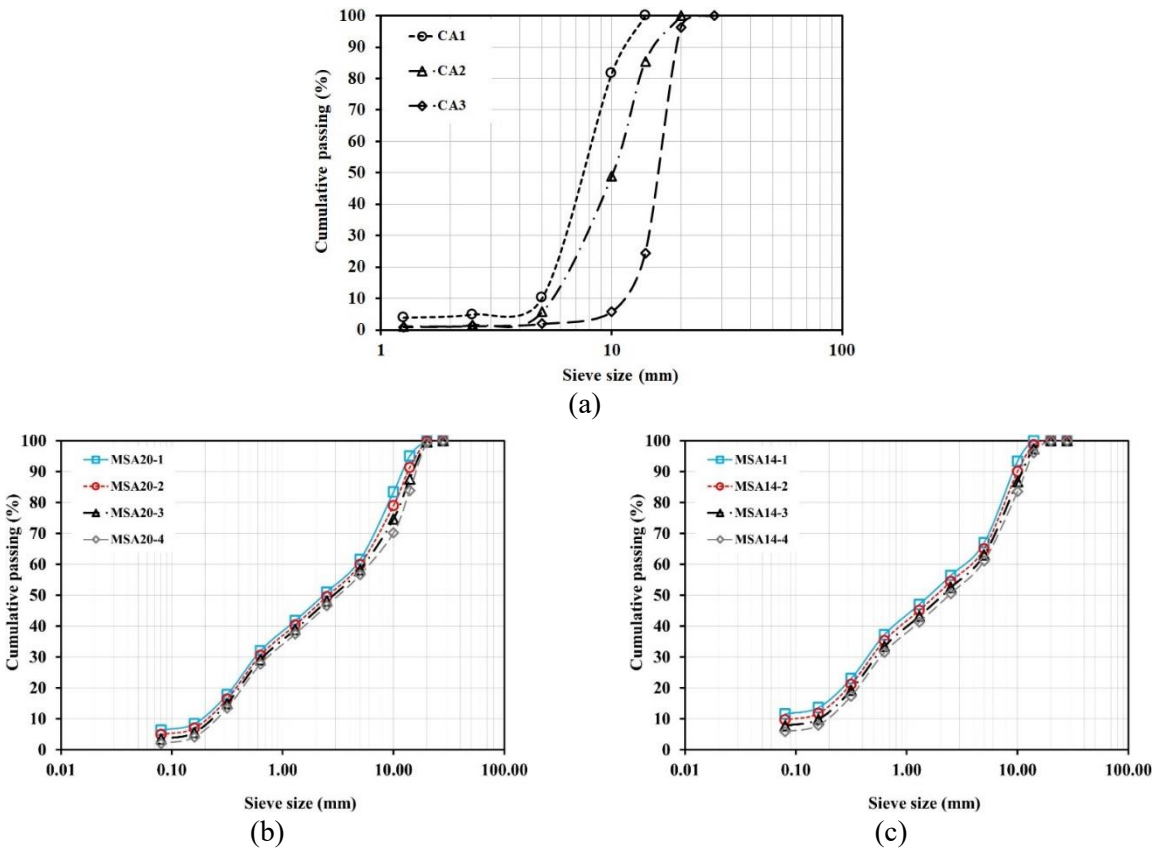
Figure 5-1 Particle-size distributions of (a) investigated coarse aggregate, and coarse aggregate mixtures for (b) precast (MSA20) and (c) repair (MSA14) applications.

Table 5-2 Physical characteristics of investigated fibers.

	Macro steel	Micro steel	PPF	PSI	TUF	IT	ST
Fiber type							
Material	Steel		Polypropylene			Polyolefin	
S.G.	7.85	7.80	0.91	0.91	0.91	0.91	0.91
L_f (mm)	30	13	38	19	38	55	42
D_f (mm)	0.55	0.20	0.39	0.12	0.69	0.92	0.79
A.R.	55	65	97	156	55	60	53
E (GPa)	200	203	3.5	-	9.5	3.9	3.9

S.G.: Specific gravity
L_f : Fiber length
D_f : Fiber diameter
A.R. : Aspect ratio
E : Modulus of elasticity
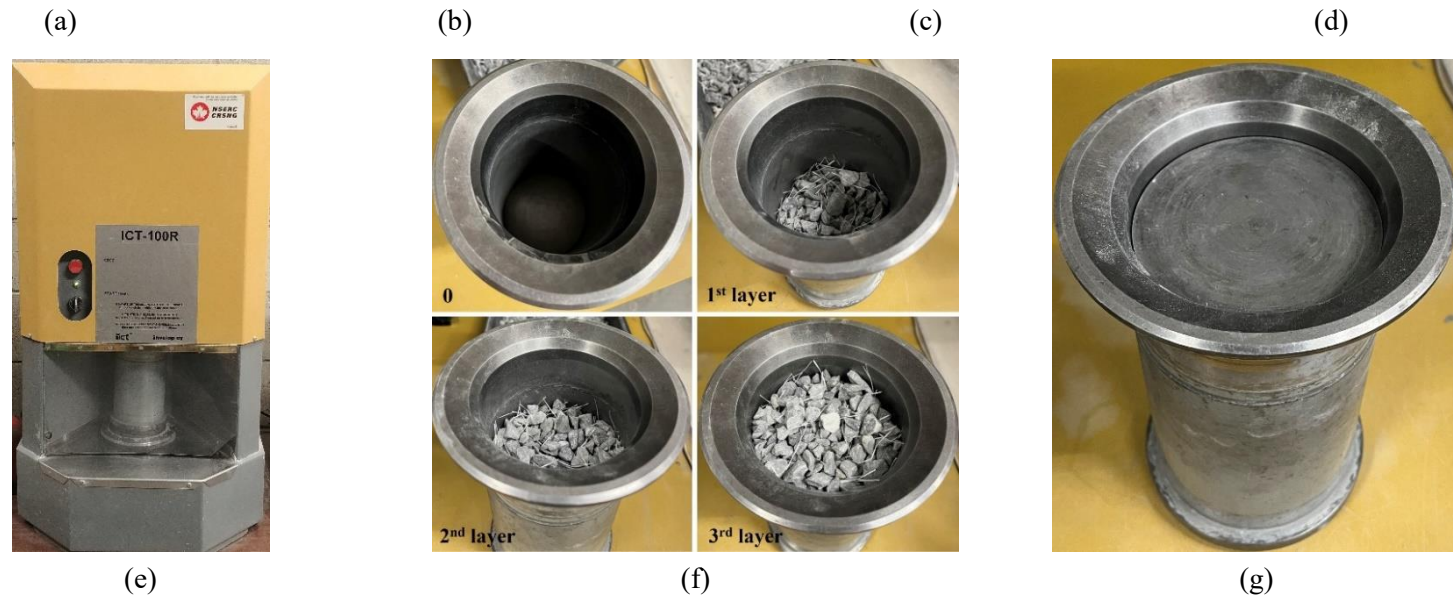
Figure 5-2 Procedure of the PD measurements, including (a) weighting different coarse aggregate classes, (b) homogenizing coarse aggregate, (c) adding fibers to the coarse aggregate, (d) homogenizing the F-A mixtures, (e) the ICT set-up, (f) layer-by-layer sampling of the cylindrical specimens, and (g) flattening the specimens' top surface.

Table 5-3 Proportioning of the FR-SCC mixtures made with macro steel fiber.

Application	Mix	Binder (kg/m^3)	Paste volume (%)	Sand (0-5 mm) (kg/m^3)	PSD of coarse aggregate	CA1 (kg/m^3)	CA2 (kg/m^3)	CA3 (kg/m^3)	Fiber (kg/m^3)	V_f in F-A mixture (%)
	R1	352	27	999	MSA14-1	825	-	-	22	0.9
	R2	352	27	999	MSA14-2	661	166	-	17	0.7
	R3	352	27	999	MSA14-3	497	333	-	9	0.4
	R4	392	30	955	MSA14-1	789	-	-	20	0.9
Repair	R5	392	30	955	MSA14-2	632	159	-	16	0.7
	R6	392	30	955	MSA14-3	475	318	-	9	0.4
	R7	431	33	910	MSA14-1	752	-	-	20	0.9
	R8	431	33	910	MSA14-2	603	151	-	15	0.7
	R9	431	33	910	MSA14-3	454	303	-	9	0.4
	P1	474	33	910	MSA20-4	-	493	268	9	0.4
	P2	474	33	910	MSA20-2	226	416	115	15	0.7
	P3	474	33	910	MSA20-3	113	455	192	11	0.5
	P4	503	35	881	MSA20-4	-	477	260	8	0.4
Precast	P5	503	35	881	MSA20-2	219	403	111	15	0.7
	P6	503	35	881	MSA20-3	110	440	185	11	0.5
	P7	532	37	852	MSA20-4	-	461	251	8	0.4
	P8	532	37	852	MSA20-2	211	389	107	14	0.7
	P9	532	37	852	MSA20-3	106	425	179	10	0.5

5.3 Results and discussions

5.3.1   Effect of fiber content on LPD of F-A mixtures

As can be observed in Figure 5-3, in the case of macro and micro steel fibers, the LPD of F-A mixtures generally increased with fiber content up to an optimum value before decreasing. For example, in the case of MSA20-3 coarse aggregate mixture, increasing the macro and micro steel fibers' content up to 0.5% and 0.7% resulted in 3.91% and 1.24% increase in the LPD, respectively. It is worthy to mention that the incorporation of macro-steel fibers resulted in a decrease in LPD of F-A combinations proportioned with MSA14 coarse aggregate mixtures, regardless of the fiber content.

Furthermore, the effect of synthetic fibers on the LPD of F-A mixtures is illustrated in Figure 5-4. As can be observed in Figures 5-4a and 5-4b, increasing ST and IT fiber content led to decrease in LPD of F-A mixtures. On the other hand, as shown in Figures 5-4c-e, the LPD of F-A mixtures containing PP fibers (i.e., PPF, PSI, and TUF) slightly increased by increasing the fiber content up to a certain value, beyond which the LPD values decreased. This can be explained by similar phenomenon causing loosening, wedging, and wall effects in mixture containing sand and coarse aggregate [15, 27]. Loosening effect happens when finer particles are added in the space between coarser aggregate. Accordingly, adding finer aggregate led to increase in packing density of the F-A mixture (Figure 5-5a). However, when the maximum packing density is achieved, increasing the volume of finer particles beyond an optimum content can disturb the packed array of the coarser aggregate skeleton and reduced the packing density of the F-A mixture. Moreover, although some finer particles fill the interparticle voids, other fine aggregate can be trapped between coarser ones and lead to more voids. This is referred to as the wedging effect (Figure 5-5b).
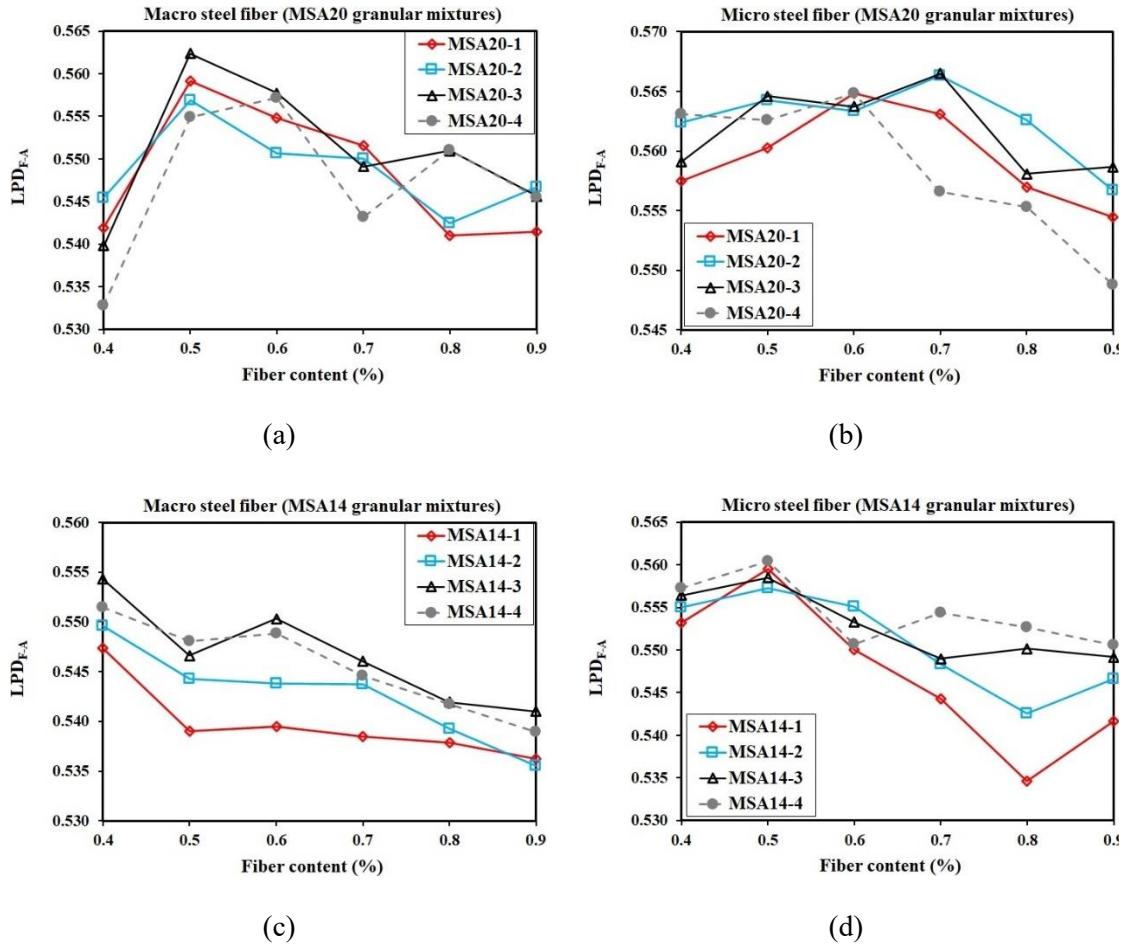
Figure 5-3 Variation of the LPD values of F-A mixtures with fiber content, including (a) macro fiber and MSA20, (b) micro steel fiber and MSA 20, (c) macro steel fiber and MSA14, and (d) micro steel fiber and MSA14.
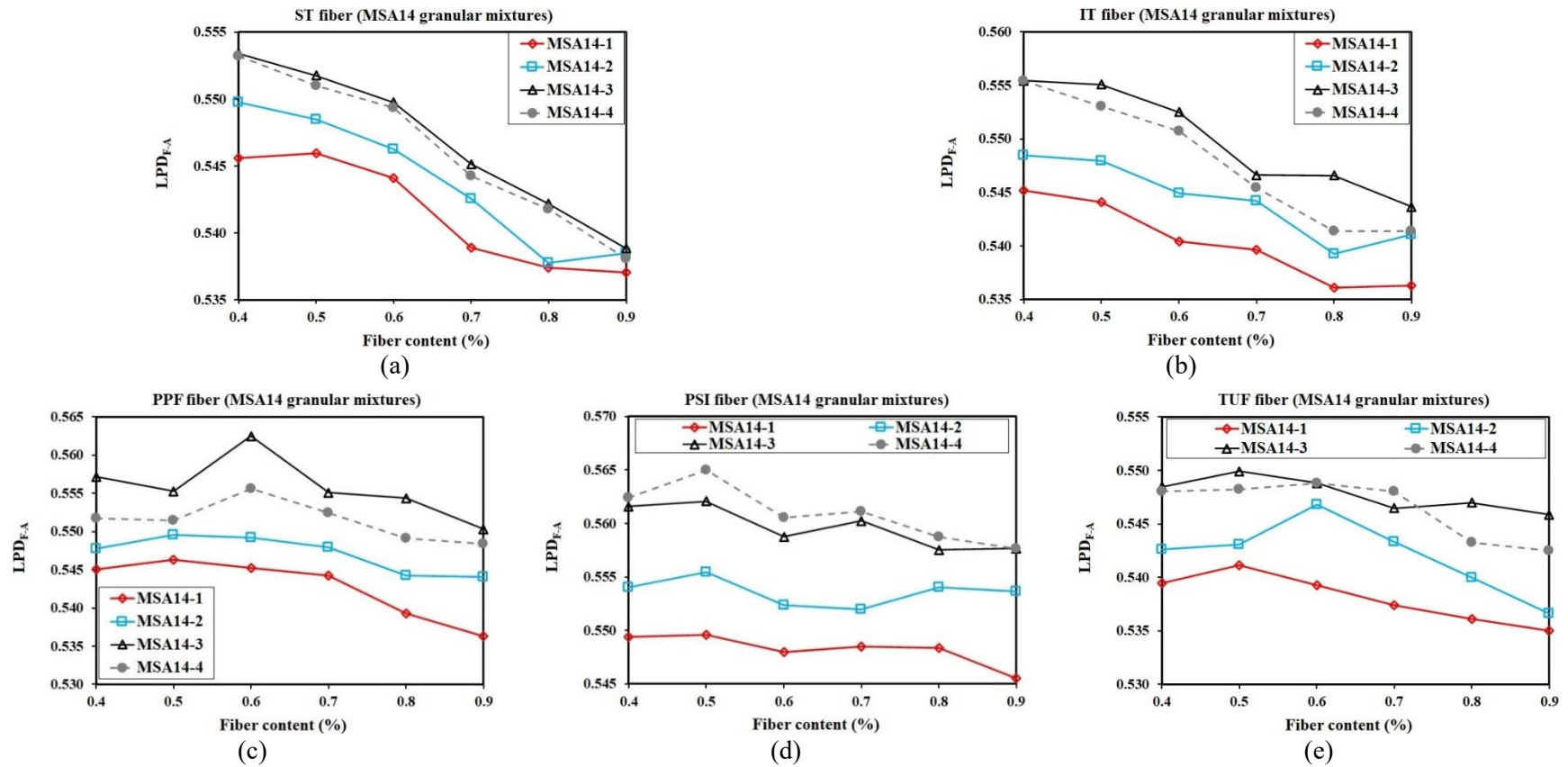
Figure 5-4 Variation of LPD of F-A mixtures with synthetic fiber volume for: (a) ST, (b) IT, (c) PPF, (d) PSI, and (e) TUF fibers with MSA14 coarse aggregate mixtures.

(a)   (b)
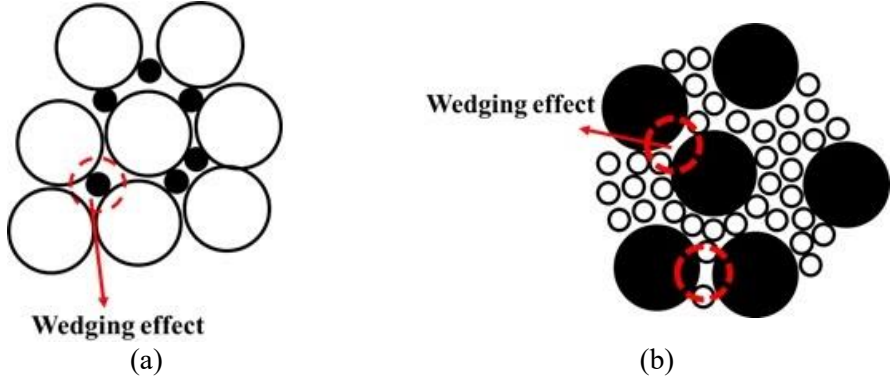
Figure 5-5 Wedging effect in (a) coarser and (b) finer PSD of aggregate [15].

On the other hand, when the content of finer particles is high, adding coarser aggregate may lead to create interparticle voids due to wall effect, which are not large enough to be filled with finer aggregate. This can result in lower packing density (Figure 5-5b). In the case of F-A combination, fibers can be cross-sectionally and longitudinally placed between aggregate, as illustrated in Figures 5-6a and 5-6b, respectively.

(a)   (b)
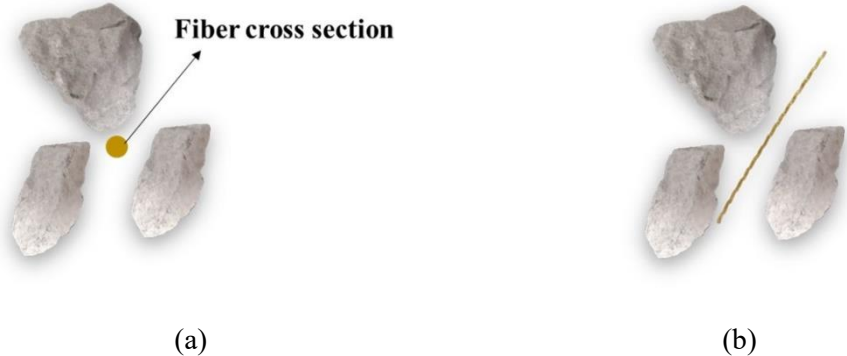
Figure 5-6 (a) Cross-sectional and (b) longitudinal placement of fibers between aggregate.

Accordingly, the packing density of F-A mixture can decrease due to the wedging effect of fibers' cross section, especially when incorporated at higher content than the optimum one, and loosening effect of finer aggregate (Figure 5-7a). On the other hand, in the presence of finer aggregate (Figure 5-7b), the packing density of F-A combination can decrease because of wedging effect of longitudinally oriented fibers and wall effect of coarser particles.
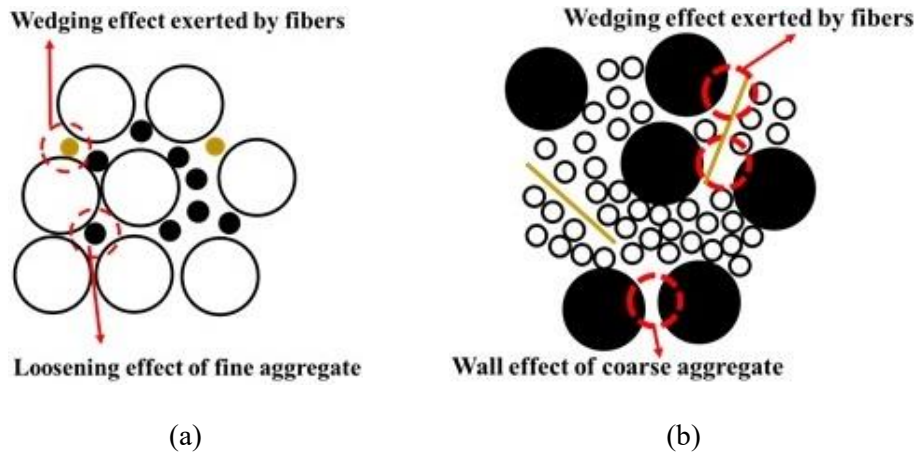
Figure 5-7 Decreasing packing density of fiber-aggregate skeleton due to wedging effect in the mixtures, including (a) coarser and (b) finer particles.

As can be observed in Figures 5-4a and 5-4b, the incorporation of polyolefin synthetic fibers (IT and ST) reduced the LPD of the investigated F-A mixtures. It can be explained by the fact that addition of polyolefin fibers beyond a certain content can increase the fiber-coarse aggregate interaction, thus leading to potential formation of fiber clumping. This can cause non-uniform fiber distribution throughout the F-A matrix, hence decreasing the LPD. On the other hand, increasing the PPF fiber content from 0.4% to 0.6% and 0.9% resulted in 1% increase and 2.1% decrease, respectively, in the LPD of F-A mixtures proportioned with MSA14-3 coarse aggregate mixture. It is worthy to mention that the accuracy of the PD measurements was evaluated using the coefficient of variation (COV_{PD}) of the PD values of three trial samples for each coarse aggregate mixture (Table 5-1) and F-A mixture (Figures 5-3 and 5-4), as follows:

$$COV_{PD} \ (\%) = \frac{SD_{PD}}{AVG_{PD}} \times 100\% \qquad\qquad \text{Equation 5-1}$$

where SD_{PD} and AVG_{PD} are the standard deviation and average of PD values of three samples for each coarse aggregate and F-A mixture, respectively. According to the carried-out error analyses, COV_{PD} values of the investigated coarse aggregate mixtures (PD_A values in Table 5-1) and F-A mixtures proportioned with macro-steel (Figures 5-3a and 5-3c), micro-steel (Figures 5-3b and 5-3d), ST (Figure 5-4a), IT (Figure 5-4b), PPF (Figure 5-4c), PSI (Figure 5-4d), and TUF (Figure 5-4e) fibers ranged from 0 to 0.10%, 0 to 0.31%, 0 to 0.28%, 0.03% to 0.16%, 0 to 0.24%, 0.03% to 0.13%, 0 to 0.21%, and 0.03% to 0.10%, respectively. It can be concluded that measurement errors are negligible compared to the reported PD values (low COV_{PD} values).

In loose state (i.e., without any compaction), adding fibers can change the arrangement of aggregate in F-A matrix depending on their size and volumetric content. Accordingly, the LPD of the coarse aggregate mixtures is compared to those incorporating different fiber contents. The PD of aggregate in F-A mixtures was evaluated, as follows:

$$\text{PD of aggregate in F-A mixture} = \frac{V_{Agg}}{V_{Total} = \pi \times r^2 \times h} \qquad \text{Equation 5-2}$$

where V_{Agg} and r correspond to the volume of coarse aggregate and radius of tested samples (50 mm), respectively, while h is the height of the sample at the end of PD measurements. The effect of fibers on PD of aggregate was then evaluated, as follows:

$$\text{Effect of fibers on PD of aggregate} = \frac{\text{PD of Agg in F-A mixture} - \text{PD}_{Agg}}{\text{PD}_{Agg}} \times 100\% \qquad \text{Equation 5-3}$$

where "PD_{Agg}" is the PD of the investigated coarse aggregate mixtures (Table 5-1) without any fibers (i.e., $V_f = 0$). The changes in PD of aggregate in F-A mixture, obtained using Equation 5-3, are plotted against the volumetric contents of the steel and synthetic fibers in Figures 5-8 and 5-9, respectively. As shown earlier, the COV_{PD} values of the PD_{Agg} measurements ranged from 0 to 0.10% which are negligible compared to the values reported in Figures 5-8 and 5-9. Hence, this can confirm the validity of the evaluated results of fiber effect on PD of coarse aggregate, presented in Figures 5-8 and 5-9.

As can be observed in Figure 5-8, increasing the steel fiber content up to an optimum value can increase the PD of coarse aggregate in F-A mixtures relative to those of the coarse aggregate mixtures without fibers. However, adding higher fiber content than the optimum value negatively affects PD of coarse aggregate. This can be due to the wedging effect of fiber on packing density of coarse aggregate skeleton (Figure 5-7). On the other hand, increasing synthetic fiber' content led to decrease in PD of coarse aggregate, as shown in Figure 5-9.

As can be observed in Figures 5-8 and 5-9, the incorporation of micro steel and PP fibers led to lower negative effect on PD of coarse aggregate compared to those obtained for F-A mixtures containing macro steel and polyolefin fibers. In order to explain this phenomenon, the DPD of different fibers were measured, using the ICT device and testing procedure explained earlier (i.e., under 50 gyratory cycles and 20 kPa normal pressure). As summarized in Table 5-4, the maximum DPD of fibers was found for PSI polypropylene fibers which also showed the higher LPD of F-A, as indicated in Figure 5-4. Moreover, micro steel and PP fibers exhibited higher DPD values than macro steel and polyolefin ones, respectively. This suggests that micro steel and PP fibers can achieve higher level of compaction within the voids of a given PSD of aggregate compared to those obtained for the macro steel and polyolefin ones. It is also worth mentioning that relatively low DPD of fibers can be due to their rod shapes. It can be concluded that the packing density of F-A mixture is a function of both fibers and aggregate characteristics in terms of fiber content, type, and PD of fibers, as well as the mean diameter of interparticle voids which directly depends on the PSD of aggregate.

Table 5-4 DPD of fibers obtained using ICT device.

Fiber type	Steel fibers		Polypropylene fibers		Polyolefin fibers		
	Macro	Micro	PPF	PSI	TUF	IT	ST
PD	0.065	0.068	0.106	0.204	0.081	0.064	0.076

(a)   (b)

(c)   (d)
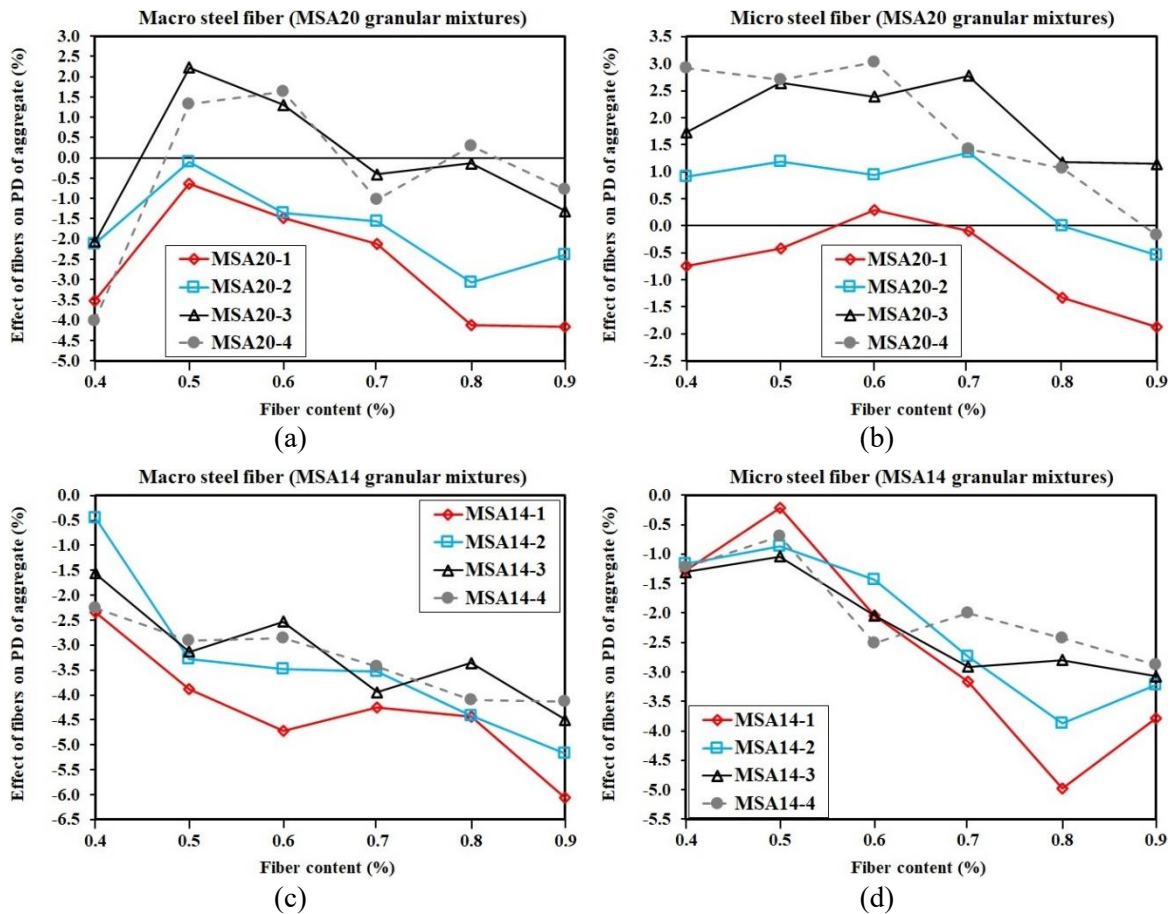
Figure 5-8 Effect of fiber content on packing density of coarse aggregate in F-A mixtures proportioned with (a, b) MSA20 and (c, d) MSA14 coarse aggregate mixtures, as well as (a, c) macro and (b, d) micro steel fibers.
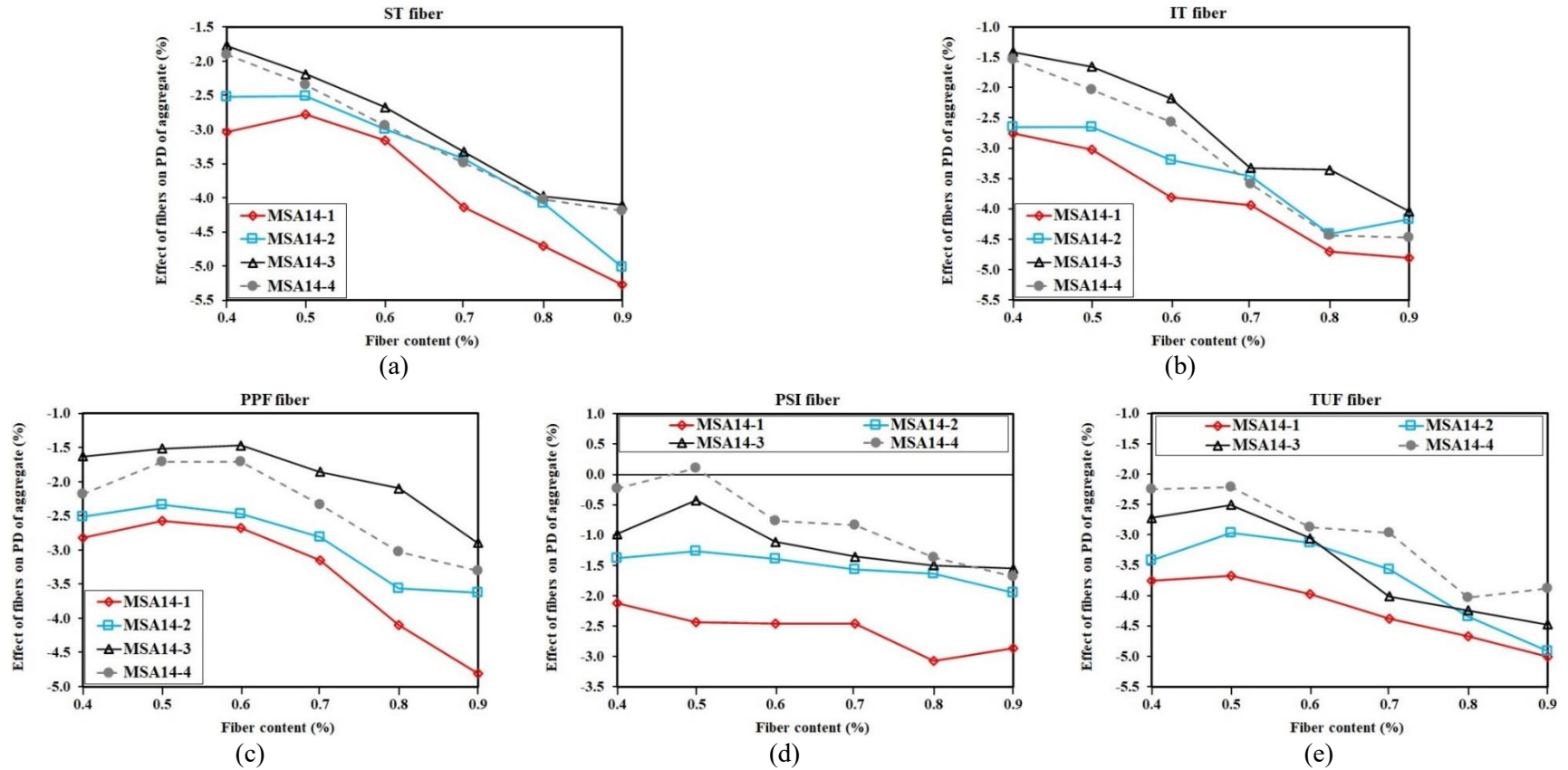
Figure 5-9 Effect of fiber content on PD of coarse aggregate in F-A mixtures proportioned with MSA14 coarse aggregate mixtures and synthetic fibers, including (a) ST, (b) IT, (c) PPF, (d) PSI, and (e) TUF fibers.

5.3.2 Effect of fiber size on LPD of the investigated F-A mixtures

As explained earlier, the LPD of F-A mixtures are dependent only on the size (length L_f and diameter D_f) of the fibers rather than their rigidity. This is reflected by non-deformed fibers after four gyratory-cycles compaction. In order to evaluate this effect, the LPD of the F-A mixtures containing relatively small and larger fibers were compared. Accordingly, for a given PSD of coarse aggregate mixture and fiber content, the LPD values obtained for the micro steel (L_f of 13 mm and D_f of 0.2 mm) and PPF fibers (L_f of 38 mm and D_f of 0.39 mm) were compared to those obtained with the macro steel (L_f of 30 mm and D_f of 0.55 mm) and TUF fibers (L_f of 38 mm and D_f of 0.69 mm), respectively, as shown in Figure 5-10.
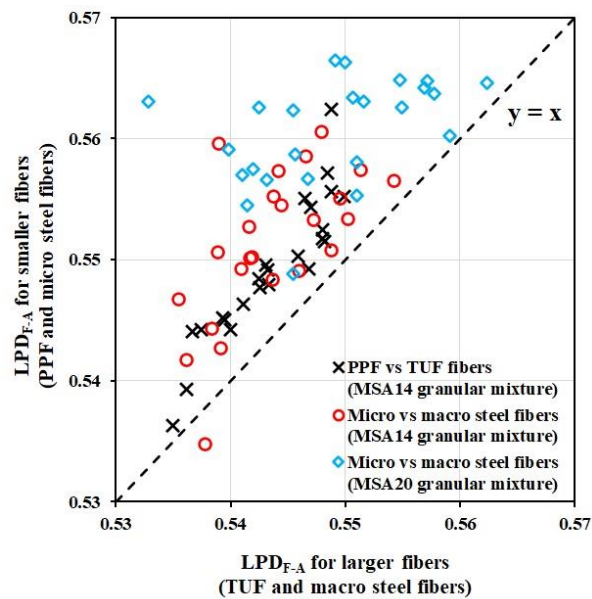
Figure 5-10 Comparison between LPD of F-A mixtures made with given
PSDs of coarse aggregate and fiber contents and different fibers' sizes
(PPF, micro steel fibers, TUF, and macro steel fibers).

As can be observed in Figure 5-10, for a given PSD of coarse aggregate, decreasing the fiber size (i.e., lower L_f and D_f) led to higher LPD of F-A mixtures. In loose state, the shorter and thinner fibers can properly fill the interparticle voids (Figure 5-11a) and, therefore, increase the LPD of the F-A mixtures. However, the longer and thicker fibers can push away aggregate particles and lower the LPD of F-A mixture (Figure 5-11b). For example, for a fiber volume of 0.5% and PSD of MSA20-4, increasing D_f and L_f of steel fibers from 0.20 to 0.55 mm and 13 to 30 mm decreased the LPD values of the F-A mixtures from 0.566 to 0.523, respectively.

(a) Small fibers   (b) Large fibers
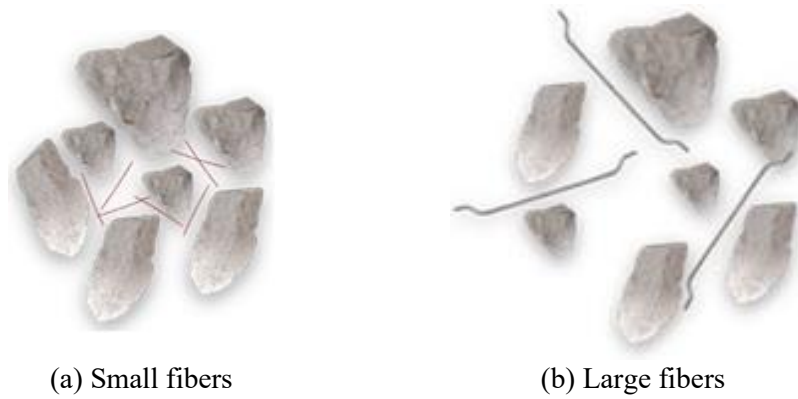
Figure 5-11 Negative effect of increasing fiber size on LPD of F-A mixtures.

5.3.3   Effect of fiber rigidity on DPD of the investigated F-A mixtures

In transition from the loosely- to densely-packed PD states, the compaction energy can lead to deform the fibers through the interparticle voids, depending on their rigidity. Therefore, the variation of PD of the investigated F-A mixtures from LPD to DPD state can reflect the effect of fibers' rigidity on PD of the F-A mixtures (Figure 5-12), for a given PSD of coarse aggregate mixtures.
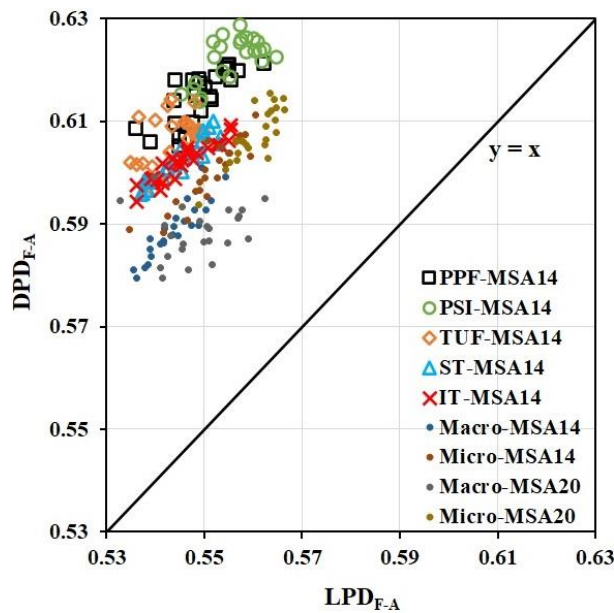
Figure 5-12 Comparison between the DPD and LPD values of
the investigated F-A mixtures.

As expected, the DPD values of the F-A mixtures obtained after 50 gyratory cycles are higher than their corresponding LPD values after four gyratory cycles (Figure 5-12). This is due to more deformation of the fibers under higher numbers of gyratory cycles, hence lowering the interparticle distances and increasing the PD. The deformation (y) of a single fiber located between two individual aggregate with an interparticle distance L_f (fiber length) and subjected to a compaction force F can be estimated, as shown in Figure 5-13a and Equation 5-4:

$$\text{Fiber deformation: } y \propto \frac{F \times L_f^3}{E \times I} \qquad\qquad \text{Equation 5-4}$$

where E and I are the modulus of elasticity and second moment of area of fiber's cross section, respectively. Therefore, for a given PSD of aggregate (i.e., given apparent interparticle distance L_f) and given compaction energy (i.e., given F), the fiber deformation (y) depends mainly on the rigidity of the fibers, which can be characterized by E × I. The variations of the DPD-to-LPD ratios of the investigated F-A mixtures with their corresponding fibers' rigidity indices (E×I) are shown in Figure 5-13b. The increase in fiber rigidity led to lower relative increase in DPD of the F-A mixtures compared to their corresponding LPD values. This is due to lower deformation of more rigid fibers under a given number of gyratory cycles. More specifically, F-A mixtures containing synthetic flexible fibers exhibited higher DPD-to-LPD ratios compared to those proportioned with rigid steel fibers. The maximum DPD-to-LPD ratio was obtained for the most flexible fibers of polypropylene PPF and TUF. As an illustrative example, the deformation of the micro- and macro-steel fibers are presented in Figures 5-14a and 5-14b, respectively. The application of 50 gyratory cycles resulted in lower deformation of macro fibers (1.6 mm / 13.4 mm = 12%) compared to that obtained for the micro fibers (1 mm / 6.5 mm = 15%). This can be attributed to the higher relative rigidity of the macro fibers compared to the micro fibers.

(a)   (b)
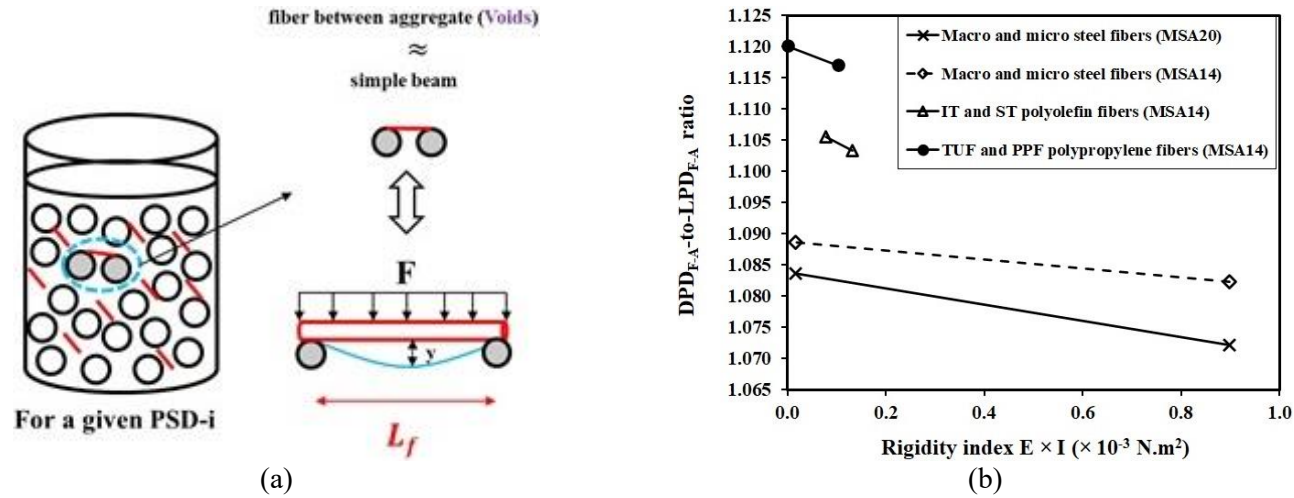
Figure 5-13 (a) Fiber deformation between aggregate and (b) variation of the DPD-to-LPD ratios of the investigated F-A mixtures versus fibers' rigidity index (E×I).

(a)   (b)
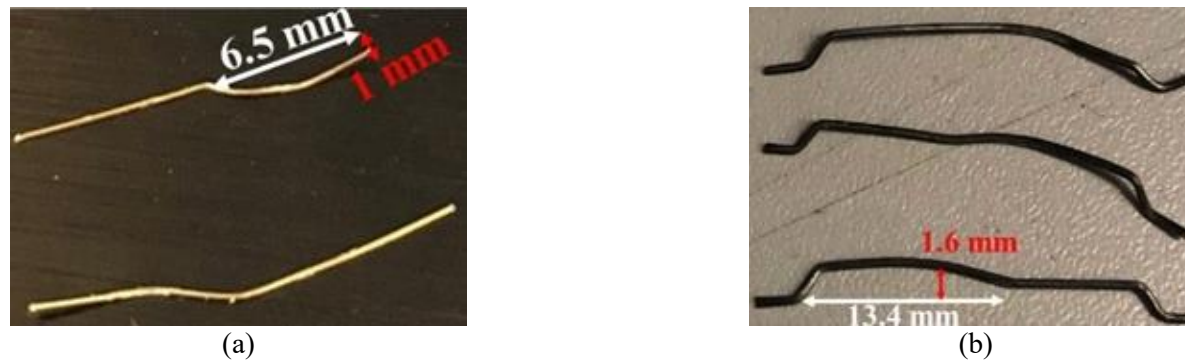
Figure 5-14 Comparison between the deformations of (a) micro- and (b) macro-steel fibers under 50 gyratory cycles and given PSD of coarse aggregate mixture.

5.3.4 Effect of PSD of coarse aggregate skeleton on LPD of the investigated F-A mixtures

In addition to fibers, LPD of F-A mixtures is influenced by aggregate characteristics. Adding a given content and type of fiber to fine and coarse PSD of aggregate can lead to opposite effects on PD of F-A mixtures. Adding fibers to a densely-packed granular mixture of finer PSD can push away the aggregate and decrease the LPD of F-A mixtures. On the other hand, in the case of a loosely-packed granular mixture of coarser PSD, fibers can fit easily in the large interparticle voids and increase the LPD of F-A mixtures.

In order to evaluate the effect of coarse aggregate on LPD of F-A mixtures, the investigated coarse aggregate mixtures were characterized in terms of their mean diameter (D_A) and mean 3D-surface area-to-volume ratio (AV_A) (Table 5-1). As shown in Figure 5-15, the incorporation of a given fiber content of 0.5% to coarser granular mixtures (i.e., higher D_A) resulted in higher LPD of F-A mixtures.
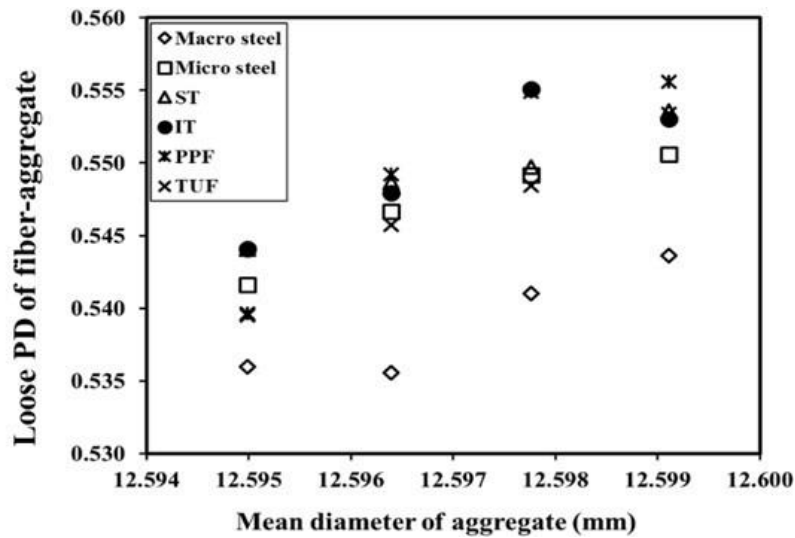
Figure 5-15 Effect of mean diameter of coarse aggregate DA on LPD
of F-A mixtures.

On the other hand, the mean diameter of voids (D_v) was calculated as the ratio of voids' volume ($V_v = 1 - LPD_{F-A}$)-to-the 3D surface area of aggregate in unit volume of F-A (A_A), as follows:

$$D_v = \frac{V_v}{A_A} = \frac{1 - LPD_{F-A}}{V_A \times AV_A} = \frac{1 - LPD_{F-A}}{(LPD_{F-A} - V_f) \times AV_A} \qquad \text{Equation 5-5}$$

where V_A and V_f are the volumetric contents of coarse aggregate and fibers in a unit volume of F-A mixture, respectively. The increase of D_v between aggregate particles leads to more available space for the fibers to be deformed under compaction, hence increasing the DPD of the F-A mixtures. As an example, illustrated in Figure 5-16, the F-A mixtures proportioned with 0.6% and 0.9% of macro steel fiber and coarse aggregate mixtures MSA20-1 and MSA20-2 were compared, respectively. It is worthy to mention that without fiber, the coarse aggregate mixture MSA20-1 exhibited higher PD_A than MSA20-2 (Table 5-1). The fiber deformation after PD measurements was evaluated by the mean values of the ratio of the fiber deflections-

to-the total fiber length (in %) using image analysis (Figure 5-16). As can be observed in Figures 5-16b and 5-17a, larger mean diameter of voids D_v, obtained for lower LPD, resulted in higher fiber deformations after PD measurements, hence increasing the DPD of F-A mixtures (Figure 5-17b).

(a)   (b)

Figure 5-16 Deformed fibers after DPD measurements of F-A mixtures proportioned with (a) MSA20-1 and (b) MSA20-2 coarse aggregate mixtures.

(a)   (b)
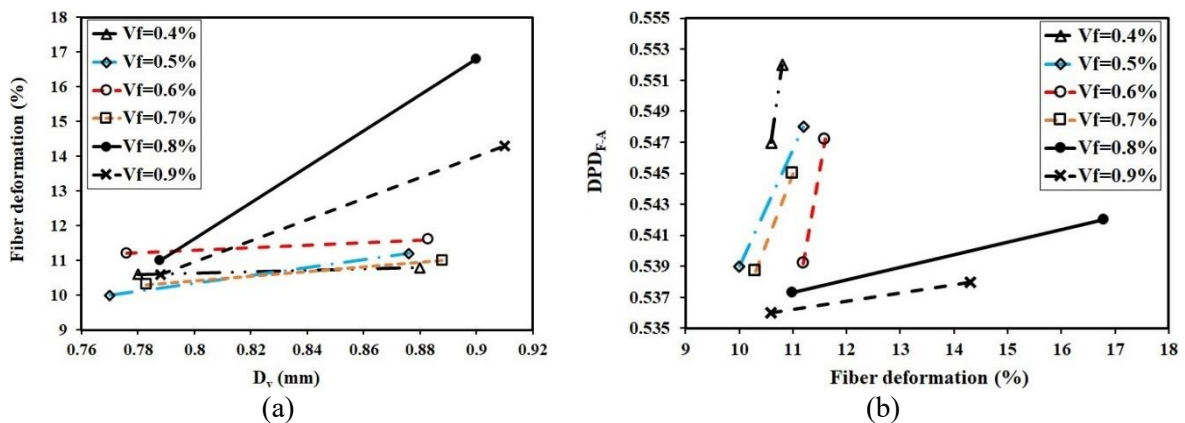
Figure 5-17 Effect of (a) mean diameter of voids Dv on fiber deformation and (b) fiber deformation on DPD of F-A mixtures proportioned with 0.6% and 0.9% macro steel fibers and coarse aggregate mixtures MSA20-1 and MSA20-2.

5.3.5 Coupled effect of fibre characteristics and coarse aggregate skeleton on PD of F-A mixtures

Given the above-mentioned observations, the coupled effect of characteristics of fibers, including volumetric content, size, and rigidity, as well as coarse aggregate skeleton, including average diameter and PD, on LPD and DPD of the investigated F-A mixtures are evaluated.

LPD model for F-A mixtures

As mentioned earlier (section 2.1), in order to investigate the LPD values, based on different PSD of coarse aggregates and fiber types and content, totally 160 F-A mixtures were prepared and tested. Then, as shown in Table 5-A.1 in Appendix, 126 F-A mixtures were selected randomly out of 160 mixtures to establish the LPD model, and the rest (34 F-A mixtures) were

used to validate this model (Table 5-A.2 in Appendix). It is worth mentioning that each F-A mixture has been entitled by an ID including: application (R for repair and P for precast application)-fiber type-fiber volume (%)-MSA of coarse aggregate-PSD code. An empirical model was established to evaluate the coupled effect of volumetric content (V_f), length (L_f), and diameter (D_f) of the fibers and the average diameter (D_A) and PD of the coarse aggregate (PD_A) on the LPD of F-A mixtures. In order to establish such model, the following conditions must be fulfilled:

(i) if $V_f = 0 \rightarrow LPD_{F-A} = PD_A$

(ii) Based on Figure 5-10: Higher $D_f \rightarrow$ Lower LPD_{F-A} values are expected.

(iii) Based on Figure 5-15: Higher $D_A \rightarrow$ Higher LPD_{F-A} values are expected.

Since any direct positive or negative effect of PD of aggregate on LPD_{F-A} values was not observed, a polynomial contribution was considered for PD_A values. This can lead to identify the optimum PD of coarse aggregate allowing higher LPD_{F-A} values. Regarding the first abovementioned condition (i), the contribution of PD_A values in the established model was assumed to be raised to the power of V_f contribution. A power law contribution was also considered for the V_f. Moreover, the effect of fibers on the LPD_{F-A} was taken into account by considering a product of power-law contributions of their content (V_f), diameter (D_f), and length (L_f) values, fulfilling the second abovementioned condition (ii). Furthermore, a power law contribution of D_A was considered in the established model, referring to the third condition (iii). Accordingly, the following pattern was applied in a Microsoft Excel solver to evaluate the coupled effect of characteristics of fibers and aggregate on LPD_{F-A} values:

$$LPD_{F-A} = \frac{\left(A' \times PD_A{}^{B'} + C' \times PD_A + D'\right)^{\left(V_f{}^{E'}\right)} \times \left(1 - V_f{}^{F'}\right)}{1 + V_f{}^{G'} \times \left(\frac{D_f}{D_A}\right)^{H'} \times L_f{}^{I'}} \times PD_A{}^{\left(J'{}^{V_f}\right)} \qquad \text{Equation 5-6 (}R^2 = 0.889\text{)}$$

The following correlation was then established using the 126 selected F-A mixtures (Table 5-A.1 in Appendix):

$$LPD_{F-A} = \frac{\left(1.9543 \times PD_A{}^{1.0812} - 0.0003 \times PD_A - 0.0170\right)^{\left(V_f{}^{0.0045}\right)} \times \left(1 - V_f{}^{146.4166}\right)}{1 + \frac{V_f{}^{0.4662} \times \left(\frac{D_f}{D_A}\right)^{0.1782}}{L_f{}^{0.0039}}} \\ \times PD_A{}^{\left(0.8105^{V_f}\right)} \qquad \text{Equation 5-7 (}R^2 = 0.889\text{)}$$

It is worth noting that the established correlation covers a wide range of fiber contents (0.40% to 1.77%) and types, including polypropylene (PPF and TUF), polyolefin (IT and ST), and steel (macro and micro) fibers of different sizes. This also includes a wide range of PSD of the coarse aggregate mixtures (Table 5-1). As shown in Figure 5-18a, the experimental LPD values of the 126 selected F-A mixtures (Table 5-1.A in Appendix) were compared to those obtained using the empirical correlation given in Equation 5-7. The accuracy of the established correlation was evaluated using the correlation coefficient (R^2) and the root-mean-square error (RMSE) defined in Equation 5-8.

$$RMSE = \sqrt{\frac{\sum_{i=1}^{N}\left(LPD_{F-A-Experimental-i} - LPD_{F-A-Theoretical-i}\right)^2}{N}} \qquad \text{Equation 5-8}$$

where N = 126 is the number of the investigated F-A mixtures to establish the empirical correlation Equation 5-7. As can be observed in Figure 5-18a, the predicted LPD values are in good agreement with their corresponding experimental ones (high R^2 of 0.889 and low RMSE of 0.0029).

As shown in Figure 5-18b, the established correlation given by Equation 5-7 was validated using 34 additional F-A mixtures (Table 5-2.A in Appendix). The proposed loose PD model is shown to predict well the loose PD values of the F-A mixtures with high R^2 of 0.845 and low RMSE of 0.0026. According to the obtained adjustment factors (A′-J′) in Equation 5-7, the PD of coarse aggregate (PD_A) and fiber content (V_f) showed the most dominant effects on LPD of F-A mixtures. Moreover, the effects of PD_A and V_f on LPD of F-A mixtures were found to be interdependent. Furthermore, among the size characteristics, diameter of fiber (D_f) and coarse aggregate (D_A) showed more significant effect than fiber length (L_f).

DPD model for F-A mixtures

As explained earlier, when the F-A mixture with a given LPD is compacted, the rigidity of fibers can negatively affect the DPD state. A Microsoft Excel solver was established to evaluate the effect of fiber rigidity on DPD of F-A mixtures (DPD_{F-A}) compared to their LPD_{F-A} values. The following empirical model was established using 127 F-A mixtures which were randomly selected among 156 F-A mixtures made with 0.4% to 1.77% fiber volume using rigid (macro and micro steel) and semi-rigid (IT and ST polyolefin) fibers, as well as eight different PSD coarse aggregate mixtures described in section 2.1 (Table 5-A.3 in Appendix). The remained 29 F-A mixtures (out of 156) in addition to 71 F-A mixtures that were taken from two lateral sections of the investigated the L-Box and T-Box tests, were then used to validate the DPD model (Table 5-A.4 in Appendix). It is worth mentioning that each F-A mixtures has been entitled by an ID including: application (R for repair and P for precast application)-volume of paste (%) of FR-SCC mixture-fiber type-fiber volume (%)-MSA of coarse aggregate-PSD code-the set-up where the sample has been extracted from (L for L-Box and T for T-Box)-sampling zone of each test (E for end and B for beginning of L-Box set-up, as well as U for tilt-up and D for tilt-down zones of T-Box set-up).

$$\text{DPD}_{F-A} = 1.0546 \times \frac{\text{LPD}_{F-A}{}^{0.9204}}{E^{0.0066} \times I^{0.0019}} \qquad \text{Equation 5-9 } (R^2 = 0.910)$$

where E and I are in GPa and mm^4, respectively. As can be observed in Figure 5-19a, the DPD_{F-A} values predicted using the empirical correlation given in Equation 5-9 ($DPD_{F-A-Theoretical}$) for the 127 F-A mixtures are in good agreement with their corresponding experimental values ($DPD_{F-A-Experimental}$), with high R^2 of 0.910 and low RMSE of 0.0033. According to the obtained adjustment power indices in Equation 5-9, it can be concluded that the LPD of the F-A mixtures dominantly control their DPD, which is itself dependent on various characteristics of fibers and coarse aggregate (Equation 5-7). Moreover, the rigidity of fibers had a negative effect on the DPD of F-A mixtures, reflected by E and I. Furthermore, the modulus of elasticity of fibers E showed more dominant effect on the DPD of the F-A mixtures compared to their second moment of area of fibers' cross section I (adjustment power index 0.0066 vs 0.0019).

As explained earlier in section 2.1, the established model defined in Equation 5-9 was validated for 100 selected F-A mixtures (Table 5-A.4 in Appendix). Accordingly, the experimental and

predicted DPD values, obtained using empirical Equation 5-9 for 100 F-A mixtures (Table 5-A.4 in Appendix) are compared in Figure 5-19b. The results indicated that the established model can successfully predict the DPD of the selected F-A mixtures with high R^2 of 0.928 and low RMSE of 0.015.
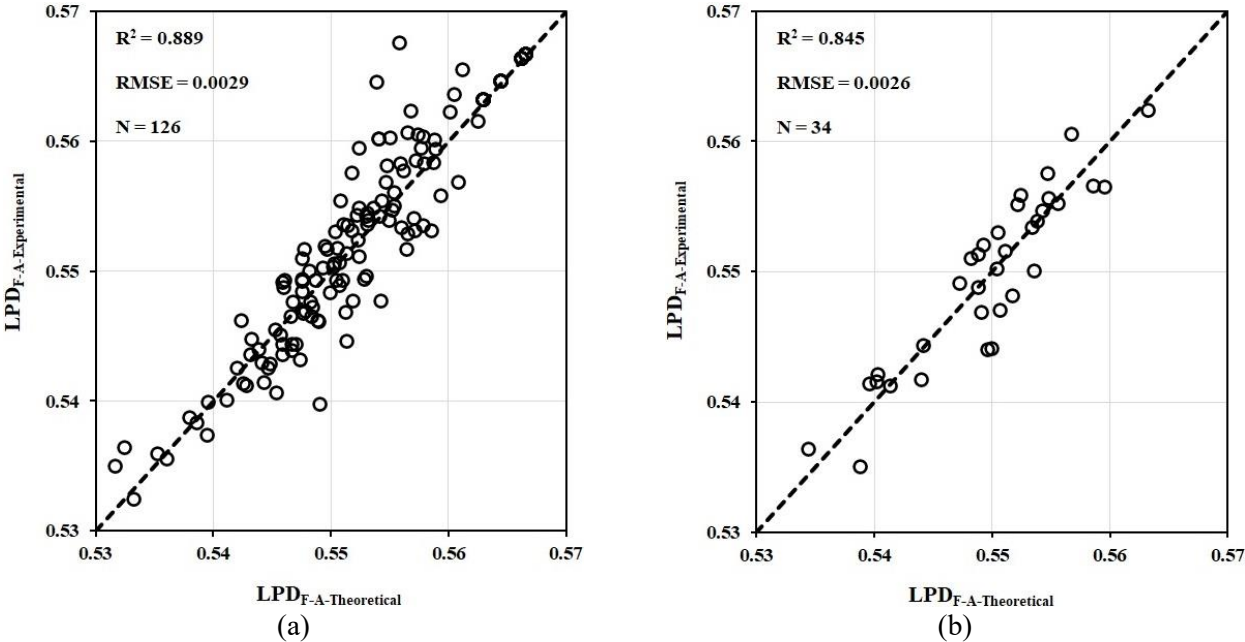
Figure 5-18 (a) Comparison between the experimental and predicted LPD of the investigated F-A mixtures (Table 5-A.1 in Appendix) and (b) validation of LPD model for F-A mixtures (Table 5-A.2 in Appendix).
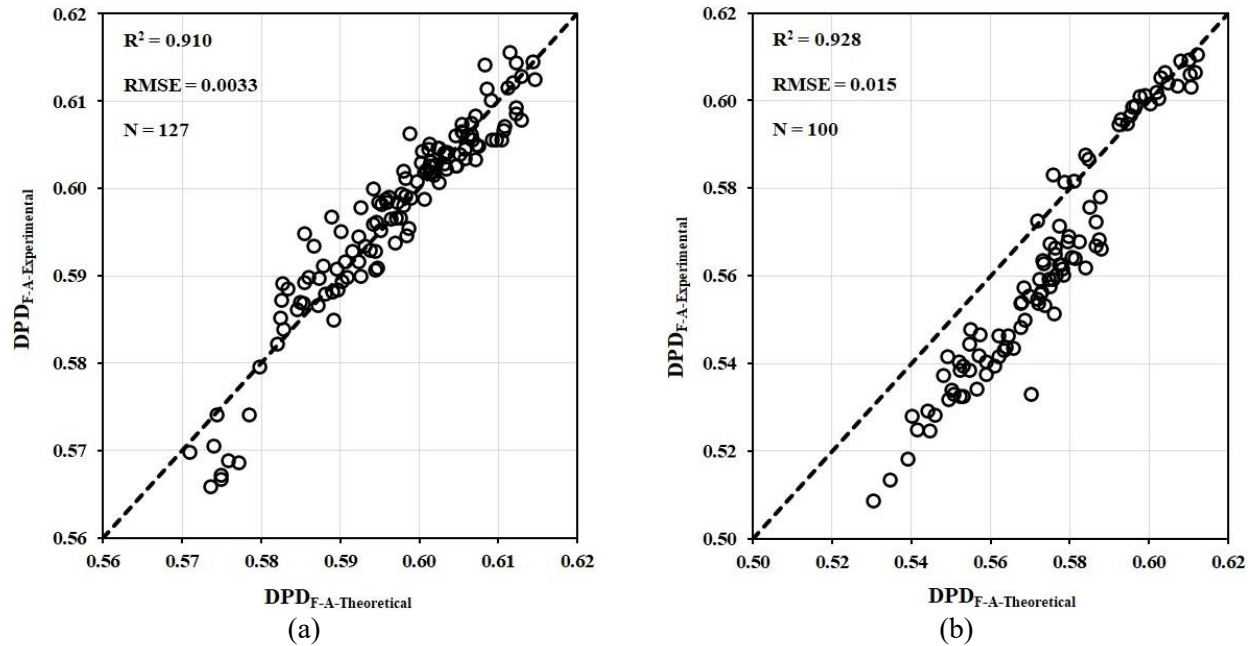
Figure 5-19 (a) Comparison between experimental values of the DPD of the F-A mixtures (Table 5-A.3 in Appendix) and those obtained using the empirical correlation (Equation 5-9) and (b) validation of the established DPD model (Equation 5-9) to predict the DPD of F-A mixtures (Table 5-A.4 in Appendix).

Robustness of LPD and DPD models to variations in the F-A mixture components

The robustness of LPD and DPD values to small variations of F-A mixture parameters, including the PD (PD_A) and mean diameter (D_A) of the coarse aggregate, as well as diameter (D_f), length (L_f), volume (V_f), and rigidity (E and I) of the fibers was investigated. Accordingly, a variation of ±5% was considered for the effective parameters of the LPD (Equation 5-7) and DPD (Equation 5-9) models.

In the case of LPD values, 1-, 2-, 3-, 4-, and 5-way robustness analyses, corresponding to single, double, triple, quadruple, and quintuple variations of the PD_A, D_A, D_f, L_f, and V_f parameters, were applied. Using the established correlation Equation 5-7, the LPDs of the F-A mixtures proportioned with fibers and coarse aggregate having characteristics with ±5% relative variations to those of the investigated F-A mixtures used to develop Equation 5-7 were evaluated. On the other hand, in the case of DPD values, the single, double, and triple ±5% variations of LPD_{F-A}, E, and I parameters were considered. Accordingly, using the established Equation 5-9, the DPDs of the F-A mixtures, considering ±5% variations of LPD_{F-A}, as well as E and I of fibers of the investigated mixtures, used to develop Equation 5-9, were calculated. In order to evaluate the robustness of the PD values of F-A mixtures, the variations in the RMSE (ΔRMSE) and coefficients of determination ($ΔR^2$) of the LPDs and DPDs of the F-A mixtures, due to single and multiple ±5% variations of the corresponding parameters, relative to those obtained for the investigated F-A mixtures, presented in Figures 5-18a and 5-19a, were calculated as follow:

$$\Delta RMSE = RMSE_{\text{with variations}} - RMSE_{\text{without variations}} \qquad \text{Equation 5-10}$$

$$\Delta R^2 = R^2_{\text{with variations}} - R^2_{\text{without variations}} \qquad \text{Equation 5-11}$$

where $RMSE_{\text{without variations}}$ (0.0029 and 0.0033) and $R^2_{\text{without variations}}$ (0.889 and 0.910) are the RMSE and R^2 values obtained for the LPD and DPD values using Equations 5-7 and 5-9 and presented in Figures 5-18a and 5-19a, respectively. The results of the robustness analyses of the LPD and DPD values are summarized in Table 5-5.

As indicated in Table 5-5, the LPD of F-A showed its maximum robustness due to any single, double, triple, and quadruple ±5% variations of volume, length, and diameter of fibers, as well as mean diameter of coarse aggregate. This was reflected by low $|\Delta RMSE|$ and $|\Delta R^2|$ values up to 0.0008 and 0.0653, respectively. On the other hand, the most sensitivity of the LPD values of F-R mixtures were observed due to any single and multiple ±5% variations of PD of coarse aggregate skeleton, reflected by increasing RMSE up to higher 0.051956 values and decreasing R^2 values up to lower 0.8893 values.

As can be observed in Table 5-5, the DPD values of F-A mixtures showed their maximum robustness due to rigidity of fibers, reflected by any single and double ±5% variations in E and I of fibers (low $|\Delta RMSE|$ and $|\Delta R^2|$ values up to 0.000031 and 0.0001, respectively). However, the most sensitivity of the DPD values were observed for any ±5% variations of LPD of the F-A mixtures, reflected by high ΔRMSE values up to 0.024704.

Table 5-5 Results of the robustness analyses carried out on the LPD of F-A mixtures.

Model	Robustness analysis method	Variations of the effective parameters								Precision		Robustness analysis results	
		PD_A	D_f	L_f	V_f	D_A	E	I	LPD_{F-A}	RMSE	R^2	ΔRMSE	ΔR^2
LPD – Equation 5-7	1-way	±5%	-	-	-	-	-	-	-	0.0512 - 0.0537	0.0013 - 0.6933	0.048335 - 0.050850	(-0.8881) - (-0.1960)
		-	±5%	-	-	-	-	-	-	0.0028 - 0.0029	0.8891 - 0.8896	0.000005 - 0.000013	(-0.000268) - (0.000220)
		-	-	±5%	-	-	-	-	-	0.0027 - 0.0028	0.8893 - 0.8894	(-0.0000001) - (0.0000001)	(-0.0000055) - (0.0000052)
		-	-	-	±5%	-	-	-	-	0.00294 - 0.00295	0.8886 - 0.8898	0.000049 - 0.000067	(-0.00077) - (0.00041)
		-	-	-	-	±5%	-	-	-	0.0028 - 0.0029	0.8891 - 0.8896	0.000005 - 0.000014	(-0.000283) - 0.000211
	2-way	±5%	±5%	-	-	-	-	-	-	0.0510 - 0.0539	0.0006 - 0.6935	0.048132 - 0.051101	(-0.8888) - (-0.1959)
		±5%	-	±5%	-	-	-	-	-	0.0512 - 0.0537	0.0012 - 0.6933	0.048331 - 0.050855	(-0.8881) - (-0.1960)
		±5%	-	-	±5%	-	-	-	-	0.0507 - 0.0544	0.00005 - 0.6935	0.047824 - 0.051472	(-0.8893) - (-0.1959)
		±5%	-	-	-	±5%	-	-	-	0.0510 - 0.0540	0.0006 - 0.6935	0.048141 - 0.051089	(-0.8887) - (-0.1959)
		-	±5%	±5%	-	-	-	-	-	0.0028 - 0.0029	0.8891 - 0.8896	0.000005 - 0.000014	(-0.00027) - (0.00022)
		-	±5%	-	±5%	-	-	-	-	0.0029 - 0.0030	0.8882 - 0.8898	0.000017 - 0.000125	(-0.0012) - (0.00045)
		-	±5%	-	-	±5%	-	-	-	0.0028 - 0.0029	0.8887 - 0.8897	0 - 0.000046	(-0.0006) - (0.0004)
		-	-	±5%	±5%	-	-	-	-	0.0029 - 0.0030	0.8886 - 0.8898	0.000048 - 0.000068	(-0.00078) - (0.00041)
		-	-	±5%	-	±5%	-	-	-	0.0028 - 0.0029	0.8891 - 0.8896	0.000004 - 0.000015	(-0.00029) - (0.00021)
		-	-	-	±5%	±5%	-	-	-	0.0029 - 0.0030	0.8882 - 0.8898	0.000015 - 0.000128	(-0.0012) - (0.00045)
	3-way	±5%	±5%	±5%	-	-	-	-	-	0.0510 - 0.0540	0.00055 - 0.6935	0.048127 - 0.051106	(-0.8888) - (-0.1959)
		±5%	±5%	-	±5%	-	-	-	-	0.0515 - 0.0546	0.00002 - 0.6936	0.047625 - 0.051718	(-0.8893) - (-0.1958)
		±5%	±5%	-	-	±5%	-	-	-	0.0508 - 0.0542	0.0002 - 0.6936	0.047940 - 0.051338	(-0.8892) - (-0.1958)
		±5%	-	±5%	±5%	-	-	-	-	0.0507 - 0.0544	0.000043 - 0.6935	0.047820 - 0.051477	(-0.8893) - (-0.1959)
		±5%	-	±5%	-	±5%	-	-	-	0.0510 - 0.0540	0.0006 - 0.6935	0.048137 - 0.051094	(-0.8888) - (-0.1959)
		-	±5%	±5%	±5%	-	-	-	-	0.0029 - 0.0030	0.8882 - 0.8898	0.000016 - 0.000127	(-0.0012) - (0.0004)

		-	±5%	±5%	-	±5%	-	-	-	0.0028 - 0.0029	0.8887 - 0.8897	0 - 0.00005	(-0.0006) - (0.0004)
		-	-	±5%	±5%	±5%	-	-	-	0.0029 - 0.0030	0.8881 - 0.8898	0.000015 - 0.00013	(-0.0012) - (0.0004)
		-	±5%	-	±5%	±5%	-	-	-	0.0029 - 0.0031	0.8877 - 0.8898	0 - 0.0002	(0.0016) - (0.0004)
		±5%	-	-	±5%	±5%	-	-	-	0.0505 - 0.0546	0.000015 - 0.6936	0.047634 - 0.051706	(-0.8893) - (-0.1958)
		±5%	±5%	±5%	±5%	-	-	-	-	0.0505 - 0.0546	0.00002 - 0.6936	0.047621 - 0.051723	(-0.8893) - (-0.1958)
	4-way	±5%	±5%	±5%	-	±5%	-	-	-	0.0508 - 0.0542	0.00016 - 0.6936	0.047935 - 0.051343	(-0.8892) - (-0.1958)
		±5%	±5%	-	±5%	±5%	-	-	-	0.0503 - 0.0548	0.00005 - 0.6937	0.047437 - 0.051951	(-0.8893) - (-0.1957)
		±5%	-	±5%	±5%	±5%	-	-	-	0.0505 - 0.0546	0.000013 - 0.6936	0.047630 - 0.051711	(-0.8893) - (-0.1958)
		-	±5%	±5%	±5%	±5%	-	-	-	0.0029 - 0.0037	0.8240 - 0.8898	0 - 0.0008	(-0.0653) - (0.0004)
	5-way	±5%	±5%	±5%	±5%	±5%	-	-	-	0.0503 - 0.0548	0.00004 - 0.6937	0.047433 - 0.051956	(-0.8893) - (-0.1957)
DPD - Equation 5-9		-	-	-	-	-	±5%	-	-	0.0032 - 0.0033	0.9098 - 0.9099	-0.000011 - 0.000022	0.001
	1-way	-	-	-	-	-	-	±5%	-	0.0032 - 0.0033	0.9099 - 0.9100	-0.000005 - 0.000005	0.001
		-	-	-	-	-	-	-	±5%	0.0276 - 0.0277	0.9099 - 0.9100	0.024361- 0.024470	0.001
		-	-	-	-	-	±5%	±5%	-	0.0032 - 0.0033	0.9098 - 0.9098	-0.000012 - 0.000031	0.0001
	2-way	-	-	-	-	-	±5%	-	±5%	0.0271 - 0.0282	0.9098 - 0.9099	0.024162 - 0.024651	0.0001
		-	-	-	-	-	-	±5%	±5%	0.0276 - 0.0278	0.9098 - 0.9098	0.024302 - 0.024523	0.0001
	3-way	-	-	-	-	-	±5%	±5%	±5%	0.0274 - 0.0280	0.9098 - 0.9098	0.024103 - 0.024704	0.0001

5.4 New workability design for FR-SCC mixtures based on the established PD models of F-A combinations

Koura et al. [32] proposed a proportioning approach for SCC mixtures as a diphasic suspension of coarse aggregate (> 1.25 mm) and fine mortars (< 1.25 mm). The authors reported that in addition to the rheological properties of fine mortar, the flowability [32], passing ability [12,32], and stability [11,13], as well as compressive strength of SCC [32] are significantly influenced by the relative-solid packing fraction of coarse aggregate. This is defined as the ratio of volumetric content (φ)-to-PD of coarse aggregate (φ/φ_{max}) in unit volume of SCC. The authors established empirical models to predict the flow and mechanical performance of SCC as a function of rheological properties of fine mortar and φ/φ_{max} of coarse aggregate. For given volume and workability of mortar, the selection of an appropriate φ/φ_{max} of coarse aggregate can lead to achieve the targeted workability characteristics and mechanical performance [32]. A similar approach can be employed to proportion FR-SCC as a diphasic suspension of suspending mortar ($\leq$ 5 mm) and suspended fiber-coarse aggregate (F-A) mixtures (A > 5 mm). The following mixtures parameters are essential in designing FR-SCC mixtures: water-to-binder ratio (w/b), volume of paste (V_{paste}), air content (V_{air}), volumetric sand-to-total aggregate ratio (S), densities of fiber (ρ_f), binder (ρ_b), water (ρ_w), coarse aggregate (ρ_{CA}), and sand (ρ_{sand}), as well as the length (L_f), diameter (D_f) , second moment of area of cross section (I_f), and modulus of elasticity (E_f) of fibers, and mean-diameter (D_{CA}) and packing density (PD_{CA}) of coarse aggregate.

First, knowing the w/b, V_{paste}, V_{air}, ρ_b, and ρ_w parameters, the required volumetric contents and masses of binder (V_b and M_b) and water (V_w and M_w) can be calculated. Second, the total volume of the sand (V_{sand}), coarse aggregate (V_{CA}), and fiber (V_f) can then be calculated, as follow:

$$V_{sand} + V_{CA} + V_f = 1 - (V_b + V_w + V_{air}) \qquad \text{Equation 5-12}$$

By knowing S, the following relationship can then be established between the V_{sand} and V_{CA}:

$$\frac{V_{sand}}{V_{sand} + V_{CA}} = S \qquad \text{Equation 5-13}$$

On the other hand, according to the empirical models and guidelines proposed by Hosseinpoor et al. [11,12] and Koura et al. [13,32], an appropriate volumetric content-to-PD ratio φ/φ_{max} of fiber-coarse aggregate combination is selected to achieve given workability and compressive strength values. Moreover, the PD of fiber-coarse aggregate combination φ_{max} can be evaluated using the proposed LPD and DPD models in this study (Equations 5-7 and 5-9). Therefore, the following relationship can be established between V_{CA}, V_f, and characteristics of fiber and coarse aggregate:

$$\frac{(V_{CA} + V_f) \times E_f^{0.0066} \times I_f^{0.0019}}{1.0546 \times \left[\dfrac{\left(1.9543 \times PD_{CA}^{1.0812} - 0.0003 \times PD_{CA} - 0.0170\right)^{\left(\left(\frac{V_f}{V_f+V_{CA}}\right)^{0.0045}\right)} \times \left(1 - \left(\frac{V_f}{V_f+V_{CA}}\right)^{146.4166}\right) \times PD_{CA}^{\left(0.8105^{\left(\frac{V_f}{V_f+V_{CA}}\right)}\right)}}{1 + \frac{\left(\frac{V_f}{V_f+V_{CA}}\right)^{0.4662} \times \left(\frac{D_f}{D_{CA}}\right)^{0.1782}}{L_f^{0.0039}}} \right]^{0.9204}} = \frac{\varphi}{\varphi_{max}}$$

Equation 5-14

Three different Equations 5-12, 5-13, and 5-14 are then simultaneously solved to calculate the volumetric contents of coarse aggregate (V_{CA}), sand (V_{sand}), and fiber (V_f). Their corresponding masses M_{CA}, M_{sand}, and M_f can then be calculated knowing their densities. A schematic flowchart of the proposed proportioning approach of FR-SCC mixtures is presented in Fig. 5-20.
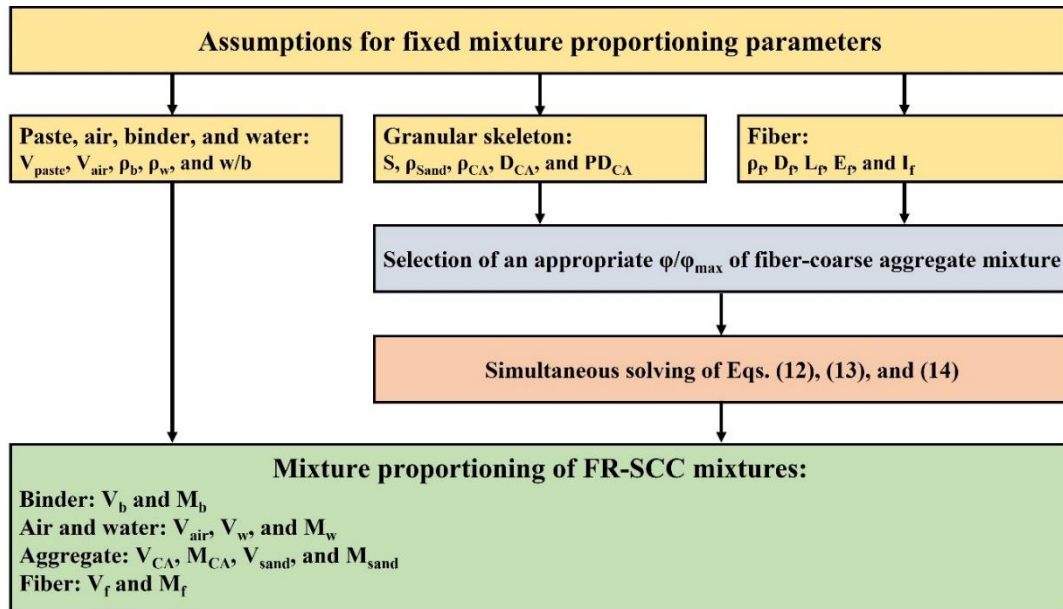
Figure 5-20 New proportioning approach of FR-SCC mixtures using the proposed models for the LPD and DPD of F-A combinations (Equations 5-7 and 5-9).

5.5 Conclusions

Understanding the coupled effect of fibers and coarse aggregate characteristics on packing density of F-A system in different compaction conditions can lead to better optimization of the performance of FR-SCC, in terms of workability and mechanical properties. In fact, enhancing the packing density of the solid skeleton, including fiber and aggregate, in FRC matrix can result in lowering the paste content for a given workability or increasing workability for a given paste content. In this study, the packing density of various fiber-coarse aggregate mixtures, under loosely- and densely-packed conditions, were investigated. Different levels of compaction was considered to simulate different packing condition during mixing and casting processes of FRC. Different types of fibers used at various volumetric contents, sizes, and rigidities, as well as different particle-size distributions of coarse aggregate were evaluated. Based on the experimental results reported in this study, two empirical models were proposed to predict the packing density of F-A mixtures in loosed and compacted conditions. The following conclusions can be established from this study:

- The loosely-packed PD (LPD) of F-A mixtures was found to be mostly affected by the volumetric content and size of the fibers, as well as the mean diameter and PD of the coarse aggregate.

- For a given PSD of coarse aggregate, the incorporation of steel and polypropylene fibers up to an optimum value resulted in higher LPD of F-A mixtures beyond which the LPD

decreased. This was found more significant for F-A mixtures proportioned with coarser PSD of granular skeleton and larger fibers. However, the incorporation of any volume of polyolefin fibers led to lower PD of aggregate compared to those obtained without any fiber.

- For a given PSD of coarse aggregate and fiber content, the incorporation of larger fibers resulted in lower LPD of the F-A mixtures. On the other hand, the incorporation of a given fiber volume to coarser PSD of coarse aggregate resulted in higher LPD of F-A mixtures.

- The densely-packed PD (DPD) of F-A mixtures were found to be more controlled by their PD in loosen state (LPD) and rigidity of the fibers. The F-A mixtures proportioned with more flexible fibers experienced higher DPD-to-LPD ratio comparing to the rigid fibers due to their higher deformation through the interparticle voids.

- Two new empirical models were proposed to predict the LPD and DPD of F-A mixtures as a function of the characteristics of the fibers and coarse aggregate skeleton. The LPD of the F-A mixtures were found in good correlations with volumetric content, length, and diameter of fibers, as well as the mean diameter and PD of coarse aggregate. The DPD of F-A mixtures were well correlated with modulus of elasticity and second moment of area of cross section of fibers, as well as their LPD values.

- Robustness analyses revealed that the LPD of F-A is quite sensitive to any variation of PD of the coarse aggregate skeleton which is directly dependent of PSD of coarse aggregate. However, the LPD values of F-A mixtures showed maximum robustness due to any single and multiple variations of volumetric content and size of fibers, as well as mean diameter of coarse aggregate. On the other hand, the DPD values of the F-A mixtures were found to be quite robust and highly sensitive to the variation of rigidity of fibers and their LPD values, respectively.

- A new workability-design approach was proposed for FR-SCC mixtures based on the established LPD and DPD models.

Declaration of Competing Interest

The authors declare that they have no known competing financial interests of personal relationships that could have appeared to influence the work reported in this paper.

Acknowledgment

Appendix

Table 5-6 A.1 Proportioning and characteristics of F-A mixtures selected to establish LPD model.

Mix. No.	F-A mixture ID	PSD of coarse aggregate	Fiber type	V_f (m³/m³)
1	R-0-14-1	MSA-14-1		
2	R-0-14-2	MSA-14-2	No fiber	0
3	R-0-14-3	MSA-14-3		
4	R-0-14-4	MSA-14-4		
5	R-MaS-0.4-14-1	MSA-14-1		0.004
6	R-MaS-0.4-14-2	MSA-14-2		0.004
7	R-MaS-0.4-14-3	MSA-14-3		0.004
8	R-MaS-0.5-14-2	MSA-14-2		0.005
9	R-MaS-0.5-14-3	MSA-14-3		0.005
10	R-MaS-0.5-14-4	MSA-14-4		0.005
11	R-MaS-0.6-14-1	MSA-14-1		0.006
12	R-MaS-0.6-14-2	MSA-14-2		0.006
13	R-MaS-0.6-14-3	MSA-14-3		0.006
14	R-MaS-0.6-14-4	MSA-14-4		0.006
15	R-MaS-0.7-14-1	MSA-14-1		0.007
16	R-MaS-0.7-14-3	MSA-14-3		0.007
17	R-MaS-0.7-14-4	MSA-14-4		0.007
18	R-MaS-0.8-14-1	MSA-14-1	Macro steel	0.008
19	R-MaS-0.8-14-2	MSA-14-2		0.008
20	R-MaS-0.8-14-4	MSA-14-4		0.008
21	R-MaS-0.9-14-1	MSA-14-1		0.009
22	R-MaS-0.9-14-2	MSA-14-2		0.009
23	R-MaS-0.9-14-3	MSA-14-3		0.009
24	R-MaS-1.62-14-1	MSA-14-1		0.0162
25	R-MaS-1.62-14-2	MSA-14-2		0.0162
26	R-MaS-1.62-14-3	MSA-14-3		0.0162
27	R-MaS-1.69-14-1	MSA-14-1		0.0169
28	R-MaS-1.69-14-2	MSA-14-2		0.0169
29	R-MaS-1.69-14-4	MSA-14-4		0.0169
30	R-MaS-1.77-14-1	MSA-14-1		0.0177
31	R-MaS-1.77-14-3	MSA-14-3		0.0177
32	R-MaS-1.77-14-4	MSA-14-4		0.0177
33	R-MiS-0.4-14-1	MSA-14-1		0.004
34	R-MiS-0.4-14-2	MSA-14-2		0.004
35	R-MiS-0.4-14-3	MSA-14-3		0.004
36	R-MiS-0.5-14-1	MSA-14-1		0.005
37	R-MiS-0.5-14-2	MSA-14-2		0.005
38	R-MiS-0.5-14-3	MSA-14-3		0.005
39	R-MiS-0.5-14-4	MSA-14-4		0.005
40	R-MiS-0.6-14-2	MSA-14-2		0.006
41	R-MiS-0.6-14-3	MSA-14-3		0.006
42	R-MiS-0.6-14-4	MSA-14-4	Micro steel	0.006
43	R-MiS-0.7-14-1	MSA-14-1		0.007
44	R-MiS-0.7-14-3	MSA-14-3		0.007
45	R-MiS-0.7-14-4	MSA-14-4		0.007
46	R-MiS-0.8-14-1	MSA-14-1		0.008
47	R-MiS-0.8-14-2	MSA-14-2		0.008
48	R-MiS-0.8-14-4	MSA-14-4		0.008
49	R-MiS-0.9-14-1	MSA-14-1		0.009
50	R-MiS-0.9-14-2	MSA-14-2		0.009
51	R-MiS-0.9-14-3	MSA-14-3		0.009

Table 5-7 A.1 Continued

Mix. No.	F-A mixture ID	PSD of coarse aggregate	Fiber type	V_f (m³/m³)
52	R-ST-0.4-14-1	MSA-14-1		0.004
53	R-ST-0.4-14-2	MSA-14-2		0.004
54	R-ST-0.4-14-3	MSA-14-3		0.004
55	R-ST-0.4-14-4	MSA-14-4		0.004
56	R-ST-0.5-14-2	MSA-14-2		0.005
57	R-ST-0.5-14-3	MSA-14-3	ST	0.005
58	R-ST-0.5-14-4	MSA-14-4		0.005
59	R-ST-0.6-14-1	MSA-14-1		0.006
60	R-ST-0.6-14-3	MSA-14-3		0.006
61	R-ST-0.6-14-4	MSA-14-4		0.006
62	R-ST-0.7-14-1	MSA-14-1		0.007

63	R-ST-0.7-14-2	MSA-14-2		0.007
64	R-ST-0.7-14-4	MSA-14-4		0.007
65	R-ST-0.8-14-1	MSA-14-1		0.008
66	R-ST-0.8-14-2	MSA-14-2		0.008
67	R-ST-0.8-14-3	MSA-14-3		0.008
68	R-ST-0.9-14-2	MSA-14-2		0.009
69	R-ST-0.9-14-3	MSA-14-3		0.009
70	R-ST-0.9-14-4	MSA-14-4		0.009
71	R-IT-0.4-14-1	MSA-14-1		0.004
72	R-IT-0.4-14-2	MSA-14-2		0.004
73	R-IT-0.4-14-4	MSA-14-4		0.004
74	R-IT-0.5-14-1	MSA-14-1		0.005
75	R-IT-0.5-14-3	MSA-14-3		0.005
76	R-IT-0.5-14-4	MSA-14-4		0.005
77	R-IT-0.6-14-1	MSA-14-1		0.006
78	R-IT-0.6-14-2	MSA-14-2		0.006
79	R-IT-0.6-14-3	MSA-14-3	IT	0.006
80	R-IT-0.7-14-1	MSA-14-1		0.007
81	R-IT-0.7-14-2	MSA-14-2		0.007
82	R-IT-0.7-14-3	MSA-14-3		0.007
83	R-IT-0.7-14-4	MSA-14-4		0.007
84	R-IT-0.8-14-3	MSA-14-3		0.008
85	R-IT-0.8-14-4	MSA-14-4		0.008
86	R-IT-0.9-14-2	MSA-14-2		0.009
87	R-IT-0.9-14-3	MSA-14-3		0.009
88	R-IT-0.9-14-4	MSA-14-4		0.009
89	R-PPF-0.4-14-2	MSA-14-2		0.004
90	R-PPF-0.4-14-3	MSA-14-3		0.004
91	R-PPF-0.4-14-4	MSA-14-4		0.004
92	R-PPF-0.5-14-1	MSA-14-1		0.005
93	R-PPF-0.5-14-3	MSA-14-3		0.005
94	R-PPF-0.6-14-1	MSA-14-1		0.006
95	R-PPF-0.6-14-2	MSA-14-2		0.006
96	R-PPF-0.6-14-3	MSA-14-3		0.006
97	R-PPF-0.6-14-4	MSA-14-4		0.006
98	R-PPF-0.7-14-1	MSA-14-1	PPF	0.007
99	R-PPF-0.7-14-2	MSA-14-2		0.007
100	R-PPF-0.8-14-3	MSA-14-3		0.007
101	R-PPF-0.8-14-1	MSA-14-1		0.008
102	R-PPF-0.8-14-2	MSA-14-2		0.008
103	R-PPF-0.8-14-3	MSA-14-3		0.008
104	R-PPF-0.8-14-4	MSA-14-4		0.008
105	R-PPF-0.9-14-1	MSA-14-1		0.009
106	R-PPF-0.9-14-3	MSA-14-3		0.009
107	R-PPF-0.9-14-4	MSA-14-4		0.009

Table 5-8 A.1 Continued

Mix. No.	F-A mixture ID	PSD of coarse aggregate	Fiber type	V_f (m³/m³)
108	R-TUF-0.4-14-1	MSA-14-1		0.004
109	R-TUF-0.4-14-2	MSA-14-2		0.004
110	R-TUF-0.4-14-3	MSA-14-3		0.004
111	R-TUF-0.4-14-4	MSA-14-4		0.004
112	R-TUF-0.5-14-1	MSA-14-1		0.005
113	R-TUF-0.5-14-3	MSA-14-3		0.005
114	R-TUF-0.5-14-4	MSA-14-4		0.005
115	R-TUF-0.6-14-1	MSA-14-1		0.006
116	R-TUF-0.6-14-2	MSA-14-2		0.006
117	R-TUF-0.6-14-3	MSA-14-3	TUF	0.006
118	R-TUF-0.7-14-1	MSA-14-1		0.007
119	R-TUF-0.7-14-2	MSA-14-2		0.007
120	R-TUF-0.7-14-4	MSA-14-4		0.007
121	R-TUF-0.8-14-1	MSA-14-1		0.008
122	R-TUF-0.8-14-2	MSA-14-2		0.008
123	R-TUF-0.8-14-4	MSA-14-4		0.008
124	R-TUF-0.9-14-1	MSA-14-1		0.009
125	R-TUF-0.9-14-3	MSA-14-3		0.009
126	R-TUF-0.8-14-4	MSA-14-4		0.009

Table 5-9 A.2 Proportioning and characteristics of F-A mixtures selected to validate the established LPD model.

Mix. No.	F-A mixture ID	PSD of coarse aggregate	Fiber type	V_f (m³/m³)
1	R-MaS-0.4-14-4	MSA-14-4		0.004
2	R-MaS-0.5-14-1	MSA-14-1		0.005
3	R-MaS-0.7-14-2	MSA-14-2		0.007
4	R-MaS-0.8-14-3	MSA-14-3	Macro steel	0.008
5	R-MaS-0.9-14-4	MSA-14-4		0.009
6	R-MaS-1.62-14-4	MSA-14-4		0.0162
7	R-MaS-1.69-14-3	MSA-14-3		0.0169
8	R-MaS-1.77-14-2	MSA-14-2		0.0177
9	R-MiS-0.4-14-4	MSA-14-4		0.004
10	R-MiS-0.6-14-1	MSA-14-1		0.006
11	R-MiS-0.7-14-2	MSA-14-2	Micro steel	0.007
12	R-MiS-0.8-14-3	MSA-14-3		0.008
13	R-MiS-0.9-14-4	MSA-14-4		0.009
14	R-ST-0.5-14-1	MSA-14-1		0.005
15	R-ST-0.6-14-2	MSA-14-2		0.006
16	R-ST-0.7-14-3	MSA-14-3	ST	0.007
17	R-ST-0.8-14-4	MSA-14-4		0.008
18	R-ST-0.9-14-1	MSA-14-1		0.009
19	R-IT-0.4-14-3	MSA-14-3		0.004
20	R-IT-0.5-14-2	MSA-14-2		0.005
21	R-IT-0.6-14-4	MSA-14-4		0.006
22	R-IT-0.7-14-1	MSA-14-1	IT	0.007
23	R-IT-0.8-14-2	MSA-14-2		0.008
24	R-IT-0.9-14-1	MSA-14-1		0.009
25	R-PPF-0.4-14-1	MSA-14-1		0.004
26	R-PPF-0.5-14-2	MSA-14-2		0.005
27	R-PPF-0.6-14-4	MSA-14-4	PPF	0.006
28	R-PPF-0.7-14-4	MSA-14-4		0.007
29	R-PPF-0.9-14-2	MSA-14-2		0.009
30	R-TUF-0.5-14-2	MSA-14-2		0.005
31	R-TUF-0.6-14-4	MSA-14-4		0.006
32	R-TUF-0.7-14-3	MSA-14-3	TUF	0.007
33	R-TUF-0.8-14-3	MSA-14-3		0.008
34	R-TUF-0.9-14-2	MSA-14-2		0.009

Table 5-10 A.3 Proportioning and characteristics of F-A mixtures selected to establish DPD model (Equation 5-9).

Mix. No.	F-A mixture ID	PSD of coarse aggregate	Fiber type	V_f (m³/m³)
1	R-MaS-0.4-14-1	MSA-14-1		0.004
2	R-MaS-0.4-14-2	MSA-14-2		0.004
3	R-MaS-0.4-14-3	MSA-14-3		0.004
4	R-MaS-0.5-14-1	MSA-14-1		0.005
5	R-MaS-0.5-14-2	MSA-14-2		0.005
6	R-MaS-0.5-14-3	MSA-14-3		0.005
7	R-MaS-0.5-14-4	MSA-14-4		0.005
8	R-MaS-0.6-14-2	MSA-14-2		0.006
9	R-MaS-0.6-14-3	MSA-14-3		0.006
10	R-MaS-0.6-14-4	MSA-14-4		0.006
11	R-MaS-0.7-14-1	MSA-14-1		0.007
12	R-MaS-0.7-14-2	MSA-14-2		0.007
13	R-MaS-0.7-14-3	MSA-14-3		0.007
14	R-MaS-0.7-14-4	MSA-14-4		0.007
15	R-MaS-0.8-14-2	MSA-14-2	Macro steel	0.008
16	R-MaS-0.8-14-3	MSA-14-3		0.008
17	R-MaS-0.8-14-4	MSA-14-4		0.008
18	R-MaS-0.9-14-1	MSA-14-1		0.009
19	R-MaS-0.9-14-3	MSA-14-3		0.009
20	R-MaS-0.9-14-4	MSA-14-4		0.009
21	R-MaS-1.62-14-1	MSA-14-1		0.0162
22	R-MaS-1.62-14-2	MSA-14-2		0.0162
23	R-MaS-1.62-14-3	MSA-14-3		0.0162
24	R-MaS-1.69-14-1	MSA-14-1		0.0169
25	R-MaS-1.69-14-2	MSA-14-2		0.0169
26	R-MaS-1.69-14-3	MSA-14-3		0.0169
27	R-MaS-1.69-14-4	MSA-14-4		0.0169
28	R-MaS-1.77-14-2	MSA-14-2		0.0177
29	R-MaS-1.77-14-3	MSA-14-3		0.0177

30	P-MaS-0.4-20-1	MSA-20-1		0.004
31	P-MaS-0.4-20-2	MSA-20-2		0.004
32	P-MaS-0.4-20-3	MSA-20-3		0.004
33	P-MaS-0.5-20-1	MSA-20-1		0.005
34	P-MaS-0.5-20-2	MSA-20-2		0.005
35	P-MaS-0.5-20-3	MSA-20-3		0.005
36	P-MaS-0.5-20-4	MSA-20-4		0.005
37	P-MaS-0.6-20-1	MSA-20-1		0.006
38	P-MaS-0.6-20-2	MSA-20-2		0.006
39	P-MaS-0.6-20-3	MSA-20-3		0.006
40	P-MaS-0.6-20-4	MSA-20-4		0.006
41	P-MaS-0.7-20-1	MSA-20-1		0.007
42	P-MaS-0.7-20-3	MSA-20-3		0.007
43	P-MaS-0.7-20-4	MSA-20-4		0.007
44	P-MaS-0.8-20-2	MSA-20-2		0.008
45	P-MaS-0.8-20-3	MSA-20-3		0.008
46	P-MaS-0.8-20-4	MSA-20-4		0.008
47	P-MaS-0.9-20-1	MSA-20-1		0.009
48	P-MaS-0.9-20-2	MSA-20-2		0.009
49	P-MaS-0.9-20-3	MSA-20-3		0.009
50	P-MaS-0.9-20-4	MSA-20-4		0.009
51	R-ST-0.4-14-2	MSA-14-2		0.004
52	R-ST-0.4-14-3	MSA-14-3		0.004
53	R-ST-0.5-14-1	MSA-14-1		0.005
54	R-ST-0.5-14-2	MSA-14-2		0.005
55	R-ST-0.5-14-3	MSA-14-3		0.005
56	R-ST-0.6-14-1	MSA-14-1		0.006
57	R-ST-0.6-14-2	MSA-14-2		0.006
58	R-ST-0.6-14-3	MSA-14-3		0.006
59	R-ST-0.6-14-4	MSA-14-4	ST	0.006
60	R-ST-0.7-14-2	MSA-14-2		0.007
61	R-ST-0.7-14-3	MSA-14-3		0.007
62	R-ST-0.7-14-4	MSA-14-4		0.007
63	R-ST-0.8-14-1	MSA-14-1		0.008
64	R-ST-0.8-14-2	MSA-14-2		0.008
65	R-ST-0.8-14-4	MSA-14-4		0.008
66	R-ST-0.9-14-1	MSA-14-1		0.009
67	R-ST-0.9-14-3	MSA-14-3		0.009
68	R-ST-0.9-14-4	MSA-14-4		0.009

Table 5-11 A.3 Continued

Mix. No.	F-A mixture ID	PSD of coarse aggregate	Fiber type	V_f (m³/m³)
69	R-MiS-0.4-14-1	MSA-14-1		0.004
70	R-MiS-0.4-14-2	MSA-14-2		0.004
71	R-MiS-0.4-14-4	MSA-14-4		0.004
72	R-MiS-0.5-14-2	MSA-14-2		0.005
73	R-MiS-0.5-14-3	MSA-14-3		0.005
74	R-MiS-0.5-14-4	MSA-14-4		0.005
75	R-MiS-0.6-14-2	MSA-14-2		0.006
76	R-MiS-0.6-14-3	MSA-14-3		0.006
77	R-MiS-0.6-14-4	MSA-14-4		0.006
78	R-MiS-0.7-14-1	MSA-14-1		0.007
79	R-MiS-0.7-14-2	MSA-14-2		0.007
80	R-MiS-0.7-14-3	MSA-14-3		0.007
81	R-MiS-0.8-14-1	MSA-14-1		0.008
82	R-MiS-0.8-14-2	MSA-14-2		0.008
83	R-MiS-0.8-14-3	MSA-14-3		0.008
84	R-MiS-0.9-14-1	MSA-14-1	Micro steel	0.009
85	R-MiS-0.9-14-2	MSA-14-2		0.009
86	R-MiS-0.9-14-3	MSA-14-3		0.009
87	R-MiS-0.9-14-4	MSA-14-4		0.009
88	P-MiS-0.4-20-1	MSA-20-1		0.004
89	P-MiS-0.4-20-2	MSA-20-2		0.004
90	P-MiS-0.4-20-3	MSA-20-3		0.004
91	P-MiS-0.5-20-1	MSA-20-1		0.005
92	P-MiS-0.5-20-2	MSA-20-2		0.005
93	P-MiS-0.5-20-4	MSA-20-4		0.005
94	P-MiS-0.6-20-1	MSA-20-1		0.006
95	P-MiS-0.6-20-2	MSA-20-2		0.006
96	P-MiS-0.6-20-3	MSA-20-3		0.006
97	P-MiS-0.6-20-4	MSA-20-4		0.006
98	P-MiS-0.7-20-1	MSA-20-1		0.007
99	P-MiS-0.7-20-2	MSA-20-2		0.007

100	P-MiS-0.7-20-3	MSA-20-3		0.007
101	P-MiS-0.7-20-4	MSA-20-4		0.007
102	P-MiS-0.8-20-1	MSA-20-1		0.008
103	P-MiS-0.8-20-3	MSA-20-3		0.008
104	P-MiS-0.8-20-4	MSA-20-4		0.008
105	P-MiS-0.9-20-1	MSA-20-1		0.009
106	P-MiS-0.9-20-2	MSA-20-2		0.009
107	P-MiS-0.9-20-3	MSA-20-3		0.009
108	P-MiS-0.9-20-4	MSA-20-4		0.009
109	R-IT-0.4-14-1	MSA-14-1		0.004
110	R-IT-0.4-14-3	MSA-14-3		0.004
111	R-IT-0.4-14-4	MSA-14-4		0.004
112	R-IT-0.5-14-1	MSA-14-1		0.005
113	R-IT-0.5-14-2	MSA-14-2		0.005
114	R-IT-0.5-14-4	MSA-14-4		0.005
115	R-IT-0.6-14-2	MSA-14-2		0.006
116	R-IT-0.6-14-3	MSA-14-3		0.006
117	R-IT-0.6-14-4	MSA-14-4		0.006
118	R-IT-0.7-14-1	MSA-14-1	IT	0.007
119	R-IT-0.7-14-2	MSA-14-2		0.007
120	R-IT-0.7-14-4	MSA-14-4		0.007
121	R-IT-0.8-14-1	MSA-14-1		0.008
122	R-IT-0.8-14-2	MSA-14-2		0.008
123	R-IT-0.8-14-3	MSA-14-3		0.008
124	R-IT-0.8-14-4	MSA-14-4		0.008
125	R-IT-0.9-14-2	MSA-14-2		0.009
126	R-IT-0.9-14-3	MSA-14-3		0.009
127	R-IT-0.9-14-4	MSA-14-4		0.009

Table 5-12 A.4 Proportioning and characteristics of F-A mixtures selected to validate the established DPD model (Equation 5-9).

Mix. No.	F-A mixture ID	Test- Sample	PSD of coarse aggregate in reference mixture	LPD_{F-A}	Fiber type	V_f in reference F-A mixture (m^3/m^3)	V_f in F-A sample mixture (m^3/m^3)
1	P-MaS-0.4-20-4		MSA-20-4	0.533		0.004	0.004
2	P-MaS-0.7-20-2		MSA-20-2	0.550		0.007	0.007
3	P-MaS-0.8-20-1		MSA-20-1	0.541		0.008	0.008
4	R-MaS-0.4-14-4		MSA-14-4	0.551		0.004	0.004
5	R-MaS-0.6-14-1	Reference	MSA-14-1	0.542		0.006	0.006
6	R-MaS-0.8-14-1		MSA-14-1	0.538		0.008	0.008
7	R-MaS-0.9-14-2		MSA-14-2	0.536		0.009	0.009
8	R-MaS-1.62-14-4		MSA-14-4	0.536		0.0162	0.0162
9	R-MaS-1.77-14-1		MSA-14-1	0.530		0.0177	0.0177
10	R-MaS-1.77-14-4		MSA-14-4	0.533		0.0177	0.0177
11	P-VP-33-MaS-0.4-20-4-L-E	L-Box - End	MSA-20-4	0.545		0.004	0.0030
12	P-VP-33-MaS-0.4-20-4-L-B	L-Box - Beginning	MSA-20-4	0.544		0.004	0.0052
13	P-VP-33-MaS-0.4-20-4-T-U	T-Box - Tilt-up	MSA-20-4	0.537		0.004	0.0024
14	P-VP-33-MaS-0.4-20-4-T-D	T-Box -Tilt-down	MSA-20-4	0.525		0.004	0.0058
15	P-VP-33-MaS-0.7-20-2-L-E	L-Box - End	MSA-20-2	0.518		0.007	0.0064
16	P-VP-33-MaS-0.7-20-2-L-B	L-Box - Beginning	MSA-20-2	0.530		0.007	0.0087
17	P-VP-33-MaS-0.7-20-2-T-U	T-Box - Tilt-up	MSA-20-2	0.523		0.007	0.0065
18	P-VP-33-MaS-0.7-20-2-T-D	T-Box -Tilt-down	MSA-20-2	0.533		0.007	0.0082
19	P-VP-33-MaS-0.5-20-3-L-E	L-Box - End	MSA-20-3	0.527		0.005	0.0047
20	P-VP-33-MaS-0.5-20-3-L-B	L-Box - Beginning	MSA-20-3	0.525		0.005	0.0054
21	P-VP-33-MaS-0.5-20-3-T-U	T-Box - Tilt-up	MSA-20-3	0.506	Macro steel	0.005	0.0045
22	P-VP-33-MaS-0.5-20-3-T-D	T-Box -Tilt-down	MSA-20-3	0.529		0.005	0.0058
23	P-VP-35-MaS-0.4-20-4-L-E	L-Box - End	MSA-20-4	0.509		0.004	0.0038
24	P-VP-35-MaS-0.4-20-4-L-B	L-Box - Beginning	MSA-20-4	0.491		0.004	0.0035
25	P-VP-35-MaS-0.4-20-4-T-U	T-Box - Tilt-up	MSA-20-4	0.511		0.004	0.0036
26	P-VP-35-MaS-0.4-20-4-T-D	T-Box -Tilt-down	MSA-20-4	0.529		0.004	0.0047
27	P-VP-35-MaS-0.7-20-2-L-E	L-Box - End	MSA-20-2	0.539		0.007	0.0072
28	P-VP-35-MaS-0.7-20-2-L-B	L-Box - Beginning	MSA-20-2	0.532		0.007	0.0080
29	P-VP-35-MaS-0.7-20-2-T-U	T-Box - Tilt-up	MSA-20-2	0.530		0.007	0.0068
30	P-VP-35-MaS-0.7-20-2-T-D	T-Box -Tilt-down	MSA-20-2	0.529		0.007	0.0087
31	P-VP-35-MaS-0.5-20-3-L-E	L-Box - End	MSA-20-3	0.516		0.005	0.0047
32	P-VP-35-MaS-0.5-20-3-L-B	L-Box - Beginning	MSA-20-3	0.487		0.005	0.0062
33	P-VP-35-MaS-0.5-20-3-T-U	T-Box - Tilt-up	MSA-20-3	0.497		0.005	0.0044
34	P-VP-35-MaS-0.5-20-3-T-D	T-Box -Tilt-down	MSA-20-3	0.510		0.005	0.0067
35	P-VP-37-MaS-0.4-20-4-L-E	L-Box - End	MSA-20-4	0.542		0.004	0.0032
36	P-VP-37-MaS-0.4-20-4-L-B	L-Box - Beginning	MSA-20-4	0.545		0.004	0.0043
37	P-VP-37-MaS-0.4-20-4-T-U	T-Box - Tilt-up	MSA-20-4	0.544		0.004	0.0034
38	P-VP-37-MaS-0.4-20-4-T-D	T-Box -Tilt-down	MSA-20-4	0.537		0.004	0.0047
39	P-VP-37-MaS-0.7-20-2-L-E	L-Box - End	MSA-20-2	0.514		0.007	0.0063
40	P-VP-37-MaS-0.7-20-2-L-B	L-Box - Beginning	MSA-20-2	0.509		0.007	0.0081
41	P-VP-37-MaS-0.7-20-2-T-U	T-Box - Tilt-up	MSA-20-2	0.501		0.007	0.0063
42	P-VP-37-MaS-0.7-20-2-T-D	T-Box -Tilt-down	MSA-20-2	0.520		0.007	0.0086

Table 5-13 A.4 Continued

Mix. No.	F-A mixture ID	Test- Sample	PSD of coarse aggregate in reference mixture	LPD_{F-A}	Fiber type	V_f in reference F-A mixture (m^3/m^3)	V_f in F-A sample mixture (m^3/m^3)
43	P-VP-37-MaS-0.5-20-3-L-E	L-Box - End	MSA-20-3	0.535		0.005	0.0036
44	P-VP-37-MaS-0.5-20-3-L-B	L-Box - Beginning	MSA-20-3	0.544		0.005	0.0060
45	P-VP-37-MaS-0.5-20-3-T-U	T-Box - Tilt-up	MSA-20-3	0.533		0.005	0.0034
46	P-VP-37-MaS-0.5-20-3-T-D	T-Box -Tilt-down	MSA-20-3	0.538		0.005	0.0058
47	R-VP-27-MaS-0.9-14-1-L-B	L-Box - Beginning	MSA-14-1	0.503		0.009	0.0118
48	R-VP-27-MaS-0.9-14-1-T-U	T-Box - Tilt-up	MSA-14-1	0.510		0.009	0.0089
49	R-VP-27-MaS-0.9-14-1-T-D	T-Box -Tilt-down	MSA-14-1	0.498		0.009	0.0108
50	R-VP-27-MaS-0.7-14-2-L-E	L-Box - End	MSA-14-2	0.524		0.007	0.0046
51	R-VP-27-MaS-0.7-14-2-L-B	L-Box - Beginning	MSA-14-2	0.521		0.007	0.0089
52	R-VP-27-MaS-0.7-14-2-T-U	T-Box - Tilt-up	MSA-14-2	0.519		0.007	0.0064
53	R-VP-27-MaS-0.7-14-2-T-D	T-Box -Tilt-down	MSA-14-2	0.521		0.007	0.0085
54	R-VP-27-MaS-0.4-14-3-L-E	L-Box - End	MSA-14-3	0.530		0.004	0.0035
55	R-VP-27-MaS-0.4-14-3-L-B	L-Box - Beginning	MSA-14-3	0.534		0.004	0.0051
56	R-VP-27-MaS-0.4-14-3-T-U	T-Box - Tilt-up	MSA-14-3	0.532		0.004	0.0038
57	R-VP-27-MaS-0.4-14-3-T-D	T-Box -Tilt-down	MSA-14-3	0.535		0.004	0.0049
58	R-VP-30-MaS-0.9-14-1-L-E	L-Box - End	MSA-14-1	0.516		0.009	0.0082
59	R-VP-30-MaS-0.9-14-1-L-B	L-Box - Beginning	MSA-14-1	0.496		0.009	0.0128
60	R-VP-30-MaS-0.9-14-1-T-U	T-Box - Tilt-up	MSA-14-1	0.505		0.009	0.0069
61	R-VP-30-MaS-0.9-14-1-T-D	T-Box -Tilt-down	MSA-14-1	0.508		0.009	0.0098
62	R-VP-30-MaS-0.7-14-2-L-E	L-Box - End	MSA-14-2	0.511	Macro steel	0.007	0.0060
63	R-VP-30-MaS-0.7-14-2-L-B	L-Box - Beginning	MSA-14-2	0.519		0.007	0.0071
64	R-VP-30-MaS-0.7-14-2-T-U	T-Box - Tilt-up	MSA-14-2	0.514		0.007	0.0057
65	R-VP-30-MaS-0.7-14-2-T-D	T-Box -Tilt-down	MSA-14-2	0.507		0.007	0.0089
66	R-VP-30-MaS-0.4-14-3-L-E	L-Box - End	MSA-14-3	0.525		0.004	0.0035
67	R-VP-30-MaS-0.4-14-3-L-B	L-Box - Beginning	MSA.14-3	0.533		0.004	0.0052
68	R-VP-30-MaS-0.4-14-3-T-U	T-Box - Tilt-up	MSA-14-3	0.532		0.004	0.0028
69	R-VP-30-MaS-0.4-14-3-T-D	T-Box -Tilt-down	MSA-14-3	0.529		0.004	0.0044
70	R-VP-33-MaS-0.9-14-1-L-E	L-Box - End	MSA-14-1	0.509		0.009	0.0083
71	R-VP-33-MaS-0.9-14-1-L-B	L-Box - Beginning	MSA-14-1	0.502		0.009	0.0118
72	R-VP-33-MaS-0.9-14-1-T-U	T-Box - Tilt-up	MSA-14-1	0.512		0.009	0.0060
73	R-VP-33-MaS-0.9-14-1-T-D	T-Box -Tilt-down	MSA-14-1	0.513		0.009	0.0111
74	R-VP-33-MaS-0.7-14-2-L-E	L-Box - End	MSA-14-2	0.525		0.007	0.0065
75	R-VP-33-MaS-0.7-14-2-L-B	L-Box - Beginning	MSA-14-2	0.529		0.007	0.0081
76	R-VP-33-MaS-0.7-14-2-T-U	T-Box - Tilt-up	MSA-14-2	0.527		0.007	0.0035
77	R-VP-33-MaS-0.7-14-2-T-D	T-Box -Tilt-down	MSA-14-2	0.506		0.007	0.0107
78	R-VP-33-MaS-0.4-14-3-L-E	L-Box - End	MSA-14-3	0.535		0.004	0.0036
79	R-VP-33-MaS-0.4-14-3-L-B	L-Box - Beginning	MSA-14-3	0.533		0.004	0.0043
80	R-VP-33-MaS-0.4-14-3-T-U	T-Box - Tilt-up	MSA-14-3	0.534		0.004	0.0029
81	R-VP-33-MaS-0.4-14-3-T-D	T-Box -Tilt-down	MSA-14-3	0.541		0.004	0.0054

Table 5-14 A.4 Continued

Mix. No.	F-A mixture ID	Test-Sample	PSD of coarse aggregate in reference mixture	LPD_{F-A}	Fiber type	V_f in reference F-A mixture (m^3/m^3)	V_f in F-A sample mixture (m^3/m^3)
82	P-MiS-0.4-20-4		MSA-20-4	0.563		0.004	0.004
83	P-MiS-0.5-20-3		MSA-20-3	0.565		0.005	0.005
84	P-MiS-0.8-20-2		MSA-20-2	0.563		0.008	0.008
85	R-MiS-0.4-14-3		MSA-14-3	0.556	Micro	0.004	0.004
86	R-MiS-0.5-14-1		MSA-14-1	0.559	steel	0.005	0.005
87	R-MiS-0.6-14-1		MSA-14-1	0.550		0.006	0.006
88	R-MiS-0.7-14-4		MSA-14-4	0.554		0.007	0.007
89	R-MiS-0.8-14-4		MSA-14-4	0.553		0.008	0.008
90	R-ST-0.4-14-1		MSA-14-1	0.546		0.004	0.004
91	R-ST-0.4-14-4	Reference	MSA-14-4	0.553		0.004	0.004
92	R-ST-0.5-14-4		MSA-14-4	0.551	ST	0.005	0.005
93	R-ST-0.7-14-1		MSA-14-1	0.539		0.007	0.007
94	R-ST-0.8-14-3		MSA-14-3	0.542		0.008	0.008
95	R-ST-0.9-14-2		MSA-14-2	0.538		0.009	0.009
96	R-IT-0.4-14-2		MSA-14-2	0.548		0.004	0.004
97	R-IT-0.5-14-3		MSA-14-3	0.555		0.005	0.005
98	R-IT-0.6-14-1		MSA-14-1	0.540	IT	0.006	0.006
99	R-IT-0.7-14-3		MSA-14-3	0.547		0.007	0.007
100	R-IT-0.9-14-1		MSA-14-1	0.536		0.009	0.009

References

[1] A. Emdadi, I, Mehdipour, N.A. Libre, M. Shekarchi, Optimized workability and mechanical properties of FRCM by using fiber factor approach: theoretical and experimental study, Materials and Structures, 48 (4) (2015) 1149-1161, https://doi.org/10.1617/s11527-013-0221-3.

[2] Y. Lu, Z. Liu, S. Li, W. Li, Behavior of steel fibers reinforced self-stressing and self-compacting concrete-filled steel tube subjected to bending, Construction and Building Materials, 156 (2017) 639-651, http://dx.doi.org/10.1016/j.conbuildmat.2017.09.019.

[3] X. Ning, Y. Ding, F. Zhang, Y. Zhang, Experimental study and prediction model for flexural behavior of reinforced SCC beam containing steel fibers, Construction and Building Materials, 93 (2015) 644-653, http://dx.doi.org/10.1016/j.conbuildmat.2015.06.024.

[4] E.V. Sarmiento, G. Zirgulis, S. Sandbakk, M.R. Geiker, T. Kanstad, Influence of concrete flow on fibre distribution, orientation and mechanical properties of fibre reinforced concrete, 8th RILEM International Symposium on Fiber Reinforced Concrete: challenges and opportunities, BEFIB2012 (2012) 418-430.

[5] K.M.A. Hossain, M. Lachemi, M. Sammour, M. Sonebi, Influence of polyvinyl alcohol, steel, and hybrid fibers on fresh and rheological properties of self-consolidating concrete, Materials in Civil Engineering, 24 (9) (2012) 1211-1220, https://doi.org/10.1061/(ASCE)MT.1943-5533.0000490.

[6] I. Mehdipour, N.A. Libre, Linking fiber factor to material performance of fiber reinforced self-consolidating cement-based materials, ACI Materials Journal, 114 (1) (2017) 77-91, http://dx.doi.org/10.14359/51689483.

[7] I. Mehdipour, N.A. Libre, M. Shekarchi, M. Khanjani, Effect of workability characteristics on the hardened performance of FRSCCMs, Construction and Building Materials, 40 (2013) 611-621, https://doi.org/10.1016/j.conbuildmat.2012.11.051.

[8] M. Nehdi, J.D. Ladanchuk, Fiber synergy in fiber-reinforced self-consolidating concrete, ACI Materials Journal, 101 (6) (2004) 508-517, http://dx.doi.org/10.14359/13490.

[9] A.S. El-Dieb, M.M.R. Taha, Flow characteristics and acceptance criteria of fiber-reinforced self-compacted concrete (FR-SCC), Construction and Building Materials, 27 (1) (2012) 585-596, https://doi.org/10.1016/j.conbuildmat.2011.07.004.

[10] K.H. Khayat, F. Kassimi, P. Ghoddousi, Mixture design and testing of fiber-reinforced self-consolidating concrete, ACI Materials Journal, 111 (2) (2014) 143, http://dx.doi.org/10.14359/51686722.

[11] M. Hosseinpoor, B.I.O. Koura, A. Yahia, Rheo-morphological investigation of static and dynamic stability of self-consolidating concrete: A biphasic approach, Cement and Concrete Composites, 121 (2021), 104072 https://doi.org/10.1016/j.cemconcomp.2021.104072.

[12] M. Hosseinpoor, B.I.O. Koura, A. Yahia, New diphasic insight into the restricted flowability and granular blocking of self-consolidating concrete: Effect of morphological characteristics of coarse aggregate on passing ability of SCC, Construction and Building Materials, 308 (2021) 125001, https://doi.org/10.1016/j.conbuildmat.2021.125001.

[13] B.I.O. Koura, M. Hosseinpoor, A. Yahia, Coupled effect of fine mortar and granular skeleton characteristics on dynamic stability of self-consolidating concrete as a diphasic material, Construction and Building Materials, 263 (2020) 120-131, https://doi.org/10.1016/j.conbuildmat.2020.120131.

[14] A.K.H. Kwan, K.W. Chan, V. Wong, A 3-parameter particle packing model incorporating the wedging effect, Powder Technology, 237 (2013) 172-179, https://doi.org/10.1016/j.powtec.2013.01.043.

[15] L. Li, G., Z. W. Zhao, J. Zhu, A. K. H. Kwan, and K. L. Zeng, Combined effects of water film thickness and polypropylene fibre length on fresh properties of mortar, Construction and Building Materials, 174 (2018), 586-593, https://doi.org/10.1016/j.conbuildmat.2018.03.259.

[16] L.G. Li, J. Zhu, Z.W. Zhao, A.K.H. Kwan, Roles of water film thickness and polypropylene fibre content in fresh properties of mortar, Advances in Cement Research, 29 (2) (2017) 71-80, https://doi.org/10.1680/jadcr.16.00102.

[17] G. Sokhansefat, M.T. Ley, M.D. Cook, R. Alturki, M. Moradian, Investigation of concrete workability through characterization of aggregate gradation in hardened concrete using X-ray computed tomography, Cement and Concrete Composites, 98 (2019), 150-161, https://doi.org/10.1016/j.cemconcomp.2019.02.008.

[18] K. Molugaram, J.S. Shanker, A. Ramesh, A study on influence of shape of aggregate on strength and quality of concrete for buildings and pavements, Advanced Materials Research, 941-944 (2014) 776-779, https://doi.org/10.4028/www.scientific.net/AMR.941-944.776.

[19] K. Ostrowski, L. Sadowski, D. Stefaniuk, D. Walach, T. Gawenda, K. Oleksik, I. Usydus, The effect of the morphology of coarse aggregate on the properties of self-compacting high-performance fiber-reinforced concrete, Materials, 11 (2018) 1-16, https://doi.org/10.3390/ma11081372.

[20] B.M. Aissoun, S.D. Hwang, K.H. Khayat, Influence of aggregate characteristics on workability of superworkable concrete, Materials and Structures, 49 (2016) 597-609, https://doi.org/10.1617/s11527-015-0522-9.

[21] R. Farokhzad, M. Mahdikhani, A. Bagheri, J. Baghdadi, Representing a logical grading zone for self-consolidating concrete, Construction and Building Materials, 115 (2016) 735-745, https://doi.org/10.1016/j.conbuildmat.2016.04.006.

[22] H. Hafid, G. Ovarlez, F. Toussaint, P.H. Jezequel, N. Roussel, Effect of particle morphological parameters on sand grains packing properties and rheology of model mortars, Cement and Concrete Research, 80 (2016), 44-51, https://doi.org/10.1016/j.cemconres.2015.11.002.

[23] L. Martinie, P. Rossi, N. Roussel, Rheology of fiber reinforced cementitious materials: classification and prediction, Cement and Concrete Research, 40 (2) (2010) 226-234, https://doi.org/10.1016/j.cemconres.2009.08.032.

[24] S.H. Chu, Y. Jiang, A.K.H. Kwan, Effect of rigid fibres on aggregate packing, Construction and Building Materials, 224 (2019), 326-335, https://doi.org/10.1016/j.conbuildmat.2019.07.072.

[25] F. de Larrard, Concrete mixture proportioning - a scientific approach, in: S. Mindess, A. Bentur (Eds.), Modern Concrete Technology Series No. 7, E&FN SPON, London (1999) ISBN 9780419235002.

[26] N. Roussel, Understanding the Rheology of Concrete, first ed., Woodhead Publishing, Sawston, Cambridge, United Kingdom, 2011, ISBN 978-0-85709-028-7.

[27] A.B. Yu, R.P. Zou, Prediction of the porosity of particle mixtures, KONA Powder and Particle Journal, 16 (1998) 68-81, https://doi.org/10.14356/kona.1998010.

[28] Z. S. Ali, M. Hosseinpoor, A. Yahia, New aggregate grading models for low-binder self-consolidating and semi-self-consolidating concrete (Eco-SCC and Eco-semi-SCC), Construction and Building Materials, 265 (2020) 120314, https://doi.org/10.1016/j.conbuildmat.2020.120314.

[29] M. Hosseinpoor, B.I.O. Koura, A. Yahia, Rheo-morphological investigation of Reynolds dilatancy and its effect on pumpability of self-consolidating concrete, Cement and Concrete Composites, 117 (2021) 103912, https://doi.org/10.1016/j.cemconcomp.2020.103912.

[30] Nordtest, Method (NT BUILD 427) for Fresh Concrete: Compactibility with IC-tester (Intensive Compaction Tester) Proj. 1005-91, Nord. Scand. Inst. (1994) 1-4, ISSN 0283-7153 www.nordtest.org.

[31] B.M. Aïssoun, Method (NT BUILD 427) for Fresh Concrete: Compactibility on the rheology of fluid concrete with adapted rheology (in French), M.Sc. thesis, Université de Sherbrooke (2011), http://savoirs.usherbrooke.ca/handle/11143/1590.

[32] B.I.O. Koura, M. Hosseinpoor, A. Yahia, E.H. Kadri, A. Kaci, A new proportioning approach of low and normal binder self-consolidating concrete based on the characteristics of fine mortar and granular skeleton, Construction and Building Materials, 239 (2020) 117892, https://doi.org/10.1016/j.conbuildmat.2019.117892.

CHAPITER 6 Homogeneous flow performance of steel-fiber reinforced self-consolidating concrete for repair application: A biphasic approach

Authors and affiliations

Naimeh Nouri : Ph.D. candidate, Cement and Concrete Research Group, Department of Civil and Building Engineering, Université de Sherbrooke, Sherbrooke, Québec, Canada, J1K 2R1.

Masoud Hosseinpoor: Research Associate, Cement and Concrete Research Group, Department of Civil and Building Engineering, Université de Sherbrooke, Sherbrooke, Québec, Canada, J1K 2R1.

Ammar Yahia: Professor, Cement and Concrete Research Group, Department of Civil and Building Engineering, Université de Sherbrooke, Sherbrooke, Québec, Canada, J1K 2R1.

Kamal H. Khayat: Professor, Missouri University of Science and Technology, Center for Infrastructure Engineering Studies, Department of Civil, Architectural and Environmental Engineering, Rolla, MO 65409.

Titre en français: Performance d'écoulement homogène du béton autoplaçant renforcé de fibres d'acier pour une application de réparation : une approche biphasique

Homogeneous flow performance of steel-fiber reinforced self-consolidating concrete for repair application: A biphasic approach

Naimeh Nouri[a], Masoud Hosseinpoor[a],*, Ammar Yahia[a], and Kamal H. Khayat[b]

[a]Université de Sherbrooke, Department of Civil and Building Engineering, Sherbrooke, Québec, Canada

[b]Missouri University of Science and Technology, Center for Infrastructure Engineering Studies, Department of Civil, Architectural and Environmental Engineering, Rolla, MO, USA

*Corresponding author: masoud.hosseinpoor@usherbrooke.ca

Abstract

In this study, fiber-reinforced self-consolidating concrete (FR-SCC) was considered as a diphasic suspension of fiber and coarse aggregate (F-A $\geq$ 5 mm) skeleton in mortar suspension with solid particles finer than 5 mm. The coupled effect of the volumetric content of fibers, coarse aggregate particle-size distribution, and rheological properties of the mortar on the passing ability and dynamic stability of various FR-SCC mixtures was investigated. Nine high-strength and 10 conventional-strength FR-SCC mixtures for repair application were proportioned with water-to-binder ratios (W/B) of 0.35 and 0.42, respectively, and macro steel fibers of 0.1%-0.5% volumetric contents. The dosages of high-range water-reducer (HRWR) admixture were optimized to achieve a targeted slump flow of 680±20 mm. The yield stress and plastic viscosity of the mortar mixtures varied between 4.6-17.7 Pa and 2.8-8.2 Pa.s., respectively. Flow performance of the investigated mixtures were evaluated in terms of flowability (slump-flow test), passing ability (J-Ring and L-Box set-ups), and dynamic stability (T-Box test). According to the established correlations, the main influencing parameters on homogeneous performance of FR-SCC include W/B, paste volume, volumetric content-to-packing density of F-A (φ/φ_{max}), HRWR dosage, fiber content, mortar rheology, and volume of excess mortar. The robustness analyses results revealed that homogeneous flow performance of FR-SCC is more sensitive due to variations of the φ/φ_{max} and paste volume rather than mortar rheology, W/B, and HRWR dosage. The characteristics of the mixture constituents for FR-SCC mixtures with different strength levels were finally recommended to ensure acceptable homogeneous performance under restricted flow conditions of repair application.

Keywords: Dynamic stability; Fiber-reinforced self-consolidating concrete; Granular blocking; Packing density; Passing ability; Rheology.

6.1 Introduction

Highly-flowable cementitious mixtures, such as self-consolidating concrete (SCC), are commonly used to facilitate the casting of highly congested reinforced elements [1,2]. However, SCC can exhibit high risk of segregation during mixing, transportation, placement, and finishing [1,3]. This is due to higher fluidity of the suspending fluid phase (i.e., cement paste or mortar matrix), which can increase the risk of dynamic and static segregation and blocking of aggregate behind reinforcing bars [4-6]. Segregation is defined as the separation of

aggregate from their surrounding paste or mortar, hence leading to heterogeneity in the formwork [4-6]. Static segregation occurs when the concrete is at rest, and coarse aggregate can settle down given their higher density compared to suspending paste/mortar matrix [7]. On the other hand, dynamic segregation occurs during flow when the mortar is not able to carry the coarse aggregate and maintain homogeneous suspension [4,5,8]. Passing across the reinforced elements, coarse aggregate can be separated from their surrounding mortar leading to blockage behind rebars [6]. Therefore, SCC is proportioned to ensure high flowability, passing ability, and stability [2].

Fibers can be used in SCC to enhance tensile strength and increase cracking resistance and strain capacity [9-14], however, this can alter the workability of FR-SCC compared to plain SCC [9]. To maintain self-consolidating ability of FR-SCC, a higher dosage of high-range water-reducer (HRWR) admixture is required allowing a given level of flowability of the reference plain SCC (no fiber). This can lead to lower viscosity of the suspending mortar of the FR-SCC mixture compared to plain SCC [9]. This can increase the risk of static/dynamic segregation of fibers-aggregate from the mortar and also the risk of blocking of solid particles during flow across narrow gaps between reinforcing bars [9,10]. These can result in non-uniform distribution and orientation of the fibers, especially with increasing fiber volume [15,16]. Such segregation can impair mechanical performance of FR-SCC [15,16]. Nehdi and Ladanchuk [17] reported that adding 1% of 38- and 50-mm long steel fibers can decrease the passing ability of FR-SCC mixtures, which was reflected by reducing the L-Box blocking ratio (h_2/h_1) by 0.30 and 0.22, respectively. The mixture proportioning of FR-SCC should be carefully designed to secure proper fluidity and stability, especially for highly reinforced elements. This includes the optimization of rheological properties of the suspending cement paste and mortar, enhancing the particle-size distribution (PSD) and packing density of the aggregate skeleton, and carefully selecting the fiber characteristics (i.e., type, volume, and aspect ratio).

The interest in repair and strengthening (rehabilitation) of structures has increased in the last decades. Indeed, repairing the existing damaged concrete structures is more cost-effective solution compared to the demolition and the reconstruction of structures. Moreover, most of the repair works are done in relatively small zones of the structural elements, with and without any reinforcement, where it is difficult to vibrate. The use of highly-flowable cementitious mixtures, such as SCC, can be beneficial solution for this type of application. SCC is proportioned with higher volume of paste (V_P) and fine particles compared to conventional concrete, which increases the risk of shrinkage [18,19]. The use of fiber-reinforced cementitious mixtures for repair application is of particular interest due to their mechanical advantages and lower shrinkage, hence leading to better durability of repaired elements. However, casting of FR-SCC in small spaces to be repaired can enface some sorts of instabilities (e.g., F-A blockage), due to altering their homogeneous flow performance passing through the restricted zones. A special attention is required on the specifications of FR-SCC mixtures, in terms of mixture proportioning, flowability, passing ability, and stability to achieve a successful repair work.

Hwang and Khayat [20] studied the effect of mixture composition on workability of FR-SCC mixtures used for repair application with 28-days compressive strength values of 43 to 54 MPa. The investigated mixtures were proportioned with water-to-binder ratio (W/B) of 0.39 to 0.42 and synthetic fibers volumes of 0.25% and 0.5% to reduce the restrained shrinkage cracking. The investigated mixtures showed good flowability having slump flow values of 660 ± 20 mm.

However, the mixtures containing higher fiber volume of 0.5% showed lower passing ability and filling ability (L-Box blocking ratios (h_2/h_1) less than 0.46 and filling capacity of 60%), compared to those proportioned with 0.25% fiber volume (h_2/h_1 of 0.62-0.84 and filling capacity of 82%-94%). Abdulhameed et al. [18], investigated the fresh and hardened performance of the FR-SCC mixtures used for repair application. The investigated mixtures were proportioned with W/B of 0.42 and 0.425 and volumetric fiber (synthetic and steel) contents of 0.1%-0.5%. The mixtures showed slump flow values of 535-635 mm, T_{50} of 4-8 s, h_2/h_1 of 0.8-1, visual stability index (VSI) of 0-1, and difference between J-Ring and slump flow spreads of 25-125 mm. Kassimi et al. [21] proportioned several FR-SCC mixtures to repair 125-mm wide zones of a beam. The mixtures were proportioned with W/B of 0.42 and steel fiber volumes of 0.3% to 0.5% having 28-days compressive strength values of 41 to 56 MPa. The investigated mixtures showed excellent flowability, reflected by slump flow values of 700 ± 20 mm and T_{50} values less than 3 s. Moreover, excellent passing ability was obtained reflected by a difference between the J-Ring and slump flow values less than 40 mm and L-Box blocking ratio (h_2/h_1) between 0.8 to 1, along with good stability (VSI values of 0 and 0.5) and deformability (V-Funnel flow times between 2 to 5 s).

Moreover, the FR-SCC mixture designed for repair application can be designed with different mechanical strength values depending on the original concrete substrate. This can affect on their W/B and V_P used for repair application. Furthermore, the maximum size of aggregate (MSA) and fiber type and size can be selected due to the dimension of the zones to be repaired. For instant, Khayat et al. [13], investigated the workability of the FR-SCC mixtures for repair application which were made by W/B of 0.42, V_P of 0.35, MSA of 10 mm, and different hooked end steel fiber (30 mm length and 0.55 aspect ratio) contents of 0.25%-0.75%. It was revealed that increasing fiber content to high value of 0.75% reduced the compressive strength from 49 to 38 MPa. This was explained due to the negative effect of extremely high fiber content on filling ability of the investigated FR-SCC mixtures, reflected by lowering the L-Box blocking ratio from 0.8 to 0.3 and J-Ring flow from 560 to 450 mm. Therefore, a maximum fiber content of 0.5% was recommended to avoid the risk of blocking. Volz et al. [22] and Arezoumandi et al. [23] investigated the fresh and hardened properties of FR-SCC mixtures (28-days compressive strength higher than 27 MP) to repair bridge structure with MSA of 12.5 and 9.5 mm, respectively. According to the aforementioned literature, the following criteria can be recommended for the FR-SCC mixtures to achieve a successful repair work: V_P of 0.27-0.35, MSA of 10-14 mm, fiber content less than 0.5%, and 28-days compressive strength higher than 27 MPa. However, depending on the dimension of the repair zone the allowed MSA can be modified. This can be concluded that different mixture characteristics must be simultaneously optimized to achieve targeted mechanical properties and also desired homogeneous flow performance passing through the narrow spaces for repair application.

The effect of mixture compositions on the homogeneous flow behavior of SCC and FR-SCC has been investigated in the literature [4-6,16,24]. For example, Jasiūnienė et al. [25] evaluated the effect of the rheological properties of FR-SCC on distribution of steel fibers using image analysis of the cut hardened beams. The most remarkable reduction in number of fibers through the length of the beam was reported for the mixture with the lowest plastic viscosity. On the other hand, the aggregate characteristics, including PSD, morphology, and packing density should also be considered. Farokhzad et al. [26] reported that increasing the size of fine aggregate can reduce their ability to fill the gaps within the coarser particles and, therefore, decrease the packing density. Lower amount of cement paste was thus available to lubricate the

granular system, hence increasing the V-Funnel time. Hafid et al. [27] reported a significant effect of morphological characteristics of fine aggregate on their packing density and rheological behavior of mortar mixtures. Ostrowski et al. [28] studied the effect of coarse aggregate morphology on fresh and hardened properties of FR-SCC. On the other hand, enhancing the packing density (PD) of solid skeleton by optimizing their PSD can lead to higher excess paste/mortar available to lubricate the aggregate and improves concrete workability [29,30].

Koura et al. [4] and Hosseinpoor et al. [5] evaluated the coupled effect of rheological properties of fine mortar (sand < 1.25 mm) and coarse aggregate (> 1.25 mm) characteristics on dynamic stability of SCC using the T-Box set-up [8]. In this test, concrete is subjected to 60 cycles of tilting motion for 120 s, which corresponds to almost 9-m flow distance travelled in the formwork [8]. The authors [4,5] proposed a dynamic segregation index (DSI), defined by the ratio of the variation of the relative-solid packing fraction (φ/φ_{max}) of coarse aggregate in the samples taken from two lateral zones of the T-Box set-up (i.e., the tilt-down and tilt-up sections) compared to that of the reference mixture [4,5]. It was revealed that increasing plastic viscosity and yield stress of fine mortar can lead to lower dynamic segregation of SCC. The authors [4,5] reported that increasing the φ/φ_{max} of coarse aggregate results in lower dynamic segregation of SCC. This is due to the higher lattice effect of denser aggregate skeleton which can push them to move along the suspending mortar. This can limit the separation of coarse aggregate and suspending phase and, consequently, improve the dynamic stability of SCC. The φ/φ_{max} of coarse aggregates showed the most dominant effect on dynamic stability of SCC rather than the mortar's rheology [4,5]. The authors recommended a maximum DSI of 25% as an acceptable limit for dynamically stable mixtures [4].

Although the SCC mixtures with high dynamic stability can properly fill the non-reinforced elements, it should be also noted that mixtures containing coarse aggregate and/or fibers can block behind the reinforcement bars. Hosseinpoor et al. [6] investigated the passing ability of SCC, as a biphasic suspension of coarse aggregate and fine mortar. The passing ability was evaluated in terms of restricted flowability and granular blocking using the L-Box set-up. The "restricted flowability" was defined as the lack of enough flowability of concrete passing through the obstacles [6]. Accordingly, the flow of a stiff concrete mixture with high yield stress can be blocked passing through the restricted elements while no separation of aggregate and mortar matrix behind the bars (granular blocking) occurs. Indeed, the flow of concrete in restricted elements under its own weight is limited due to its high yield stress and plastic viscosity. Indeed, due to shear-induced particle migration, solid particles migrate from high-shear rate zones towards the lower shear-rate zones. Hosseinpoor et al. [6] reported that the shear-rate gradient increases due to the presence of reinforcement bars which can result in higher risk of segregation of particles and mortar matrix behind the rebars. The aggregate arches formed behind the rebars can resist against the drag force exerted by the mortar and thus be blocked [6].

Hosseinpoor et al. [6] evaluated the passing ability of SCC using the L-Box blocking ratio (h_2/h_1) as the ratio of the final profile heights at the end of the L-Box channel (h_2)-to-the one measured behind the rebars in vertical compartment of the set-up (h_1). On the other hand, the granular blocking corresponds to variation of the φ/φ_{max} of coarse aggregate by passing among the reinforcing bars. It can be noted that a highly flowable concrete can still show a high h_2/h_1 ratio while exhibiting high granular blocking where mostly the mortar matrix passes, and aggregate get jammed behind the L-Box obstacles. The authors [6] introduced a new index to evaluate the granular blocking through the L-Box set-up (BI_{LB}), defined as the ratio of variation of φ/φ_{max} of coarse aggregate in the samples taken from the zones behind the rebars (vertical compartment) and end of the horizontal channel of the L-Box set-up, respectively, -to- the φ/φ_{max} of the reference mixture. The authors [6] reported that increasing the rheological properties of the mortar matrix can reduce the risk of granular blocking but negatively affect the h_2/h_1 ratio of SCC. Also, the study revealed that increasing the φ/φ_{max} of coarse aggregate can significantly decrease the passing ability reflected by higher BI_{LB} index and lower h_2/h_1 ratio. Moreover, increasing the W/B, HRWR dosage, and V_P led to higher BI_{LB} index and h_2/h_1 ratio. The optimization of φ/φ_{max} of coarse aggregate was found as a more effective approach to minimize the granular blocking of SCC rather than the volume and constituents of cement paste (i.e., V_P, W/B, and HRWR dosage) [6].

However, in the case of FR-SCC, no clear correlation was found between the passing ability results of the standard J-Ring [31] and the L-Box test to the fiber factor ($V_f \times L_f / d_f$) [13]. Khayat et al. [13] reported considerable blockage when the standard J-Ring test [31] with 16 bars to evaluate the passing ability of steel FR-SCC. This was due to the interactions between the fibers, coarse aggregate, and the reinforcing bars in the passing ability tests of FR-SCC compared to the plain SCC. Modified test set-ups were thus recommended by reducing the number of rebars from 16 to 8 (or 6) and 3 to 1 for the J-Ring and L-Box tests, respectively. These modifications lead to higher clear distance between the rebars and correspond to up to 2.5 times relative to the fiber length, thus enabling the assessment of the passing ability of FR-SCC [13].

In this study the homogeneous flow performance of various steel-fiber reinforced SCC (FR-SCC) mixtures for repair application were evaluated in terms of flowability, passing ability, granular blocking, and dynamic stability. The investigated mixtures, corresponding to conventional and high strength levels, were proportioned with different MSA, W/B, and V_P. The investigated FR-SCC mixtures were considered as a biphasic suspension of fiber and coarse aggregate (solid F-A phase $\geq$ 5 mm) in suspending mortar containing solid particles finer than 5 mm. The mortar matrix was assumed as the stable-liquid phase that does not undergo any instability during flow. Accordingly, the coupled effect of F-A characteristics and mortar rheology on flow performance of the investigated FR-SCC mixtures was evaluated. The study seeks to recommend a workability-based classification that can be employed to design FR-SCC for repair application with different strength levels to secure high flowability and adequate resistance to dynamic segregation and granular blocking.

6.2 Experimental study

Two different sets of FR-SCC mixtures for repair applications were proportioned with a macro steel fiber, MSA of 14-20 mm, W/B of 0.35-0.42, and V_P of 27%-37% corresponding to conventional (CSR) and high (HSR) strength levels. The workability of the investigated FR-

SCC mixtures was evaluated using the slump flow (flowability), spread in modified J-Ring set-up (with 8 bars), and L-Box blocking ratio (h_2/h_1 in presence of 2 bars) (passing ability). The homogeneous performance of the investigated mixtures was evaluated in terms of granular blocking in the L-Box set-up (BI_{LB} index) and dynamic segregation through the T-Box set-up (DSI index), as a diphasic suspension of F-A combination in mortar matrix. The rheological properties of the investigated mortar mixtures corresponding to the CSR and HSR FR-SCC mixtures were also evaluated.

6.2.1   FR-SCC mixture proportioning

Three different classes of crushed-limestone coarse aggregate with grain-size distributions of 5-10 mm (CA1), 5-14 mm (CA2), and 5-20 mm (CA3) and one natural-river sand (0-5 mm) were used. The specific gravities of these aggregates are 2.72, 2.73, 2.76, and 2.67, respectively. The PSDs of the aggregates are shown in Figure 6-1. The CSR and HSR mixtures were proportioned with MSAs of 14 (MSA14) and 20 mm (MSA20), respectively. As shown in Table 6-1 and Figure 6-2, each of the MSA14 and MSA20 series were proportioned using three different combinations of CA1-3, leading to different levels of packing density (PD) values. This allowed to assess the effect of PSD and PD of coarse aggregate on flow performance of FR-SCC. These include MSA20-1 to MSA20-3 and MSA14-1 to MSA14-3, as shown in Table 1. The investigated FR-SCC mixtures were proportioned with a volumetric sand-to-total aggregate ratio (S/A) of 0.55. Moreover, hooked-end steel fibers with 0.55-mm diameter and 30-mm length were used (Table 6-2).

The PD of fiber-coarse aggregate (F-A) mixtures were firstly measured. Accordingly, different volumetric contents of fibers of 0.4%-0.9% were mixed with the six investigated coarse-aggregate combinations (Table 6-1) corresponding to the CSR and HSR mixtures. The PD of the investigated F-A mixtures were measured using the intensive compaction tester (ICT) and dry method [32-34]. Then, three fiber-coarse aggregate mixtures corresponding to the minimum ($PD_{minimum}$), medium (PD_{medium}), and maximum ($PD_{maximum}$) PD values for CSR and HSR applications were then selected to proportion the investigated FR-SCC mixtures. These correspond to the PD values of 0.536, 0.544, and 0.554 for CSR, and 0.533, 0.550, and 0.562 for HSR applications, respectively. Furthermore, an additional 1.77% fraction of fibers relative to F-A volume, was also considered, corresponding to a fiber volume of 0.5% in unit volume of concrete. This was done to achieve the maximum recommended fiber volume in literature (0.5%) [21]. Therefore, the fibers with volumetric fraction of 1.77% were mixed with coarse aggregate mixture of MSA14-3, resulting to a PD of 0.534.

Ten FR-SCC mixtures were then proportioned with coarse aggregate MSA14, W/B of 0.42, and paste volumes (V_P) of 0.27, 0.30, and 0.33 for CSR series (30 MPa < 28-days compressive strength f'_{c-28d} < 50 MPa). On the other hand, nine FR-SCC mixtures were proportioned with MSA20 coarse aggregate, V_P of 0.33, 0.35, and 0.37, and a W/B of 0.35 for HSR series (60 MPa < f'_{c-28d}) (Figure 6-3 and Table 6-3). Moreover, a ternary blended cement (TerC^3) containing approximately 70% general use Portland cement (GU), 25% class F fly ash, and 5% silica fume was used as binder. A polycarboxylate-based HRWR and an air-entraining agent (AEA) was used to achieve targeted slump-flow of 680 ± 20 mm and air content of 5%-8%, respectively. All the investigated FR-SCC mixtures were prepared in batches of 65 L using a rotating drum mixer.
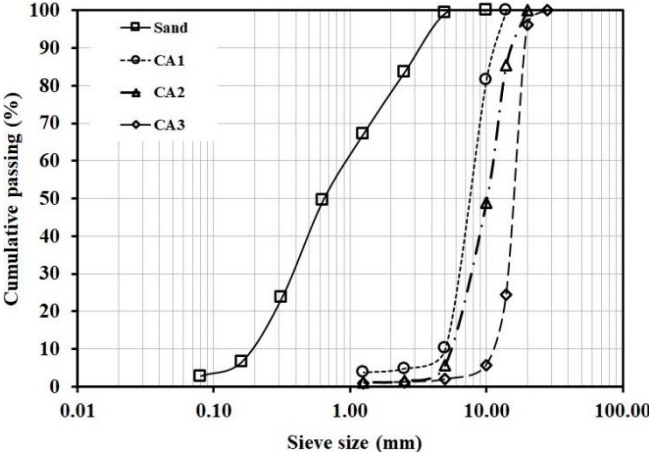
Figure 6-1 Particle-size distribution of the sand and coarse aggregate.

Table 6-1 Volumetric proportions of the investigated coarse aggregate combinations.

Application	Granular mixtures	CA1: 5-10 mm (%)	CA2: 5-14 mm (%)	CA3: 5-20 mm (%)
HSR	MSA20-1	30	55	15
	MSA20-2	15	60	25
	MSA20-3	-	65	35
CSR	MSA14-1	100	-	-
	MSA14-2	80	20	-
	MSA14-3	60	40	-

(a)   (b)
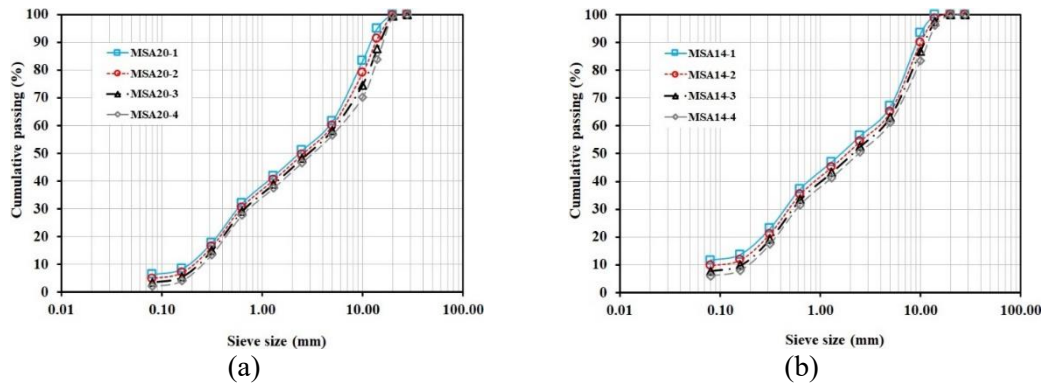
Figure 6-2 Particle-size distribution of coarse-aggregate combinations used to proportion the investigated **(a)** HSR and **(b)** CSR fiber reinforced SCC mixtures.

Table 6-2 Characteristics of steel fibres.

Type	Length (mm)	Diameter (mm)	Aspect ratio	Specific gravity	Modulus of elasticity (GPa)
Hooked end	30	0.55	55	7.85	200

(a)   (b)
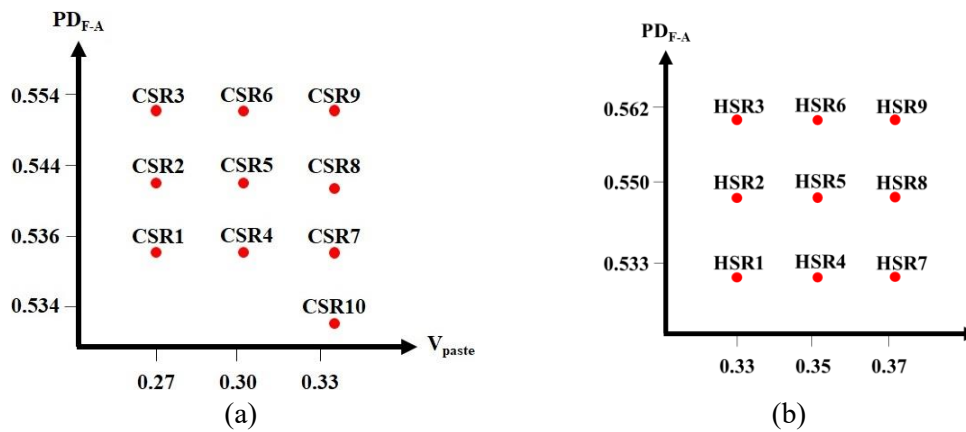
Figure 6-3 Mixture design of the investigated FR-SCC mixtures based on different volume of pastes and PSD of aggregate for (a) CSR and (b) HSR applications.

Table 6-3 Proportioning, slump flow, and compressive strength of the investigated FR-SCC mixtures (HRWR and AEA dosages are in mL/100 kg of binder).

Series	Mix	Binder (kg/m³)	V_P (%)	Sand (kg/m³)	CA1 (kg/m³)	CA2 (kg/m³)	CA3 (kg/m³)	Fiber (kg/m³)	V_f in concrete (%)	φ/φ_{max} of F-A	HRWR	AEA	Air content (%)	Slump flow (mm)	$f'_{c\text{-}28d}$ (MPa)
	CSR1	352	27	999	825	0	0	22	0.28	0.571	3300	5.0	6.3	667	30.2
	CSR2	352	27	999	661	166	0	17	0.22	0.563	2860	5.0	6.1	665	31.6
	CSR3	352	27	999	497	333	0	9	0.11	0.552	2600	5.0	7.6	662	33.2
	CSR4	392	30	955	789	0	0	20	0.25	0.546	1500	5.0	7.4	700	38.9
CSR	CSR5	392	30	955	632	159	0	16	0.20	0.538	1350	10.0	6.7	673	39.9
	CSR6	392	30	955	475	318	0	9	0.11	0.528	1180	8.0	7.2	656	47.8
	CSR7	431	33	910	752	0	0	20	0.25	0.521	1140	9.0	7.8	678	42.9
	CSR8	431	33	910	603	151	0	15	0.19	0.513	980	7.0	7.9	685	44.7
	CSR9	431	33	910	454	303	0	9	0.11	0.503	820	7.0	7.5	694	46.0
	CSR10	431	33	910	447	299	0	39	0.50	0.523	1036	7.0	7.7	675	49.4
	HSR1	474	33	910	0	493	268	9	0.11	0.524	1070	8.0	7.9	683	65.0
	HSR2	474	33	910	226	416	115	15	0.19	0.508	1070	5.0	7.6	678	62.6
	HSR3	474	33	910	113	455	192	11	0.14	0.496	1070	6.0	7.3	694	60.4
	HSR4	503	35	881	0	477	260	8	0.10	0.507	965	7.5	8	678	66.9
HSR	HSR5	503	35	881	219	403	111	15	0.19	0.491	965	9.0	7.1	695	66.1
	HSR6	503	35	881	110	440	185	11	0.14	0.480	965	6.0	7.2	697	65.3
	HSR7	532	37	852	0	461	251	8	0.10	0.490	870	10.0	7.5	694	74.6
	HSR8	532	37	852	211	389	107	14	0.18	0.475	870	10.0	8.0	690	71.0
	HSR9	532	37	852	106	425	179	10	0.13	0.464	870	10.0	6.9	695	67.7

6.2.2 Rheological evaluation of the suspending phase (paste/mortar)

The rheological properties of mortar matrices (containing aggregate finer than 5 mm) of the investigated FR-SCC mixtures were evaluated. It is worthy to mention that the viscometer ConTec 6 was firstly employed. However, no reasonable results were obtained. As an alternative approach, the investigated mortars were considered as diphasic suspensions of coarser portion of sand particles greater than 1.25 in fine mortar, containing aggregate finer than 1.25 mm, to allow precise rheological measurements. On the other hand, the fine mortar itself is considered as a diphasic suspension of fine sand (< 1.25 mm) in cement paste. Hosseinpoor et al. [35,36] proposed empirical models to predict the plastic viscosity ($\mu_{p\text{-FM}}$) and yield stress ($\tau_{0\text{-FM}}$) of fine mortar as functions of the relative-solid packing fraction of fine sand (φ/φ_{max}) in fine mortar and rheological properties of cement paste ($\mu_{p\text{-P}}$ and $\tau_{0\text{-P}}$), as follows:

$$\mu_{p\text{-FM}} = \mu_{p\text{-P}} \times \prod_{i=1}^{5} \left[\frac{978022.775^{\left(\frac{\varphi_{FS_i}}{\varphi_{max\text{-}FS_i}}\right)} \times 0.0000358^{\left[\frac{\left(\frac{\varphi_{FS_i}}{\varphi_{max\text{-}FS_i}}\right)}{\left(1-\frac{\varphi_{FS_i}}{\varphi_{max\text{-}FS_i}}\right)^{1.100}}\right]}}{\left(1-\frac{\varphi_{FS_i}}{\varphi_{max\text{-}FS_i}}\right)^{\left[\frac{2.865}{\left(1-\frac{\varphi_{FS_i}}{\varphi_{max\text{-}FS_i}}\right)}\right]}} \right] \qquad \text{Equation 6-1}$$

$$\tau_{0\text{-FM}} = \tau_{0\text{-P}} \times \prod_{i=1}^{5} \left[\frac{0.023^{\left(\frac{\varphi_{FS_i}}{\varphi_{max\text{-}FS_i}}\right)} \times 3.557^{\left[\frac{\left(\frac{\varphi_{FS_i}}{\varphi_{max\text{-}FS_i}}\right)}{\left(1-\frac{\varphi_{FS_i}}{\varphi_{max\text{-}FS_i}}\right)^{3.350}}\right]}}{\left(1-\frac{\varphi_{FS_i}}{\varphi_{max\text{-}FS_i}}\right)^{\left[\frac{1.215}{\left(1-\frac{\varphi_{FS_i}}{\varphi_{max\text{-}FS_i}}\right)}\right]}} \right] \qquad \text{Equation 6-2}$$

where i = 1 to 5 are different size classes of fine sand, corresponding to successive standard sieves of 0-0.080, 0.080-0.160, 0.160-0.315, 0.315-0.630, and 0.630-1.25 mm, respectively (Table 6-4). Moreover, φ_{max-FS_i} is the maximum packing density of subclass "i" of fine sand (Table 6-4), and φ_{FS_i} is the volumetric content of subclass "i" in a suspension of the fine-sand particles finer or equal to subclass "i" (i.e., ≤ i) in cement paste with plastic viscosity μ_{p-P} and yield stress τ_{0-P}.

On the other hand, the plastic viscosity (μ_{p-M}) and yield stress (τ_{0-M}) of the investigated mortar mixtures, containing aggregate finer than 5 mm, were evaluated by considering the product of dispersed different subclasses of coarser portion of sand (CS) of 1.25-2.5, 2.5-5, and 5-10 mm (i = 6 to 8 in Table 6-4) in fine-mortar mixtures according to the following models reported in literature [37-40]:

$$\mu_{p-M} = \mu_{p-FM} \times \prod_{i=6}^{8} \left[\left(1 - \frac{\varphi_{CS_i}}{\varphi_{max-CS_i}} \right)^{-1 \times \eta^*_i \times \varphi_{max-CS_i}} \right]$$

Equation 6-3

$$\tau_{0-M} = \tau_{0-FM} \times \prod_{i=6}^{8} \sqrt{ (1 - \varphi_{CS_i}) \left(1 - \frac{\varphi_{CS_i}}{\varphi_{max-CS_i}} \right)^{-1 \times \eta^*_i \times \varphi_{max-CS_i}} }$$

Equation 6-4

where φ_{max-CS_i} is the maximum packing density of subclass "i" of coarse sand (i = 6 to 8 in Table 6-4) and φ_{CS_i} is its volumetric content in suspension of the coarse sand, finer or equal to subclass "i" (i.e., ≤ i) in a fine mortar with plastic viscosity μ_{p-FM} and yield stress τ_{0-FM}. Moreover, the η^*_i parameter in Equations 6-3 and 6-4 refers to the shape-dependent intrinsic viscosity of coarse sand subclass "i", which equals 2.5 for spheres [26-28]. It is worthy to mention that the η^*_i of coarse subclasses of sand were extrapolated by Hosseinpoor et al. [36] using the empirical model proposed by Struble et al. [41] and presented in Table 6-4. It is worthy to mention that the $\varphi_{FS_{i=1 \text{ to } 5}}$ and $\varphi_{CS_{i=6 \text{ to } 8}}$ values were identified using the PSD of sand (Figure 6-1) and sand content (Table 6-1) in each of the investigated FR-SCC mixtures.

Table 6-4 Characteristics of different subclasses of sand (< 5 mm).

Sand subclass No. (i)	Size threshold	Sieve size range (mm)	Packing density (φ_{max-FS_i} and φ_{max-CS_i})	Intrinsic viscosity (η^*_i)
1		0.-0.080	0.613	
2		0.080-0.160	0.587	
3	Fine sand (FS < 1.25 mm)	0.160-0.315	0.580	-
4		0.315-0.630	0.575	
5		0.630-1.25	0.561	
6		1.25-2.5	0.570	3.64
7	Coarse sand (CS > 1.25 mm)	2.5-5	0.537	4.37
8		5-10	0.511	3.87

The rheological properties of the paste mixtures were assessed using a coaxial-cylinders rheometer equipped with serrated-inner and smooth outer cylinders with diameters of 26.660 and 28.911 mm, respectively. The plastic viscosity (μ_{p-P}) and yield stress (τ_{0-P}) of the investigated cement pastes were measured by applying a pre-shearing of 150 s^{-1} for 2 min (red zone in Figure 6-4) followed by stepwise decreasing of shear rate from 150 s^{-1} to 1 s^{-1} for 105 s (blue zone in Figure 6-4). Stability of the investigated cement paste mixtures was checked by re-applying a shear rate of 100 s^{-1} at the end of the shear protocol (green zone in Figure 6-4).

The stability of the paste was confirmed by comparing the shear stresses obtained at the first and second 100 s^{-1} shear rates.
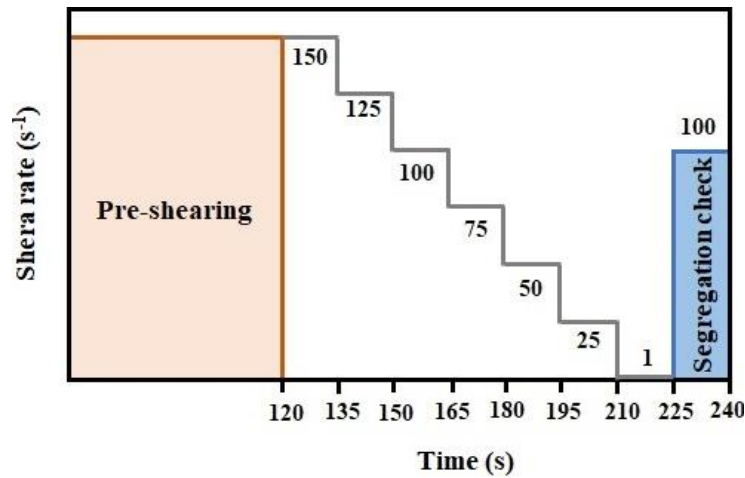
Figure 6-4 Shear protocol used to evaluate the rheological properties of the investigated cement paste mixtures [35].

In total, 13 cement paste mixtures, including 10 for CSR and 3 for HSR series, were prepared and their rheological properties were evaluated (Figures 6-5a and 6-5b and Table 6-5). It is worthy to mention that in order to reproduce the suspending phases exist in the investigated concrete suspensions, the cement paste mixtures were proportioned using the same dosages of HRWR and AEA of their corresponding FR-SCC mixtures. The obtained flow curves of the investigated cement pastes are presented in Figures 6-5a and 6-5b. Moreover, as can be observed in Figure 6-5c, the shear stress values obtained under both primary and secondary 100 s^{-1}-shear rates are in good agreement, confirming a good stability of the investigated cement paste mixture

(a)

(b)

(c)
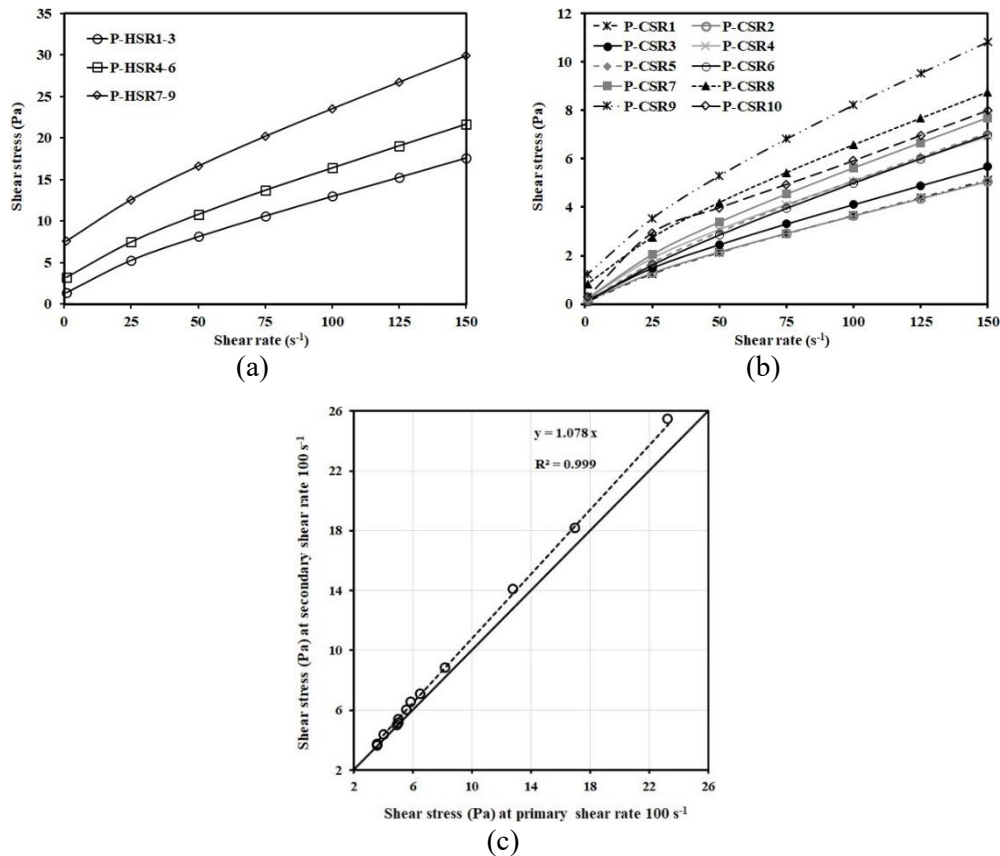
Figure 6-5 Flow curves obtained for the investigated cement paste mixtures, corresponding to the (a) HSR and (b) CSR series, as well as (c) comparison between the shear stress values obtained at the primary and secondary applied 100 s-1-shear rates for the investigated cement paste mixtures.

Table 6-5 Rheological properties of the investigated cement paste mixtures.

Application	Cement paste No.	Corresponding FR-SCC mixture	$\tau_{0\text{-}P}$ (Pa)	$\mu_{P\text{-}P}$ (Pa.s)
CSR	P-CSR1	R1	0.61	0.029
	P-CSR2	R2	0.76	0.0287
	P-CSR3	R3	0.95	0.032
	P-CSR4	R4	1.01	0.040
	P-CSR5	R5	1.09	0.040
	P-CSR6	R6	1.22	0.040
	P-CSR7	R7	1.27	0.043
	P-CSR8	R8	1.69	0.047
	P-CSR9	R9	2.85	0.053
	P-CSR10	R10	1.58	0.045
HSR	P-HSR1-3	P1-3	2.16	0.104
	P-HSR4-6	P4-6	4.39	0.122
	P-HSR7-9	P7-9	7.71	0.141

As presented in Table 6-6, the rheological properties of the investigated mortars corresponding to the investigated FR-SCC mixtures were then evaluated using the rheological properties of their corresponding cement paste mixtures (Table 6-5) and Equations 6-1 to 6-4.

Table 6-6 Rheological properties of the investigated mortar mixtures (sand < 5 mm).

Application	Mortar No.	Corresponding FR-SCC mixture	Corresponding cement paste mixture	V_P in mortar	$\tau_{0\text{-}M}$ (Pa)	$\mu_{p\text{-}M}$ (Pa.s)
CSR	M-CSR1	CSR1	P-CSR1	0.39	8.75	2.83
	M-CSR2	CSR2	P-CSR2	0.39	10.91	2.80
	M-CSR3	CSR3	P-CSR3	0.39	13.49	3.07
	M-CSR4	CSR4	P-CSR4	0.42	6.58	3.55
	M-CSR5	CSR5	P-CSR5	0.42	7.05	3.54
	M-CSR6	CSR6	P-CSR6	0.42	7.96	3.55
	M-CSR7	CSR7	P-CSR7	0.46	4.61	3.24
	M-CSR8	CSR8	P-CSR8	0.46	6.12	3.55
	M-CSR9	CSR9	P-CSR9	0.46	10.33	4.02
	M-CSR10	CSR10	P-CSR10	0.46	5.78	3.39
HSR	M-HSR1-3	HSR1-3	P-HSR1-3	0.46	8.49	8.03
	M-HSR4-6	HSR4-6	P-HSR4-6	0.48	12.54	8.20
	M-HSR7-9	HSR7-9	P-HSR7-9	0.50	17.68	8.27

6.2.3 Workability measurements

Immediately after mixing, the air content, slump flow [42], J-Ring [31], L-Box [13], and T-Box [4,5,8] tests were carried out. The passing ability and granular blocking of the investigated FR-SCC mixtures were evaluated using both the J-Ring and L-Box test set-ups. The J-Ring test was carried out using eight reinforcing bars of 16-mm diameter. The ratio of the spread between the concrete flow diameters after the J-Ring (JRF) and slump flow tests-to-the slump flow values (SF) was considered to evaluate the passing ability of the investigated mixtures, as follows:

$$\Delta_{JR} \ (\%) = \frac{SF - JRF}{SF} \times 100\% \qquad \text{Equation 6-5}$$

Moreover, the L-Box test was performed using two 10-mm diameter reinforcement bars located right after the gate that provide a 60-mm clear spacing between the bars (Figure 6-6a). The L-Box blocking ratio (h_2/h_1) was calculated to evaluate the passing ability of the investigated FR-SCC mixtures. Moreover, the granular blocking of the investigated FR-SCC mixtures using two cylindrical samples, measuring 100-mm diameter and 200-mm height, taken from the beginning (behind bars) and end of the horizontal channel of the L-Box set-up, immediately after the test (Figure 6-6a).

Furthermore, the T-Box test [4,5,8] was performed to evaluate the dynamic stability of the investigated mixtures. As shown in Figure 6-6b, a 16-L sample of concrete was placed in the horizontal channel. The box is then subjected to 120 s of 60 tilting cycles (2 s/cycle). Similar to the granular blocking measurements, in order to evaluate the dynamic segregation of the investigated FR-SCC mixtures, two cylindrical samples (100 mm in diameter and 200 mm in height) were taken from each tilt-up and tilt-down sections, immediately after the test (Figure 6-6b).

The fiber-coarse aggregate portions of the concrete samples taken from the L-Box and T-Box set-ups were extracted by wet-sieving on a 5-mm sieve and then dried. The fibers were then separated from the aggregate using a magnet. Extracted dry coarse aggregate and fibers were then weighed. For each sample, the volumetric content of the extracted fibers and coarse aggregate and the PSD of the extracted coarse aggregate were determined. The fibers were then

mixed with the coarse aggregate to achieve a homogeneous dispersion. The PD of the extracted fiber-coarse aggregate mixtures were determined by means of the ICT device using the same method applied for the F-A mixtures in section 2.1. It is worthy to mention that in order to calculate the PD of the F-A samples, it is required to evaluate the volume of coarse aggregate in each sample. Accordingly, the density values of the extracted coarse aggregate were estimated using the arithmetic volumetric average of the density values of different classes of aggregate in each coarse aggregate sample. The volumetric contents of different classes of aggregate in each extracted coarse aggregate sample were evaluated using PSD of the extracted coarse aggregate. The volume of the extracted coarse aggregate sample was then measured by dividing their mass to their estimated density.

(a)   (b)
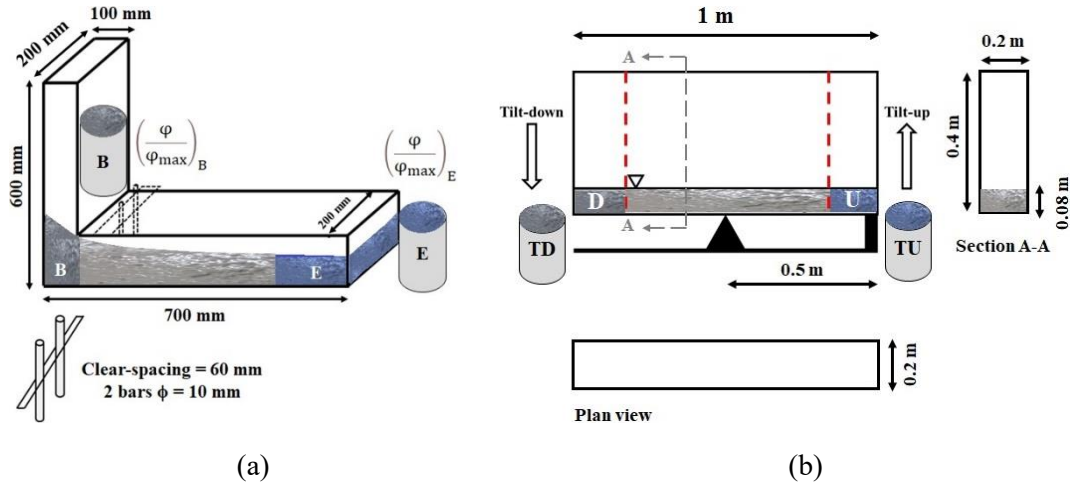
Figure 6-6 (a) Sampling method for (a) L-Box and (b) T-Box tests.

According to the methods proposed by Koura et al. [4] and Hosseinpoor et al. [5,6], the blocking (BI) and dynamic segregation indices (DSI) of the investigated FR-SCC mixtures through the L-Box and T-Box set-ups were evaluated using the variation of the ratio of the volumetric content (φ)-to-packing density (φ_{max}) of the fiber-coarse aggregate mixtures (φ/φ_{max}) in different zones of the set-ups, relative to the reference mixtures, as follow:

$$\text{BI (\%)} = \frac{\left(\frac{\varphi}{\varphi_{max}}\right)_B - \left(\frac{\varphi}{\varphi_{max}}\right)_E}{\left(\frac{\varphi}{\varphi_{max}}\right)_{Ref}} \times 100\% \qquad \text{Equation 6-6}$$

$$\text{DSI (\%)} = \frac{\left(\frac{\varphi}{\varphi_{max}}\right)_{TD} - \left(\frac{\varphi}{\varphi_{max}}\right)_{TU}}{\left(\frac{\varphi}{\varphi_{max}}\right)_{Ref}} \times 100\% \qquad \text{Equation 6-7}$$

where $\left(\frac{\varphi}{\varphi_{max}}\right)_B$, $\left(\frac{\varphi}{\varphi_{max}}\right)_E$, $\left(\frac{\varphi}{\varphi_{max}}\right)_{TD}$, $\left(\frac{\varphi}{\varphi_{max}}\right)_{TU}$, and $\left(\frac{\varphi}{\varphi_{max}}\right)_{Ref}$ are the volumetric content-to-packing density ratios of the fiber-aggregate mixtures corresponding to the samples taken behind the rebars and end of the horizontal channel of the L-Box set-up, tilt-down and tilt-up zones of the

T-Box set-up, and reference mixture, respectively. The results of the workability tests are presented in Table 6-7.

Table 6-7 Workability results of investigated FR-SCC mixtures.

Application	Mix	Passing ability		Granular blocking	Dynamic segregation
		ΔJR (%)	h_2/h_1	BI (%)	DSI (%)
CSR	CSR1	15.15	0.002	79.69	0.42
	CSR2	9.16	0.636	47.33	17.66
	CSR3	3.01	0.789	11.98	12.23
	CSR4	4.44	0.696	19.52	20.40
	CSR5	3.79	0.800	14.34	18.44
	CSR6	2.19	0.808	18.06	40.25
	CSR7	2.86	0.800	14.64	49.58
	CSR8	0.71	0.909	16.67	71.37
	CSR9	2.07	0.750	9.83	54.77
	CSR10	2.22	0.727	11.39	40.64
HSR	HSR1	3.66	0.808	34.02	35.69
	HSR2	2.95	0.900	25.71	45.13
	HSR3	0.72	1.000	19.10	62.33
	HSR4	4.42	0.750	28.73	32.63
	HSR5	3.74	0.800	22.35	43.06
	HSR6	1.43	0.878	13.50	57.74
	HSR7	7.35	0.682	27.74	27.62
	HSR8	5.07	0.762	21.27	30.39
	HSR9	4.32	0.800	10.43	46.40

6.3 Results and discussions

According to the experimental results, the coupled effect of different mixture constituents, as well as the rheological properties of the mortar mixtures (sand < 5 mm) and φ/φ_{max} of F-A (> 5 mm) on heterogeneous behavior of FR-SCC mixtures were evaluated. These include passing ability (ΔJR and h_2/h_1), BI, and DSI indices.

6.3.1 Effect of paste volume and fiber-coarse aggregate characteristics on HRWR demand

The mixture proportioning of FR-SCC includes the simultaneous optimization of several influencing factors to achieve the targeted flow and mechanical properties. These factors include the W/B, volume of paste (V_P), HRWR and AEA dosage rates, and characteristics of coarse aggregate and fibers. In this study, the HRWR dosages were adjusted to achieve a targeted slump flow of 680 ± 20 mm. The effect of W/B, fiber-coarse aggregate characteristics, and V_P on HRWR demand was evaluated. As can be observed in Figure 6-7, the HRWR demand (mL/100 kg of binder) is in good agreement with the W/B, φ/φ_{max} of fiber-coarse aggregate combination, and V_P (%) (Table 6-3). Relationships with high coefficient of determination (R^2) of 0.993 and low root-mean squared-error (RMSE) of 60.1 mL/100 kg of binder was established. According to the correlation, the FR-SCC mixtures proportioned with higher W/B and paste volume, as well as fiber-coarse aggregate combination with lower φ/φ_{max} required lower HRWR demand. This can be explained by higher volume of paste available to lubricate the aggregate and fibers, hence increasing the fluidity of the mixture for a given HRWR and W/B. Lower HRWR (mL/100 kg binder) is then required to achieve a given flowability.

$$HRWR\left(\frac{mL}{100 \text{ kg of Binder}}\right) = 198.912 - \frac{136.385}{\left(\frac{W}{B}\right)^{0.766} \times \left[1.460 \times \sqrt{\frac{\varphi}{\varphi_{max}}} \times \ln\left(\frac{\varphi}{\varphi_{max}}\right) + \frac{374.826}{V_p^2} + 0.044\right] - 0.013}$$
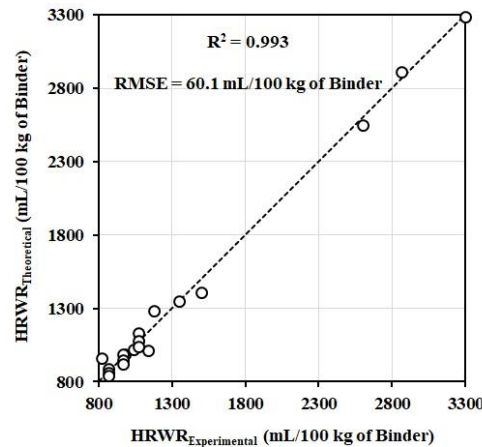
Figure 6-7 Relationship between the HRWR demand, W/B, paste volume, and φ/φ_{max} of the fiber-coarse aggregate of the investigated FR-SCC mixtures.

The robustness of the HRWR demands due to small variations of FR-SCC mixture parameters, including the water content, paste volume (V_P), and φ/φ_{max} of fiber-coarse aggregate combination was evaluated. According to the European guideline [43], a maximum variation of ± 10 L/m³ in water content can be considered. Moreover, the sensitivity of the established correlation (Figure 6-7) to the variation of ± 5% in V_P and φ/φ_{max} values was assessed, as recommended by Hosseinpoor et al. [6] for plain SCC. The 1-way, 2-way, and 3-way robustness analyses, corresponding to single, double, and triple variations of the mixture parameters, respectively, were then employed. Using the established correlation in Figure 6-7, the HRWR demand of mixtures proportioned with ± 10 L/m³ water content, ± 5% V_P, and ± 5% φ/φ_{max} values was estimated. The variations in the RMSE (ΔRMSE) and coefficients of determination (ΔR²) of the HRWR demand, induced by the single, double, and triple variations of the mixture parameters, relative to the experimental HRWR dosage, were calculated and summarized in Table 6-8. It is worthy to mention that the ΔRMSE and ΔR² values were calculated, as follows:

$$\Delta RMSE = RMSE_{\text{with variations}} - RMSE_{\text{without variations}} \qquad \text{Equation 6-8}$$

$$\Delta R^2 = R^2_{\text{with variations}} - R^2_{\text{without variations}} \qquad \text{Equation 6-9}$$

where RMSE$_{\text{without variations}}$ (60.1 ml/100 kg of Binder) and R²$_{\text{without variations}}$ (0.993) are the RMSE and R² values of the correlation established in Figure 6-7 determined using the initial mixture parameters (i.e., without any variation), respectively.

Table 6-8 Results of the robustness analysis carried out on HRWR demand due to the coupled effect of FR-SCC mixture parameters.

Robustness analysis method	Mixture parameters			Precision		Robustness analysis results	
	Water content	V_P	φ/φ_{max}	RMSE (mL/100 kg of binder)	R^2	ΔRMSE (mL/100 kg of binder)	ΔR^2
1-way	$\pm$ 10 L/m^3	-	-	77.9 - 81.2	0.99285 - 0.99289	17.9 - 21.1	(-0.00003) - 0.00001
	-	$\pm$ 5%	-	377.3 - 1629.4	0.95964 - 0.98730	317.3 - 1569.3	(-0.03324) - (-0.00557)
	-	-	$\pm$ 5%	332.2 - 804.1	0.98029 - 0.98903	272.1 - 744.1	(-0.01259) - (-0.00385)
2-way	$\pm$ 10 L/m^3	$\pm$ 5%	-	340.9 - 1669.4	0.95647 - 0.98759	280.9 - 1609.3	(-0.03641) - (-0.00529)
	$\pm$ 10 L/m^3	-	$\pm$ 5%	293.7 - 859.3	0.97904 - 0.98929	233.6 - 799.2	(-0.01384) - (-0.00359)
	-	$\pm$ 5%	$\pm$ 5%	107.2 - 20678.8	0.10703 - 0.99246	47.1 - 20618.8	(-0.88585) - (-0.00042)
3-way	$\pm$ 10 L/m^3	$\pm$ 5%	$\pm$ 5%	85.9 - 32473.1	0.03360 - 0.99253	25.8 - 32413.0	(-0.95928) - (-0.00035)

As shown in Table 6-8, HRWR demand showed its maximum robustness due to single variation of water content, leading to low ΔRMSE and ΔR^2 of up to 21.1 mL/100 kg of binder and 0.00001, respectively. However, HRWR was found highly sensitive to any single or multiple variations of V_P and φ/φ_{max} of fiber-coarse aggregate. Moreover, the robustness analyses revealed that HRWR demand is more affected by the variation of φ/φ_{max} of fiber-coarse aggregate rather than paste volume, leading to higher ΔRMSE and ΔR^2 values.

6.3.2   Passing ability and granular blocking

In order to achieve the targeted flow performance of the FR-SCC mixtures through the restricted elements, it is necessary to understand the influencing parameters and predict their coupled effect on passing ability and granular-blocking resistance. In this section, the coupled effect of fiber-aggregate characteristics and cement paste-related factors, including W/B, HRWR dosage, and V_P on passing ability of the investigated FR-SCC mixtures was first evaluated. The coupled effect of biphasic constituents of FR-SCC, including φ/φ_{max} of fiber-coarse aggregate combination (solid phase) and rheological properties of mortar (suspending phase) on passing ability and granular blocking of the investigated mixtures was then assessed.

Passing ability

The results of the passing ability evaluation of the investigated FR-SCC mixtures are summarized in Table 6-7 in terms of ΔJR and h_2/h_1 values, obtained using the J-Ring and L-Box tests, respectively. As can be observed in Figure 6-8, the passing ability results obtained using the J-Ring and L-Box tests are well correlated to each other (high R^2 of 0.992). According to the established correlation in Figure 6-8, lower differences between the concrete final spreads at slump flow and J-Ring tests (ΔJR) are expected for the FR-SCC mixtures showing higher h_2/h_1 ratios through the L-Box test. This corresponds to high flowability through the restricted element.

$$\frac{h_2}{h_1} = \sqrt{0.818 - 0.054 \times \Delta JR}$$

$$R^2 = 0.992$$
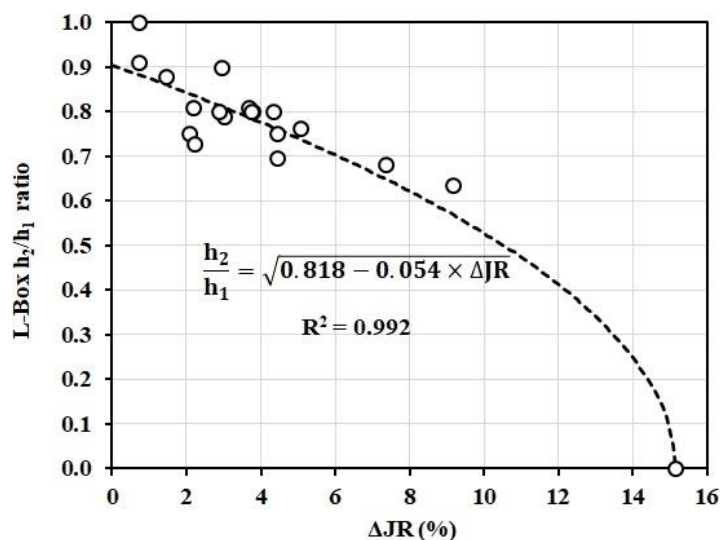
Figure 6-8 Relationship between the passing ability results of the investigated FR-SCC mixtures, including L-Box h_2/h_1 ratio versus ΔJR values.

Considering the good agreement between the ΔJR and h_2/h_1 values, the coupled effect of different mixture constituents on passing ability of the investigated FR-SCC mixtures were only evaluated for the J-Ring test results. As shown in Figure 6-9, the obtained ΔJR values

were well correlated to different mixture parameters, including W/B, HRWR dosage, V_P, and φ/φ_{max} of fiber-coarse aggregate, reflected by high R^2 and low RMSE values of 0.761 and 1.607%, respectively.

$$\Delta JR = 14.436 + 53.874 \times \left| \left[\frac{V_p}{\left(\frac{\varphi}{\varphi_{max}} \right)} \right] \right| \times \ln \left[\frac{V_p}{\left(\frac{\varphi}{\varphi_{max}} \right)} \right] + 13.627 \times \left(HRWR \times \frac{W}{B} \right)^2 \times \ln \left(HRWR \times \frac{W}{B} \right)$$

$$R^2 = 0.761$$
$$RMSE = 1.607\%$$

Figure 6-9 Coupled effect of the HRWR dosage, W/B, paste volume, and φ/φ_{max} of the fiber-coarse aggregate combination on passing ability (ΔJR values) of the investigated FR-SCC mixtures.

The robustness analyses of the ΔJR results due to ± 10 kg/m^3 variation of water content and ± 5 % variations in paste volume, HRWR dosage, and φ/φ_{max} of fiber-coarse aggregate (single and multiple variations) were carried out using the established correlation in Figure 6-9 and presented in Table 6-9. According to the obtained low ΔRMSE and ΔR^2 values in Table 6-9, it can be concluded that the passing ability of the investigated FR-SCC mixtures, evaluated using the J-Ring set-up, is highly robust due to any single or multiple slight variations in paste volume and φ/φ_{max} of fiber-coarse aggregate. However, obtaining relatively higher ΔRMSE and ΔR^2 values, the ΔJR results were found to be more sensitive to the single and multiple variations of water content and HRWR dosage.

Moreover, the coupled effect of mortar rheology and fiber-coarse aggregate characteristics on passing ability of the investigated mixtures were evaluated considering the biphasic approach. As can be observed in Figure 6-10, the ΔJR values of the investigated FR-SCC mixtures were correlated to the yield stress of their corresponding mortar matrices (τ_{0-M} in Table 6-6) and relative-solid packing fraction of the fiber-coarse aggregate portion (φ/φ_{max} in Table 6-3). High R^2 of 0.833 and low RMSE of 1.344% were obtained. According to the established correlation in Figure 6-10, increasing both the yield stress of mortar and φ/φ_{max} of fiber-coarse aggregate led to lower passing ability, reflected by higher ΔJR values. This can be due to higher interparticle interactions in the mixtures proportioned with higher φ/φ_{max} values, hence leading to higher frictional stresses between the suspending mortar, fibers, and coarse aggregate. This can limit the flow of concrete in presence of the reinforcing bars. In the case of high-yield stress mortar mixtures, the gravity-induced and inertial stresses cannot overcome the abovementioned shear and frictional stresses and lower passing ability is obtained. However, the φ/φ_{max} of fiber-coarse aggregate showed more dominant effect on passing ability of FR-SCC rather than mortar yield stress, as reflected by higher power indices in the established correlation.

Table 6-9 Results of the robustness analyses carried out on the passing ability of FR-SCC mixtures.

Robustness analysis method	Mixture constituents				Precision		Robustness analysis results	
	V_P	φ/φ_{max}	HRWR	Water content	RMSE (%)	R^2	ΔRMSE (%)	ΔR^2
1-way	±5%	-	-	-	1.649 - 1.666	0.749 - 0.751	0.042 - 0.059	(-0.012) - (-0.0099)
	-	±5%	-	-	1.646 - 1.673	0.747 - 0.752	0.039 - 0.066	(-0.0138) - (-0.0092)
	-	-	±5%	-	1.701 - 1.754	0.754 - 0.761	0.094 - 0.146	(-0.0067) - (-0.0002)
	-	-	-	±10 L/m³	1.772 - 1.869	0.751 - 0.758	0.165 - 0.262	(-0.0099) - (-0.0027)
2-way	±5%	±5%	-	-	1.608 - 1.931	0.694 - 0.761	0.0003 - 0.3242	(-0.0669) - (-0.0001)
	±5%	-	±5%	-	1.690 - 1.844	0.722 - 0.762	0.083 - 0.237	(-0.0387) - 0.0009
	±5%	-	-	±10 L/m³	1.748 - 1.971	0.707 - 0.765	0.141 - 0.364	(-0.0536) - 0.0042
	-	±5%	±5%	-	1.689 - 1.839	0.719 - 0.762	0.082 - 0.232	(-0.042) - 0.0015
	-	±5%	-	±10 L/m³	1.748 - 1.965	0.703 - 0.765	0.141 - 0.358	(-0.0578) - 0.0046
	-	-	±5%	±10 L/m³	1.622 - 2.394	0.737 - 0.762	0.014 - 0.787	(-0.0242) - 0.0014
3-way	±5%	±5%	±5%	-	1.701 - 2.097	0.622 - 0.761	0.094 - 0.4899	(-0.1389) - (-0.0002)
	±5%	±5%	-	±10 L/m³	1.761 - 2.176	0.589 - 0.758	0.154 - 0.568	(-0.1722) - (-0.0027)
	±5%	-	±5%	±10 L/m³	1.643 - 2.521	0.638 - 0.770	0.036 - 0.913	(-0.1227) - 0.0095
	-	±5%	±5%	±10 L/m³	1.641 - 2.514	0.631 - 0.770	0.033 - 0.906	(-0.1297) - 0.0092
4-way	±5%	±5%	±5%	±10 L/m³	1.622 - 2.657	0.468 - 0.762	0.014 - 1.050	(-0.2929) - 0.0014

$$\Delta JR = 50.661 + \frac{0.272 \times \left(\frac{\varphi}{\varphi_{max}}\right)^{30.211}}{\left(1 - \frac{\varphi}{\varphi_{max}}\right)^{24.514}} - \frac{52.652}{\tau_{0-M}^{0.0448}}$$

$$R^2 = 0.833$$

$$RMSE = 1.344\%$$
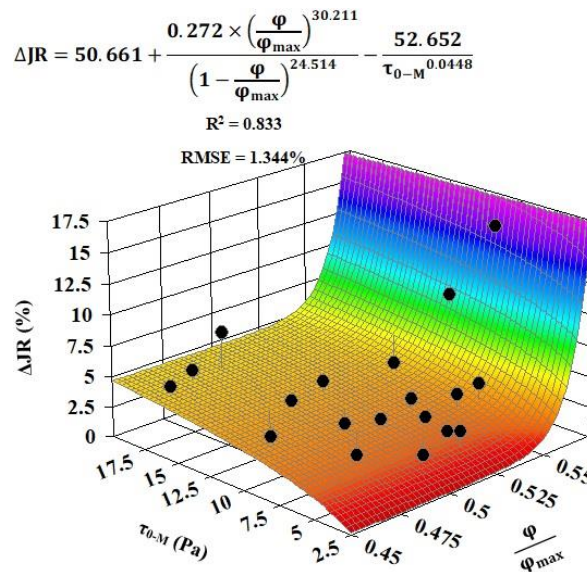
Figure 6-10 Coupled effect of mortar's yield stress and φ/φ_{max} of the fiber-coarse aggregate combination on ΔJR results of the investigated FR-SCC mixtures.

Granular blocking

As can be observed in Figure 6-11, the granular blocking indices of the investigated FR-SCC mixtures using the L-Box set-up (BI) are in good agreement with the mixture parameters, including W/B, HRWR dosage (L/100 kg of binder), paste volume (V_P), and φ/φ_{max} of fiber-coarse aggregate combination, reflected by an acceptable R^2 of 0.703 and low RMSE of 8.754%. According to the established correlation, increasing φ/φ_{max} of fiber-coarse aggregate and lowering paste volume led to higher granular blocking behind the bars in the L-Box set-up. This can be explained by the lower mean distance between the coarse aggregate and fibers due to lower paste volume and higher relative solid packing fraction of coarse aggregate and fibers. This consequently led to higher interlocking between the coarse aggregate and rigid fibers. This can result in higher possibility of blockage of fibers and coarse aggregate passing across the reinforcing bars. On the other hand, regarding the correlated power-law effect, for a given paste volume and compacity of the fiber-coarse aggregate (i.e., given φ/φ_{max}), increasing the W/B and HRWR dosage led to higher BI indices. This can result in higher fluidity of the mortar phase, hence lowering the drag forces exerted on the fibers and coarse aggregate. The highly-flowable mortar matrices cannot sufficiently push the fibers and coarse aggregate to pass through the reinforcing bars, hence higher blocking is expected.

The robustness analyses of the BI indices due to single and multiple variations of 10 L/m³ water content and 5% in paste volume, φ/φ_{max} of fiber-coarse aggregate combination, and HRWR dosage is presented in Table 6-10. As can be observed, due to lower $\Delta RMSE$ values, granular blocking of the investigated FR-SCC mixtures is only relatively robust due to single variations of HRWR dosage and water content. On the other hand, the BI indices were found to be dominantly controlled by the V_P and φ/φ_{max} of fiber-coarse aggregate, reflected by high $\Delta RMSE$ values for their any single or multiple variations. According to the carried-out robustness analyses (Tables 6-9 and 6-10), it can be concluded that in order to enhance the passing ability of FR-SCC, optimizing the volumetric contents of cement paste, fiber, and aggregate, as well as packing density of fiber-coarse aggregate combinations is a more effective approach rather than optimizing the HRWR dosage and W/B.

$$BI = 0.0399 \times 5.088^{\left[1 \middle/ \left(\frac{v_p}{\varphi}\middle/\left(\frac{\varphi}{\varphi_{max}}\right)\right)\right]^2} \times \left(HRWR \times \frac{W}{B}\right)^{\left[2.610 \times \ln\left(HRWR \times \frac{W}{B}\right)\right]}$$
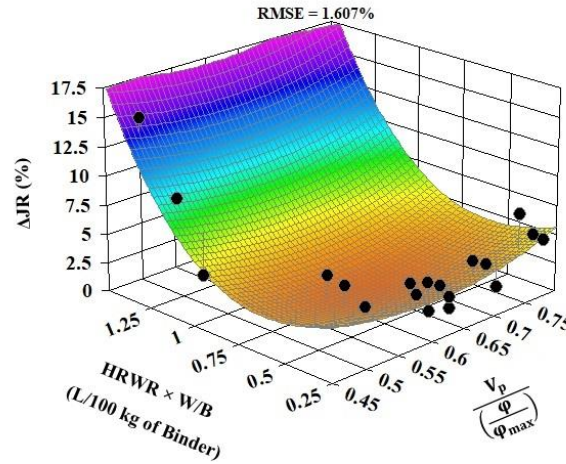
$$R^2 = 0.703$$

$$RMSE = 8.754\%$$

Figure 6-11 Coupled effect of the HRWR dosage, W/B, paste volume, and φ/φ_{max} of the fiber-coarse aggregate combination on granular blocking indices (BI) of the investigated FR-SCC mixtures in the L-Box test.

Table 6-10 Results of the robustness analyses carried out on the granular blocking of FR-SCC mixtures

Robustness analysis method	Mixture constituents				Precision		Robustness analysis results	
	V_P	φ/φ_{max}	HRWR	Water Content	RMSE (%)	R^2	ΔRMSE (%)	ΔR^2
1-way	±5%	-	-	-	12.796 - 32.146	0.653 - 0.742	4.042 - 23.392	(-0.050) - 0.039
	-	±5%	-	-	13.130 - 30.206	0.644 - 0.743	4.375 - 21.452	(-0.059) - 0.039
	-	-	±5%	-	8.796 - 12.514	0.642 - 0.751	0.042 - 3.760	(-0.061) - 0.048
	-	-	-	±10 L/m³	9.169 - 13.297	0.615 - 0.749	0.415 - 4.543	(-0.088) - 0.046
2-way	±5%	±5%	-	-	8.754 - 95.517	0.387 - 0.742	0.0001 - 86.763	(-0.316) - 0.039
	±5%	-	±5%	-	13.227 - 34.757	0.367 - 0.748	4.473 - 26.003	(-0.336) - 0.045
	±5%	-	-	±10 L/m³	13.176 - 35.210	0.320 - 0.750	4.422 - 26.456	(-0.383) - 0.047
	-	±5%	±5%	-	13.517 - 32.930	0.350 - 0.746	4.763 - 24.176	(-0.353) - 0.043
	-	±5%	-	±10 L/m³	13.525 - 33.415	0.304 - 0.749	4.771 - 24.661	(-0.399) - 0.046
	-	-	±5%	±10 L/m³	8.748 - 21.797	0.314 - 0.744	0.007 - 13.043	(-0.389) - 0.041
3-way	±5%	±5%	±5%	-	8.796 - 101.245	0.100 - 0.751	0.042 - 92.491	(-0.603) - 0.048
	±5%	±5%	-	±10 L/m³	9.169 - 104.360	0.076 - 0.749	0.415 - 95.605	(-0.627) - 0.046
	±5%	-	±5%	±10 L/m³	12.719 - 44.894	0.070 - 0.754	3.965 - 36.140	(-0.633) - 0.051
	-	±5%	±5%	±10 L/m³	13.057 - 43.116	0.063 - 0.755	4.303 - 34.362	(-0.640) - 0.052
4-way	±5%	±5%	±5%	±10 L/m³	8.748 - 115.043	0.003 - 0.753	0.007 - 106.289	(-0.700) - 0.050

The coupled effect of fiber-coarse aggregate (> 5 mm) characteristics and mortar (solid particles < 5 mm) rheology on granular blocking of the investigated HSR and CSR mixtures were evaluated using the Equations 6-10 and 6-11, respectively, established using a biphasic approach. As shown in Figure 6-12, the BI indices of the investigated FR-SCC mixtures are in very good agreement with volumetric fiber content (V_f) and φ/φ_{max} of fiber-coarse aggregate combination, as well as yield stress (τ_{0-M}) and plastic viscosity (μ_{p-M}) of their corresponding mortar matrices (high R^2 of 0.959 and low RMSE of 3.255%). It is worth mentioning that according to Hosseinpoor et al. [6], the "$1 - \frac{\varphi}{\varphi_{max}}$" term represents the excess volume of mortar (V_{EM}) which contributes in lubricating the solid phase and governing the fluidity of concrete.

$$\text{BI}_{\text{HSR}}(\%) = 22.854 \times \frac{V_f^{0.721} \times \left(\dfrac{\varphi}{\varphi_{\text{max}}}\right)^{0.368}}{\tau_{0\text{-M}}^{0.097} \times \mu_{p\text{-M}}^{26.254} \times \left(1 - \dfrac{\varphi}{\varphi_{\text{max}}}\right)^{38.969}} + 14.470 \qquad \text{Equation 6-10}$$

$$\text{BI}_{\text{CSR}}(\%) = 216.586 \times \frac{V_f^{0.0001} \times \left(\dfrac{\varphi}{\varphi_{\text{max}}}\right)^{0.835}}{\tau_{0\text{-M}}^{0.0001} \times \mu_{p\text{-M}}^{0.0001} \times \left(1 - \dfrac{\varphi}{\varphi_{\text{max}}}\right)^{0.327}} - 127.140 \qquad \text{Equation 6-11}$$
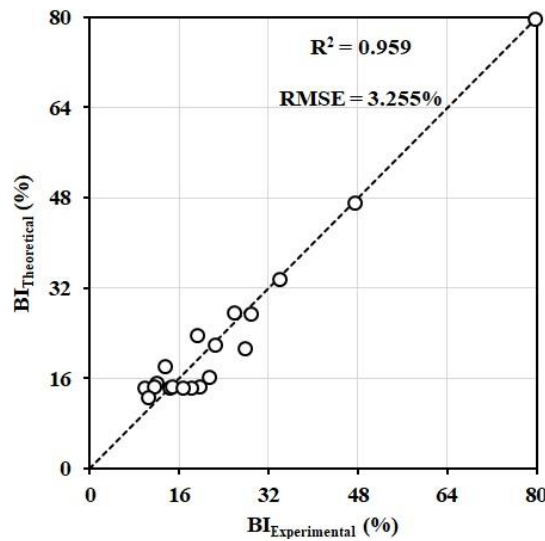
Figure 6-12 Comparison between experimental BI indices of the investigated HSR and CSR mixtures and those obtained using the established correlations Equations 6-10 and 6-11, respectively.

The negative effect of higher $\varphi/\varphi_{\text{max}}$ of fiber-coarse aggregate on passing ability of the investigated FR-SCC mixtures reflected by the established correlations Equations 6-10 and 6-11, are consistent with those explained earlier in the case of correlation presented in Figure 6-12. Furthermore, according to the established correlations, higher fiber content can increase the granular blocking potential of FR-SCC. Indeed, higher fraction of rigid steel fibers can increase the interaction between the aggregate and fibers, hence leading to higher jamming potential when passing through the narrow gaps between the reinforcing bars. Moreover, according to the Equations 6-10 and 6-11, the FR-SCC mixtures proportioned with higher yield-stress and plastic-viscosity mortar matrices exhibited lower blocking indices. Indeed, increasing plastic viscosity of suspending mortar results in higher drag forces exerted on coarse aggregate and fibers, hence limiting their relative velocity compared to the mortar matrix. Mortars with higher yield stress values can resist the forces applied on coarse aggregate and fibers and avoid their separation from surrounding mortars. Thus, lower blocking-induced segregations in the FR-SCC mixtures can be achieved.

On the other hand, the adjustment factors obtained in the established correlations Equations 6-10 and 6-11 revealed that granular blocking of the FR-SCC mixtures for HSR application is more affected by rheological properties of mortars, fiber content, and excess volume of mortar V_{EM}. However, in the case of the CSR mixtures, the BI indices are more controlled by the $\varphi/\varphi_{\text{max}}$ of fiber-coarse aggregate portion. This can be explained by the fact that these mixtures

were proportioned with lower paste and mortar content rather than those corresponding to the HSR mixtures. On the other hand, the φ/φ_{max} of fiber-coarse aggregate in CSR mixtures were higher than those used to proportion the HSR mixtures. The heterogeneous performance of HSR and CSR mixtures in the presence of reinforcing bars are thus more dependent on the characteristics of mortar (rheological properties and volume of excess mortar) and φ/φ_{max} of fiber-coarse aggregate combination, respectively.

6.3.3 Dynamic stability

Effect of mixture constituents

The coupled effect of mixture constituents on DSI obtained using the T-Box set-up was evaluated. As can be observed in Figure 6-13, the DSI values were well correlated to W/B, HRWR dosage, V_P, and φ/φ_{max} of fiber-coarse aggregate (high $R^2 = 0.716$ and low RMSE = 9.507%). According to the established correlation in Figure 6-13, lower W/B, HRWR dosage, and paste volume, as well as higher φ/φ_{max} of fiber-coarse aggregate can lead to higher dynamic stability of the FR-SCC mixtures. This is due to higher lattice effect of the fiber-aggregate combination with higher φ/φ_{max} values which push them to move and limit their dynamic segregation. On the other hand, the mortar matrices of the FR-SCC mixtures proportioned with higher W/B, HRWR dosage, and paste volume exhibit relatively higher fluidity. This leads to lower drag force exerted on coarse aggregate and fiber to keep their homogeneity during flow. Therefore, higher DSI are expected in presence of higher flowable mortar mixtures.

$$DSI = 66.318 - 316.189 \times \ln\left[\frac{V_p}{\left(\frac{\varphi}{\varphi_{max}}\right)}\right] \times \left[\frac{V_p}{\left(\frac{\varphi}{\varphi_{max}}\right)}\right]^{3.412} - 262.528 \times \left[1 - \frac{V_p}{\left(\frac{\varphi}{\varphi_{max}}\right)}\right]^{1.849} - \frac{0.0201}{\left(HRWR \times \frac{W}{B}\right)^{6.537}}$$

$$R^2 = 0.716$$
$$RMSE = 9.507\%$$

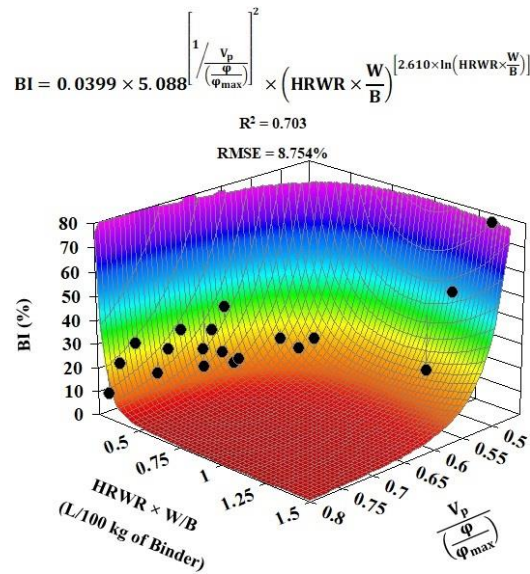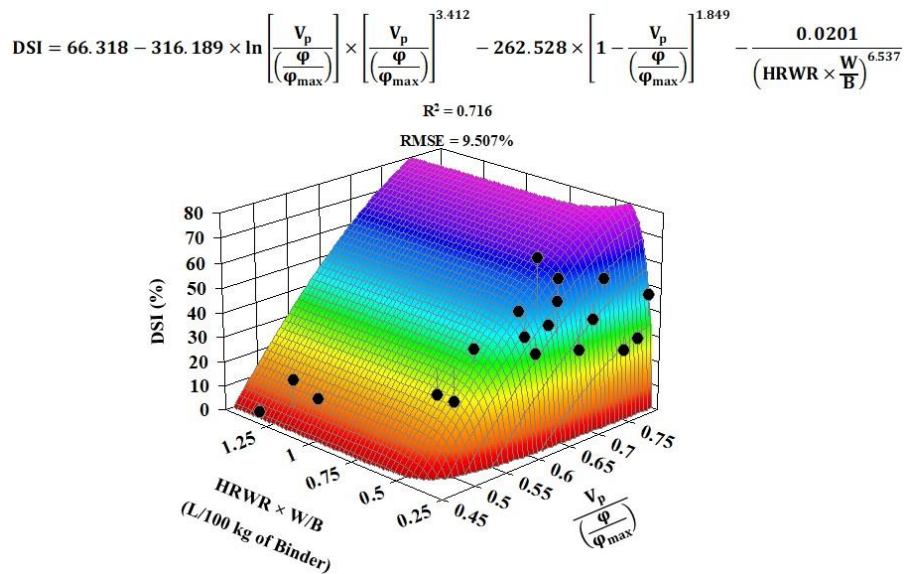

Figure 6-13 Coupled effect of the HRWR dosage, W/B, paste volume, and φ/φ_{max} of the fiber-coarse aggregate combination on DSI of the investigated FR-SCC mixtures.

The robustness of the dynamic stability of the investigated FR-SCC mixtures due to the single and multiple variations of ±10 L/m^3 of water content and $\pm5\%$ of HRWR dosage, paste volume, and φ/φ_{max} of fiber-coarse aggregate was determined and presented in Table 6-11. As can be observed, dynamic stability showed its maximum robustness reflected by relatively lower ΔRMSE and ΔR^2 values due to single variations with regard to paste content and φ/φ_{max} of fiber-coarse aggregate. On the other hand, dynamic stability of the investigated FR-SCC mixtures was found highly sensitive due to multiple variations of different mixture constituents.

Table 6-11 Results of the robustness analyses carried out on the DSI of the investigated FR-SCC mixtures.

Robustness analysis method	Mixture constituents				Precision		Robustness analysis results	
	V_P	φ/φ_{max}	HRWR	Water content	RMSE (%)	R^2	ΔRMSE (%)	ΔR^2
1-way	±5%	-	-	-	12.142 - 12.370	0.700 - 0.714	2.634 - 2.863	(-0.016) - (-0.002)
	-	±5%	-	-	12.114 - 12.370	0.698 - 0.714	2.606 - 2.862	(-0.018) - (-0.001)
	-	-	±5%	-	11.377 - 13.006	0.584 -0.667	1.870 - 3.499	(-0.132) - (-0.049)
	-	-	-	±10 L/m³	11.647 - 13.729	0.559 - 0.662	2.140 - 4.221	(-0.157) - (-0.054)
2-way	±5%	±5%	-	-	9.507 - 18.593	0.633 - 0.716	0.001 - 9.086	(-0.082)-0.001
	±5%	-	±5%	-	11.656 - 17.713	0.508 - 0.691	2.149 - 8.206	(-0.207) - (-0.0250)
	±5%	-	-	±10 L/m³	11.690 - 18.582	0.481 - 0.687	2.182 - 9.074	(-0.235) - (-0.028)
	-	±5%	±5%	-	11.513 - 17.412	0.504 - 0.692	2.006 - 7.905	(-0.212) - (-0.023)
	-	±5%	-	±10 L/m³	11.559 - 18.277	0.476 - 0.688	2.051 - 8.770	(-0.240) - (-0.027)
	-	-	±5%	±10 L/m³	9.527 - 24.767	0.215 - 0.715	0.019 - 15.260	(-0.500) - (-0.001)
3-way	±5%	±5%	±5%	-	11.377 - 24.401	0.389 - 0.699	1.870 - 14.894	(-0.327) - (-0.017)
	±5%	±5%	-	±10 L/m³	11.647 - 25.294	0.362 - 0.698	2.140 - 15.787	(-0.353) - (-0.018)
	±5%	-	±5%	±10 L/m³	11.774 - 29.828	0.172 - 0.718	2.266 - 20.321	(-0.544) - 0.003
	-	±5%	±5%	±10 L/m³	11.963 - 29.533	0.170 - 0.718	2.455 - 20.026	(-0.546) - 0.003
4-way	±5%	±5%	±5%	±10 L/m³	9.527 - 36.246	0.118 - 0.715	0.019 - 26.739	(-0.597) - (-0.001)

Coupled effect of rheological properties of mortar and fiber-coarse aggregate characteristics on dynamic stability of FR-SCC

The dynamic segregation of the investigated FR-SCC mixtures was evaluated using the diphasic approach. Accordingly, the coupled effect of characteristics of fiber-aggregate combination (solid phase) and rheological properties of mortar (suspending phase) was evaluated. As can be observed in Figures 6-14a and 6-14b, the DSI indices obtained using the T-Box test were well correlated to the φ/φ_{max} of fiber-coarse aggregate mixtures as well as plastic viscosity (μ_{p-M}) and yield stress (τ_{0-M}) of mortar matrix. Increasing φ/φ_{max} of fiber-coarse aggregate led to lower DSI indices due to higher lattice effect, as shown earlier in Figure 6-13. From a rheological point of view, increasing both plastic viscosity and yield stress of mortar enhanced the dynamic stability of the investigated FR-SCC mixtures. This is due to higher drag forces exerted on the solid dispersion (i.e., fibers and aggregate). Moreover, from a macro scale point of view, higher φ/φ_{max} of fiber-coarse aggregate and rheological properties of mortar led to higher rheological properties of the FR-SCC mixture. This can remarkably decrease the flow velocity and, consequently, the shear rate magnitudes during the tilting motion of the T-Box channel. This can lead to lower possibility of collisions between the coarse aggregate and fibers. Hence, lower shear-induced particle migration (lower DSI) is expected.
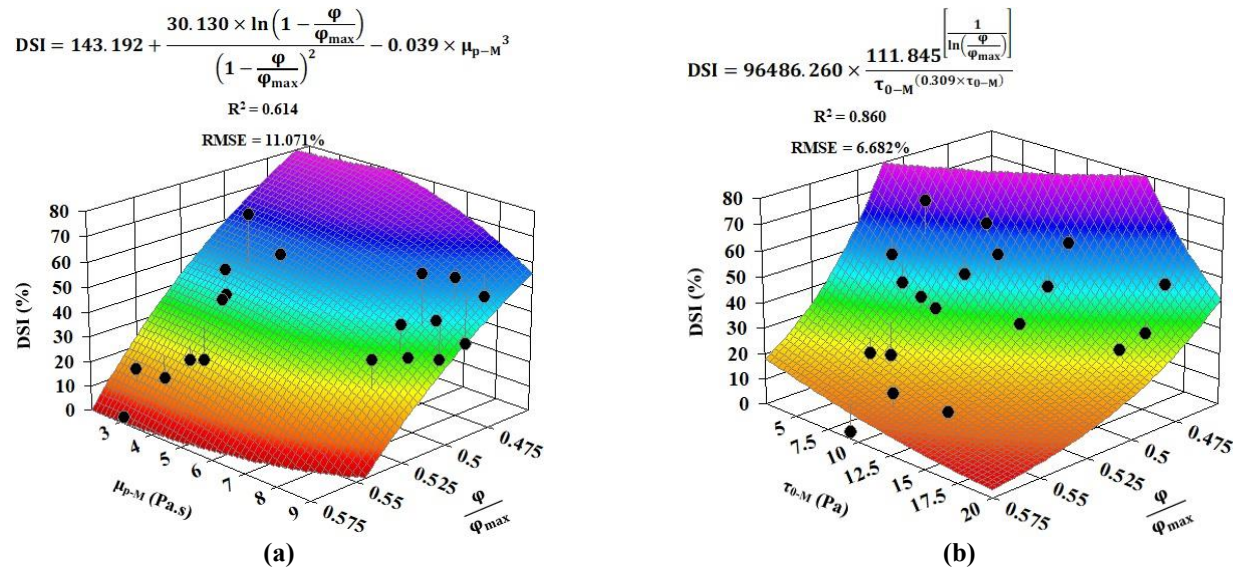
Figure 6-14 Coupled effect of φ/φ_{max} of the fiber-coarse aggregate combination, (a) plastic viscosity (μ_{p-M}), and (b) yield stress (τ_{0-M}) of mortar and on DSI values of the investigated FR-SCC mixtures.

6.3.4 A workability-based classification of FR-SCC

The workability properties of the investigated FR-SCC reaching a targeted slump flow of 680 ± 20 mm were assessed in terms of passing ability (ΔJR and h_2/h_1), dynamic stability (DSI), and granular-blocking resistance (BI). Based on the workability results of the investigated FR-SCC mixtures, three different classes of workability corresponding to low, medium, and high were defined, as shown in Table 6-12.

Table 6-12 Classification of FR-SCC based on workability levels.

Workability level	Passing ability		Dynamic stability	Granular-blocking resistance
	ΔJR (%)	h_2/h_1	DSI (%)	BI (%)
Low	> 12	< 0.33	> 50	> 54
Medium	$6 \leq \Delta$JR ≤ 12	$0.33 \leq h_2/h_1 \leq 0.67$	$25 \leq$ DSI ≤ 50	$27 \leq$ BI ≤ 54
High	< 6	> 0.67	< 25	< 27

The investigated mixtures are classified using the defined workability classes. As shown in Figure 6-15, the BI indices, ΔJR, and h_2/h_1 ratio results were plotted versus the DSI indices (Table 6-7). The FR-SCC mixtures with medium to high dynamic stability and passing ability characteristics (green zones in Figure 6-15) were then identified. These include the CSR3, CSR4, CSR5, CSR6, and CSR10 mixtures for CSR and HSR2, HSR5, HSR8, and HSR9 mixtures for HSR applications. According to these mixtures' proportions, the recommended characteristics of the mixture constituents to ensure medium to high workable FR-SCC mixtures for repair applications and different level of strength are summarized in Table 6-13.

Table 6-13 Characteristics of mixture constituents of medium to high workable FR-SCC mixtures.

Mixture constituents		Conventional-strength repair mixtures			High-strength repair mixtures		
	Paste content	Low	Medium	High	Low	Medium	High
Cement paste	V_P (%)	27	30	33	33	35	37
	τ_{0-P} (Pa)	0.95	1.01 - 1.22	1.58	2.16	4.39	7.71
	μ_{p-P} (Pa.s)	0.032	0.040	0.045	0.104	0.122	0.141
Mortar	τ_{0-M} (Pa)	13.49	6.58 - 7.96	5.78	8.49	12.54	17.68
	μ_{p-M} (Pa.s)	3.07	3.54 - 3.55	3.39	8.03	8.20	8.27
Aggregate	S/A	0.55	0.55	0.55	0.55	0.55	0.55
	PSD of CA	MSA14-3	MSA14-1-3	MSA14-3	MSA20-1	MSA20-1	MSA20-1-2
Fiber	V_f (%)	0.12	0.12 - 0.26	0.50	0.20	0.19	0.13 - 0.18
Fiber-coarse aggregate combination	φ_{max}	0.554	0.536 - 0.554	0.534	0.550	0.550	0.550 - 0.562
	φ/φ_{max}	0.552	0.528 - 0.546	0.523	0.508	0.491	0.464 - 0.475
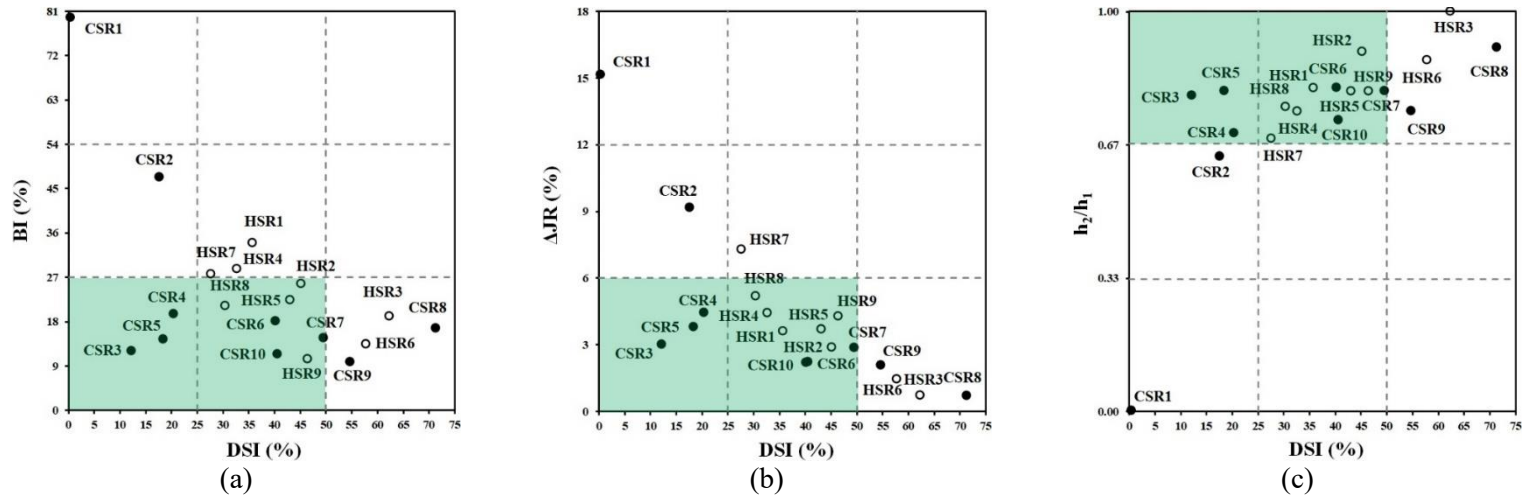
Figure 6-15 Workability-based classifications of investigated FR-SCC mixtures: Dynamic stability (DSI) versus passing ability properties, including (a) BI, (b) ΔJR, and (c) h_2/h_1 results.

6.4 Conclusions

In this study, the workability characteristics of 19 FR-SCC mixtures for repair application with different conventional and high strength levels were investigated. The passing ability, granular-blocking resistance, and dynamic stability of the investigated mixtures were evaluated. The mixtures were considered as biphasic suspensions of macro-steel fibers and coarse aggregate ($\geq$ 5 mm) in a mortar suspension with solid particles finer than 5 mm. Based on the test results, the following conclusions can be drawn:

- The HRWR demand to secure a targeted slump flow of 680 $\pm$20 mm corelated well with the W/B, V_P, and φ/φ_{max} of fiber-coarse aggregate combination (F-A). Increasing the W/B and V_P, as well lowering the φ/φ_{max} of F-A led to reduced HRWR demand. Moreover, the HRWR demand was quite robust given some variations in water content but highly sensitive to any change in V_P and/or φ/φ_{max} of F-A.

- Good correlations were established between the passing ability results evaluated using the J-Ring and L-Box tests for the investigated FR-SCC mixtures. Moreover, the ΔJR results were found to be robust given a single variation of different mixture constituents, including water content, HRWR dosage, V_P, and φ/φ_{max} of F-A. However, the passing ability was more sensitive to small variations in water content and HRWR dosage than changes in V_P and φ/φ_{max} of F-A.

- Increasing the yield stress of the suspending mortar and φ/φ_{max} of F-A led to lower passing ability (higher ΔJR).

- The proposed BI and DSI can be employed to evaluate the variation of φ/φ_{max} of F-A portion flowing through restricted and non-restricted flow conditions, respectively. The proposed BI and DSI indices can enable proper assessment of the blocking- and shear-induced changes in the relative volume and particle-size distribution of coarse aggregate and fiber contents.

- The BI indices were found to be in good agreement with the mixture parameters, including W/B, HRWR dosage, V_P, and φ/φ_{max} of F-A. Accordingly, FR-SCC mixtures proportioned with higher φ/φ_{max} of F-A, W/B, and HRWR dosage, as well as lower V_P exhibited higher granular blockage behind reinforcing bars. Moreover, optimizing the V_P, fiber content, volumetric content and PSD of coarse aggregate was found more effective to decrease the risk of blockage in restricted zones rather than controlling the W/B and optimizing the HRWR dosage.

- The BI indices of FR-SCC were found in good agreements with φ/φ_{max} of F-A and mortar rheological properties. Higher yield stress and plastic viscosity of the mortar led to lower risk of blocking of fibers and coarse aggregate behind reinforcing bars. The risk of granular blocking of the HSR and CSR, FR-SCC mixtures in reinforced elements were found to be more controlled by the rheological properties and volume of excess mortar and φ/φ_{max} of F-A, respectively.

- The DSI obtained using the T-Box set-up were well correlated to mixture constituents, including the W/B, HRWR dosage, V_P, and φ/φ_{max} of F-A. The dynamic stability of FR-SCC can be enhanced by decreasing the W/B, HRWR dosage, and V_P, as well as increasing the φ/φ_{max} of F-A. Unlike the results reported for plain SCC mixtures (no fibers), dynamic stability of FR-SCC mixtures is more robust due to small variations of

V_P and φ/φ_{max} of F-A but more sensitive to variations in water content and HRWR dosage. Moreover, the DSI indices for FR-SCC can be correlated to the φ/φ_{max} of F-A and plastic viscosity and yield stress of the suspending mortar. According to the established biphasic correlation, increasing the plastic viscosity and yield stress of the mortar can enhance the dynamic stability of FR-SCC.

- A new workability-based classification is proposed based on the established trade-offs between flow performance under restricted and non-restricted conditions, including passing ability, blocking resistance, and dynamic stability. Characteristics of mixture constituents for FR-SCC mixtures with conventional- and high-strength levels were then recommended to ensure an acceptable homogeneous flow performance under restricted flow conditions of repair application.

Acknowledgment

References

[1] K.H. Khayat, Workability, testing, and performance of self-consolidating concrete, ACI Materials Journal, 96 (3) (1999) 346-353, https://dx.doi.org/10.14359/632.

[2] K.H. Khayat, C. Hu, H. Monty, Stability of self-consolidating concrete, advantages, and potential applications, in: A. Skarendahl, O. Petersson (Eds.), Proceedings of the first International RILEM Symposium on Self Compacting Concrete, Stockholm, Sweden, (1999), 143-152.

[3] A. Yahia, P.-C. Aïtcin, Self-consolidating concrete, in: Science and Technology of Concrete Admixtures, Woodhead Publishing, (2016), 491-502, https://doi.org/10.1016/B978-0-08-100693-1.00026-6.

[4] B.I.O. Koura, M. Hosseinpoor, A. Yahia, Coupled effect of fine mortar and granular skeleton characteristics on dynamic stability of self-consolidating concrete as a diphasic material, Construction and Building Materials, 263 (2020) 120131, https://doi.org/10.1016/j.conbuildmat.2020.120131.

[5] M. Hosseinpoor, B.I.O. Koura, A. Yahia, Rheo-morphological investigation of static and dynamic stability of self-consolidating concrete: A biphasic approach, Cement and Concrete Composites, 121 (2021) 104072, https://doi.org/10.1016/j.cemconcomp.2021.104072.

[6] M. Hosseinpoor, B.I.O. Koura, A. Yahia, New diphasic insight into the restricted flowability and granular blocking of self-consolidating concrete: Effect of morphological characteristics of coarse aggregate on passing ability of SCC, Construction and Building Materials, 308 (2021) 125001, https://doi.org/10.1016/j.conbuildmat.2021.125001.

[7] N. Roussel, A theoretical frame to study stability of fresh concrete, Materials and Structures, 39 (1) (2006) 81-91, https://doi.org/10.1617/s11527-005-9036-1.

[8] B. Esmaeilkhanian, D. Feys, K.H. Khayat, A. Yahia, New test method to evaluate dynamic stability of self-consolidating concrete, ACI Materials Journal, 111 (3) (2014) 299-308, https://doi.org/10.14359/51686573.

[9] L. Ferrara, P. Bamonte, A. Caverzan, A. Musa, I. Sanal, A comprehensive methodology to test the performance of Steel Fibre Reinforced Self-Compacting Concrete (SFR-SCC), Construction and Building Materials, 37 (2012) 406-424, https://doi.org/10.1016/j.conbuildmat.2012.07.057.

[10] I. Mehdipour, N.A. Libre, Linking fiber factor to material performance of fiber-reinforced self-consolidating cement-based materials, ACI Materials Journal, 114 (1) (2017) 77-91, https://doi.org/10.14359/51689483.

[11] L. Ferrara, A. Meda, Relationships between fibre distribution, workability and the mechanical properties of SFRC applied to precast roof elements, Materials and Structures, 39 (4) (2006) 411-420, https://doi.org/10.1617/s11527-005-9017-4.

[12] T. Ponikiewski, J. Katzer, Properties of fresh SCC mix reinforced by different types of steel and polymer fibre, Construction and Building Materials, 62 (2014) 96-101, https://doi.org/10.1016/j.conbuildmat.2014.03.037.

[13] K.H. Khayat, F. Kassimi, P. Ghoddousi, Mixture design and testing of fiber-reinforced self-consolidating concrete, ACI Materials Journal, 111 (2) (2014) 143-152, https://doi.org/10.14359/51686722.

[14] W. Si, M. Cao, L. Li, Establishment of fiber factor for rheological and mechanical performance of polyvinyl alcohol (PVA) fiber reinforced mortar, Construction and Building Materials, 265 (2020) 120347, https://doi.org/10.1016/j.conbuildmat.2020.120347.

[15] R. Zerbino, J.M. Tobes, M.E. Bossio, G. Giaccio, On the orientation of fibres in structural members fabricated with self compacting fibre reinforced concrete, Cement and Concrete Composites, 34 (2) (2012) 191-200, https://doi.org/10.1016/j.cemconcomp.2011.09.005.

[16] G. Žirgulis, O. Švec, E.V. Sarmiento, M.R. Geiker, A. Cwirzen, T. Kanstad, Importance of quantification of steel fibre orientation for residual flexural tensile strength in FRC, Materials and Structures, 49 (2016) 3861-3877, https://doi.org/10.1617/s11527-015-0759-3.

[17] M. Nehdi, J.D. Ladanchuk, Fiber synergy in fiber-reinforced self-consolidating concrete, ACI Materials Journal, 101 (6) (2004) 508-517, https://dx.doi.org/10.14359/13490.

[18] H.A. Abdulhameed, H. Nassif, K.H. Khayat, Use of fiber-reinforced self-consolidating concrete to enhance serviceability performance of damaged beams, Transportation Research Record, 2672 (27) (2018) 45-55, https://doi.org/10.1177/0361198118787983.

[19] K.H. Khayat, W.J. Long, Shrinkage of precast, prestressed self-consolidating concrete, ACI Materials Journal, 107 (3) (2010) 231-238, https://dx.doi.org/10.14359/51663751.

[20] S.-D. Hwang, K.H. Khayat, Effect of mixture composition on restrained shrinkage cracking of self-consolidating concrete used in repair, ACI Materials journal, 105 (5) (2008) 499-509, https://dx.doi.org/10.14359/19980.

[21] F. Kassimi, A.K. El-Sayed, K.H. Khayat, Performance of fiber-reinforced self-consolidating concrete for repair of reinforced concrete beams, ACI Structural Journal, 111 (6) (2014) 1277-1286, https://dx.doi.org/10.14359/51687031.

[22] J.S. Volz, J.T. Drury, J.G. Choate, C.M. Wirkman, Volume IV: Performance of Fiber-Reinforced Self-Consolidating Concrete for Repair of Bridge Sub-Structures and Fiber Reinforced Super Workable Concrete for Infrastructure Construction, Report number: RECAST UTC# 00042134-05-3A (2020), https://rosap.ntl.bts.gov/view/dot/54649.

[23] M. Arezoumandi, C. Wirkman, J.S. Volz, Performance of fiber-reinforced self-consolidating concrete for repair of bridge substructures, Structures, 15 (2018) 320-328, https://doi.org/10.1016/j.istruc.2018.07.015.

[24] Q. Song, R. Yu, Z. Shui, X. Wang, S. Rao, Z. Lin, Optimization of fibre orientation and distribution for a sustainable Ultra-High Performance Fibre Reinforced Concrete (UHPFRC): Experiments and mechanism analysis, Construction and Building Materials, 169 (2018) 8-19, https://doi.org/10.1016/j.conbuildmat.2018.02.130.

[25] E. Jasiūnienė, V. Cicėnas, P. Grigaliūnas, Ž. Rudžionis, A.A. Navickas, Influence of the rheological properties on the steel fibre distribution and orientation in self-compacting concrete, Materials and Structures, 51 (2018) 103, https://doi.org/10.1617/s11527-018-1231-y.

[26] R. Farokhzad, M. Mahdikhani, A. Bagheri, J. Baghdadi, Representing a logical grading zone for self-consolidating concrete, Construction and Building Materials, 115 (2016) 735-745, https://doi.org/10.1016/j.conbuildmat.2016.04.006.

[27] H. Hafid, G. Ovarlez, F. Toussaint, P.H. Jezequel, N. Roussel, Effect of particle morphological parameters on sand grains packing properties and rheology of model mortars, Cement and Concrete Research, 80 (2016) 44-51, https://doi.org/10.1016/j.cemconres.2015.11.002.

[28] K. Ostrowski, K. Oleksik, Comparative analysis of the coarse aggregate shapes used to manufacturing high performance self-compacting concrete, Technical Transaction, 7 (2018) 75-86, https://doi.org/10.4467/2353737XCT.18.101.8796.

[29] F.V. Mueller, O.H. Wallevik, K.H. Khayat, Linking solid particle packing of Eco-SCC to material performance, Cement and Concrete Composites, 54 (2014) 117-125, https://doi.org/10.1016/j.cemconcomp.2014.04.001.

[30] I. Mehdipour, K.H. Khayat, Understanding the role of particle packing characteristics in rheo-physical properties of cementitious suspensions: A literature review, Construction and Building Materials, 161 (2018) 340-353, https://doi.org/10.1016/j.conbuildmat.2017.11.147.

[31] ASTM C1621/C1621M-17, Standard test method for passing ability of self-consolidating concrete by J-Ring, West Conshohocken, PA; ASTM International (2017), https://dx.doi.org/10.1520/C1621_C1621M-17.

[32] Nordtest, Method (NT BUILD 427) for Fresh Concrete: Compactibility with IC-tester (Intensive Compaction Tester) Proj. 1005-91, Nord. Scand. Inst. (1994) 1-4, ISSN 0283-7153, www.nordtest.org.

[33] B.M. Aïssoun, Étude de l'influence des caractéristiques des granulats sur la performance des bétons fluides à rhéologie adaptée (in French), M.Sc. thesis, Université de Sherbrooke (2011), http://savoirs.usherbrooke.ca/handle/11143/1590.

[34] N. Nouri, M. Hosseinpoor, A. Yahia, K.H. Khayat, Coupled effect of fiber and granular skeleton characteristics on packing density of fiber-aggregate mixtures, Construction and Building Materials, 342 (2022) 127932, https://doi.org/10.1016/j.conbuildmat.2022.127932.

[35] M. Hosseinpoor, B.I.O. Koura, A. Yahia, E.H. Kadri, Diphasic investigation of the visco-elastoplastic characteristics of highly flowable fine mortars, Construction and Building Materials, 270 (2021) 121425, https://doi.org/10.1016/j.conbuildmat.2020.121425.

[36] M. Hosseinpoor, B.I.O. Koura, A. Yahia, Rheo-morphological investigation of Reynolds dilatancy and its effect on pumpability of self-consolidating concrete, Cement and Concrete Composites, 117 (2021) 103912, https://doi.org/10.1016/j.cemconcomp.2020.103912.

[37] C.F. Ferraris, L.E. Brower, Comparison of concrete rheometers: international tests at MB (Cleveland OH, USA) in 2003. National Institute of Standards and Technology Interagency Report, NISTIR 7145.

[38] X. Chateau, G. Ovarlez, K.L. Trung, Homogenization approach to the behavior of suspensions of noncolloidal particles in yield stress fluids, Journal of Rheology, 52 (2) (2008) 489-506, https://doi.org/10.1122/1.2838254.

[39] H. Hafid, G. Ovarlez, F. Toussaint, P.H. Jezequel, N. Roussel, Estimating measurement artifacts in concrete rheometers from MRI measurement on model materials, In: Khayat, K., Feys, D. (eds) Proceedings of SCC2010: Design, Production and Placement of Self-Consolidating Concrete, Montreal, Canada (2010), RILEM Bookseries, vol 1. Springer, Dordrecht, 127-137, https://doi.org/10.1007/978-90-481-9664-7_11.

[40] S.D. Jo, C.K. Park, J.H. Jeong, S.H. Lee, S.H. Kwon, A computational approach to estimating a lubricating layer in concrete pumping, Computers Materials and Continua, 27 (3) (2012) 189-210, https://doi.org/10.3970/CMC.2011.027.189.

[41] L. Struble, R. Szecsy, W.-G. Lei, G.-K. Sun, Rheology of cement paste and concrete, Cement, Concrete and Aggregates, 20 (2) (1998) 269-277, https://dx.doi.org/10.1520/CCA10421J.

[42] ASTM C1611/C1611M-21 Standard test method for slump flow of self-consolidating concrete, West Conshohocken, PA; ASTM International (2021), https://dx.doi.org/10.1520/C1611_C1611M-21.

[43] EFNARC, European Project Group, The European guidelines for self-compacting concrete: specification, Production and Use (2005).

CHAPITER 7 Homogenous flow performance of steel fiber-reinforced self-consolidating concrete for repair applications: Developing a new empirical set-up

Authors and affiliations

Naimeh Nouri : Ph.D. candidate, Cement and Concrete Research Group, Department of Civil and Building Engineering, Université de Sherbrooke, Sherbrooke, Québec, Canada, J1K 2R1.

Masoud Hosseinpoor: Research Associate, Cement and Concrete Research Group, Department of Civil and Building Engineering, Université de Sherbrooke, Sherbrooke, Québec, Canada, J1K 2R1.

Ammar Yahia: Professor, Cement and Concrete Research Group, Department of Civil and Building Engineering, Université de Sherbrooke, Sherbrooke, Québec, Canada, J1K 2R1.

Kamal H. Khayat: Professor, Missouri University of Science and Technology, Center for Infrastructure Engineering Studies, Department of Civil, Architectural and Environmental Engineering, Rolla, MO 65409.

Titre en français: Performance d'écoulement homogène du béton autoplaçant renforcé de fibres d'acier pour les applications de réparation : développement d'une nouvelle configuration empirique

Homogenous flow performance of steel fiber-reinforced self-consolidating concrete for repair applications: Developing a new empirical set-up

Naimeh Nouri[a], Masoud Hosseinpoor[a],*, Ammar Yahia[a], and Kamal H. Khayat[b]

[a]Université de Sherbrooke, Department of Civil and Building Engineering, Sherbrooke, Québec, Canada

[b]Missouri University of Science and Technology, Center for Infrastructure Engineering Studies, Department of Civil, Architectural and Environmental Engineering, Rolla, MO, USA

*Corresponding author: masoud.hosseinpoor@usherbrooke.ca

Abstract

In this study, a new empirical Square-Box test was employed to evaluate the homogeneous flow performance of fiber-reinforced self-consolidating concrete (FR-SCC) under confined-flow conditions that are typical of repair applications. The Square-Box set-up consisted of a closed-circuit box, providing 2.4-m flow distance and a closed-surface cross section of 100-mm width and 200-mm height, equipped with 0 and 4 rows of reinforcing bar grids with 45-mm clear spacing. The flow performance was assessed in terms of dynamic stability and passing ability. The investigated mixtures were considered as diphasic suspensions of fiber-coarse aggregate (F-A > 5 mm) in suspending mortars containing particles finer than 5 mm. According to the experimental results, the dynamic segregation and blocking indices of the investigated mixtures were found in good agreements with characteristics of F-A combination and rheology of mortar. The investigated mixtures exhibited significantly higher blocking indices through the Square-Box set-up compared to those obtained using the L-Box test. Furthermore, the characteristics of F-A and rheology of mortar showed opposite effects on dynamic segregation assessed using Square-Box and conventional T-Box set-ups. Under confined flow conditions, higher dynamic segregation led to more dissimilar compressive strength values at different flow distances through the proposed Square-Box set-up. A new filling ability classification was established based on the experimental dynamic stability and passing ability results of the proposed empirical test.

Keywords: Blocking, Dynamic segregation; Fiber-reinforced self-consolidating concrete; Repair; Rheology; Square-Box test.

7.1 Introduction

Self-consolidating concrete (SCC) has gained high interest in construction industry given its ability to facilitate the casting of highly congested elements and filling narrow gaps in formwork systems. However, cementitious materials are generally considered as brittle, with low tensile and flexural strengths and weak strain capacity [1]. Concrete is thus reinforced by reinforcement bars [2] and steel fibers [3] to improve strength-strain capacity and ductility of concrete structures. Conventional reinforcement bars can be partially replaced by steel fibers while maintaining the required flexural and tensile strengths [4,5]. Steel fibers can improve the crack resistance and energy absorption (toughness), as well as impact and fatigue resistance [6,7]. Song et al. [8] reported an improvement of flexural strength of ultra-high-performance fiber-reinforced concrete by increasing the steel fiber content. Zhang et al. [9] reported that increasing

the fiber content from 0.5% to 2% can enhance compressive, tensile, and flexural strengths of fiber-reinforced concrete (FRC) by 4%-24%, 33%-122%, and 25%-111%, respectively.

Combining the advantages of SCC and FRC [4], fiber-reinforced self-consolidating concrete (FR-SCC) has gained acceptance in different applications, such as precast industry [5], rehabilitation of transportation infrastructure [3], construction of slabs on grade [10], slabs on piles [11], and tunneling applications [11]. However, adding fibers to SCC can significantly decrease its workability [12]. This can increase the risk of blockage of fibers and aggregate behind the reinforcing bars during casting [13]. An uneven fiber-aggregate distribution and fiber orientation can negatively affect the mechanical performance of FR-SCC [14]. The fiber distribution is a function of rheological properties of concrete, flow distance, and arrangement of reinforcing bars [4,13,15]. Jasiūnienė et al. [15] reported the most uneven fiber distribution through a beam for the FR-SCC mixtures with the lowest viscosity. Ferrara et al. [4] reported the negative effect of lowering the viscosity of FR-SCC on its static stability. Moreover, Jasiūnienė et al. [15] and Yoo et al. [16] reported a heterogeneous distribution of fibers at longer flow distances in the formwork. On the other hand, Žirgulis et al. [13] highlighted the effect of reinforcing bars configuration on fiber distribution. The authors reported the maximum fiber blockage within two layers of reinforcing bars compared to the configuration equipped with one layer of reinforcement.

FR-SCC is also frequently specified as a promising repair material due to its advantages in both fresh and hardened states [17-20]. FR-SCC can properly fill the narrow sections to be repaired and pass through the congested reinforcement bars under its own weight with low risk of blockage and instability which cannot be achieved using conventional concrete. Unlike free-surface flow in casting process of concrete, close-surface flows are encountered in repair applications, hence leading to extremely higher confinement. This can increase the interactions between the fibers and aggregate with formwork walls and reinforcing bars, hence leading to high risks of granular blocking and flow instabilities in repair applications. FR-SCC mixture design should be tailored by taking into account the specifications of repaired elements, such as the clear space between the formwork and original substrate and configuration of the rebars. The type and volume of fibers, particle-size distribution of aggregate, as well as the workability and rheological properties of the paste/mortar matrix must be optimized. Understanding the coupled effect of the aforementioned parameters on homogenous performance of FR-SCC allows to secure proper mechanical performance of the cast element. Indeed, high flowability, dynamic stability, and passing ability of FR-SCC can ensure successful casting and targeted mechanical performance at different flow distances passing through the reinforced elements.

Voigt et al. [21] investigated the performance of FRC mixtures using a diphasic concept. The granular skeleton and fibers, as the solid phase, and the mortar matrix, as the liquid phase filling the interparticle voids and lubricating the solid dispersions, were investigated. Koura et al. [22] and Hosseinpoor et al. [23,24] studied the workability of SCC as a biphasic suspension of coarse aggregate (> 1.25 mm) and fine mortar (< 1.25 mm). Koura et al. [22] investigated the coupled effect of coarse aggregate characteristics and fine mortar rheology on dynamic stability of SCC. The dynamic segregation of SCC was measured by variation of the relative-solid packing-fraction of coarse aggregate (φ/φ_{max}), defined by the ratio of their volumetric content (φ)-to-their packing density (φ_{max}), in the T-Box set-up [25]. The φ/φ_{max} of coarse aggregate showed a dominant effect on dynamic stability of SCC compared to the rheological properties of fine mortar [22]. Hosseinpoor et al. [24] evaluated the blocking resistance of SCC by variation of the φ/φ_{max} of coarse aggregate passing across the rebars in the J-Ring [26] and L-Box [27] set-ups. The authors reported the negative effect of decreasing rheological properties of fine mortar, as well as increasing φ/φ_{max} of coarse aggregates on passing ability of SCC. Moreover, the study

revealed a decrease of risk of blocking by lowering the water-to-binder ratio (W/B), dosage of high-range water-reducer (HRWR), and the paste volume (V_P).

The flow performance of SCC and FR-SCC mixtures can be evaluated using different empirical tests, such as slump flow [28], J-Ring [26], U-Box [27,29], L-Box [27], and filling-box [30] test set-ups. However, the short flow distance through slump flow, J-Ring, and L-Box test is not representative to those traveled by concrete during real-scale castings. Accordingly, Jasiūnienė et al. [15] and Ferrara et al. [4] used beams of 1.35 ± 0.15 m length to evaluate the flow homogeneity and fiber orientation of FR-SCC mixtures. However, these beams were not equipped with reinforcement bars. The heterogeneity of concrete can be more critical in the presence of reinforcing bars and formwork walls (blocking and wall effect), which are more critical in confined repair sections. The arrangement, diameter, and spacing of reinforcing bars can significantly affect the passing ability of FR-SCC mixtures containing rigid fibers.

Conventional workability tests used for SCC and those developed for FRC cannot be properly applied to evaluate the flow performance of FR-SCC for repair applications. A new empirical method is required to simulate concrete flow in confined and restricted flow conditions, such as those encountered in repair applications. A new empirical Square-Box set-up was developed to evaluate the coupled effect of fiber volume, φ/φ_{max} of fiber-coarse aggregate combination, as well as the rheological properties of the suspending mortar on dynamic stability and passing ability of FR-SCC. The Square-Box test allows concrete to travel a horizontal distance of 2.4 m passing through a close-surface and close-circuit narrow channel (100-mm width) equipped with various congested reinforcing bars with clear spacing of 45 mm. FR-SCC mixtures exhibiting high passing ability and good dynamic stability determined using conventional L-Box and T-Box tests were selected. The study aimed at proposing a filling ability classification for FR-SCC that can secure adequate homogeneous flow performance in confined areas. The impact of heterogeneous flow on the uniformity of in-situ mechanical properties was also evaluated.

7.2 Experimental study

7.2.1   Proportioning of the investigated FR-SCC mixtures: Materials and characterizations

A natural-river sand (0-5 mm) and two different classes of crushed-limestone coarse aggregate of 5-10 mm (CA1) and 5-14 mm (CA2) were used (Table 7-1). As shown in Table 7-1, three different combinations (PSD-1 to PSD-3) of coarse aggregate were considered to achieve different levels of packing densities. The investigated FR-SCC mixtures were proportioned with a volumetric sand-to-total aggregate ratio of 0.55. Moreover, a hooked end steel fiber with 30-mm length, 0.55-mm diameter (aspect ratio of 55), and modulus of elasticity of 200 GPa was also used.

Table 7-1 Particle-size distribution of the fine and coarse aggregates and their combinations (PSD-1-3) made with different volumetric proportions of CA1-3 coarse aggregate classes.

Sieve size (mm)	Sand	CA1	CA2	PSD-1 100% CA1	PSD-2 80% CA1 + 20% CA2	PSD-3 60% CA1 + 40% CA2
20	100	100	100	100	100	100
14	100	100	85.5	100	97.1	94.2
10	100	81.7	48.9	81.7	75.1	68.6
5	99.4	10.2	5.7	10.2	9.3	8.4
2.5	83.6	4.9	1.5	4.9	4.2	3.5
1.25	67.3	3.9	1.2	3.9	3.3	2.8
0.630	49.5	-	-	-	-	-
0.315	23.7	-	-	-	-	-
0.160	6.6	-	-	-	-	-
0.080	2.9	-	-	-	-	-
Specific gravity	2.67	2.72	2.73	-	-	-

Various fiber volumes of 0.4% to 0.9% were mixed with the 3 coarse aggregate mixtures PSD1-3. The packing density of the investigated F-A mixtures were evaluated using the dry method and intensive compaction tester (ICT) [31-33]. Three F-A mixtures corresponding to the minimum, medium, and maximum packing density (PD) values of 0.536, 0.544, and 0.554 were selected to cover a wide range of packing density. Nine FR-SCC mixtures (FRC-1-9) were then proportioned with coarse aggregate combinations PSD1-3, W/B of 0.42, and V_P of 0.27, 0.30, and 0.33, as summarized in Table 7-2. Khayat et al. [3] recommended an upper limit of fiber volume of 0.5% of macro steel fibers (out of unit volume of concrete) to ensure proper workability for SCC. Accordingly, an additional F-A mixture was proportioned with PSD3 and 1.77% fiber volume. This F-A mixture corresponded to 0.5% fiber volume in 1 m^3 of concrete mixture (FRC-10) containing V_P of 0.33 (Table 7-2).

A ternary-blended cement made with 70% general use Portland cement (GU), 25% class F fly ash, and 5% silica fume was used. A polycarboxylate-based HRWR and an air-entraining agent (AEA) was used to achieve a targeted slump-flow value of 680 ± 20 mm and air content of 5%-8%, respectively. All the mixtures were prepared in batches of 65 L using a rotating drum mixer. The 28-day compressive strength (f'_{c-Ref}) determined using cylindrical samples measuring 100-mm diameter and 200-mm height are presented in Table 7-2.

Table 7-2 Proportioning and workability results of the investigated FR-SCC mixtures (HRWR and AEA dosages are in ml/100 kg of binder).

Mix	Binder (kg/m³)	V_P (%)	Sand (kg/m³)	PSD of CA	CA1 (kg/m³)	CA2 (kg/m³)	Fiber (kg/m³)	V_f in F-A (%)	V_f in concrete (%)	φ_{max}-of F-A	φ/φ_{max} of F-A	AEA	Slump flow (mm)	$f'_{c\text{-Ref}}$ (MPa)*	UBI_{LB} (%)	DSI_{TB} (%)
FRC-1	352	27	999	PSD-1	825	0	22	0.9	0.28	0.536	0.571	5	667	30.2	79.7	0.4
FRC-2	352	27	999	PSD-2	661	166	17	0.7	0.22	0.544	0.563	5	665	31.6	47.3	17.7
FRC-3	352	27	999	PSD-3	497	333	9	0.4	0.12	0.554	0.552	5	662	33.2	11.9	12.2
FRC-4	392	30	955	PSD-1	789	0	20	0.9	0.26	0.536	0.546	5	700	38.9	19.5	20.4
FRC-5	392	30	955	PSD-2	632	159	16	0.7	0.20	0.544	0.538	10	673	39.9	14.3	18.4
FRC-6	392	30	955	PSD-3	475	318	9	0.4	0.12	0.554	0.528	8	656	47.8	18.1	40.3
FRC-7	431	33	910	PSD-1	752	0	20	0.9	0.25	0.536	0.521	9	678	42.9	14.6	49.6
FRC-8	431	33	910	PSD-2	603	151	15	0.7	0.20	0.544	0.513	7	685	44.7	16.7	71.4
FRC-9	431	33	910	PSD-3	454	303	9	0.4	0.11	0.554	0.503	7	694	46.0	9.8	54.8
FRC-10	431	33	910	PSD-3	447	299	39	1.77	0.50	0.534	0.523	7	675	49.4	11.4	40.6

*Standard deviations of all the compressive strength measurements ranged between 0.1 and 1.3 MPa.

7.2.2   Conventional workability measurements

The blocking resistance and dynamic stability of the investigated mixtures were firstly evaluated using the L-Box and T-Box tests, respectively. The L-Box set-up has a vertical part measuring 600-mm, a horizontal channel of 700-mm length and 200 mm in width [3]. Two 10-mm diameter reinforcing bars are installed right after the separating gate. Two 100×200-mm cylindrical samples were taken from the fresh concrete at the two lateral sides of the L-Box set-up. The concentration and packing density of F-A portions in the samples taken behind the rebars and end of the horizontal channel of the L-Box set-up were determined. The ultimate blocking index in the L-Box test (UBI$_{LB}$) was evaluated, as follows:

$$\text{UBI}_{LB}\ (\%) = \frac{\left(\frac{\varphi}{\varphi_{max}}\right)_B - \left(\frac{\varphi}{\varphi_{max}}\right)_E}{\left(\frac{\varphi}{\varphi_{max}}\right)_{Ref}} \times 100\% \qquad \text{Equation 7-1}$$

where $\left(\frac{\varphi}{\varphi_{max}}\right)_B$, $\left(\frac{\varphi}{\varphi_{max}}\right)_E$, and $\left(\frac{\varphi}{\varphi_{max}}\right)_{Ref}$ corresponds to the relative-solid packing fraction of F-A mixtures in samples taken from behind the rebars and end of horizontal channel of the L-Box set-up, as well as reference mixture, respectively. Moreover, the dynamic stability of the investigated FR-SCC mixtures was investigated using the T-Box set-up [25] (16-L sample) under 60 tilting cycles of 2-s period. Two cylindrical samples were taken from the tilt-up (TU) and tilt-down (TD) sections. The volumetric content and packing density of the F-A portion of the taken samples were determined. The dynamic segregation of the investigated mixtures in T-Box test was assessed, as follow:

$$\text{DSI}_{TB}\ (\%) = \frac{\left(\frac{\varphi}{\varphi_{max}}\right)_{TD} - \left(\frac{\varphi}{\varphi_{max}}\right)_{TU}}{\left(\frac{\varphi}{\varphi_{max}}\right)_{Ref}} \times 100\% \qquad \text{Equation 7-2}$$

where $\left(\frac{\varphi}{\varphi_{max}}\right)_{TD}$, $\left(\frac{\varphi}{\varphi_{max}}\right)_{TU}$, and $\left(\frac{\varphi}{\varphi_{max}}\right)_{Ref}$ are the volumetric content-to-packing density ratios of the F-A mixtures corresponding to the samples taken from tilt-down and tilt-up zones of the T-Box set-up, and reference mixture, respectively. The results of the workability tests are summarized in Table 7-2. It is worth mentioning that due to the highly restricted flow conditions of repair application, a particular attention should be considered to ensure high passing ability of FR-SCC for repair application rather than their dynamic stability. Therefore, according to the workability results presented in Table 7-2, six mixtures exhibiting high passing ability and medium to high dynamic stability, corresponding to the UBI$_{LB}$ values less than 27% and DSI$_{TB}$ values less than 50%, respectively, were selected for further analyses.

7.2.3   Rheological evaluation of suspending paste/mortar

The rheological properties of the suspending mortar (< 5 mm) of the FR-SCC mixtures were assessed considering a diphasic approach proposed by Hosseinpoor et al. [34,35]. The mortar matrix (< 5 mm) was considered as a diphasic suspension of coarser particles of sand (> 1.25 mm) and fine mortar (< 1.25 mm). Similarly, the fine mortar was investigated as a suspension of fine sand particles (< 1.25 mm) in a suspending cement paste. According to the diphasic models proposed by Hosseinpoor et al. [34,35], the volumetric content and packing density of fine (FS < 1.25 mm) and coarse (1.25 mm < CS < 5 mm) particles of sand suspended in cement pastes and fine mortars, respectively, as well as the yield stress and plastic viscosity of cement paste ($\tau_{0\text{-}P}$, $\mu_{p\text{-}P}$) and fine mortar ($\tau_{0\text{-}FM}$, $\mu_{p\text{-}FM}$) mixtures were considered. The rheological

properties ($\tau_{0\text{-FM}}$, $\mu_{p\text{-FM}}$) of fine mortar mixtures (< 1.25 mm) were evaluated as functions of the rheological properties of their corresponding cement pastes ($\tau_{0\text{-P}}$, $\mu_{p\text{-P}}$) and relative-solid packing fraction of fine sand ($\varphi_{FS}/\varphi_{max\text{-FS}}$) suspended in the cement pastes. Subsequently, the yield stress ($\tau_{0\text{-M}}$) and plastic viscosity ($\mu_{p\text{-M}}$) of the mortar matrices (< 5 mm) were evaluated as functions of yield stress ($\tau_{0\text{-FM}}$) and plastic viscosity ($\mu_{p\text{-FM}}$) of their corresponding fine mortars and relative-solid packing fraction of fine sand ($\varphi_{CS}/\varphi_{max\text{-CS}}$) suspended in the fine mortars. It is worth mentioning that the rheological properties of the cement paste mixtures were evaluated using a 50-mm diameter parallel-plates system and a 4-mm gap. The shear protocol included applying a pre-shearing of 150 s^{-1} for 120 s, then stepwise descending shear rate values from 150 s^{-1} to 1 s^{-1} during 150 s in 6 steps. The rheological properties of the investigated mortar mixtures and their corresponding cement paste mixtures are summarized in Table 7-3.

Table 7-3 Rheological properties of the investigated cement paste and mortar mixtures.

Mortar No.	Corresponding FR-SCC mixture	$\tau_{0\text{-P}}$ (Pa)	$\mu_{p\text{-P}}$ (Pa.s)	$\tau_{0\text{-M}}$ (Pa)	$\mu_{p\text{-M}}$ (Pa.s)
M3	FRC-3	0.95	0.032	13.49	3.07
M4	FRC-4	1.01	0.040	6.58	3.55
M5	FRC-5	1.09	0.040	7.05	3.54
M6	FRC-6	1.22	0.040	7.96	3.55
M7	FRC-7	1.27	0.043	4.61	3.24
M10	FRC-10	1.58	0.045	5.78	3.39

7.2.4 Workability measurements using new Square-Box set-up

A new Square-Box test set-up is proposed to investigate the homogeneous flow of FR-SCC under confined flow conditions. As shown in Figure 7-1, the Square-Box set-up consists of a close-circuit of four close-surface rectangular channels measuring 200 mm in height, 700 mm in length, and 100 mm in width, yielding a box with 700 × 700 mm outer dimensions, 500 × 500 mm inner dimensions, and a height of 200 mm. In total, 48 L of concrete was cast in a continuous manner from one corner during almost 18 s corresponding to a casting rate of 2.7 L/s (9.6 m^3/h). The passing ability of the investigated mixtures was evaluated using the Square-Box set-up equipped with four rows of 10-mm diameter reinforcing bar grids positioned in horizontal and vertical configurations, in addition to one longitudinal rebar through the whole length of the set-up (Figure 7-1). The reinforcing-bar grids were placed in the middle of each of the four close-surfaced channels. Moreover, the dynamic stability of the investigated mixtures was evaluated by carrying out this test without presence of any reinforcing bars. It is worth mentioning that the geometry of the proposed Square-Box test led to more confined and restricted flow conditions compared to the T-Box and L-Box set-ups. Indeed, the channel width of 100 mm is 50% tighter than those of the T-Box and L-Box set-ups of 200 mm [25,27]. On the other hand, the clear spacing between the vertical rebars and the Square-Box set-up's walls is 45 mm which is lower than that of the L-Box set-up of 60 mm. Furthermore, the closed surface of the Square-Box set-up led to more restricted and confined flow condition compared to those of the conventional L-Box and T-Box set-ups.

As shown in Figure 7-2a, immediately after casting, the cast beam was divided in 5 different sections (i = 1 to 5) using separators inserted just behind the reinforcing grids at middle of the channels. Then, 5 cylindrical samples measuring 100 mm in diameter and 200 mm in height were taken from each section i = 1 to 5 to evaluate the variation of concentration and distribution of coarse aggregate and steel fibers at different distances from the casting point.

The extracted samples from each section were wet-sieved on 5-mm sieve and then dried. The extracted fibers and coarse aggregate were then separated using a magnet and weighted. The

volumetric content of fiber-coarse aggregate samples in unit volume of concrete and the PSD of extracted coarse aggregate were determined for each sample. The fibers and coarse aggregate were remixed to determine the packing density of fiber-coarse aggregate combination using the ICT device [31-33]. The variation of ratio of the volumetric content ($\varphi_{F-i} + \varphi_{CA-i}$)-to-the packing density ($\varphi_{max-F-A-i}$) of fiber-coarse aggregate combination obtained at different distances (i = 1 to 5) from the casting point relative to the reference mixture ($\varphi_{F+CA-Ref} / \varphi_{max-F+CA-Ref}$) was calculated.

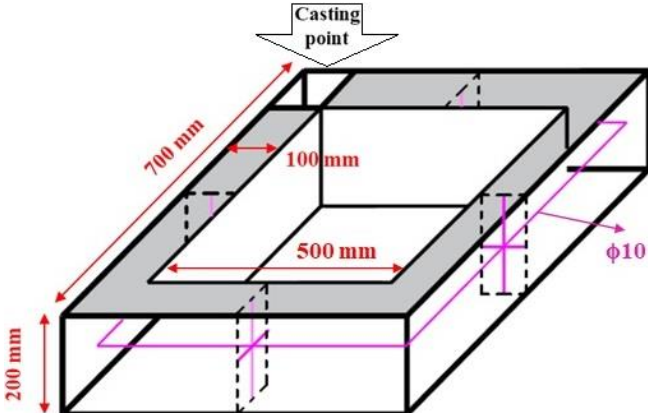Figure 7-1 Schematics of the proposed Square-Box test to evaluate the passing ability and dynamic stability of the FR-SCC mixtures.
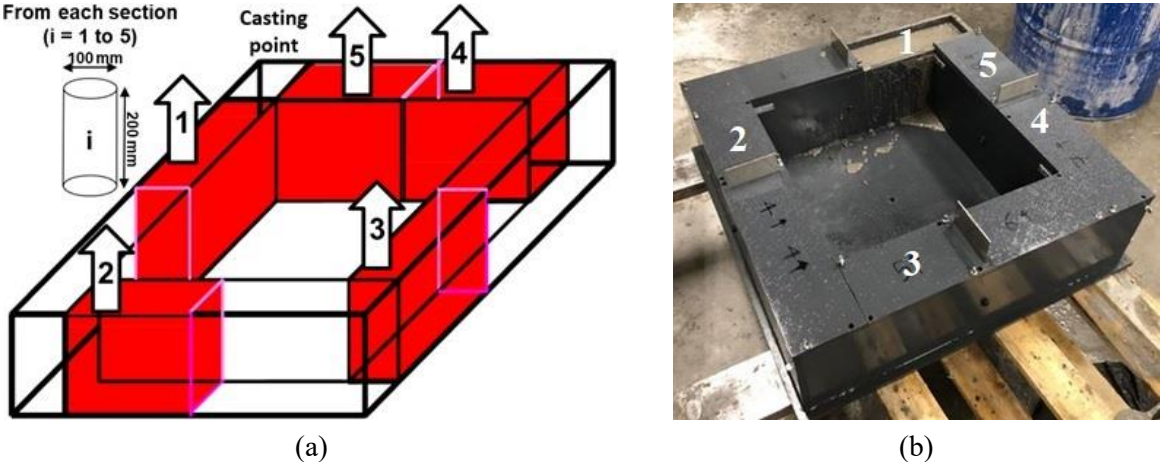

(a)   (b)

Figure 7-2 (a) Sampling method from each section (i = 1 - 5) of (b) the proposed Square-Box test set-up.

Accordingly, a heterogeneity index (HI_{F+CA-i}) to assess the dynamic stability and passing ability of the investigated FR-SCC mixtures was defined, as follows:

$$HI_{F+CA-i} = \frac{\dfrac{\varphi_{F-i} + \varphi_{CA-i}}{\varphi_{max-F+CA-i}}}{\dfrac{\varphi_{F-Ref} + \varphi_{CA-Ref}}{\varphi_{max-F+CA-Ref}}} \times 100\% \qquad \text{Equation 7-3}$$

where φ_{F-i}, φ_{CA-i}, φ_{F-Ref}, and φ_{CA-Ref} are the volumetric contents of fibers and coarse aggregate in sample i (i = 1 to 5) and reference mixture, respectively. Moreover, $\varphi_{max-F+CA-i}$ and $\varphi_{max-F+CA-Ref}$ are the packing density values of fiber-coarse aggregate combinations obtained in each section (i = 1 to 5) and reference mixture, respectively. The blocking (BI) and dynamic segregation (DSI) indices of the investigated mixtures were evaluated using the coefficient of variation (C.O.V.) of HI_{F+CA-i} values obtained at five sections (i = 1 to 5) of the testing set-up with and without reinforcing bars, respectively, as follows:

$$BI = COV(HI_{F+CA-i})_{i=1\,to\,5} = \frac{\sigma(HI_{F+CA-i})_{i=1\,to\,5}}{Avg(HI_{F+CA-i})_{i=1\,to\,5}} \times 100\%, \text{ in presence of reinforcing bars} \qquad \text{Equation 7-4}$$

$$DSI = COV(HI_{F+CA-i})_{i=1\,to\,5} = \frac{\sigma(HI_{F+CA-i})_{i=1\,to\,5}}{Avg(HI_{F+CA-i})_{i=1\,to\,5}} \times 100\%, \text{ without reinforcing bars} \qquad \text{Equation 7-5}$$

where $\sigma(HI_{F+CA-i})_{i=1\,to\,5}$ and $Avg(HI_{F+CA-i})_{i=1\,to\,5}$ are the standard deviation and average of HI_{F+CA-i} values obtained in sections i = 1 to 5. The obtained BI and DSI indices for the investigated FR-SCC mixtures are summarized in Table 7-4.

Table 7-4 Workability results of the investigated FR-SCC mixtures.

Mix	FRC-3	FRC-4	FRC-5	FRC-6	FRC-7	FRC-10
BI (%)	12.9	26.0	19.1	11.3	9.9	19.1
DSI (%)	7.2	11.9	2.8	3.2	1.3	4.5

7.3 Results and discussion

The coupled effects of flow distance, relative-solid packing-fraction (φ/φ_{max}) of fiber-coarse aggregate combination (> 5 mm), and rheological properties of the mortars on passing ability and dynamic stability of the investigated FR-SCC mixtures (BI and DSI indices - Equations 7-4 and 7-5) were evaluated in this section.

7.3.1   Effect of flow distance on heterogeneous performance of FR-SCC

The HI values (Equation 7-3) obtained at different distances from the casting point in the Square-Box without and with presence of reinforcing bars are presented in Figures 7-3a and 7-3b, respectively. It is worth mentioning that the distance from the casting point, illustrated in Fig. 3, correspond to the distance travelled by concrete to reach the middle of each section.

As can be observed in Figure 7-3, lower HI values (< 100%) were obtained at longer flow distances. This reflects the decrease in relative-solid packing-fraction of fiber-coarse aggregate combination with the flow distance from the casting point relative to the reference mixture. This can be due to dynamic segregation and blocking of fibers and coarse aggregate across the Square-Box test. The maximum and minimum variations in the φ/φ_{max} of fiber-coarse aggregate

were obtained for FRC-4 and FRC-7 mixtures, respectively. This can be attributed to the rheology of their corresponding mortar mixtures, their fiber content, and fiber-coarse aggregate characteristics, which is further discussed in the following sections. Moreover, the results presented in Figures 7-3a and 7-3b revealed higher variations in HI indices in the presence of reinforcing bars (70.7% < HI-with bar < 126.4%) compared to those obtained without any obstacles (82.7% < HI-without bar < 109.7%). This can be attributed to the blockage of fibers and coarse aggregate due to presence of reinforcing bars.

(a)   (b)
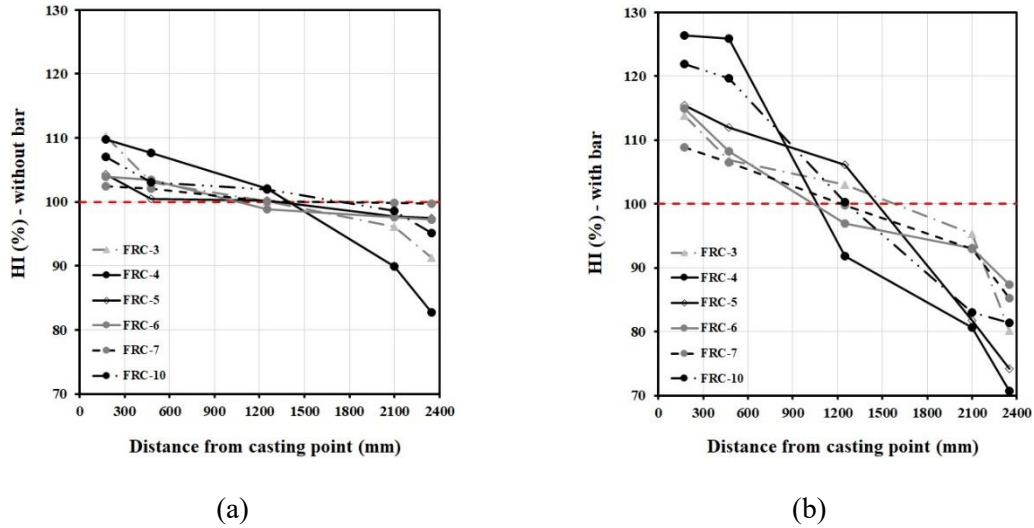
Figure 7-3 Effect of flow distance on fiber-coarse aggregate distribution in the Square-Box test (a) without and (b) in presence of reinforcing bars.

7.3.2 Blocking

The blocking indices (BI) of the investigated FR-SCC mixtures were correlated to their relative solid packing-fraction (φ/φ_{max}) of fiber-coarse aggregate combinations, as well as the yield stress ($\tau_{0\text{-M}}$) and plastic viscosity ($\mu_{p\text{-M}}$) values of their corresponding mortar mixtures, as follows:

$$\text{BI (\%)} = A_1 \times V_f^{A_2} \times \left(\frac{\varphi}{\varphi_{max}}\right)^{A_3} \times A_4^{\tau_{0\text{-M}}} \times A_5^{\mu_{p\text{-M}}} + A_6 \qquad \text{Equation 7-6}$$

where V_f is volumetric content of fibers and A_1 to A_6 are the adjustment factors reflecting the effect of different characteristics of suspended and suspending phases. A Microsoft Excel solver was then developed to obtain the adjustment factors leading to the closest BI values to the experimental ones. The results of the established correlation are shown in Equation 7-7 and Figure 7-4. As can be observed in Figure 7-4, the blocking indices of the investigated FR-SCC mixtures are in good agreement with the fiber content, φ/φ_{max} of fiber-coarse aggregate combinations, and rheological properties of their corresponding mortar matrix (R^2 of 1.0 and RMSE of 0.111%).

$$\text{BI (\%)} = 587.869 \times \frac{V_f^{0.630} \times \left(\frac{\varphi}{\varphi_{max}}\right)^{11.4549}}{0.967^{\tau_{0\text{-M}}} \times 0.288^{\mu_{p\text{-M}}}} + 0.564 \qquad \text{Equation 7-7}$$
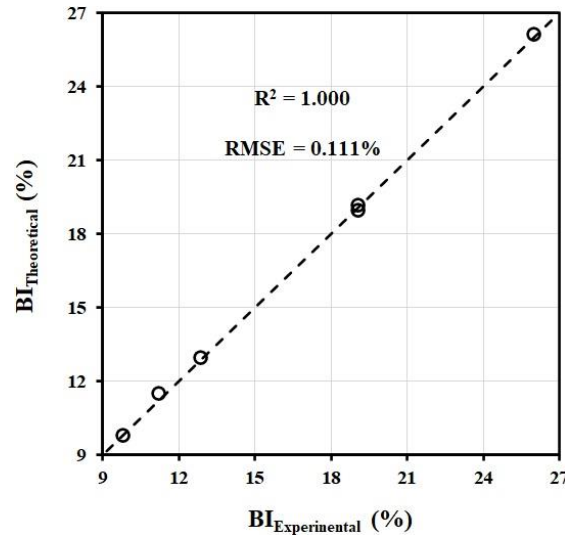
Figure 7-4 Comparison between the experimental BI indices of the investigated FR-SCC mixtures and those obtained using Equation 7-7.

According to the obtained adjustment factors in Equation 7-7, increasing the fiber content and φ/φ_{max} of fiber-coarse aggregate and decreasing the yield stress and plastic viscosity of the mortar resulted in higher blockage indices. The increasing in fibers and coarse aggregate contents can result in higher interaction between the solid phase (fibers and coarse aggregate) with the reinforcing bars and confining formwork walls, hence leading to higher blockage. On the other hand, mortar mixtures with higher yield stress and plastic viscosity can exert higher drag forces on fibers and coarse aggregate, hence leading to lower risk of separation of the suspended and suspending phases (lower BI values). Among different parameters, φ/φ_{max} of fiber-coarse aggregate combinations showed the most significant effect on passing ability of the investigated mixtures, rather than fiber content and rheology of mortar.

Furthermore, the passing ability of FR-SCC mixtures evaluated using the proposed Square-Box test is compared to the blocking indices obtained from the L-Box set-up (UBI_{LB} in Table 7-3). The ultimate blocking indices in the proposed Square-Box test (UBI_{set-up}) were firstly evaluated, as follows:

$$UBI_{set-up} \; (\%) = \frac{\left(\dfrac{\varphi}{\varphi_{max}}\right)_1 - \left(\dfrac{\varphi}{\varphi_{max}}\right)_5}{\left(\dfrac{\varphi}{\varphi_{max}}\right)_{Ref}} \times 100\% \qquad\qquad \text{Equation 7-8}$$

where $\left(\dfrac{\varphi}{\varphi_{max}}\right)_1$, $\left(\dfrac{\varphi}{\varphi_{max}}\right)_5$, and $\left(\dfrac{\varphi}{\varphi_{max}}\right)_{Ref}$ correspond to the relative-solid packing-fraction of fiber-coarse aggregate mixtures in samples taken from sections 1 and 5 of the proposed Square-Box set-up (Figure 7-2a) and reference mixture, respectively. As can be observed in Figure 7-5, the investigated mixtures exhibited significantly higher blocking in the Square-Box test (UBI_{set-up} of 23.6% to 55.7%) compared to those obtained in the L-Box set-up (UBI_{LB} of 11.4% to 19.5%). This can be due to higher flow distance travelled by the concrete through the proposed Square-Box test (2.4 m) compared to the horizontal channel (0.7 m) of the L-Box set-up.

Moreover, as mentioned earlier, the concrete is subjected to more restricted and confined flow conditions in the proposed Square-Box test compared to that in the L-Box test. Indeed, the L-Box and Square-Box set-ups are equipped with 1 and 4 rows of reinforcing bars with clear spacings of 60 and 45 mm between the rebars and Square-Box walls, respectively. Furthermore, the flow in the L-Box set-up is a free-surface flow type while it was confined at 4 sides in the

Square-Box test. These can lead to higher interaction between the reinforcing bars and fiber-coarse aggregate skeleton in the Square-Box test, hence leading to higher flow-induced blockage compared to the L-Box flow. This suggests that the L-Box set-up cannot sufficiently simulate the confined flow conditions of FR-SCC mixtures compared to the Square-Box test. Accordingly, low blocking indices in L-Box test may not guarantee high passing ability passing through the narrow zones such those that can be encountered in repair applications. This can highlight the proficiency of the proposed Square-Box test to simulate the flow conditions that FR-SCC experiences in repair applications.
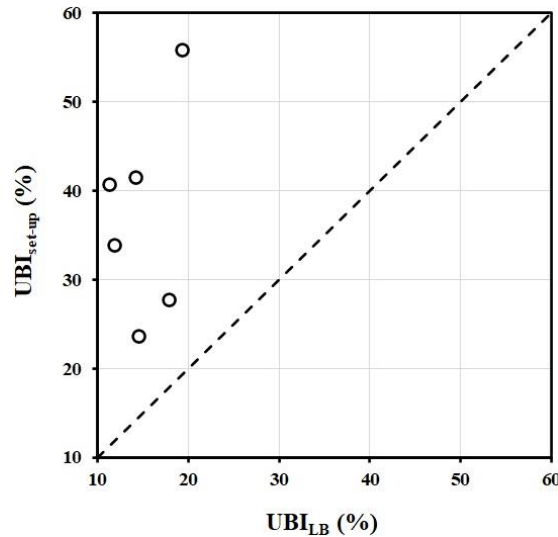
Figure 7-5 Comparison between the blocking results of the investigated FR-SCC mixtures in the L-Box (UBI_{LB}) and proposed Square-Box tests (UBI_{set-up}).

7.3.3 Dynamic stability

The coupled effect of rheological properties of mortar, fiber content, and φ/φ_{max} of fiber-coarse aggregate combinations on dynamic segregation of the investigated FR-SCC mixtures was evaluated. This was carried out similarly to the BI indices, using Equation 7-6 and a developed Microsoft Excel solver. The results of the established correlation are shown in Equation 7-9 and Figure 7-6.

$$\text{DSI (\%)} = 0.0012 \times \frac{V_f^{6.526} \times \left(\dfrac{\varphi}{\varphi_{max}}\right)^{57.933}}{0.248^{\tau_{0\text{-M}}} \times 0.000005^{\mu_{\text{p-M}}}} + 1.926 \qquad \text{Equation 7-9}$$
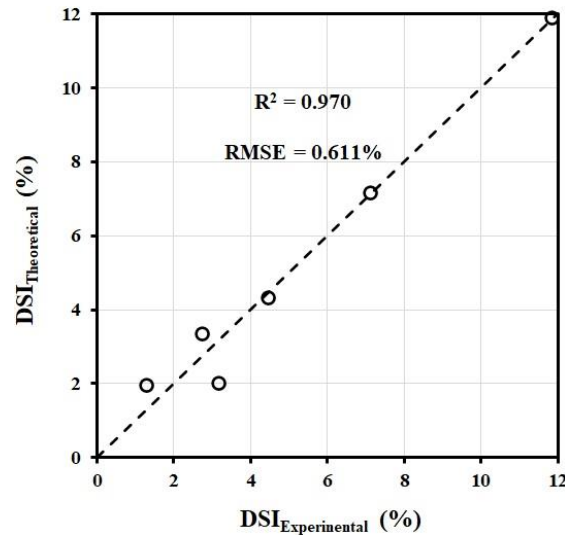
Figure 7-6 Comparison between the experimental DSI indices of the investigated FR-SCC mixtures and those obtained using Equation 7-9.

As can be observed in Figure 7-6, the established Equation 7-9 can well predict the dynamic segregation of the investigated FR-SCC mixtures as a function of volumetric content of fibers (V_f), φ/φ_{max} of fiber-coarse aggregate combination, as well as yield stress (τ_{0-M}) and plastic viscosity (μ_{p-M}) of their corresponding mortar matrices (R^2 of 0.970 and RMSE of 0.611%). According to the obtained adjustment factors in Equation 7-9, increasing yield stress and plastic viscosity of mortar led to higher dynamic stability of the investigated FR-SCC mixtures. This can be attributed to higher drag forces exerted on fibers and coarse aggregate, hence reducing the risk of separation of the solid phase (fibers and coarse aggregate) and suspending mortar.

On the other hand, the risk of dynamic segregation of the investigated FR-SCC mixtures increased for higher fiber volume and φ/φ_{max} of fiber-coarse aggregate. This is in contradiction to the positive effect of the φ/φ_{max} of coarse aggregate on dynamic stability of plain SCC mixtures through the T-Box set-up, as reported in literature [22]. This can be due to different flow conditions through the T-Box and Square-Box tests. In fact, the flow through the proposed Square-Box test is two times more confined (100-mm width) compared to the T-Box test (200-mm wide channel). Moreover, the T-Box flow is free-surface while concrete flow in the Square-Box test is surrounded by 4 walls. Furthermore, unlike the straight flow direction in the T-Box test, the investigated FR-SCC mixtures were subjected to three 90°-turning directions at the corners of the close-circuit in Square-Box set-up. These can lead to higher risk of interlocks between the coarse aggregate and fibers, as well as higher interactions between the solid phase (fibers and coarse aggregate) and the Square-Box set-up's walls for the mixtures proportioned with higher φ/φ_{max} of fiber-coarse aggregate combinations.

The dynamic stability of FR-SCC mixtures assessed using the Square-Box test is compared to the dynamic segregation indices obtained from the T-Box set-up (UDSI$_{TB}$ in Table 7-2). The ultimate dynamic segregation index in the Square-Box set-up (UDSI$_{set-up}$) was evaluated, as follows:

$$\text{UDSI}_{\text{set-up}} \ (\%) = \frac{\left(\dfrac{\varphi}{\varphi_{max}}\right)_1 - \left(\dfrac{\varphi}{\varphi_{max}}\right)_5}{\left(\dfrac{\varphi}{\varphi_{max}}\right)_{Ref}} \times 100\% \qquad \text{Equation 7-10}$$

where $\left(\dfrac{\varphi}{\varphi_{max}}\right)_1$, $\left(\dfrac{\varphi}{\varphi_{max}}\right)_5$, and $\left(\dfrac{\varphi}{\varphi_{max}}\right)_{Ref}$ corresponds to the relative-solid packing fraction of fiber-coarse aggregate mixtures in samples taken from sections 1 and 5 of the Square-Box test (without reinforcing bars: Figure 7-2b), and the reference mixture, respectively.

As can be observed in Figure 7-7, the majority of the investigated mixtures showed relatively higher dynamic segregation indices in the T-Box set-up (UDSI$_{TB}$ of 12.2% to 49.6%) compared to those obtained in the Square-Box test (UDSI$_{set-up}$ of 2.7% to 27.0%) for majority of the investigated mixtures. This can be related to the higher flow distance that concrete travels in the T-Box test (9.0 m) [36] than that in the Square-Box test (2.4 m). Although the T-Box set-up allowed longer flow distance, the confined flow conditions in repair application are more realistically reproduced using the proposed Square-Box test, as mentioned earlier. This may suggest that the dynamic segregation in T-Box test is overestimated compared to that can occur under confined flow conditions of the repair application.
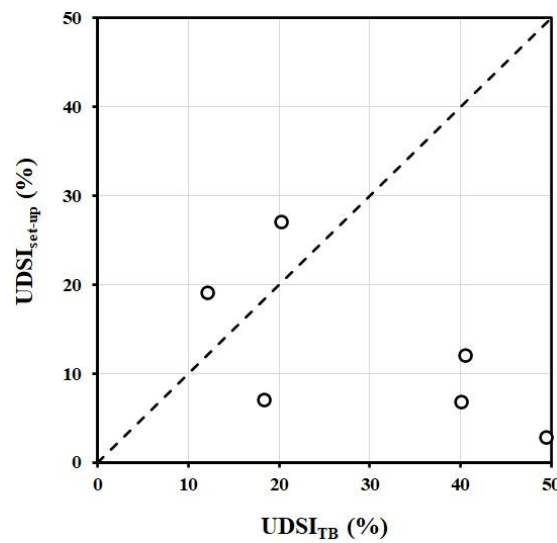
Figure 7-7 Comparison between the dynamic segregation results of the investigated FR-SCC mixtures in the T-Box (UDSITB) and proposed Square-Box tests (UDSIset-up).

7.3.4 Filling ability classification of FR-SCC mixtures

The filling ability of the investigated FR-SCC mixtures can be classified by plotting their blocking indices (BI – Equation 7-6) to dynamic segregation indices (DSI - Equation 7-7) presented in Table 7-5. As shown in Table 7-5, three different classes corresponding to relatively low, medium, and high dynamic stability and passing ability were defined according to the measured DSI and BI values. As shown in Figure 7-8, the investigated FR-SCC mixtures were classified in three different filling ability levels, including (i) high filling ability (Green zone: low DSI and BI values), (ii) medium filling ability (Purple zone: low to medium DSI and BI values), and (iii) low filling ability (Red zone: high DSI and BI values).

Table 7-5 Recommended dynamic stability and passing ability criteria to establish the filling ability classification of FR-SCC.

Flow performance level	Low	Medium	High
Dynamic stability	DSI > 8%	4% ≤ DSI ≤ 8%	DSI < 4%
Passing ability	BI > 21%	15% ≤ BI ≤ 21%	BI < 15%
Filling ability	Low filling ability	Medium filling ability	High filling ability
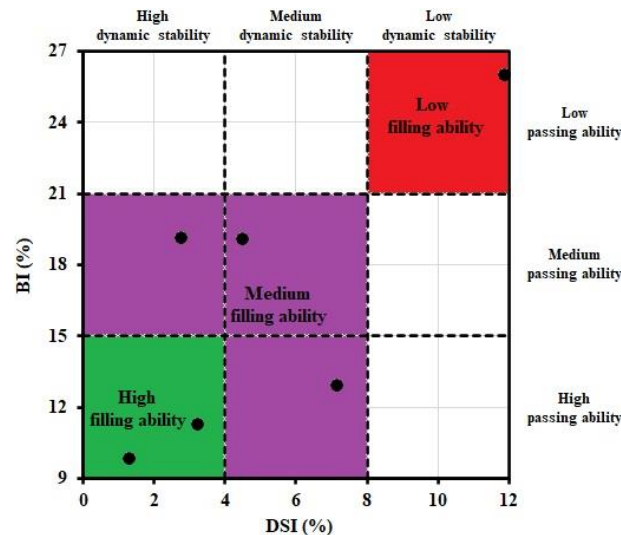
Figure 7-8 Filling ability-based classifications of the investigated FR-SCC mixtures: passing ability (BI) versus dynamic stability (DSI) indices.

According to the established classification, the majority of the investigated mixtures exhibited medium and high filling ability levels, except the FRC-4 mixture (low filling ability). On the other hand, the FRC-6 and FRC-7 mixtures showed the highest filling ability among the investigated FR-SCC mixtures. Accordingly, the characteristics of FR-SCC mixtures with high filling ability are summarized in Table 7-6 based on the properties of their corresponding cement paste (volumetric content and rheology), mortar matrix (rheology), PSD of aggregate, macro-steel fiber content, and fiber-coarse aggregate (volumetric content and packing density). This is worth mentioning that the characteristics summarized in Table 7-6 are only preliminary recommendations established based on limited FR-SCC mixtures investigated in this study. Further studies are thus required to establish more comprehensive recommendations considering wider ranges of characteristics of coarse aggregate (PSD and PD), volume and type of fibers, W/B ratio, and paste volume.

Table 7-6 Preliminary recommendation of characteristics of FR-SCC mixtures that can exhibit high filling ability.

Mixture constituents	Properties	Recommended ranges
	Paste volume: V_P (%)	30 - 33
Cement paste	Yield stress: $\tau_{0\text{-}P}$ (Pa)	1.22 - 1.27
	Plastic viscosity: $\mu_{p\text{-}P}$ (Pa.s)	0.040 - 0.043
Mortar	Yield stress: $\tau_{0\text{-}M}$ (Pa)	4.61 - 7.96
	Plastic viscosity: $\mu_{p\text{-}M}$ (Pa.s)	3.24 - 3.55
Aggregate	Volumetric sand-to-total aggregate ratio: S/A	0.55
	Particle-size distribution of coarse aggregate	PSD-1 and PSD-3
Macro steel fiber	Fiber volume: V_f (%)	0.12 - 0.25
Fiber-coarse aggregate combination	Packing density: φ_{max}	0.536 - 0.554
	Relative-solid packing-fraction: φ/φ_{max}	0.521 - 0.528

7.3.5 Impact of flow-induced heterogeneity on mechanical performance of FR-SCC

As shown in the previous sections, the FR-SCC mixtures exhibited heterogeneous distribution of fibers and aggregate due to dynamic segregation and blocking in the Square-Box test. This was reflected by the variations of volumetric content and packing density of the fiber-coarse aggregate compared to the reference mixture. Inadequate homogeneities can impact mechanical performance of FR-SCC. Unfavorable mechanical performance of FR-SCC can lead to lower

bond with the substrate concrete [18]. The effect of flow-induced heterogeneity on dissimilar mechanical properties of the investigated mixtures determined at different distances from the casting point was evaluated.

In addition to the samples taken for dynamic segregation measurements, two cylindrical samples, measuring 100 mm in diameter and 200 mm in height, were taken from each section (i = 1 to 5) of the Square-Box set-up with no reinforcing bars to determine compressive strength. It is worthy to mention that these samples could not be taken for the configuration with presence of reinforcing bars. Indeed, enough quantity of concrete was not available to be sampled for compressive strength measurements after sampling for blocking measurements. It was due to blockage occurred in first three sections of the reinforced Square-Box set-up. The compressive strength (f'_{c-i}) of the taken samples corresponding to each section (i = 1 to 5) was measured after 28 days of curing at 100% relative humidity condition. The flow-induced dissimilarity in compressive strength values across the cast element was evaluated using a compressive-strength heterogeneity index (CSHI). The CSHI is defined as the coefficient of variation (C.O.V.) of the ratio of f'_{c-i} values obtained in sections i = 1 to 5-to-the compressive strength of the investigated reference mixtures before any segregation (f'_{c-Ref} values in Table 7-3), as follows:

$$\text{CSHI (\%)} = \text{COV}\left(\frac{f'_{c-i}}{f'_{c-Ref}}\right)_{i\,=\,1\text{ to }5} = \frac{\sigma\left(\frac{f'_{c-i}}{f'_{c-Ref}}\right)_{i\,=\,1\text{ to }5}}{\text{Avg}\left(\frac{f'_{c-i}}{f'_{c-Ref}}\right)_{i\,=\,1\text{ to }5}} \times 100\%, \text{ without reinforcing bars} \qquad \text{Equation 7-11}$$

where $\sigma\left(\dfrac{f'_{c-i}}{f'_{c-Ref}}\right)_{i\,=\,1\text{ to }5}$ and $\text{Avg}\left(\dfrac{f'_{c-i}}{f'_{c-Ref}}\right)_{i\,=\,1\text{ to }5}$ are the standard deviation and average of the relative compressive strength of the samples at each section (i = 1 to 5) to that of the reference mixture, respectively. As can be observed in Figure 7-9, the CSHI values determined using Equation 7-11 are in good agreement with dynamic segregation indices of the investigated mixtures in the Square-Box test, obtained using Equation 7-5 (DSI in Table 7-4). According to the established correlation, higher dynamic segregation can lead to more dissimilar compressive strength values at different sections of the cast element. Therefore, it can be concluded that an appropriate and uniform mechanical performance across the repaired element can be achieved by ensuring homogeneous flow performance of the used FR-SCC.
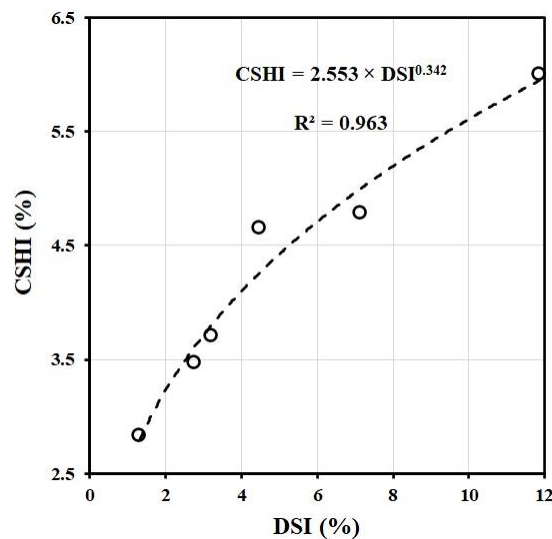

Figure 7-9 Relationship between the CSHI and DSI indices of the investigated FR-SCC mixtures.

7.4 Conclusions

In this study, workability of various FR-SCC mixtures for repair applications was investigated as biphasic suspension of steel fibers and coarse aggregate (> 5 mm) in a suspending mortar, containing cement paste and aggregate finer than 5 mm. The mixtures exhibiting high passing ability and medium to high dynamic stability in the conventional L-Box and T-Box set-ups were identified. However, these conventional tests cannot properly simulate the confined and restricted flow conditions. Accordingly, a new empirical Square-Box test was proposed to evaluate the passing ability and dynamic stability of the selected FR-SCC mixtures under confined flow conditions in presence and without reinforcing bars, respectively. The proposed Square-Box test consisted of a close-surface and close-circuit of four rectangular channel, hence providing more confined and restricted flow conditions compared to the T-Box and L-Box set-ups. Based on the obtained experimental results, the following concluding remarks can be drawn:

- Unlike the conventional L-Box and T-Box tests, the proposed Square-Box test could successfully simulate the flow conditions during casting of FR-SCC mixtures, including the flow distance and confinement, wall effect, and presence of highly congested reinforcing bars.

- The obtained dynamic segregation and blocking indices in the Square-Box are well correlated to the coupled effect of fiber volume, relative-solid packing-fraction (φ/φ_{max}) of fiber-coarse aggregate combination, and rheological properties of mortar matrix.

- The volumetric content and φ/φ_{max} of fibers and coarse aggregate showed negative effect on both dynamic stability and passing ability of FR-SCC mixtures. On the other hand, increasing yield stress and plastic viscosity of the suspending mortar mixtures enhanced the homogeneous performance of the investigated FR-SCC mixtures. The flow-induced heterogeneities of the investigated FR-SCC mixtures were found more controlled by characteristics of fibers and coarse aggregate rather than the rheology of mortar.

- The investigated FR-SCC mixtures exhibited significantly higher blocking indices through the proposed Square-Box test (UBI$_{set-up}$ values of 24% to 56%) compared to those obtained using the L-Box test (UBI$_{LB}$ values of 11% to 20%). On the other hand, the dynamic segregation indices obtained using the T-Box set-up (UDSI$_{TB}$ values of 12% to 50%) were found overestimated (UDSI$_{set-up}$ values of 3% to 27% in the proposed Square-Box test). Furthermore, the fiber volume and φ/φ_{max} of fiber-coarse aggregate showed opposite effects on dynamic segregation indices determined using the T-Box and Square-Box tests, due to their different flow conditions.

- A new filling ability classification was established for FR-SCC mixtures. The specifications of the FR-SCC mixtures with high dynamic stability and passing ability properties were recommended. These include the appropriate ranges of volumetric content and rheology of cement paste, viscoplastic properties of mortar, PSD of aggregate, macro-steel fiber content, and φ/φ_{max} of fiber-coarse aggregate combination for confined and restricted flow conditions (e.g., repair application).

- The heterogeneous flow performance of the investigated FR-SCC mixtures was found in good agreement with heterogeneous mechanical performance obtained at different flow distances. According to the established correlation, higher dynamic segregation led to higher dissimilar compressive strength values across the repaired/cast element.

Acknowledgment

References

[1] J. Wang, Q. Dai, R. Si, Y. Ma, S. Guo, Fresh and mechanical performance and freeze-thaw durability of steel fiber-reinforced rubber self-compacting concrete (SRSCC), Journal of Cleaner Production, 277 (2020) 123180, https://doi.org/10.1016/j.jclepro.2020.123180.

[2] S. Cattaneo, F. Giussani, F. Mola, Flexural behaviour of reinforced, prestressed and composite self-consolidating concrete beams, Construction and Building Materials, 36 (2012) 826-837, https://doi.org/10.1016/j.conbuildmat.2012.06.001.

[3] K.H. Khayat, F. Kassimi, P. Ghoddousi, Mixture design and testing of fiber-reinforced self-consolidating concrete, ACI Materials Journal, 111 (2) (2014) 143-152, https://doi.org/10.14359/51686722.

[4] L. Ferrara, P. Bamonte, A. Caverzan, A. Musa, I. Sanal, A comprehensive methodology to test the performance of Steel Fibre Reinforced Self-Compacting Concrete (SFR-SCC), Construction and Building Materials, 37 (2012) 406-424, https://doi.org/10.1016/j.conbuildmat.2012.07.057.

[5] H.B. Dhonde, Y.L. Mo, T.T.C. Hsu, J. Vogel, Fresh and hardened properties of self-consolidating fiber-reinforced concrete, ACI Materials journal, 104 (5) (2007) 491-500, https://dx.doi.org/10.14359/18905.

[6] ASTM C1399/C1399M-10, Standard test method for obtaining average residual-strength of fiber-reinforced concrete, West Conshohocken, PA; ASTM International (2015), https://dx.doi.org/10.1520/C1399_C1399M-10R15.

[7] ASTM C1609/C1609M-19a, Standard Test Method for Flexural Performance of Fibre-Reinforced Concrete (Using Beam With Third Point Loading), West Conshohocken, PA; ASTM International (2020), https://dx.doi.org/10.1520/C1609_C1609M-19A.

[8] Q. Song, R. Yu, Z. Shui, X. Wang, S. Rao, Z. Lin, Optimization of fibre orientation and distribution for a sustainable Ultra-High Performance Fibre Reinforced Concrete (UHPFRC): Experiments and mechanism analysis, Construction and building materials, 169 (2018) 8-19, https://doi.org/10.1016/j.conbuildmat.2018.02.130.

[9] L. Zhang, J. Zhao, C. Fan, Z. Wang, Effect of surface shape and content of steel fiber on mechanical properties of concrete, Advances in Civil Engineering, 2020 (2020) 8834507, https://doi.org/10.1155/2020/8834507.

[10] L.G. Sorelli, A. Meda, G.A. Plizzari, Steel fiber concrete slabs on ground: A structural matter, ACI Structural Journal, 103 (4) (2006) 551-558, https://doi.org/10.14359/16431.

[11] M. Di Prisco, M. Mauri, M. Scola, A new design for stabilizing ground slopes, In: Proceedings of the 2nd fib congress, Napoli, Italy, 2006, ID 4-1 on CD-ROM, http://hdl.handle.net/11311/536592.

[12] A.S. El-Dieb, M.M. Reda Taha, Flow characteristics and acceptance criteria of fiber-reinforced self-compacted concrete (FR-SCC), Construction and Building Materials, 27 (1) (2012) 585-596, https://doi.org/10.1016/j.conbuildmat.2011.07.004.

[13] G. Žirgulis, O. Švec, M.R. Geiker, A. Cwirzen, T. Kanstad, Influence of reinforcing bar layout on fibre orientation and distribution in slabs cast from fibre-reinforced self-compacting concrete (FRSCC), Structural Concrete, 17 (2) (2016) 245-256, https://doi.org/10.1002/suco.201500064.

[14] B. Boulekbache, M. Hamrat, M. Chemrouk, S. Amziane, Flowability of fibre-reinforced concrete and its effect on the mechanical properties of the material, Construction and Building Materials, 24 (9) (2010) 1664-1671, https://doi.org/10.1016/j.conbuildmat.2010.02.025.

[15] E. Jasiūnienė, V. Cicėnas, P. Grigaliūnas, Ž. Rudžionis, A.A. Navickas, Influence of the rheological properties on the steel fibre distribution and orientation in self-compacting concrete, Materials and Structures, 51 (2018) 103, https://doi.org/10.1617/s11527-018-1231-y.

[16] D.Y. Yoo, G. Zi, S.T. Kang, Y.S. Yoon, Biaxial flexural behavior of ultra-high-performance fiber-reinforced concrete with different fiber lengths and placement methods, Cement and Concrete Composites, 63 (2015) 51-66, https://doi.org/10.1016/j.cemconcomp.2015.07.011.

[17] M. Safdar, T. Matsumoto, K. Kakuma, Flexural behavior of reinforced concrete beams repaired with ultra-high performance fiber reinforced concrete (UHPFRC), Composite Structures, 157 (2016) 448-460, https://doi.org/10.1016/j.compstruct.2016.09.010.

[18] F. Kassimi, A.K. El-Sayed, K.H. Khayat, Performance of fiber-reinforced self-consolidating concrete for repair of reinforced concrete beams, ACI Structural Journal, 111 (6) (2014) 1277-1286, https://dx.doi.org/10.14359/51687031.

[19] F. Kassimi, A.K. El-Sayed, K.H. Khayat, Flexural behavior of fiber-reinforced SCC for monolithic and composite beams, Journal of Advanced Concrete Technology, 19 (8) (2021) 937-949, https://doi.org/10.3151/jact.19.937.

[20] M. Arezoumandi, C. Wirkman, J.S. Volz, Performance of fiber-reinforced self-consolidating concrete for repair of bridge substructures, In Structures, 15 (2018) 320-328, https://doi.org/10.1016/j.istruc.2018.07.015.

[21] T. Voigt, V.K. Bui, S.P. Shah, Drying shrinkage of concrete reinforced with fibers and welded-wire fabric, ACI Materials Journal, 101 (3) (2004) 233-241, https://doi.org/10.14359/13119.

[22] B.I.O. Koura, M. Hosseinpoor, A. Yahia, Coupled effect of fine mortar and granular skeleton characteristics on dynamic stability of self-consolidating concrete as a diphasic material, Construction and Building Materials, 263 (2020) 120131, https://doi.org/10.1016/j.conbuildmat.2020.120131.

[23] M. Hosseinpoor, B.I.O. Koura, A. Yahia, Rheo-morphological investigation of static and dynamic stability of self-consolidating concrete: A biphasic approach, Cement and Concrete Composites, 121 (2021) 104072, https://doi.org/10.1016/j.cemconcomp.2021.104072.

[24] M. Hosseinpoor, B.I.O. Koura, A. Yahia, New diphasic insight into the restricted flowability and granular blocking of self-consolidating concrete: Effect of morphological characteristics of coarse aggregate on passing ability of SCC, Construction and Building Materials, 308 (2021) 125001, https://doi.org/10.1016/j.conbuildmat.2021.125001.

[25] B. Esmaeilkhanian, D. Feys, K.H. Khayat, A. Yahia, New test method to evaluate dynamic stability of self-consolidating concrete, ACI Materials Journal, 111 (3) (2014) 299-307, https://doi.org/10.14359/51686573.

[26] ASTM C1621/C1621M-17, Standard Test Method for Passing Ability of Self-Consolidating Concrete by J-Ring, West Conshohocken, PA; ASTM International (2017), https://dx.doi.org/10.1520/C1621_C1621M-17.

[27] EFNARC, European Project Group, The European Guidelines for Self-Compacting Concrete: Specification, Production and Use (2005).

[28] ASTM C1611/C1611M-18, Standard Test Method for Slump Flow of Self-Consolidating Concrete, West Conshohocken, PA; ASTM International (2018), https://dx.doi.org/10.1520/C1611_C1611M-18.

[29] S. Kuroiwa, Y. Matsuoka, M. Hayakawa, T. Shindoh, Application of super workable concrete to construction of a 20-story building, ACI Symposium Publication, 140 (1993) 147-162.

[30] K.H. Khayat, Workability, testing, and performance of self-consolidating concrete, ACI Materials Journal, 96 (3) (1999) 346-353, https://dx.doi.org/10.14359/632.

[31] Nordtest, Method (NT BUILD 427) for Fresh Concrete: Compactibility with IC-tester (Intensive Compaction Tester) Proj. 1005-91, Nord. Scand. Inst. (1994) 1-4, ISSN 0283-7153, www.nordtest.org.

[32] B.M. Aïssoun, Étude de l'influence des caractéristiques des granulats sur la performance des bétons fluides à rhéologie adaptée (in French) (in French), M.Sc. thesis, Université de Sherbrooke (2011), http://savoirs.usherbrooke.ca/handle/11143/1590.

[33] N. Nouri, M. Hosseinpoor, A. Yahia, K.H. Khayat, Coupled effect of fiber and granular skeleton characteristics on packing density of fiber-aggregate mixtures, Construction and Building Materials, 342 (2022) 127932, https://doi.org/10.1016/j.conbuildmat.2022.127932.

[34] M. Hosseinpoor, B.I.O. Koura, A. Yahia, E.H. Kadri, Diphasic investigation of the visco-elastoplastic characteristics of highly flowable fine mortars, Construction and Building Materials, 270 (2021) 121425, https://doi.org/10.1016/j.conbuildmat.2020.121425.

[35] M. Hosseinpoor, B.I.O. Koura, A. Yahia, Rheo-morphological investigation of Reynolds dilatancy and its effect on pumpability of self-consolidating concrete, Cement and Concrete Composites, 117 (2021) 103912, https://doi.org/10.1016/j.cemconcomp.2020.103912.

[36] B. Esmaeilkhanian, K. H. Khayat, A. Yahia, D. Feys, Effects of mix design parameters and rheological properties on dynamic stability of self-consolidating concrete, Cement and Concrete Composites, 54 (2014) 21-28, https://doi.org/10.1016/j.cemconcomp.2014.03.001.

CHAPITER 8 Fiber orientation and distribution of steel fiber-reinforced self-consolidating concrete in reinforced and confined elements

Authors and affiliations

Naimeh Nouri : Ph.D. candidate, Cement and Concrete Research Group, Department of Civil and Building Engineering, Université de Sherbrooke, Sherbrooke, Québec, Canada, J1K 2R1.

Masoud Hosseinpoor: Research Associate, Cement and Concrete Research Group, Department of Civil and Building Engineering, Université de Sherbrooke, Sherbrooke, Québec, Canada, J1K 2R1.

Ammar Yahia: Professor, Cement and Concrete Research Group, Department of Civil and Building Engineering, Université de Sherbrooke, Sherbrooke, Québec, Canada, J1K 2R1.

Kamal H. Khayat: Professor, Missouri University of Science and Technology, Center for Infrastructure Engineering Studies, Department of Civil, Architectural and Environmental Engineering, Rolla, MO 65409.

Fiber orientation and distribution of steel fiber-reinforced self-consolidating concrete in reinforced and confined elements

Naimeh Nouri[a], Masoud Hosseinpoor[a],*, Ammar Yahia[a], and Kamal H. Khayat[b]

[a]Université de Sherbrooke, Department of Civil and Building Engineering, Sherbrooke, Québec, Canada

[b]Missouri University of Science and Technology, Center for Infrastructure Engineering Studies, Department of Civil, Architectural and Environmental Engineering, Rolla, MO, USA

*Corresponding author: masoud.hosseinpoor@usherbrooke.ca

Abstract

In this study, the coupled effect of mixture constituents and casting conditions on fiber orientation and distribution (FOD) of FR-SCC being cast in confined flow conditions was investigated. The studied mixture constituents include the volumetric content-to-packing density ratio (φ/φ_{max}) of fiber-coarse aggregate combination (F-A), fiber volume (V_f), and rheological properties of suspending mortar. Moreover, the casting conditions were investigated in terms of flow distance, formwork-wall effect, and presence of reinforcing bars. A new Square-Box test method was used to simulate the confined flow conditions. In total, six FR-SCC mixtures with high passing ability and dynamic stability properties were investigated. The FOD of the investigated mixtures cast through the Square-Box set-up was evaluated in terms of distribution frequency in horizontal and vertical directions, as well as in-plane and out-of-plane orientations of fibers. Different empirical indices are developed to evaluate the effect of reinforcing bars and formwork walls on FOD. The proposed indices were found in good agreements with the φ/φ_{max} of F-A, V_f, and rheological properties of mortar. Increasing the φ/φ_{max} of F-A and rheological properties of mortar reduced the negative effect of flow distance and formwork wall but increased the negative effect of the presence of reinforcing bars on homogeneous fiber distribution. Similarly, higher φ/φ_{max} of F-A led to more negative effect of reinforcing bars on desired fiber orientation. However, the fiber orientation of FR-SCC mixtures proportioned with high plastic viscosity of mortar and φ/φ_{max} of F-A were less affected by flow distance.

Keywords: Fiber distribution; Fiber orientation; Fiber-reinforced self-consolidating concrete; Packing density; Reinforcing bar; Rheology.

8.1 Introduction

Fiber-reinforced Fiber-reinforced self-consolidating concrete (FR-SCC) is frequently used for structural and non-structural applications to accelerate the casting [1], increase the flexural performance [2], and decrease shrinkage [3]. The fresh and mechanical properties of FR-SCC were widely investigated in literature [1,4-6]. Good workability of FR-SCC can be ensured by optimizing the volume of paste, type and volume of fibers, and particle-size distribution of aggregate [7]. For instant, Khayat and Roussel [7] reported a maximum volume of steel fibers of 0.5% to secure high flowability and passing ability of FR-SCC. Khayat et al. [5] and Gencel et al. [8] reported an increase in compressive and flexural strengths of FR-SCC mixtures up to 28% and 52% by adding 0.25% volume and 60 kg/m^3 content of steel fibers, respectively.

In addition to the primary effect of fiber content, mechanical performance of FR-SCC is significantly affected by the homogeneous distribution and desired orientation of fibers through

the cast elements [9,10]. By taking advantage of the high flowability of FR-SCC to eliminate the vibration, homogeneous distribution of fibers can be achieved at different flow distances, hence resulting in uniform distribution of mechanical performance through the cast element [1]. Moreover, it was reported in literature that higher flexural strength and toughness are achieved for FR-SCC due to orientation of majority of fibers parallel to the flow direction and perpendicular to the cross section of the cast elements [1,11]. The fiber orientation and distribution (FOD) of FR-SCC significantly depend on the flow conditions [12]. Torrijos et al. [13] reported the remarkable effect of casting method (flow direction) on FOD and, consequently, the mechanical performance of structural FR-SCC elements. Alberti et al. [14] and Zerbino et al. [15] highlighted the effect of flow distance on FOD. However, a significant decrease of fiber efficiency on mechanical properties was reported for random orientation of fibers compared to those fully aligned in the flow direction [16,17]. Then, FOD should be properly controlled to ensure proper mechanical performance.

Orientation of fibers can be quantified using the angle between the fibers' alignment and cross-section plane of the cast elements. This can identify the efficiency of the fibers to carry the uniaxial-tensile stresses perpendicularly applied to the cross section of the elongated structural elements, such as beams [17]. In the case of multiaxial stress distribution in the wide elements, such as slabs [18], the orientation of fibers can be effective on mechanical performance of the cast elements in all directions, not only perpendicular to their cross-section plane [19]. Accordingly, both in-plane and out-of-plane orientation angles of fibers in the cross sections are considered.

FOD have been evaluated using different experimental methods, such as image analysis [20], X-ray tomography [21], electromagnetic induction [22], and active microwave thermography [23]. Lataste et al. [24] evaluated segregation of fibers using the electrical conductivity measurements. However, the results are dependent on the concrete age and only applicable for the conductive fibers, such as carbon and steel fibers. Torrents et al. [25] proposed an inductive method to limit the effect of the concrete age for steel fiber-reinforced mixtures. Mehdipour et al. [26] evaluated the distribution of steel fibers in fiber-reinforced cement-based mortar using near-field microwave reflectometry. The results indicated that at 3 GHz frequency of microwave signals, increasing fiber content from 0% to 1% and 2% increased the reflection coefficients up to an optimum value of 2% and then decreases. This can be explained by an improper FOD induced by the fiber balling in the case of a high fiber content of 2%. The authors reported that both microwave and image-analysis methods can successfully evaluate the FOD. Image analysis is generally employed to evaluate FOD due to its high accuracy and low cost. In this method, the investigated cross sections are pictured using high-resolution cameras. Dark-color inks are generally used for painting the coarse aggregate and mortar matrix to enhance their contrast compared to that of the cut fibers. The taken images are then converted to binary format (black and white pixels) and analysed using computational techniques. The FOD are evaluated using the number, position, and geometrical properties (dimension, form, and orientation) of the cut fibers through the investigated cross sections.

Martinie and Roussel [12] noted that the FOD change with the flow distances travelled by fiber reinforced concrete (FRC), which consequently affects the mechanical performance. The variations in fibers concentration at different flow distances can reflect the dynamic stability and passing ability of FRC across the non-reinforced and reinforced elements, respectively. Spangenberg et al. [27] reported lower volumetric fraction of solid particles of flowable concrete at longer flow distances, whereas the maximum concentration of solid particles was found in the vicinity of the casting point. Ferrara et al. [11] reported that increasing the distance from casting point led to a decrease in fiber content from 80 to 29 kg/m^3 through a 1.5-m length beam, reflecting the dynamic segregation of fibers. The authors reported that the uneven

distribution of fibers negatively affects the mechanical performance of FRC elements. However, fibers displaced to longer flow distances were found mostly oriented parallel to the flow direction which can enhance the mechanical properties in such zones [28]. This can refer to the controversial effects of flow distance on homogeneous distribution and desired orientation of fibers.

Effect of rheological properties of fiber reinforced concrete (FRC) on FOD was also investigated in literature [11,28]. Ferrara et al. [11] and Jasiūnienė et al. [28] reported that low plastic viscosity and yield stress of FRC led the fibers to be mostly orientated perpendicular to the cross section. However, low rheological properties of FRC showed negative influence on uniform distribution of fibers. Indeed, despite their proper orientation, lower volume of fibers at longer flow distance led to lower flexural strength values compared to the zones closer to the casting point. It can thus be concluded that optimization of the rheological properties of FR-SCC in fresh state can ensure proper mechanical performance depending on the casting conditions.

The use of fibers allows to reduce the reinforcement density and enhance the flexural behavior of FRC structural elements [28,29]. The FOD can be locally disturbed in the vicinity of the rebars due to their interactions [30]. Žirgulis et al. [31] investigated the effect of different reinforcing configurations on FOD through casting in FRC slabs. The authors reported the fiber blockage and uneven fiber orientation in the vicinity of rebars, resulting in negative effect on the mechanical performance [31]. Accordingly, Khayat et al. [5] recommended a minimum clear distance of 2.5 times the fiber length to be considered between the reinforcing bars to reduce the risk of fibers' blockage.

FR-SCC is recently used for repair applications [32-34]. The efficiency of repair concrete depends on its capacity to properly fill the narrow zones and encapsulate the reinforcing bars of the repaired sections [35]. Thus, the use of FR-SCC for casting in the restricted and confined zones, which are typical for repair applications, is highly advantageous. In order to ensure a proper mechanical performance of repaired elements, the FR-SCC mixtures should be optimized to achieve high dynamic stability and passing ability, in addition to a proper FOD. This includes the optimization of characteristics of fibers, aggregate, and rheological behavior of FR-SCC, depending on the casting conditions, such as casting flow rate, flow confinement, and reinforcement density. It was revealed that the effect of formwork walls on fiber orientation depends on the ratios between the formwork width and aspect ratio (length/diameter) of fibers [36]. Petersson [37] reported that longer fibers (higher aspect ratio) are more oriented parallel to the flow direction unlike the random orientation of short fibers. However, higher risks of balling, blockage, and improper distribution were reported for longer fibers (higher aspect ratio) [38]. This can be more critical for confined flow conditions [32]. Accordingly, Khayat and Roussel [7] recommended a maximum size of aggregate of 10 mm, volumetric sand-to-paste ratio of 0.6-0.8, and maximum fiber content of 0.5% to minimize any blockage.

In this study, the coupled effect of fiber-coarse aggregate characteristics, and mortar rheology, as well as reinforcing bars arrangement and formwork wall on FOD of FR-SCC mixtures under restricted and confined flow conditions was evaluated. A new Square-Box test set-up was proposed to simulate the confined and restricted flow conditions which are typical for repair applications. The set-up consisted in a closed surface and close-square circuit box, equipped with several horizontal, vertical, and longitudinal reinforcing bars. Several steel-fiber reinforced SCC mixtures, proportioned with 0.12% to 0.50% macro steel fibers and showing high passing ability and appropriate dynamic stability properties were investigated. The investigated FR-SCC mixtures were considered as diphasic suspensions of fiber-coarse aggregate combination (> 5 mm) and mortar matrix, containing aggregate finer than 5 mm. The FOD was then evaluated using image analysis of the hardened cut sections taken from the cast

proposed Square-Box set up. The results of this study can help to better optimize the mixture proportioning and rheological properties of FR-SCC mixtures to ensure proper FOD and, consequently, appropriate mechanical performance of cast/repaired elements by taking into account the reinforcing arrangement and formwork confinement.

8.2 Experimental study

8.2.1   Materials and characteristics

In this study, 10 FR-SCC mixtures were proportioned with a water-to-binder ratio (W/B) of 0.42 and paste volume (V_P) of 0.27 to 0.33, which are typical for repair applications, and macro steel fiber volume of 0.12% to 0.50%. The investigated mixtures were optimized to achieve a targeted slump flow of 680 ± 20 mm. The mixture design parameters and characteristics of the materials used to proportion the investigated mixtures, as well as the grading of fine and coarse aggregate are summarized in Tables 1 and 2, respectively.

Table 8-1 Mixture design parameters and characteristics of the materials used to proportion the investigated FR-SCC mixtures.

Materials		Properties	Proportioning in the investigated FR-SCC mixtures
Water-to-binder ratio (W/B)		By mass	0.42
Volume of paste (V_P)		By volume	0.27, 0.30, and 0.33
Binder (B): [a]Ternary blended cement		[b]S.G.: 2.96	352, 392, and 431 kg/m^3
High-range water-reducer (HRWR)		[c]PCE	Optimized to achieve targeted slump flow of 680 ± 20 mm : 0.82-3.30 L/100 kg of binder
Air-entraining admixture (AEA)		Liquid	Optimized to achieve targeted air content of 5% - 8% : 5-10 ml/100 kg of binder
Fine aggregate: Natural river sand	0 – 5 mm	[b]S.G.: 2.67	Volumetric sand-to-total aggregate ratio = 0.55
Coarse aggregate: Crushed limestone	CA1 (5 – 10 mm)	[b]S.G.: 2.72	▪ Three coarse-aggregate combinations (vol. %): • PSD1: 100% CA1 • PSD2: 80% CA2 + 20% CA1
	CA2 (5 – 14 mm)	[b]S.G.: 2.73	• PSD3: 60% CA1 + 40% CA2
Hook-ended macro steel fibers		[d]L$_f$: 30 mm [e]D$_f$: 0.55 mm [f]E$_f$: 200 GPa	[g]V$_f$: 0.12%-0.50%
Fiber-Coarse aggregate combinations (F-A)		By volume	▪ 0.4%-0.9% V_f mixed with PSD1-3. Three F-A mixtures F-A1-3 corresponding to minimum, medium, and maximum [h]φ_{max} were selected for proportioning of the FR-SCC mixtures, as follows: • F-A1: 0.9% fiber + 99.1% PSD1 (φ_{max} : 0.536) • F-A2: 0.7% fiber + 99.3% PSD2 (φ_{max} : 0.544) • F-A3: 0.4% fiber + 99.6% PSD3 (φ_{max} : 0.554) ▪ F-A4 mixture, corresponding to [g]V_f of 0.50% was considered, as follows: • F-A4: 1.77% fiber + 98.23% PSD3 (φ_{max} : 0.534)
FR-SCC mixtures		10 mixtures	▪ 9 mixtures FRC-1-9 were proportioned with F-A1-3 and V_P of 0.27, 0.30, and 0.33 ([h]φ/φ_{max} : 0.503 - 0.571) ▪ One additional FRC-10 mixture was proportioned with F-A4 and V_P of 0.33 ([h]φ/φ_{max} : 0.523)
Air content (%)		By volume	6.1 – 7.9
Slump flow (mm)		Initial	662 – 700
Compressive strength (MPa)		28 days of moist curing	30.2 – 49.4

[a]Ternary blended cement : 70% general use Portland cement, 25% class F fly ash, and 5% silica fume
[b]S.G.: Specific gravity
[c]PCE: Polycarboxylate ether
[d]L$_f$: Fiber length
[e]D$_f$: Fiber diameter
[f]E$_f$: Modulus of elasticity of fibers
[g]V$_f$: Volume of fibers in 1m^3 of concrete
[h]φ_{max} : Packing density of F-A combinations, obtained using the dry method [40-42]
[h]φ/φ_{max} : Volumetric content-to-packing density ratio of F-A combinations in 1m^3 of concrete

Table 8-2 Particle-size distribution of the aggregates (cumulative passing percentages).

Sieve size (mm)	0.080	0.160	0.315	0.630	1.25	2.5	5	10	14	20
Sand	2.9	6.6	23.7	49.5	67.3	83.6	99.4	100	100	100
CA1	-	-	-	-	3.9	4.9	10.2	81.7	100	100
CA2	-	-	-	-	1.2	1.5	5.7	48.9	85.5	100

The passing ability and dynamic stability of the investigated mixtures were evaluated using the L-Box set-up equipped with two 10-mm rebars [5], and T-Box [43] set-up, respectively. The blocking indices (BI) of the investigated mixtures were evaluated by the ratio of difference of relative-solid packing-fraction (φ/φ_{max}) of fiber-coarse aggregate (F-A) mixtures (> 5 mm) sampled behind the rebars and at the end of the L-Box channel-to-those of the reference mixtures. On the other hand, dynamic segregation indices (DSI) of the investigated mixtures were evaluated by the ratio of difference of the φ/φ_{max} of F-A mixtures determined on samples taken from the tilt-down and tilt-up zones of the T-Box set-up-to-those of the reference mixtures. As shown in Table 3, the BI and DSI indices of the 10 investigated mixtures ranged from 9.8% to 79.7% and 0.4% to 71.4%, respectively. Subsequently, in total, six mixtures exhibiting high passing ability (BI < 25%) and medium to high dynamic stability (DSI < 50%) were selected to be tested under confined and restricted flow conditions. These include FRC-3, FRC-4, FRC-5, FRC-6, FRC-7, and FRC-10 mixtures.

Table 8-3 Blocking and dynamic segregation indices of the investigated FR-SCC mixtures.

Mix	FRC-1	FRC-2	FRC-3	FRC-4	FRC-5	FRC-6	FRC-7	FRC-8	FRC-9	FRC-10
BI (%)	79.7	47.3	11.9	19.5	14.3	18.1	14.6	16.7	9.8	11.4
DSI (%)	0.4	17.7	12.2	20.4	18.4	40.3	49.6	71.4	54.8	40.6

The rheological properties of the mortar (sand < 5 mm) of the selected mixtures were evaluated using the diphasic approaches proposed by Hosseinpoor et al. [44,45]. First, the rheological properties of the cement paste mixtures were measured using a parallel-plates system of 50-mm diameter and 4-mm gap. The mortar was pre-sheared for 120 s at a shear rate of 150 s^{-1} followed by descending shear rate to 1 s^{-1} in six 25-s steps. The rheological properties of the fine mortar, containing sand particles finer than 1.25 mm (FS < 1.25 mm) and cement paste were estimated using the diphasic approach [44] as functions of volumetric content and packing density of FS in unit volume of fine mortars and rheological properties of their corresponding cement paste mixtures. Subsequently, the yield stress (τ_0) and plastic viscosity (μ_p) of the mortar mixtures (0-5 mm) of the selected FR-SCC mixtures were finally evaluated as function of the yield stress and plastic viscosity of their corresponding fine mortar mixtures, as well as the volumetric content and packing density of sand particles larger than 1.25 mm, using the diphasic method proposed by Hosseinpoor et al. [45]. The rheological properties of the mortar mixtures of the selected FR-SCC mixtures are summarized in Table 4.

Table 8-4 Rheological properties of the investigated mortar mixtures (< 5 mm).

Mortar	M3	M4	M5	M6	M7	M10
Corresponding FR-SCC mixture	FRC-3	FRC-4	FRC-5	FRC-6	FRC-7	FRC-10
τ_0 (Pa)	13.49	6.58	7.05	7.96	4.61	5.78
μ_p (Pa.s)	3.07	3.55	3.54	3.55	3.24	3.39

8.2.2 Proposed set-up to evaluate FOD of FR-SCC for repair applications

A Square-Box test set-up is proposed to simulate the confined and restricted flow conditions such those encountered in repair applications. As shown in Fig. 1, the set-up consisted in a

closed-circuit of four closed-surface channels of 0.7-m length, 0.2-m height, and 0.1-m width. The set-up is equipped with four rows of 10-mm diameter reinforcing-bar frames located at the middle of each channel, as well as a 10-mm diameter longitudinal rebar across the whole set-up length (Fig. 1a). The reinforcing-bar frames consisted in one 0.1-m horizontal bar and one 0.2-m vertical steel rebars of 10-mm diameter (Fig. 1a). The test was also carried out without the presence of rebars (Fig. 1b). A 48-L concrete sample was cast into the channels from one corner over 18 s without any vibration (Figs. 1a and 1b). The hardened concrete was demoulded after 24 h and cut perpendicularly to the flow direction at the middle of the first and third channels wherein concrete flowed, identified as sections #1 and #2 in Figs. 1a and 1b. The FODs at the cut sections corresponding to the reinforced (Fig. 1c) and non-reinforced (Fig. 1d) tests were then compared to evaluate the effect of reinforcing bars on FOD.
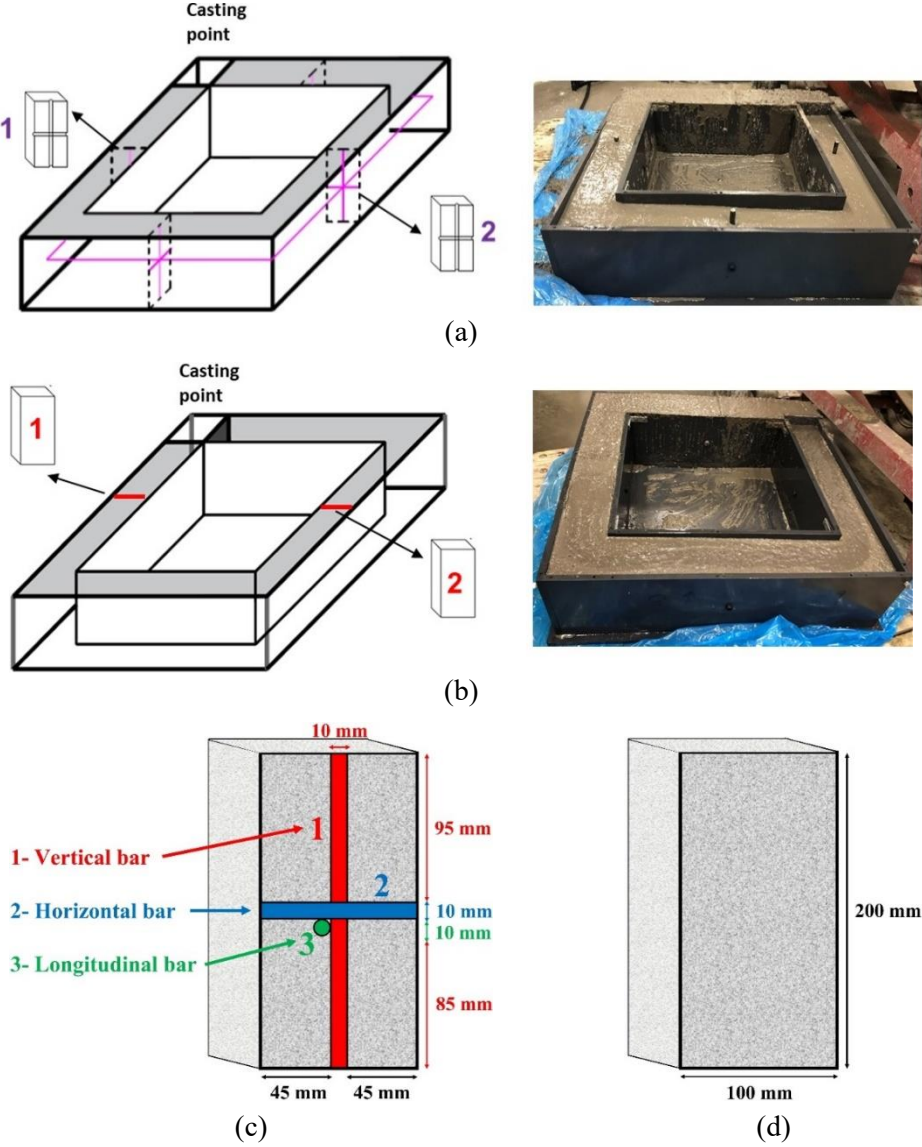

(a)

(b)

(c)   (d)

Figure 8-1 Square-Box set-up, (a) in presence and (b) without reinforcing bars, cut sections of (c) reinforced and (d) non-reinforced set-ups.

8.2.3   Image analysis of the cut sections

As shown in Fig. 2a, the coarse aggregate appeared in the cut sections were painted using a black ink to enhance the contrast between the fibers and the concrete matrix, and then pictured using a 12-MP camera. As shown in Fig. 2b, the picture was then converted to a binary format

where the white and black pixels represent the cut fibers and concrete matrix, respectively. ImageJ software and Shape Filter plugin [46] were used to determine the number, vertical and horizontal positions, circular or elliptic form, dimensions, and orientation angle of cut fibers in each cut-cross section.
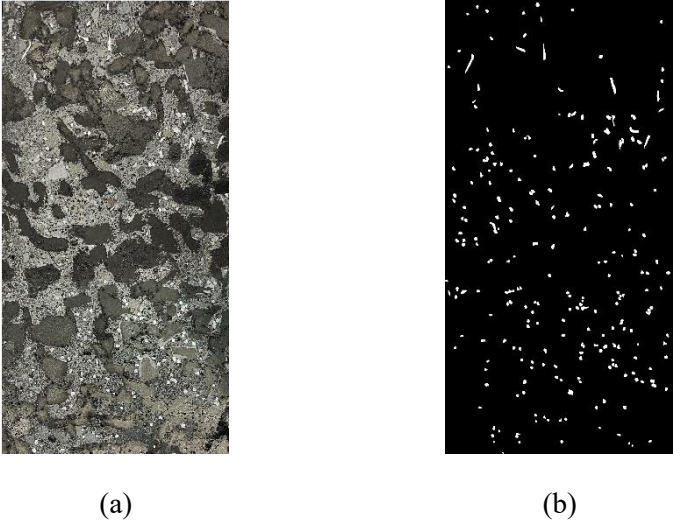

(a)   (b)

Figure 8-2 An example of (a) cut-cross section image and (b) its corresponding converted binary format.

8.2.4   Horizontal and vertical distribution of fibers

As shown in Fig. 3, the 100×200 mm binary images of each cross section were divided into seven horizontal and seven vertical units, according to the placement of the horizontal, vertical, and longitudinal rebars. The total number and shape characteristics of cut fibers were identified in whole cut sections and each unit. The horizontal and vertical distributions of fibers in each cut-cross section were evaluated by their distances to the left and bottom sides of the formwork, respectively.
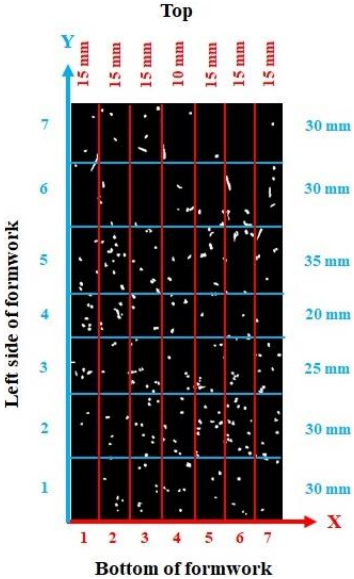

Figure 8-3 Horizontal and vertical units of a cut-cross section.

8.2.5 In-plane and out-of-plane orientations of fibers

As illustrated in Fig. 4a, assuming that the fiber is a rigid and uniform slender cylinder, the 3D orientation of a single fiber in a cut-cross section plane (XY) can be represented by the unit vector "P" directed toward the fiber axis. As can be observed in Fig. 4a, the fiber made an in-plane orientation angle of Φ with the X axis and an out-of-plane angle of θ with the cut cross section plane XY. The orientation of fibers was then evaluated by characterizing the elliptical form of their cut cross section (Fig. 4b).
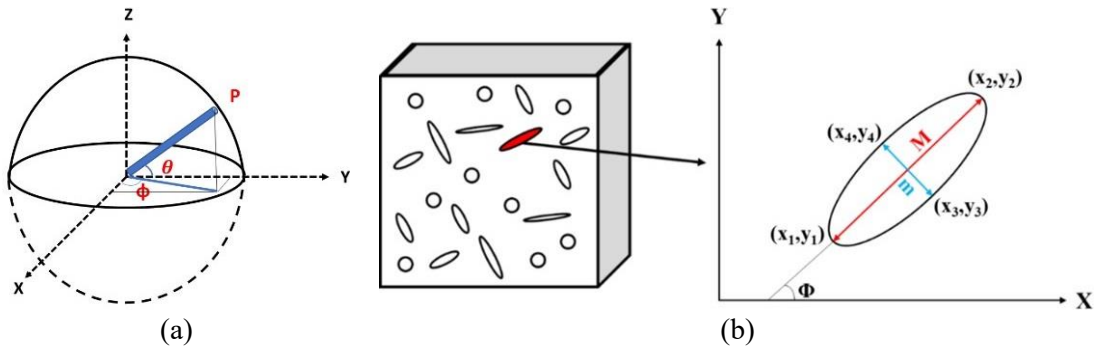

Figure 8-4 (a) Representation of the fiber alignment in cut-cross section plane XY [47,48] and (b) schematic illustration of the form characteristics of a cut fiber.

The coordinates of the four ends of the elliptical cut fiber, corresponding to its major (M) and minor (m) axes, were then determined. The (x_1,y_1) and (x_2,y_2) represent the major axis (M). On the other hand, the minor axis (m) was represented by (x_3,y_3) and (x_4,y_4) coordinates. The major and minor lengths of the cut fiber section were calculated, as follows:

$$M = \sqrt{(x_2 - x_1)^2 + \left(y_2 - y_1\right)^2} \qquad \text{Equation 8-1}$$

$$m = \sqrt{(x_4 - x_3)^2 + \left(y_4 - y_3\right)^2} \qquad \text{Equation 8-2}$$

The in-plane (Φ) and out-of-plane (θ) orientation angles were then calculated, as follows:

$$0° \leq \Phi \leq 90° = \min\left[\cos^{-1}\left(\frac{x_2 - x_1}{M}\right), 180 - \cos^{-1}\left(\frac{x_2 - x_1}{M}\right)\right] \qquad \text{Equation 8-3}$$

$$0° \leq \theta \leq 90° = 90 - \cos^{-1}\left(\frac{m}{M}\right) \qquad \text{Equation 8-4}$$

It is worth mentioning that according to Eq. (3), the in-plane orientation angle Φ refers to the angle between the major axis of the cut fiber and bottom of the mold (Fig. 4b). Therefore, the extreme Φ values of 0° and 90° correspond to the cut fibers oriented parallel and perpendicular to the bottom side of the formwork, respectively. On the other hand, according to Eq. (4), the extreme out-of-plane angles θ of 0° and 90° correspond to the cut fibers oriented fully parallel and perpendicular to the cross-section plane (XY in Fig. 4a), respectively. Statistical analyses were then conducted to evaluate the FOD through the concrete cut cross-section samples (#1 and #2 in Fig. 1).

8.3 Results and discussions

The FOD of the investigated mixtures cast through the Square-Box set-up was evaluated at different flow distances using the carried-out image analyses. New empirical indices were proposed to evaluate the effect of flow distance, formwork walls, and reinforcing bars on FOD in different horizontal and vertical units (Fig. 3). The proposed indices were then correlated to the coupled contributions of rheological properties of mortar matrix (τ_0 and μ_p in Table 4), relative-solid packing-fraction (φ/φ_{max}) of fiber-coarse aggregate combination, and volume of fibers (V_f).

8.3.1   Distribution of fibers

Effect of flow distance

The total number of fibers in cut sections #1 and #2 at different flow distances of the non-reinforced set-up (Fig. 1b) is presented in Fig. 5. As can be observed, lower number of fibers was observed in section #2 corresponding to longer flow distance compared to that obtained in section #1 which is closer to the casting point. This can reflect the shear- and gravity-induced segregation of fibers during flow.
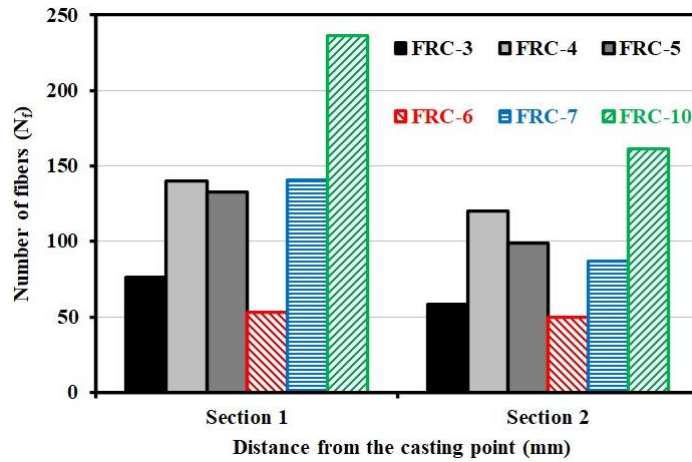

Figure 8-5 Number of fibers detected at cross sections #1 and #2 of the non-reinforced Square-Box specimens.

The dynamic segregation of fibers was then evaluated by the difference between the number of fibers detected in sections #1 and #2 ($\Delta N_f = N_{f-1} - N_{f-2}$). The ΔN_f values were then correlated to the coupled effect of the relative-solid packing fraction of fiber-coarse aggregate combination (φ/φ_{max}) and fiber content (V_f), as well as yield stress (τ_0) and plastic viscosity (μ_p) of mortar using a Microsoft Excel solver. The results of the established correlation are presented in Eq. (5) and Fig. 6, as follows:

$$\Delta N_f\ (\%) = 5.300 \times \frac{V_f^{1.433} \times \mu_p^{2.324}}{\left(\frac{\varphi}{\varphi_{max}}\right)^{8.964} \times \tau_0^{2.975}} + 12.999 \qquad \text{Equation 8-5}$$
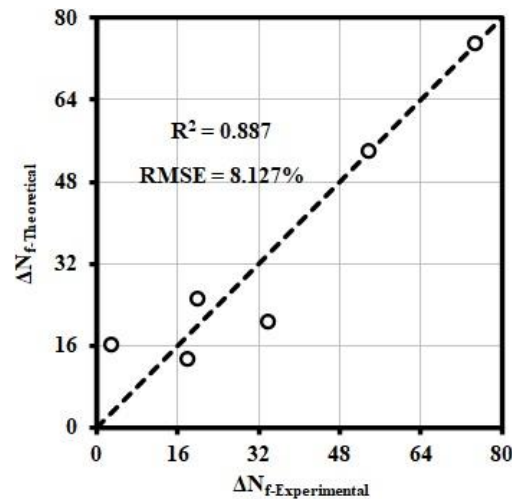
Figure 8-6 Comparison between experimental ΔN_f values and those obtained theoretically using Eq. (5).

As can be observed in Fig. 6, ΔN_f values are in good agreement with the characteristics of fiber-coarse aggregate and rheology of mortars. Increasing V_f increased the dynamic segregation of fibers, and higher fiber volume is shown to increase the interaction of fibers and creation of fiber balling. Consequently, clustered fibers gain larger masses and settle down over the flow distance. Lower amounts of fibers can then reach to longer flow distances. For a given flow velocity, increasing μ_p of the suspending mortar is expected to increase the drag forces exerted on the embedded fibers, thus pushing them to reach longer flow distances. However, according to the established correlation, higher μ_p of mortar led to higher dynamic segregation. This can be due to the fact that higher μ_p values of mortar covering fiber surfaces can lead to higher risk of the interfacial adhesion of fibers and promoting the fiber balling, hence increasing the risk of gravity-induced segregation of the steel fibers. On the other hand, higher φ/φ_{max} of fiber-coarse aggregate combination led to lower dynamic segregation of fibers due to higher lattice effect of the solid particles. This is in agreement with the results reported by Koura et al. [49] and Hosseinpoor et al. [50] on the positive effect of using a relative-solid packing fraction on dynamic stability of SCC. Moreover, according to the established correlation, higher yield stress of mortars increased the dynamic stability of fibers. Indeed, high yield stress mortar can better resist separating forces exerted on fibers and maintain their homogeneity during casting. Given the obtained power indices in Eq. (5), the φ/φ_{max} of fiber-coarse aggregate combination showed more significant effect on homogeneous distribution of fibers through the flow distance compared to the fiber volume and mortar rheology. Therefore, optimizing the volumetric content and packing density of fiber-coarse aggregate is more effective in improving the dynamic stability of FR-SCC mixtures compared to adjusting the rheological properties of mortar.

Effect of horizontal reinforcing bars

The presence of horizontal reinforcing bars (#2 in Fig. 1c) can affect the distribution of fibers in the vertical direction. The frequency of relative number of fibers detected in each vertical unit (1 to 7 in Fig. 3) to the total number of fibers was calculated for the cross-section #2 samples (Figs. 1a and 1b) of both non-reinforced (N) and reinforced (R) set-ups and is presented in Fig. 7. It is worth mentioning that the effect of bars on fiber distribution was only evaluated in cross section #2 samples (longer flow distance). This is due to the fact that the flow pattern is more developed at longer distances (section #2), and the significance of the presence of bars is less affected by any existing flow turbulence in shorter flow distance

(section #1) where flow velocity is higher. Moreover, FRC-3 and FRC-4 mixtures could not fully fill the cross section #2, therefore only the FRC-5, FRC-6, FRC-7, and FRC-10 mixtures were investigated.

The arithmetic average of the relative frequency of number of fibers (F_i) in the vertical units located on the top side of the position of the horizontal reinforcing bars (i.e., i = 4 to 7 in Fig. 3: 85-200 mm) was calculated for the cut cross sections #2 (Figs. 1a and 1b) taken from both reinforced (R) and non-reinforced (N) slabs. The effect of horizontal reinforcing bars on the vertical distribution of fibers (HB$_{FD}$) was then evaluated as the difference between the average values calculated at the reinforced and non-reinforced concrete specimens, as follows:

$$\text{HB}_{\text{FD}} (\%) = \left[\frac{\left[\sum_{i=4}^{7}(F_i \times \Delta Y_i)\right]_R}{\left(\sum_{i=1}^{7} \Delta Y_i\right)_R} - \frac{\left[\sum_{i=4}^{7}(F_i \times \Delta Y_i)\right]_N}{\left(\sum_{i=1}^{7} \Delta Y_i\right)_N} \right] \times 100\% \qquad \text{Equation 8-6}$$

where F_i and ΔY_i are the frequency of number of fibers and thickness of the vertical unit "i" (i = 1 to 7) presented in Fig. 3, respectively. As shown in Fig. 7, all the HB$_{FD}$ values are positive, which refer to higher frequency of fibers in the upper half (i = 4 to 7: 85-200 mm) of the cross-sections #2 samples of the reinforced sections compared to those of the non-reinforced sections. This reflects that the horizontal reinforcing bars limited the sedimentation of fibers toward the lower layers (i = 1 to 3: 0-85 mm), hence leading to a higher number of fibers accumulated in the upper zones of the cross section (i = 4 to 7: 85-200 mm). The bottom layers of the cut-cross sections of the non-reinforced channel contained greater number of fibers. This can indicate that gravity-induced migration of fibers toward the bottom layers in the absence of any rebar. As can be observed in Eq. (7) and Fig 8, the obtained HB$_{FD}$ values are very well correlated to the coupled effect of φ/φ_{max} of fiber-coarse aggregate combination and fiber content (V_f), as well as yield stress (τ_0) and plastic viscosity (μ_p) of mortar.

$$\text{HB}_{\text{FD}} (\%) = 0.136 \times \frac{\left(\frac{\varphi}{\varphi_{max}}\right)^{4.233} \times \mu_p^{8.017}}{V_f^{0.364} \times \tau_0^{1.653}} - 9.203 \qquad \text{Equation 8-7}$$
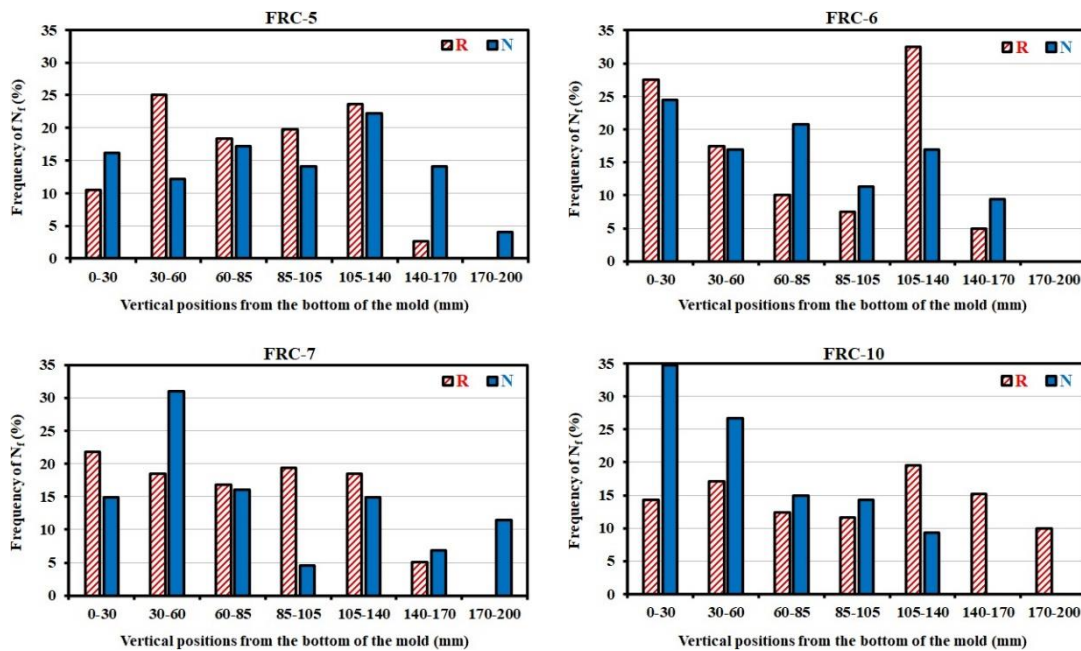

Figure 8-7 Fig. 7. Frequency of number of fibers across the vertical units of cross-section #2 samples of reinforced (R) and non-reinforced (N) Square-Box specimens.
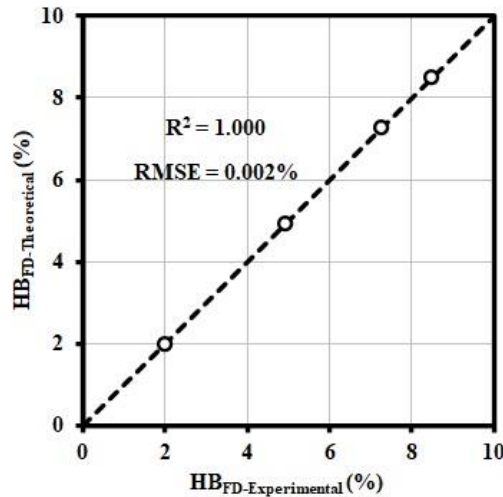
Figure 8-8 Comparison between the experimental HB_{FD} values
and those obtained theoretically using Eq. (7).

According to the established correlation, increasing the φ/φ_{max} of fiber-coarse aggregate combination led to higher risk of fiber blockage on upper layers. This is due to more interaction between fibers and coarse aggregate with horizontal rebars. Moreover, higher HB_{FD} values were obtained for lower yield stress of mortar. Indeed, low yield stress mortar cannot resist against the frictional and collision forces that rebars exert on fibers, which leads to accumulation of fibers on the upper layers. On the other hand, higher plastic viscosity of mortars covering the fibers can increase the possibility of the interfacial adhesion of fibers and increase the risk of fiber balling that can promote blocking in the upper layers of the rebars (i.e., higher HB_{FD} values). Increasing the fiber volume was expected to increase the fiber blockage. However, according to the adjustment factor obtained for fiber volume, lower fiber blockage resulted by higher fiber volume. As reported by Nouri et al. [42], the variation in fiber volume (V_f) can significantly affect the packing density (φ_{max}) of the fiber-coarse aggregate mixture, and its effect cannot be solely concluded from Eq. (7).

Effect of vertical reinforcing bars

The The presence of vertical reinforcing bars (#1 in Fig. 1c) can affect the horizontal distribution of fibers. Accordingly, the frequency of relative number of fibers in each horizontal unit (i = 1 to 7 in Fig. 3) to the total number of fibers were calculated for the cross-sections #2 samples of both non-reinforced (N) and reinforced (R) set-ups and presented in Fig. 9. As shown in Fig. 9, lower number of fibers were observed in the center of the cross section #2 (i = 4: 45-55 mm) compared to its adjacent units of i = 3 (30-45 mm) and i = 5 (55-70 mm) for both reinforced and non-reinforced set-ups. The difference between the average decrease in frequency of number of fibers (F_i) from horizontal units i = 3 to 4 and i = 5 to 4 was calculated for the reinforced (R) and non-reinforced (N) set-ups to evaluate the effect of vertical bar on horizontal fiber distribution, as follows:

$$VB_{FD}\ (\%) = \left[\frac{(F_3-F_4)+(F_5-F_4)}{2}\right]_R - \left[\frac{(F_3-F_4)+(F_5-F_4)}{2}\right]_N \qquad \text{Equation 8-8}$$

As can be observed in Eq. (9) and Fig. 10, the obtained VB_{FD} values were well correlated to the coupled effect of the φ/φ_{max} of fiber-coarse aggregate combination and volume of fibers (V_f), as well as yield stress (τ_0) and plastic viscosity (μ_p) of mortar.

$$VB_{FD} \ (\%) = 2.080 \times \frac{\left(\frac{\varphi}{\varphi_{max}}\right)^{0.320} \times \mu_p^{2.253}}{V_f^{0.345} \times \tau_0^{1.021}} - 3.374 \qquad \text{Equation 8-9}$$
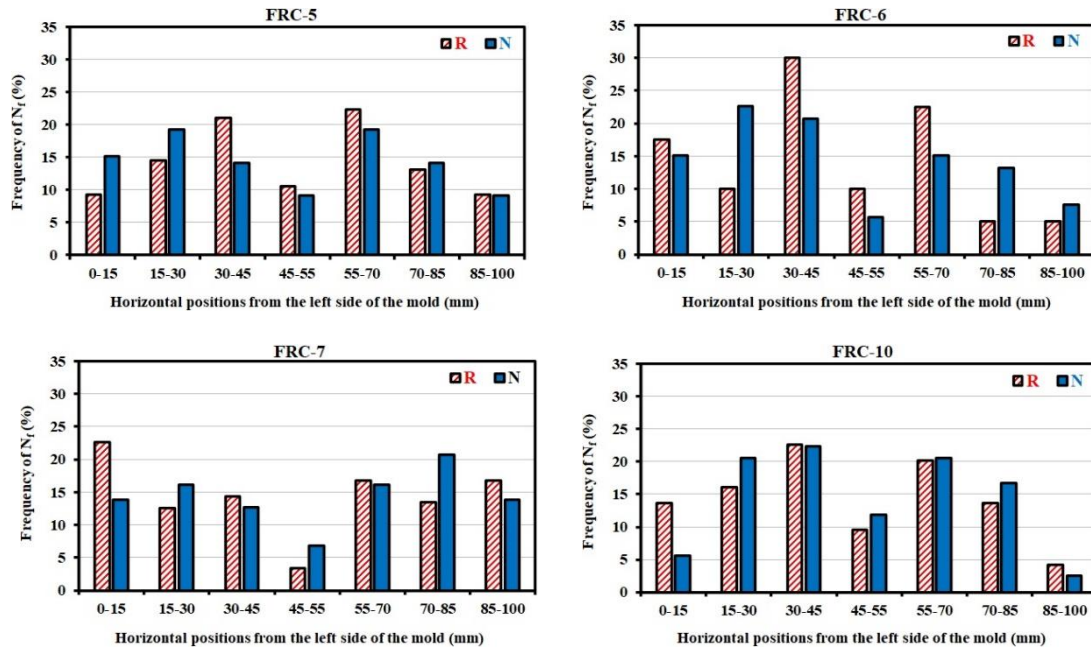

Figure 8-9 Frequency of number of fibers across horizontal units of the cross-section #2 samples of reinforced (R) and non-reinforced (N) Square-Box specimens.
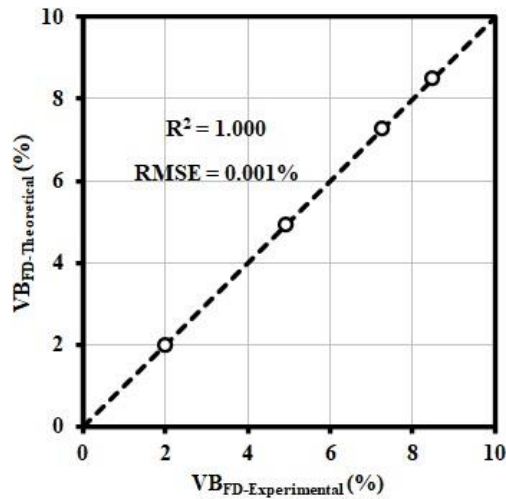
Figure 8-10 Comparison between experimental VBFD values and those obtained theoretically using Eq. (9).

According to the adjustment factors obtained in Eq. (9), the effects of characteristics of fibers, coarse aggregate, and mortar matrix on VB_{FD} indices are in agreement with those reported earlier for the horizontal bars (HB_{FD} indices in Eq. (7)). Accordingly, the vertical bars showed more negative effect on the distribution of fibers of the mixtures proportioned with higher φ/φ_{max} of fiber-coarse aggregate combination and plastic viscosity (μ_p) of mortar, as well as lower volume of fibers (V_f) and yield stress (τ_0) of mortar.

Formwork-wall effect

The effect of formwork walls on distribution of fibers across the cut-cross section samples was evaluated in the non-reinforced set-up (Fig. 1b). The frequency of number of fibers in each horizontal unit 1 to 7 (Fig. 3), relative to the total number of fibers was evaluated in cut-cross section #2 samples (Fig. 1b), as shown in Fig. 11. As can be observed in Fig. 11, lower frequency of number of fibers (Fi) was obtained in vicinity of the formwork walls, i.e., horizontal units i =1 (0-15 mm) and i = 7 (85-100 mm), compared to their adjacent units i = 2 (15-30 mm) and i = 6 (70-85 mm), respectively. Accordingly, the formwork-wall effect on fiber distribution (WEFD) of the investigated mixtures was evaluated using the mean values of decreasing of the frequency of number of fibers in the horizontal units close to the formwork walls, as follows:

$$WE_{FD} \ (\%) = \frac{(F_2 - F_1) + (F_6 - F_7)}{2}$$
<div align="right">Equation 8-10</div>

The obtained WEFD values were then correlated to the φ/φ_{max} of fiber-coarse aggregate combination and V_f, as well as $\tau 0$ and μ_p of mortar. The results of the established correlation are presented in Eq. (11) and Fig. 12, as follow:

$$WE_{FD} \ (\%) = 0.00016 \times \frac{V_f^{0.544} \times \tau_0^{1.408}}{\left(\frac{\varphi}{\varphi_{max}}\right)^{15.130} \times \mu_p^{0.061}} - 6.982$$
<div align="right">Equation 8-11</div>

As can be observed in Fig. 12, the WE$_{FD}$ values are in very good agreement with the characteristics of fiber-coarse aggregate, rheology of mortar, and volume of fiber. As reflected by the established correlation, the WE$_{FD}$ values are highly dependent on the φ/φ_{max} of fiber-coarse aggregate, reflected by highest adjustment factor (15.1) wherein increasing the φ/φ_{max} values can significantly decrease the effect of formwork walls on distribution of fibers in their vicinity. In fact, more concentrated fiber-coarse aggregate skeleton can push the fibers and coarse aggregate towards the formwork walls due to their higher lattice effect. Therefore, higher number of fibers can be placed in vicinity of formwork walls, reflected by lower WE$_{FD}$ values.

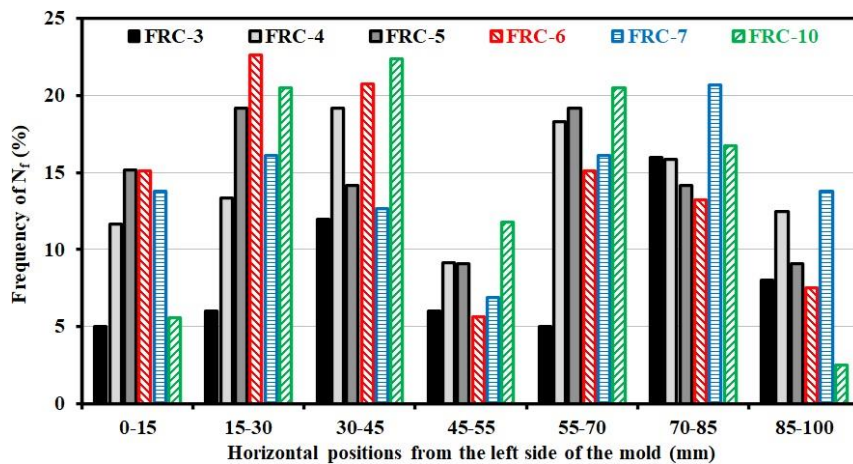Figure 8-11 The frequency of number of fibers in cross section #2 of the non-reinforced set-up at different horizontal units i = 1-7.
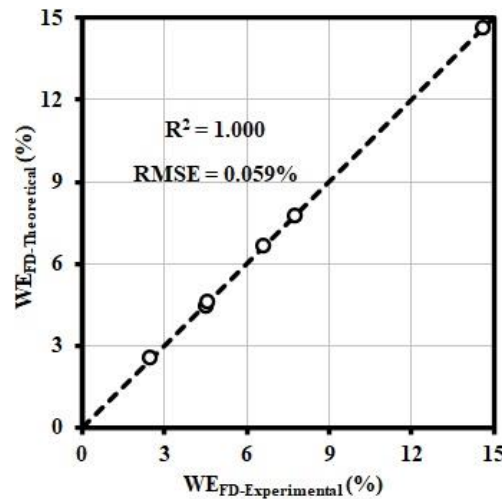
Figure 8-12 Comparison between experimental WEFD values
and those obtained theoretically using Eq. (11).

On the other hand, increasing the volume of fibers led to higher wall effect. This can be explained by the fact that higher fiber content can increase the interactions between the formwork walls, fibers, and coarse aggregate, hence pushing the coarse aggregate away and reducing the packing density of fiber-coarse aggregate in the vicinity of the formwork walls. Furthermore, the yield stress and plastic viscosity of mortar showed opposite effects on WE_{FD} values. Indeed, according to the obtained adjustment factor in the established correlation, the yield stress of mortar showed more significant effect on WE_{FD} values compared to plastic viscosity values. The increasing effect of yield stress on WE_{FD} can be explained by the fact that during flow, the lattice of solid particles cannot overcome the high yield stress values of mortar matrix. Therefore, fibers cannot be well compacted in the vicinity of formwork walls, hence leading to higher WE_{FD} values for FR-SCC mixtures with higher yield stress of their corresponding mortar matrices. On the other hand, fibers covered with mortars with higher viscosity can better stick to the formwork walls, hence reducing the WE_{FD} values.

8.3.2 Orientation of fibers

Effect of flow distance on out-of-plane orientation (θ)

The average values of out-of-plane orientation angles (θ_{avg}) of all the cut fibers detected in both cross sections #1 and #2, located at different flow distances of the non-reinforced set-up (Fig. 1b), are presented in Fig. 13. As can be observed, higher θ_{avg} values were obtained at longer flow distances (section #2). Indeed, fibers are more randomly oriented closer to the casting point due to higher turbulence and velocity of concrete flow in section #1. Subsequently, at longer flow distances, fibers tend to be reoriented following the concrete flow velocity direction which is perpendicular to the cross sections.
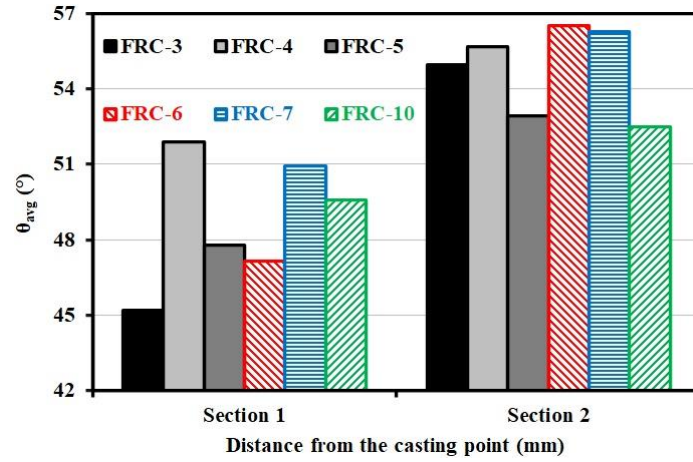
Figure 8-13 Average out-of-plane orientation angles θ_{avg} of fibers detected in different cross sections #1 and #2, located in different flow distances of the non-reinforced Square-Box specimens.

The coupled effect of the φ/φ_{max} of fiber-coarse aggregate combination and V_f, as well as τ_0 and μ_p of mortar on increasing the θ_{avg} values from section #1 to #2 ($\Delta\theta_{avg} = \theta_{avg-2} - \theta_{avg-1}$) was evaluated using a Microsoft Excel solver and is presented in Eq. (12) and Fig. 14, as follow:

$$\Delta\theta_{avg} \ (°) = 0.080 \times \frac{\tau_0^{0.175}}{\left(\frac{\varphi}{\varphi_{max}}\right)^{6.599} \times \mu_p^{1.746} \times V_f^{1.080}} + 0.938 \qquad \text{Equation 8-12}$$

As can be observed in Fig. 14, the $\Delta\theta_{avg}$ values are in good agreement with the coupled contributions of fiber-coarse aggregate characteristics and mortar rheology. Increasing the volume of fibers, φ/φ_{max} of fiber-coarse aggregate combinations, and plastic viscosity of mortar led to lower $\Delta\theta_{avg}$. This can be attributed to more limited rotation of higher volume of fibers in more compacted granular skeleton and viscous suspending matrix. Moreover, for given characteristics of fiber-coarse aggregate combination, higher plastic viscosity of mortar can result in higher viscosity of the FR-SCC mixture, hence leading to lower flow velocity. Lower reorientation of fibers can therefore be expected for lower flow velocity magnitudes. However, yield stress of mortar showed opposite effects on reorientation of fibers for longer flow distances. This can be concluded that the mortar matrices with lower plastic viscosity and high yield stress are recommended to achieve more desired orientation of fibers in elongated elements, such as beams. For example, FRC-3 with the highest τ_0 of 13.5 Pa and lowest μ_p of 3.1 Pa.s showed the highest $\Delta\theta_{avg}$ of 9.8°. On the other hand, FRC-10 with the maximum fiber volume of 0.5% exhibited the lowest $\Delta\theta_{avg}$ of 2.9°.
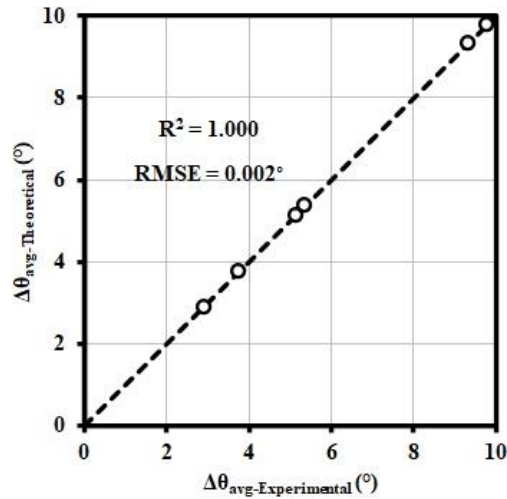
Figure 8-14 Comparison between the experimental $\Delta\theta_{avg}$ values and those obtained theoretically using Eq. (12).

Effect of horizontal bar on out-of-plane orientation of fibers (θ)

As shown in Fig. 15, the presence of horizontal reinforcing bars (#2 in Fig. 1c) can affect the orientation of fibers in vertical direction. Once the flow passes across the horizontal bars, fibers are reoriented depending on their vertical distance to the obstacle. The average of out-of-plane orientation angles (θ_{avg}) of fibers in each vertical unit (1 to 7 in Fig. 3) is presented in Fig. 16 for cross section #2 samples of both non-reinforced (N) and reinforced (R) Square-Box specimens.

.
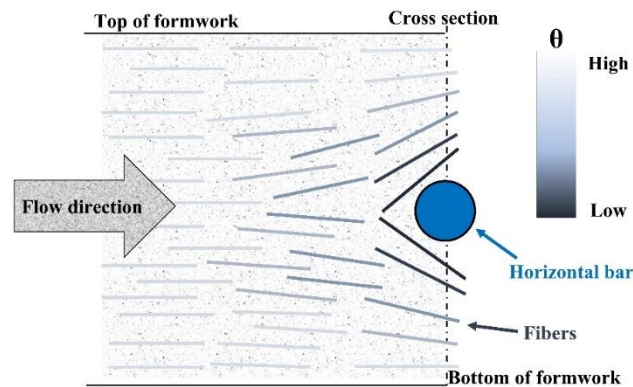
Figure 8-15 Schematic effect of horizontal bars on out-of-plane orientation (θ) of fibers.

As can be observed in Fig. 16, the θ_{avg} values decreased in the vicinity of the horizontal bars (i.e., vertical units i = 3 to 5 in Fig. 3: 60-140 mm). The effect of horizontal bar on fiber orientation (HB$_{FO}$) was evaluated by the difference between the mean θ values (θ_{avg-i}) in vicinity of the horizontal bar obtained in the non-reinforced (N) and reinforced (R) set-ups. This was calculated in the vertical units i = 3 to 5 in Fig. 3, corresponding to the zone located at 60-140-mm distances to the bottom of the formwork. The HB$_{FO}$ was evaluated, as follows:

$$HB_{FO} \ (°) = \left[\frac{\sum_{i=3}^{5}(\theta_{avg-i} \times \Delta Y_i)}{\sum_{i=3}^{5} \Delta Y_i}\right]_N - \left[\frac{\sum_{i=3}^{5}(\theta_{avg-i} \times \Delta Y_i)}{\sum_{i=3}^{5} \Delta Y_i}\right]_R \qquad \text{Equation 8-13}$$

where, ΔY_i is the thickness of vertical unit "i", as shown in Figure 8-3.

Figure 8-16 Average out-of-plane orientation of fibers (θ_{avg}) in different vertical units of cross-section #2 samples of reinforced (R) and non-reinforced (N) Square-Box specimens.

The coupled effect of the φ/φ_{max} of fiber-coarse aggregate combination, fiber volume, and rheological properties of mortar on HB_{FO} of the investigated mixtures were then evaluated using a Microsoft Excel solver and presented in Eq. 14. As can be observed in Fig. 17, the effect of horizontal bar on the out-of-plane orientation is in good agreement with characteristics of fiber-coarse aggregate and rheology of mortar.

$$HB_{FO} \ (°) = 0.352 \times \frac{\left(\frac{\varphi}{\varphi_{max}}\right)^{2.596} \times \mu_p^{2.942} \times \tau_0^{0.183}}{V_f^{0.748}} - 3.452 \qquad \text{Equation 8-14}$$

Figure 8-17 Comparison between the experimental HB_{FO} values
and those obtained theoretically using Equation 8-14.

According to the established correlation, the horizontal bar showed higher effect on the out-of-plane orientation of the FR-SCC mixtures proportioned with fiber-coarse aggregate with higher φ/φ_{max}, lower fiber volume (V_f), and mortar with higher yield stress (τ_0) and plastic viscosity (μ_P) values.

Effect of vertical bar on out-of-plane orientation of fibers (θ)

The out-of-plane orientation angle (θ) of fibers can be changed due to the presence of vertical reinforcing bars (#1 in Fig. 1c). The average of θ angles (θ_{avg}) of fibers in each horizontal unit (1 to 7 in Fig. 3) of cross section #2 samples of both non-reinforced (N) and reinforced (R) set-ups is presented in Fig. 18. As can be observed in the reinforced set-up, the θ_{avg} values decreased in the vicinity of the vertical bar (horizontal unit i = 4: 45-55 mm) compared to their adjacent horizontal units i = 3 (30-45 mm) and i = 5 (55-70 mm). The difference between the average of decreases in the θ_{avg} values from horizontal units i = 3 (30-45 mm) and i = 5 (55-70 mm) to the central horizontal unit i = 4 (45-55 mm), obtained in the reinforced (R) and non-reinforced (N) set-ups was calculated to evaluate the effect of the vertical bar on out-of-plane orientation of fibers (VB_{FO}), as follows:

$$VB_{FO} (°) = \left[\frac{(\theta_{avg-3}-\theta_{avg-4})+(\theta_{avg-5}-\theta_{avg-4})}{2}\right]_R - \left[\frac{(\theta_{avg-3}-\theta_{avg-4})+(\theta_{avg-5}-\theta_{avg-4})}{2}\right]_N \qquad \text{Equation 8-15}$$

As can be observed in Eq. (16) and Fig 19, the obtained VB_{FO} values were well correlated to the coupled effect of the φ/φ_{max} of fiber-coarse aggregate and fiber content (V_f), as well as the yield stress (τ_0) and plastic viscosity (μ_P) of mortar.

$$VB_{FO} (°) = 11.086 \times \frac{\mu_P^{6.241}}{\left(\frac{\varphi}{\varphi_{max}}\right)^{13.486} \times \tau_0^{31.248} \times V_f^{22.507}} + 6.757 \qquad \text{Equation 8-16}$$
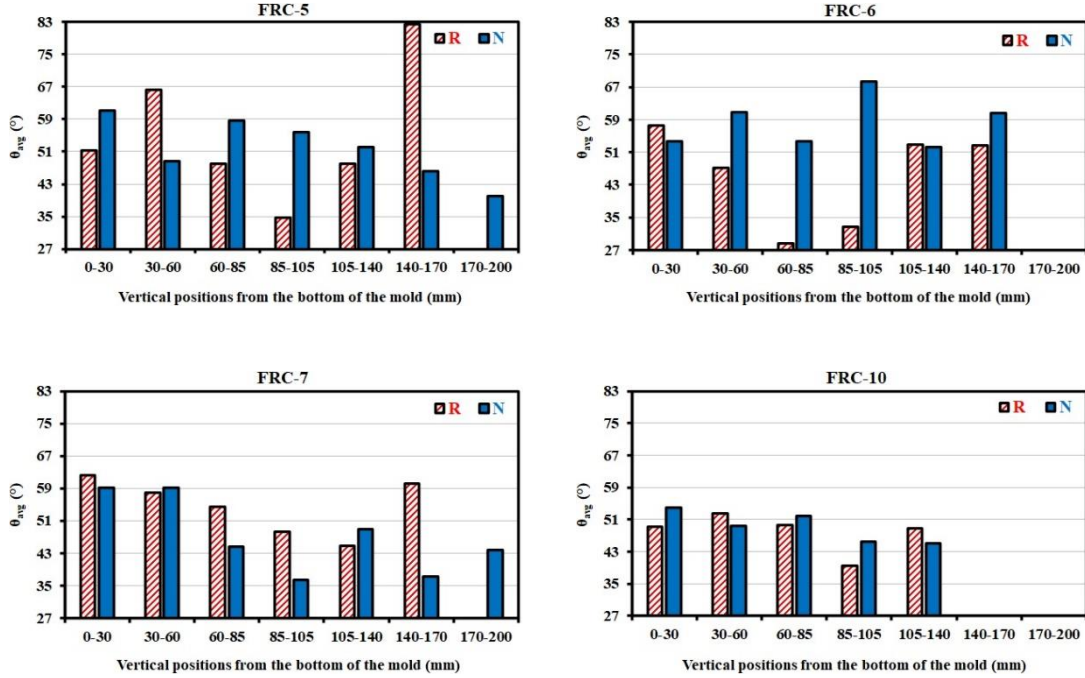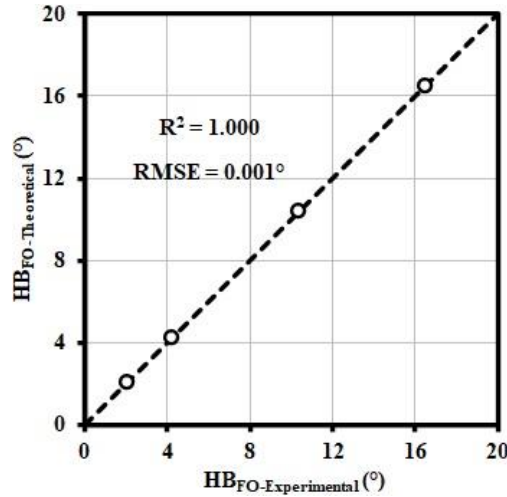
Figure 8-18 Average out-of-plane orientation of fibers (θ_{avg}) in different horizontal units of cross-section #2 samples of reinforced (R) and non-reinforced (N) Square-Box specimens.
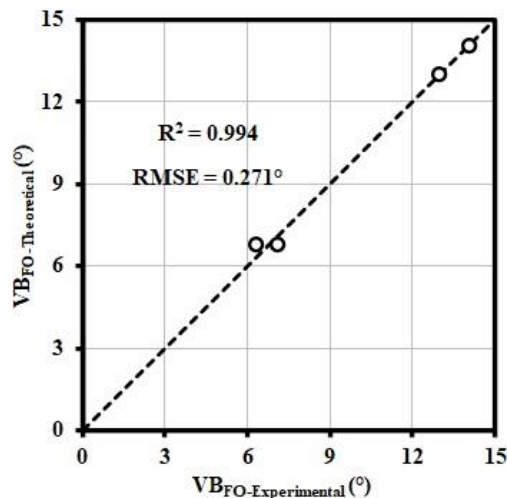
Figure 8-19 Comparison between experimental VB$_{FO}$ values and those obtained theoretically using Eq. (16).

According to the stablished correlation, the effect of vertical bar on out-of-plane orientation of fibers increases for FR-SCC mixtures containing fiber-coarse aggregate mixtures with lower φ/φ_{max}, lower volume of fibers V_f, as well as lower yield stress τ_0 and higher plastic viscosity μ_p of mortar.

Effect of longitudinal bar on in-plane orientation of fibers (Φ)

The presence of the longitudinal bar can only affect the in-plane orientation of fibers (Φ). The average of Φ angles in different vertical units 1 to 7 (Fig. 3) of the cross-section #2 samples of both non-reinforced (N) and reinforced (R) set-ups (Figs. 1a and 1b) was evaluated and presented in Fig. 20. As can be observed, the Φ angles of fibers decreased in the vicinity of the

longitudinal bar. This can be associated with the filling process of FR-SCC mixtures in the Square-Box set-up (Fig. 21). Indeed, once the concrete reaches the longer flow distance (cross section #2), first fills the bottom layers, and gradually comes up to fully fill the formwork height. In the case of non-reinforced set-up, fibers are randomly oriented in the middle vertical zones, in terms of in-plane orientation angle (Φ). However, in the case of reinforced set-up, once the concrete level reaches the middle of the section height and fibers touch the longitudinal bar, the in-plane orientation of fibers is changed mostly parallel to the formwork bottom (tangential to the longitudinal bar). Moreover, as shown in section 3.1.2, the settled down fibers in upper layers get blocked on top side of the horizontal bar which is close to the longitudinal-bar level. Therefore, the in-plane orientation angle (Φ) of fibers decreases in vicinity of the longitudinal bar (i.e., from vertical units i = 3 (65-85 mm) and i = 5 (105-140 mm) to the middle unit i = 4 (85-105 mm)). The difference in the average decreases in Φ values from the vertical units i = 3 and 5 to the middle unit i = 4, obtained in the reinforced (R) and non-reinforced (N) set-ups was calculated to evaluate the effect of longitudinal bar on in-plane orientation of fibers (LB$_{FO}$), as follows:

$$LB_{FO} \ (°) = \left[\frac{(\Phi_{avg\text{-}3}-\Phi_{avg\text{-}4})+(\Phi_{avg\text{-}5}-\Phi_{avg\text{-}4})}{2} \right]_R - \left[\frac{(\Phi_{avg\text{-}3}-\Phi_{avg\text{-}4})+(\Phi_{avg\text{-}5}-\Phi_{avg\text{-}4})}{2} \right]_N \qquad \text{Equation 8-17}$$

The coupled effect of the φ/φ_{max} of fiber-coarse aggregate combination, fiber volume, and rheological properties of mortar on LB$_{FO}$ of the investigated FR-SCC mixtures are presented in Eq. 18 and Fig. 22. According to the established correlation, increasing the φ/φ_{max} of fiber-coarse aggregate combination, as well as lower fiber volume and rheological properties of mortar led to higher influence of longitudinal bars on in-plane orientation of fibers.

$$LB_{FO} \ (°) = 0.905 \times \frac{\left(\frac{\varphi}{\varphi_{max}} \right)^{0.142}}{V_f^{2.720} \times \mu_p^{0.133} \times \tau_0^{1.019}} + 5.250 \qquad \text{Equation 8-18}$$
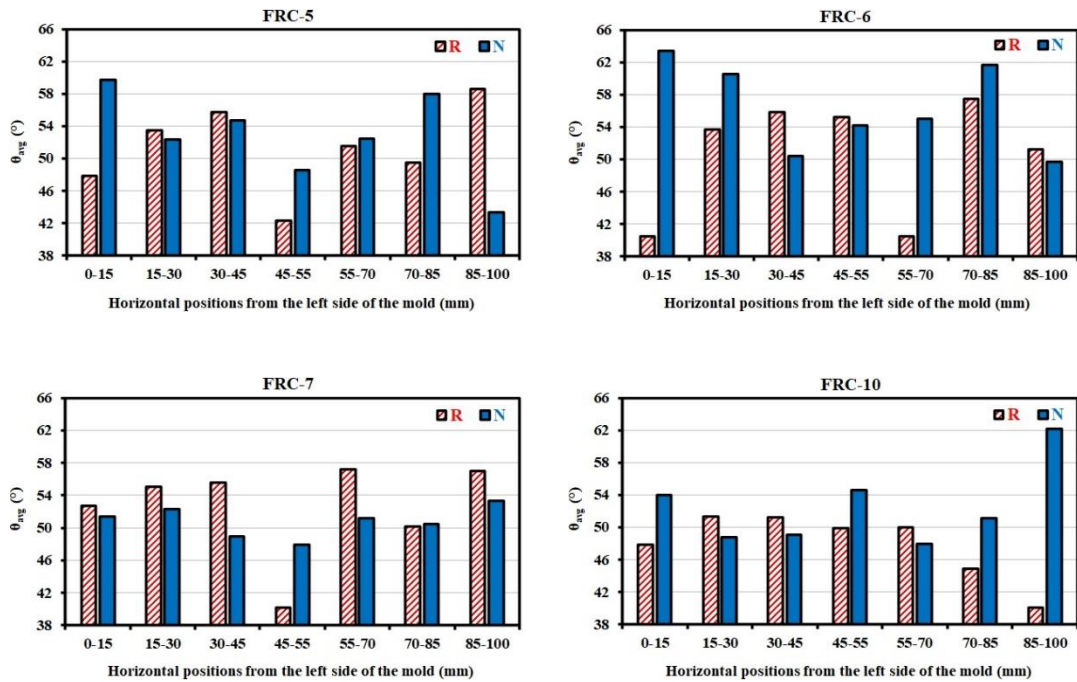

Figure 8-20 Average in-plane orientation of fibers (Φ_{avg}) in different vertical units of cross-section #2 samples of both reinforced (R) and non-reinforced (N) Square-Box specimens.
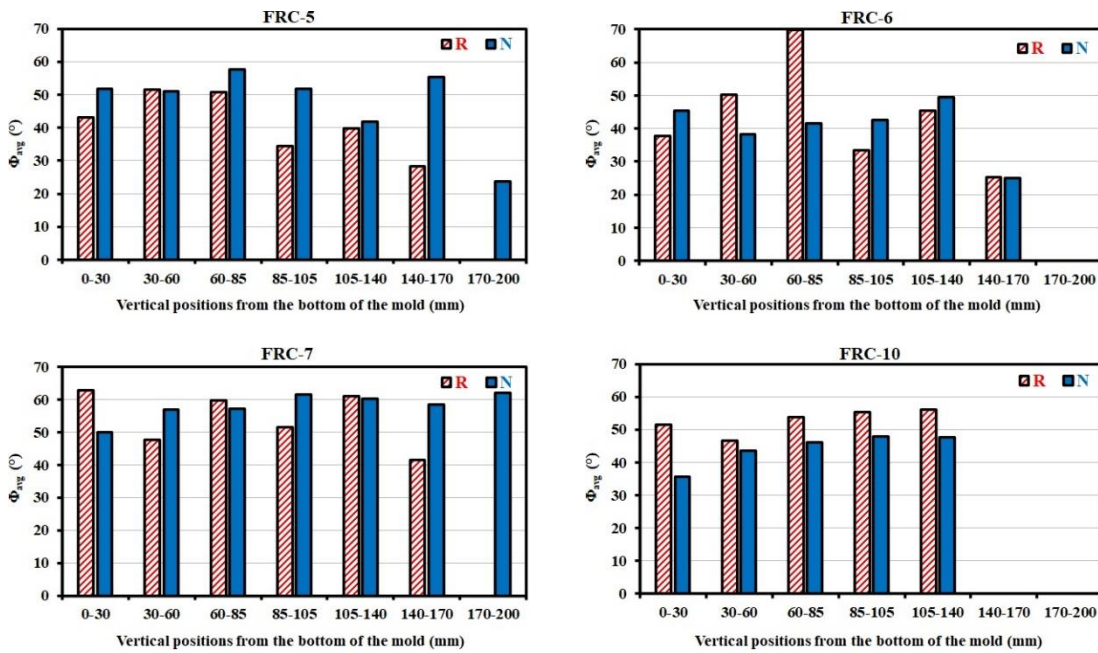
(a) Initial filling of the bottom layers | (b) Filling of the middle layers | (c) Filling of the upper layers
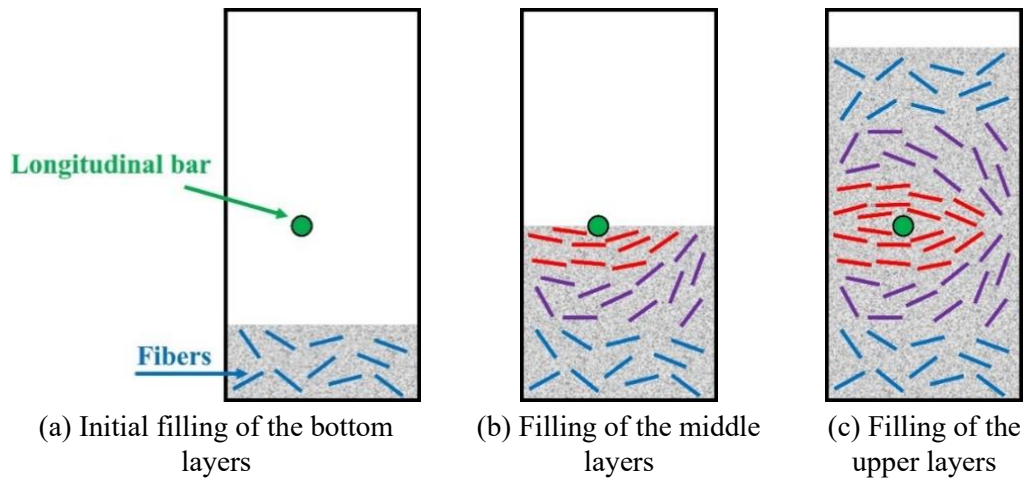
Figure 8-21 Filling process of cross section #2: Effect of longitudinal bar on in-plain orientation of fibers (Blue, purple, and red-color fibers correspond to random, medium, and low in-plane orientation angles, respectively).
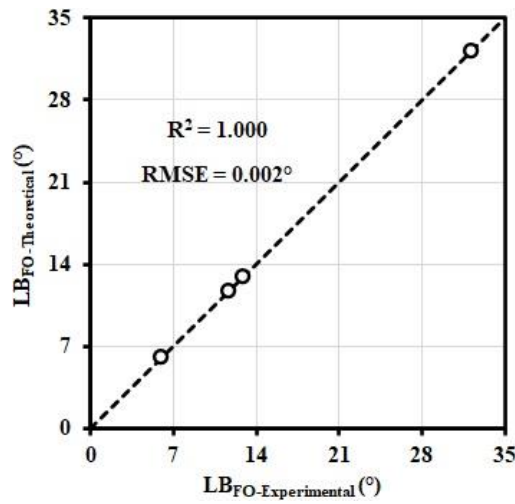
Figure 8-22 Comparison between experimental LBFO values and those obtained theoretically using Eq. (18).

Effect of formwork walls on in-plane orientation of fibers (Φ)

The effect of formwork walls on in-plane orientation of fibers was evaluated for the non-reinforced set-up. First, the average of Φ angles in each horizontal unit 1 to 7 (Fig. 3) in the cross-section #2 samples (Fig. 1b) were evaluated and shown in Fig. 23. As can be observed, the Φ values increased in the vicinity of the formwork walls (i.e., horizontal units i = 1 (0-15 mm) and i = 7 (85-100 mm), compared to their adjacent horizontal units i = 2 (15-30 mm) and i = 6 (70-85 mm), respectively. The wall effect on in-plane orientation of fibers (WE$_{FO}$) was evaluated by the average decrease in the Φ_{avg} values in the vicinity of the formwork walls from horizontal units i = 1 and 7 to the horizontal units i = 2 and 6, respectively (Eq. (19), and summarized in Table 5.

$$\mathrm{WE_{FO}}\ (°) = \frac{\left(\Phi_{avg\text{-}1} - \Phi_{avg\text{-}2}\right) + \left(\Phi_{avg\text{-}7} - \Phi_{avg\text{-}6}\right)}{2} \qquad \text{Equation 8-19}$$

Table 8-5 WE_{FO} values of the investigated FR-SCC mixtures.

Mix	FRC-3	FRC-4	FRC-5	FRC-6	FRC-7	FRC-10
WE_{FO} (°)	3.1	5.8	11.7	2.9	13.6	12.5

As presented in Fig. 23 and Table 5, due to the boundary wall-effect, in-plane orientation of fibers is changed to parallelly oriented to the vertical formwork walls or perpendicular to the bottom side of the formwork (larger Φ values). Moreover, among the investigated FR-SCC mixtures, the highest WE_{FO} values were obtained for the FRC-7 and FRC-10 mixtures proportioned with the lowest φ/φ_{max} of fiber-coarse aggregate combinations and yield stress of mortar. This can be due to larger reorientation of fibers in vicinity of the formwork walls for lower packing of fibers, coarse aggregate, and formwork walls (lower lattice effect). Furthermore, the exerted forces on fibers in vicinity of the formwork walls can easier resist against lower yield stress of mortars and change the orientation of fibers.

Figure 8-23 Average in-plane orientation of fibers (Φavg) in different horizontal units of cross-section #2 samples of non-reinforced set-up.
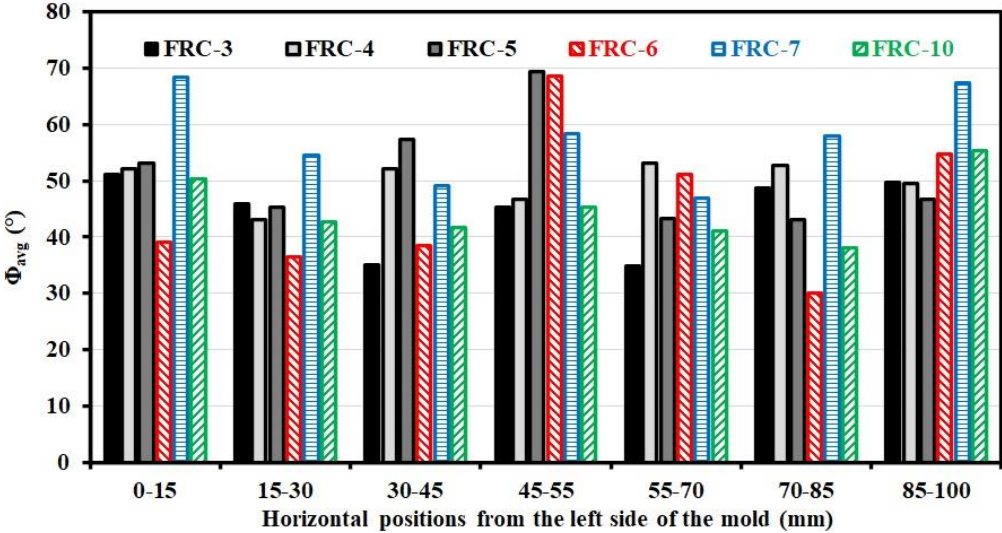
8.4 Conclusions

In this study, fiber orientation and distribution (FOD) of six FR-SCC mixtures proportioned with macro steel fibers measuring 30 mm in length were investigated using image analysis. A new Square-Box test set-up was proposed to simulate the confined and restricted flow conditions that can be used for repair applications. The Square-Box set-up allows a flow distance of 2.4 m in narrow cross sections in the presence of horizontal, vertical, and longitudinal reinforcing bars. The FOD was evaluated by determining the number of fibers at different horizontal and vertical sections, as well as the in-plane and out-of-plane orientation angles of the cut fibers in cross sections located at different flow distances. The effect of flow distance, formwork walls, and reinforcing bars on FOD of the investigated FR-SCC mixtures were evaluated using new empirical indices. The coupled effect of fibers, coarse aggregate, and mortar on FOD in the vicinity of formwork walls and in presence of different arrangement of the reinforcing bars was evaluated. According to the experimental results, the following concluding remarks can be pointed out:

- The proposed Square-Box test set-up can be used to successfully simulate the confined and restricted flow conditions of FR-SCC. Moreover, the effect of flow distance, formwork walls, and the presence of reinforcing bars on the FOD of the investigated FR-SCC mixtures were found in good agreements with the coupled contribution of the φ/φ_{max} of fiber-coarse aggregate combination (> 5 mm), volume of fibers, and rheological properties of mortar, containing sand particles finer than 5 mm.

- Greater fiber segregation was obtained at longer flow distances. The dynamic stability of fibers at longer flow distances was enhanced for higher φ/φ_{max} of fiber-coarse aggregate combination and yield stress of mortar, as well as lower volume of fibers and plastic viscosity of mortar. The φ/φ_{max} of fiber-coarse aggregate combination showed more significant effect on homogeneous distribution of fibers through the formwork length. Moreover, proper out-of-plane orientation of fibers (i.e., more perpendicular to the cross section, was obtained at longer flow distances). Decreasing the φ/φ_{max} of fiber-coarse aggregate combination, fiber volume, and plastic viscosity of mortar, as well as higher yield stress of mortar led to more desired out-of-plane orientation of fibers across the cut-cross sections.

- Higher number of fibers were obtained in the upper layers of the horizontal bars. The effect of horizontal bars on vertical distribution of fibers increased for higher φ/φ_{max} of fiber-coarse aggregate combination and plastic viscosity of mortars and decreased for higher volume of fibers and yield stress of mortar. Moreover, lower out-of-plane orientation angles were obtained in the vicinity of the horizontal bars. The negative effect of horizontal bars on out-of-plane orientation of fibers increased for higher φ/φ_{max} of fiber-coarse aggregate combination and rheological properties of mortars, as well as lower volume of fibers.

- Lower number of fibers were obtained in the vicinity of vertical bars. Increasing the φ/φ_{max} of fiber-coarse aggregate and plastic viscosity of mortar and reducing fiber volume and yield stress of the suspending mortar led to greater impact of vertical bars on fiber distribution. Moreover, the out-of-plane orientation angles of fibers decreased in the vicinity of the vertical bars. The vertical bars showed more negative effect on out-of-plane orientation of fibers of mixtures proportioned with higher plastic viscosity of mortar and lower φ/φ_{max} of fiber-coarse aggregate combination, volume of fibers, and yield stress of mortar.

- Lower in-plane orientation angles were obtained for fibers placed in the vicinity of longitudinal bar (i.e., oriented more parallel to the bottom of the formwork). The effect of longitudinal bar on in-plane orientation of fibers increased for higher φ/φ_{max} of fiber-coarse aggregate combination and lower volume of fibers and rheological properties of mortar.

- Lower number of fibers were obtained in the vicinity of the formwork walls. The formwork walls showed more significant effect on fiber distribution of the FR-SCC mixtures proportioned with higher volume of fibers and yield stress of mortars, as well as lower φ/φ_{max} of fiber-coarse aggregate combination and plastic viscosity of mortar. Moreover, higher in-plane orientation angles were obtained for the fibers located in the vicinity of the formwork walls. The formwork walls showed more significant effect on in-plane orientation of fibers of FR-SCC mixtures proportioned with the lowest φ/φ_{max} of fiber-coarse aggregate combinations and yield stress of mortar.

Acknowledgment

References

[1] R.A. Raju, S. Lim, M. Akiyama, T. Kageyama, Effects of concrete flow on the distribution and orientation of fibers and flexural behavior of steel fiber-reinforced self-compacting concrete beams, Construction and Building Materials, 262 (2020) 119963, https://doi.org/10.1016/j.conbuildmat.2020.119963.

[2] D.Y. Yoo, N. Banthia, S.T. Kang, Y.S. Yoon, Effect of fiber orientation on the rate-dependent flexural behavior of ultra-high-performance fiber-reinforced concrete, Composite Structures, 157 (2016) 62-70, https://doi.org/10.1016/j.compstruct.2016.08.023.

[3] N. Banthia, R. Gupta, Influence of polypropylene fiber geometry on plastic shrinkage cracking in concrete, Cement and Concrete Research, 36 (7) (2006) 1263-1267, https://doi.org/10.1016/j.cemconres.2006.01.010.

[4] L. Ferrara, N. Ozyurt, M. di Prisco, High mechanical performance of fibre reinforced cementitious composites: the role of "casting-flow induced" fibre orientation, Materials and Structures, 44 (2011) 109-128, https://doi.org/10.1617/s11527-010-9613-9.

[5] K.H. Khayat, F. Kassimi, P. Ghoddousi, Mixture design and testing of fiber-reinforced self-consolidating concrete, ACI Materials Journal, 111 (2) (2014) 143-152, https://doi.org/10.14359/51686722.

[6] I. Mehdipour, N.A. Libre, Linking fiber factor to material performance of fiber-reinforced self-consolidating cement-based materials, ACI Materials Journal, 114 (1) (2017) 77-91, https://doi.org/10.14359/51689483.

[7] K.H. Khayat, Y. Roussel, Testing and performance of fiber-reinforced, self-consolidating concrete, Materials and Structures, 33 (2000) 391-397, https://doi.org/10.1007/BF02479648.

[8] O. Gencel, W. Brostow, T. Datashvili, M. Thedford, Workability and mechanical performance of steel fiber-reinforced self-compacting concrete with fly ash, Composite Interfaces, 18 (2) (2011) 169-184, https://doi.org/10.1163/092764411X567567.

[9] E.V. Sarmiento, Flowable fibre-reinforced concrete for structural applications: A modelling approach that can take anisostropic and inhomogeneous fibre configuration into account, Ph.D. Thesis, Norwegian University of Science and Technology (2015), http://hdl.handle.net/11250/2373312.

[10] P. Stähli, R. Custer, J.G.K. van Mier, On flow properties, fibre distribution, fibre orientation and flexural behaviour of FRC, Materials and Structures, 41 (2008) 189-196, https://doi.org/10.1617/s11527-007-9229-x.

[11] L. Ferrara, P. Bamonte, A. Caverzan, A. Musa, I. Sanal, A comprehensive methodology to test the performance of Steel Fibre Reinforced Self-Compacting Concrete (SFR-SCC), Construction and Building Materials, 37 (2012) 406-424, https://doi.org/10.1016/j.conbuildmat.2012.07.057.

[12] L. Martinie, N. Roussel, Simple tools for fiber orientation prediction in industrial practice, Cement and Concrete Research, 41 (10) (2011) 993-1000, https://doi.org/10.1016/j.cemconres.2011.05.008.

[13] M.C. Torrijos, B.E. Barragán, R.L. Zerbino, Placing conditions, mesostructural characteristics and post-cracking response of fibre reinforced self-compacting concretes, Construction and Building Materials, 24 (6) (2010) 1078-1085, https://doi.org/10.1016/j.conbuildmat.2009.11.008.

[14] M.G. Alberti, A. Enfedaque, J.C. Gálvez, A. Ferreras, Pull-out behavior and interface critical parameters of polyolefin fibres embedded in mortar and self-compacting concrete matrixes, Construction and Building Materials, 112 (2016) 607-622, https://doi.org/10.1016/j.conbuildmat.2016.02.128.

[15] R. Zerbino, J.M. Tobes, M.E. Bossio, G. Giaccio, On the orientation of fibres in structural members fabricated with self-compacting fibre reinforced concrete, Cement and Concrete Composites, 34 (2) (2012) 191-200, https://doi.org/10.1016/j.cemconcomp.2011.09.005.

[16] R.N. Swamy, Fibre reinforcement of cement and concrete, Materials and Structures, 8 (1975) 235-254, https://doi.org/10.1007/BF02475172.

[17] N. Ozyurt, T.O. Mason, S.P. Shah, Non-destructive monitoring of fiber orientation using AC-IS: An industrial-scale application, Cement and Concrete Research, 36 (9) (2006) 1653-1660, https://doi.org/10.1016/j.cemconres.2006.05.026.

[18] H. Salehian, J.A.O. Barros, Assessment of the performance of steel fibre reinforced self-compacting concrete in elevated slabs, Cement and Concrete Composites, 55 (2015) 268-280, https://doi.org/10.1016/j.cemconcomp.2014.09.016.

[19] J. Kim, D.J. Kim, G. Zi, Improvement of the biaxial flexure test method for concrete, Cement and Concrete Composites, 37 (2013) 154-160, https://doi.org/10.1016/j.cemconcomp.2012.11.001.

[20] B.Y. Lee, J.-K. Kim, J.-S. Kim, Y.Y. Kim, Quantitative evaluation technique of Polyvinyl Alcohol (PVA) fiber dispersion in engineered cementitious composites, Cement and Concrete Composites, 31 (6) (2009) 408-417, https://doi.org/10.1016/j.cemconcomp.2009.04.002.

[21] M. Tausif, B. Duffy, S. Grishanov, H. Carr, S.J. Russell, Three-dimensional fiber segment orientation distribution using X-ray microtomography, Microscopy and Microanalysis, 20 (4) (2014) 1294-1303, https://doi.org/10.1017/S1431927614000695.

[22] J. Kobaka, J. Katzer, T. Ponikiewski, A combined electromagnetic induction and radar-based test for quality control of steel fibre reinforced concrete, Materials, 12 (21) (2019) 3507, https://doi.org/10.3390/ma12213507.

[23] A. Foudazi, I. Mehdipour, K.M. Donnell, K.H. Khayat, Evaluation of steel fiber distribution in cement-based mortars using active microwave thermography, Materials and Structures, 49 (2016) 5051-5065, https://doi.org/10.1617/s11527-016-0843-3.

[24] J.F. Lataste, M. Behloul, D. Breysse, Characterisation of fibres distribution in a steel fibre reinforced concrete with electrical resistivity measurements, Ndt & E International, 41 (8) (2008) 638-647, https://doi.org/10.1016/j.ndteint.2008.03.008.

[25] J.M. Torrents, A. Blanco, P. Pujadas, A. Aguado, P. Juan-García, M.Á. Sánchez-Moragues, Inductive method for assessing the amount and orientation of steel fibers in concrete, Materials and Structures, 45 (2012) 1577-1592, https://doi.org/10.1617/s11527-012-9858-6.

[26] I. Mehdipour, M. Horst, R. Zoughi, K.H. Khayat, Use of near-field microwave reflectometry to evaluate steel fiber distribution in cement-based mortars, Journal of Materials in Civil Engineering, 29 (7) (2017) 04017029, https://doi.org/10.1061/(ASCE)MT.1943-5533.0001850.

[27] J. Spangenberg, N. Roussel, J.H. Hattel, H. Stang, J. Skocek, M.R. Geiker, Flow induced particle migration in fresh concrete: Theoretical frame, numerical simulations and experimental results on model fluids, Cement and Concrete Research, 42 (4) (2012) 633-641, https://doi.org/10.1016/j.cemconres.2012.01.007.

[28] E. Jasiūnienė, V. Cicėnas, P. Grigaliūnas, Ž. Rudžionis, A.A. Navickas, Influence of the rheological properties on the steel fibre distribution and orientation in self-compacting concrete, Materials and Structures, 51 (2018) 103, https://doi.org/10.1617/s11527-018-1231-y.

[29] X. Ning, Y. Ding, F. Zhang, Y. Zhang, Experimental study and prediction model for flexural behavior of reinforced SCC beam containing steel fibers, Construction and Building Materials, 93 (2015) 644-653, https://doi.org/10.1016/j.conbuildmat.2015.06.024.

[30] Y. Ding, Z. You, S. Jalali, The composite effect of steel fibres and stirrups on the shear behaviour of beams using self-consolidating concrete, Engineering Structures, 33 (1) (2011) 107-117, https://doi.org/10.1016/j.engstruct.2010.09.023.

[31] G. Žirgulis, O. Švec, M.R. Geiker, A. Cwirzen, T. Kanstad, Influence of reinforcing bar layout on fibre orientation and distribution in slabs cast from fibre-reinforced self-compacting concrete (FRSCC), Structural Concrete, 17 (2) (2016) 245-256, https://doi.org/10.1002/suco.201500064.

[32] F. Kassimi, A.K. El-Sayed, K.H. Khayat, Performance of fiber-reinforced self-consolidating concrete for repair of reinforced concrete beams, ACI Structural Journal, 111 (6) (2014) 1277-1286, https://doi.org/10.14359/51687031.

[33] M. Arezoumandi, C. Wirkman, J.S. Volz, Performance of fiber-reinforced self-consolidating concrete for repair of bridge substructures, Structures, 15 (2018) 320-328, https://doi.org/10.1016/j.istruc.2018.07.015.

[34] C.A. Issa, J.J. Assaad, Stability and bond properties of polymer-modified self-consolidating concrete for repair applications, Materials and Structures, 50 (1) (2017) 28, https://doi.org/10.1617/s11527-016-0921-6.

[35] G. Martinola, A. Meda, G.A. Plizzari, Z. Rinaldi, Strengthening and repair of RC beams with fiber reinforced concrete, Cement and Concrete Composites, 32 (9) (2010) 731-739, https://doi.org/10.1016/j.cemconcomp.2010.07.001.

[36] M.C. Torrijos, B. Barragán, R. Zerbino, Placing conditions, mesostructural characteristics and post-cracking response of fibre reinforced self-compacting concretes, Construction and Building Materials, 24 (6) (2010) 1078-1085, https://doi.org/10.1016/j.conbuildmat.2009.11.008.

[37] Ö. Petersson, Preliminary mix-design, Brite EuRam Program: Rational production and improved working environment through using self-compacting concrete, Task 1 (1998) 1-41.

[38] D.R. Lankard, Prediction of the flexural strength properties of steel fibrous concrete, in: Proceedings of CERL Conference on Fibrous Concrete, Construction Engineering Research Laboratory, Champaign, USA, May 1972, 101-123.

[39] ASTM C260/C260M-10a(2016), Standard Specification for Air-Entraining Admixtures for Concrete, West Conshohocken, PA; ASTM International (2016), https://dx.doi.org/10.1520/C0260_C0260M-10AR16.

[40] Nordtest, Method (NT BUILD 427) for Fresh Concrete: Compactibility with IC-tester (Intensive Compaction Tester) Proj. 1005-91, Nord. Scand. Inst. (1994) 1-4, ISSN 0283-7153, www.nordtest.org

[41] B.M. Aïssoun, Étude de l'influence des caractéristiques des granulats sur la performance des bétons fluides à rhéologie adaptée (in French). M.Sc. Thesis, Université de Sherbrooke (2011), http://savoirs.usherbrooke.ca/handle/11143/1590

[42] N. Nouri, M. Hosseinpoor, A. Yahia, K.H. Khayat, Coupled effect of fiber and granular skeleton characteristics on packing density of fiber-aggregate mixtures. Construction and Building Materials, 342 (Part B) (2022) 127932, https://doi.org/10.1016/j.conbuildmat.2022.127932.

[43] B. Esmaeilkhanian, D. Feys, K.H. Khayat, A. Yahia, New test method to evaluate dynamic stability of self-consolidating concrete, ACI Materials Journal, 111 (3) (2014) 299-307, https://doi.org/10.14359/51686573.

[44] M. Hosseinpoor, B.I.O. Koura, A. Yahia, E.H. Kadri, Diphasic investigation of the visco-elastoplastic characteristics of highly flowable fine mortars, Construction and Building Materials, 270 (2021) 121425, https://doi.org/10.1016/j.conbuildmat.2020.121425.

[45] M. Hosseinpoor, B.I.O. Koura, A. Yahia, Rheo-morphological investigation of Reynolds dilatancy and its effect on pumpability of self-consolidating concrete, Cement and Concrete Composites, 117 (2021) 103912, https://doi.org/10.1016/j.cemconcomp.2020.103912.

[46] T. Wagner, H.-G. Lipinski, An ImageJ library for connected component analysis and shape analysis, Journal of Open Research Software, 1 (1) (2013) p.e6, http://doi.org/10.5334/jors.ae.

[47] B.-Y. Lee, Fiber distribution evaluation using digital image processing and its effect on tensile behavior of fiber reinforced cement composites, Ph.D. Thesis, Korea Advanced Institute of Science and Technology (2009), http://hdl.handle.net/10203/30654.

[48] B.Y. Lee, S.-T. Kang, H.-B. Yun, Y.Y. Kim, Improved sectional image analysis technique for evaluating fiber orientations in fiber-reinforced cement-based materials, Materials, 9 (1) (2016) 42, https://doi.org/10.3390/ma9010042.

[49] B.I.O. Koura, M. Hosseinpoor, A. Yahia, Coupled effect of fine mortar and granular skeleton characteristics on dynamic stability of self-consolidating concrete as a diphasic material, Construction and Building Materials, 263 (2020) 120131, https://doi.org/10.1016/j.conbuildmat.2020.120131.

[50] M. Hosseinpoor, B.I.O. Koura, A. Yahia, New diphasic insight into the restricted flowability and granular blocking of self-consolidating concrete: Effect of morphological characteristics of coarse aggregate on passing ability of SCC, Construction and Building Materials, 308 (2021) 125001, https://doi.org/10.1016/j.conbuildmat.2021.125001.

CHAPITER 9 Conclusions and perspectives (English)

This study aims to evaluate the coupled the coupled effect of aggregate-fiber-reinforcing bars on flow and structural performance of fiber-reinforced self-consolidating concrete (FR-SCC). The study consists in evaluating dynamic stability and passing ability of fiber-aggregate combinations as well as distribution and orientation of fibers at different distances from the casting point. The study was carried out in 4 different phases. In the first phase of this study, the coupled effect of fibers and coarse aggregate characteristics on packing density of fiber-coarse aggregate (F-A) system in different compaction conditions has been successfully tailored through comprehensive experimental program. The combinations of F-A include various contents of steel (rigid) and synthetic (flexible) fibers, as well as different particle-size distributions of coarse aggregate (> 5 mm). Furthermore, the packing density of various fiber-coarse aggregate mixtures were evaluated under loosely- and densely-packed conditions to simulate different packing conditions during mixing and casting processes of fiber-reinforced self-consolidating concrete for precast and repair applications. In this phase, the following conclusions can be summarized as follows:

- The volumetric content and size of fibers as well as the mean diameter and PD of the coarse aggregate, which is a function of their particle-size distribution (PSD), showed the most significant effect on the loosely-packed PD (LPD) of F-A mixtures.

- The LPD of F-A mixtures is a function of the size (length and diameter) of fibers rather than their rigidity. Indeed, for a given PSD of coarse aggregate, the addition of larger fibers showed negative effect on LPD of fiber-coarse aggregate mixtures. This can be related to the fact that in loose state, the longer and thicker fibers can push away aggregate from each other which leads to decreasing the loose packing density of F-A.

- LPD of F-A mixtures was influenced by aggregate characteristics, in addition to fibers. For a given fiber type and content, the incorporation of fibers to a densely-packed granular mixture of finer PSD can push away the aggregate and decrease the LPD of F-A mixtures. On the other hand, in the case of a loosely-packed granular mixture of coarser PSD, fibers can fit easily in the large interparticle voids and increase the LPD of F-A mixtures.

- In the case of densely-packed PD (DPD) state, the compaction energy can lead to deformation of fibers through the interparticle voids between aggregate, depending on their rigidity. Increasing the fiber rigidity led to decreasing DPD of fiber-aggregate due to lower deformation of rigid fibers under a given level of compaction.

- Two new empirical models were proposed to predict the loose and dense packing density of F-A mixtures as a function of the characteristics of both fibers and coarse aggregate. A good correlation was found between the loose packing density of F-A with volumetric content, length, and diameter of fibers, as well as the mean diameter and PD of coarse aggregate. On the other hand, the dense packing density of F-A mixtures was well correlated with modulus of elasticity and second moment of area of cross section of fibers, as well as their LPD values. Accordingly, a new workability-design approach was proposed for FR-SCC mixtures based on the established LPD and DPD models.

In Phase 2 of this study, the coupled effect of fiber-aggregate characteristics in terms of φ/φ_{max}, V_P, W/B, HRWR dosage as well as rheological properties of mortar on homogeneous performance of 19 FR-SCC mixtures were investigated. This includes of passing ability (using J-Ring and L-Box), granular blocking (L-Box), and dynamic segregation (T-Box). The FR-SCC mixture was considered as biphasic suspension of fibers-coarse aggregate (≥ 5 mm) in a mortar suspension with solid particles finer than 5 mm. Based on the test results, the following conclusions can be drawn:

- The passing ability of FR-SCC mixtures was sensitive to variation in water content and HRWR dosage than changes in volume of paste (V_P) and (φ/φ_{max}) of F-A. Moreover, good correlations were established between the passing ability evaluated using the J-Ring and L-Box tests for the investigated FR-SCC mixtures.

- In the case of rheological properties of mortar, increasing the yield stress of mortar showed negative effect on passing ability of FR-SCC mixtures. However, higher yield stress and plastic viscosity of the mortar decreased the risk of blocking of fibers and coarse aggregate behind reinforcing bars.

- New dynamic segregation (DSI) and blocking (BI) indices were proposed to evaluate the homogeneous performance of FR-SCC mixtures through restricted and non-restricted flow conditions. The proposed BI and DSI indices can enable proper assessment of the blocking- and shear-induced changes in the relative volume and particle-size distribution of coarse aggregate and fiber contents.

- The BI indices of FR-SCC were found to be more controlled by the rheological properties and volume of excess mortar and φ/φ_{max} of F-A. On the other hand, DSI indices were well correlated to W/B, HRWR dosage, V_P, and φ/φ_{max} of F-A. More specifically, decreasing the W/B, HRWR dosage, and V_P, as well as increasing the φ/φ_{max} of F-A improved the dynamic stability of the investigated FR-SCC mixtures.

According to the results of the comprehensive experimental program of this phase, a new workability-based classification is proposed based on the established correlations between passing ability, blocking resistance, and dynamic stability of FR-SCC mixtures under restricted and non-restricted conditions. According to the proposed classification, characteristics of mixture constituents for FR-SCC mixtures were then recommended to ensure an acceptable homogeneous flow performance of repair application. Accordingly, 6 FR-SCC mixtures out of 19 mixtures with medium to high dynamic stability and high passing ability were introduced as workable FR-SCC mixtures.

In the third phase of this study, a new empirical Square-Box test was employed to evaluate the homogeneous flow performance of FR-SCC under confined-flow conditions that are typical of repair applications. The proposed Square-Box test consisted of a close-surface and close-circuit of four rectangular channels, which provides more confined and restricted flow conditions compared to the traditional test set-ups (T-Box and L-Box). The selected FR-SCC mixtures (Phase 2) were cast through the Square-Box to assess its flowability in 2.8-m length. Then, the variation of φ/φ_{max} of fiber-coarse aggregate at different distances from the casting point was evaluated. To evaluate the dynamic stability and passing ability of 6 selected FR-SCC mixtures, the Square-Box set-up without and with reinforcement bar were used. The results showed that unlike the traditional T-

Box and L-Box tests, the proposed Square-Box test could simulate the flow distance and confinement, wall effect, and presence of reinforcing bars on performance of FR-SCC mixtures.

Furthermore, the obtained DSI and BI indices in the Square-Box are well correlated to the coupled effect of V_f, φ/φ_{max} of F-A combination, and rheological properties of mortar matrix. It was found that increasing φ/φ_{max} of F-A can negatively reduce the dynamic stability and passing ability of FR-SCC mixtures. However, enhancing yield stress and plastic viscosity of mortar led to more homogeneous performance of fiber-reinforced concrete mixtures. More specifically, the heterogeneous performance of the investigated FR-SCC mixtures was found mostly controlled by characteristics of fibers and coarse aggregate rather than the rheology of mortar. Therefore, optimising the characteristics of fiber-aggregate skeleton is more promising approach to achieve a workable FR-SCC mixture than rheological properties of mortar.

In the Phase 4 of this study, the 6 FR-SCC mixtures investigated in Phase 3 were cast in the proposed Square-Box set-up and left to be hardened for 24 hours. Then the fiber orientation and distribution (FOD) of selected FR-SCC mixtures were investigated using the image analysis method. The FOD were evaluated by assessing the number of fibers at different horizontal and vertical units, as well as the in-plane and out-of-plane orientation angles of fibers detected at cross sections located at different distances from casting point. New empirical indices were proposed. Furthermore, the coupled effect of the fibers, coarse aggregate, and mortar rheology on the FOD was evaluated. According to the experimental results, the flow distance showed negative effect on homogeneous performance of fibers, but positive effect on desired out of-plain fiber orientation.

It was found that the presence of reinforcement bar can change the pattern of fiber orientation, as well as blockage of fibers over reinforcing rebars. The risk of blockage increased with higher φ/φ_{max} of F-A due to the interaction between solid particles and reinforcing rebars.

Moreover, increasing the φ/φ_{max} of F-A and rheological properties of mortar reduced the negative effect of flow distance and formwork wall on fiber distribution, but increased the negative effect of presence of reinforcing bars on homogeneous fiber distribution. Similarly, higher φ/φ_{max} of F-A led to more negative effect of reinforcing bars on desired fiber orientation. However, the fiber orientation of FR-SCC mixtures proportioned with high plastic viscosity of mortar and φ/φ_{max} of F-A were less affected by flow distance.

In the future work, the correlation between homogeneous performance of FR-SCC in fresh state with the mechanical performance of the investigated mixtures in the hardened state must be evaluated. Therefore, different samples should be taken from different distances from casting point for flexural and young modulus tests. Then, a correlation can be stablished between the fresh performance of concrete, fiber distribution and orientation, as well as mechanical performance of FR-SCC. Moreover, it is recommended to modify the existing prediction models or to propose new models for FR-SCC mixtures incorporating synthetic fibers with different size and rigidity characteristics.

CHAPITER 10 Conclusions et perspectives (Français)

Dans la première phase de cette étude, l'effet couplé des fibres et des caractéristiques des granulats grossiers sur la compacité du système fibre-granulats grossiers (F-A) a été étudié avec succès dans différentes conditions de compactage grâce à un programme expérimental complet. Les combinaisons de F-A comprennent divers teneurs et types de fibres métalliques (rigides) et synthétiques (souples), ainsi que de différents profils granulométriques des granulats grossiers (> 5 mm). En outre, deux états de compacité ont été définis et étudiés pour chacun des mélanges F-A ; un état de compacité faible (LPD) et un état de compacité forte (DPD). Cela permet de simuler les niveaux de densification que le béton fibré autoplaçant peut subir pendant les processus de mélange et de coulée dans les applications de préfabrication et de réparation.

Dans cette étude, les conclusions peuvent être résumées comme suit :

- La teneur en volume et la taille des fibres, le diamètre moyen des granulats grossiers et leur compacité, qui est fonction de la distribution granulométrique (PSD), sont les paramètres qui ont montré l'effet le plus significatif sur la compacité des systèmes F-A faiblement compactés.

- Les résultats ont révélé que la compacité faible (LDP) des mélanges F-A est fonction de la taille (longueur et diamètre) des fibres plutôt que de leur rigidité. En effet, pour un PSD donné de granulats grossiers, l'ajout de fibres plus grosses a affecté négativement le LPD des mélanges fibres-granulats grossiers. Cela peut être lié au fait qu'à l'état lâche, les fibres plus longues et plus épaisses peuvent repousser les agrégats les uns des autres, ce qui entraîne une diminution de la densité de tassement lâche de F-A.

- Il a été constaté qu'à l'état de compacité forte (DPD), l'énergie de compactage peut conduire à la déformation des fibres à travers les vides interparticulaires, en fonction de leur rigidité. Ainsi, l'augmentation de la rigidité des fibres a entraîné une diminution de la DPD de l'agrégat de fibres en raison d'une moindre déformation des fibres rigides sous un niveau de compactage donné.

- La LPD des mélanges F-A A été influence par les caractéristiques des agrégats, en plus des fibres. Pour un type et une teneur donnée des fibres, l'incorporation de ces fibres dans un mélange granulaire dense, une PSD plus fine peut repousser l'agrégat et diminuer la LPD des mélanges F-A. D'autre part, dans le cas d'un mélange granulaire moins compact et de PSD plus grossière, les fibres peuvent s'insérer facilement dans les grands vides interparticulaires et augmenter le LPD des mélanges F-A.

- Deux nouveaux modèles empiriques ont été proposés pour prédire les compacités faible (LPD) et forte (DPD) des mélanges F-A en fonction des caractéristiques des fibres et des granulats grossiers. Une bonne corrélation a été trouvée entre la LPD de F-A et la teneur volumétrique, la longueur et le diamètre des fibres, ainsi que le diamètre moyen et la compacité des agrégats grossiers. D'autre part, la DPD des mélanges F-A était bien corrélée avec le module d'élasticité et le second moment d'aire de la section transversale des fibres, ainsi qu'avec la valeur de la LPD. En conséquence, une nouvelle approche de conception de

la maniabilité a été proposée pour les mélanges de Béton Autoplaçant Renforcé de Fibres BAP-F basée sur les modèles LPD et DPD établis.

Dans la deuxième phase de cette recherche, une étude à paramètres multiples a été menée sur 19 mélanges BAP-F destinés à des applications de réparation pour but d'évaluer l'effet sur les performances d'écoulement homogène (capacité de passage, blocage, et stabilité dynamique). Cela inclut l'effet couplé des caractéristiques fibres-granulats en termes de teneur volumétrique sur la compacité de la combinaison F-A (φ/φ_{max}), le volume de pâte (V_P), le rapport eau/liant (W/B), le dosage HRWR ainsi que les propriétés rhéologiques du mortier sur la capacité de passage (en utilisant J-Ring et L-Box), blocage granulaire (L-Box), et indices de ségrégation dynamique (T-Box). À cet effet, le mélange BAP-F a été considéré comme une suspension biphasique de fibres-agrégats grossiers (≥ 5 mm) dans une suspension de mortier avec des particules solides plus fines que 5 mm. Sur la base des résultats des tests, les conclusions suivantes peuvent être tirées :

- La capacité de passage des mélanges BAP-F était plus sensible à la variation de la teneur en eau et du dosage HRWR qu'aux variations du volume de pâte (V_P) et (φ/φ_{max}) des mélanges F-A. De plus, de bonnes corrélations ont été établies entre les résultats de capacité de passage évalués à l'aide des tests J-Ring et L-Box pour les BAP-F étudiés.

- Dans le cas des propriétés rhéologiques du mortier, il a été révélé que l'augmentation de la limite d'élasticité du mortier a un effet négatif sur la capacité de passage des mélanges BAP-F. Cependant, une limite d'élasticité et une viscosité plastique plus élevées du mortier ont réduit le risque de blocage des fibres et des granulats grossiers derrière les barres d'armature.

- De nouveaux indices de ségrégation dynamique (DSI) et de blocage (BI) ont été proposés dans cette phase pour évaluer les performances d'écoulement homogène des mélanges BAP-F dans des conditions de débit restreint et non restreint. Les indices BI et DSI proposés peuvent permettre une évaluation correcte des changements induits par le blocage et le cisaillement dans le volume relatif et la distribution granulométrique des teneurs en agrégats grossiers et en fibres.

- Les indices BI de BAP-F se sont avérés être plus contrôlés par les propriétés rhéologiques et le volume de mortier en excès et φ/φ_{max} des mélanges F-A. D'autre part, les indices DSI étaient bien corrélés à W/B, dosage HRWR, V_P et φ/φ_{max} de ces mélanges. Plus précisément, la diminution du W/B, du dosage HRWR et du V_P, ainsi que l'augmentation du rapport φ/φ_{max} a amélioré la stabilité dynamique des BAP-F étudiés.

Selon les résultats du programme expérimental complet de cette phase, une nouvelle classification basée sur la maniabilité est proposée fondée sur les corrélations établies entre la capacité de passage, la résistance au blocage et la stabilité dynamique des mélanges BAP-F dans des conditions restreintes et non restreintes. Selon la classification proposée, les caractéristiques des constituants du mélange pour les mélanges BAP-F ont été recommandées pour assurer une performance d'écoulement homogène acceptable pour l'application de réparation. En conséquence, à partir des 19 mélanges BAP-F étudiés, 6 mélanges ayant une stabilité dynamique moyenne à élevée et une capacité de passage élevée ont été introduits en tant que mélanges BAP-F utilisables.

Dans la troisième phase de cette étude, un nouveau test empirique Square-Box a été utilisé pour évaluer les performances d'écoulement homogène du BAP-F dans des conditions d'écoulement confiné typiques des applications de réparation. Les mélanges BAP-F sélectionnés (Phase 2) ont été coulés dans le Square-Box et ont coulé sous leur propre poids sur une longueur de 2,8 m. Ensuite, à l'aide de la méthode d'échantillonnage, la variation de φ/φ_{max} des granulats fibreux grossiers à différentes distances du point de coulée a été évaluée. Pour évaluer la stabilité dynamique et la capacité de passage de 6 mélanges BAP-F sélectionnés, la configuration Square-Box sans et avec une barre de renforcement a été utilisée. Le test Square-Box proposé consistait en une surface fermée et un circuit fermé de 4 canaux rectangulaires, ce qui fournit des conditions d'écoulement plus confinées et restreintes par rapport aux configurations de test traditionnelles (T-Box et L-Box). Les résultats ont montré que, contrairement aux tests traditionnels T-Box et L-Box, le test Square-Box proposé pouvait simuler la distance d'écoulement et le confinement, l'effet de paroi et la présence de barres d'armature sur les performances des mélanges BAP-F.

De plus, les indices de ségrégation et de blocage dynamiques obtenus dans la Square-Box sont bien corrélés à l'effet couplé du volume de fibres, φ/φ_{max} de la combinaison F-A et des propriétés rhéologiques de la matrice de mortier. Il a été constaté que l'augmentation de φ/φ_{max} des mélanges F-A peut réduire négativement la stabilité dynamique et la capacité de passage des mélanges BAP-F. Cependant, l'amélioration de la limite d'élasticité et de la viscosité plastique du mortier a conduit à une performance plus homogène des mélanges de béton renforcé de fibres. Plus précisément, les performances hétérogènes des mélanges BAP-F étudiés ont été trouvées plus contrôlées par les caractéristiques des fibres et des granulats grossiers plutôt que par la rhéologie du mortier. Par conséquent, l'optimisation des caractéristiques du squelette fibre-agrégat est une approche plus prometteuse pour obtenir un mélange BAP-F exploitable que les propriétés rhéologiques du mortier.

Dans la dernière phase de ce projet, 6 mélanges BAP-F (identiques à la Phase 3) ont été coulés dans la configuration Square-Box proposée et laissés durcir pendant 24 heures. Ensuite, l'orientation et la distribution des fibres (FOD) des mélanges BAP-F sélectionnés ont été étudiées à l'aide des méthodes d'analyse d'images. Le FOD a été évalué par le nombre de fibres à différentes unités horizontales et verticales, ainsi que les angles d'orientation dans le plan et hors du plan des fibres coupées détectées à des sections transversales situées à différentes distances du point de coulée à l'aide de nouveaux indices empiriques. De plus, l'effet couplé des fibres, des granulats grossiers et des caractéristiques du mortier sur le FOD a été évalué. Selon les résultats expérimentaux, la distance d'écoulement a montré un effet négatif sur la performance homogène des fibres, mais un effet positif sur l'orientation désirée des fibres unies.

Il a été constaté que la présence de boîte modifie le modèle d'orientation des fibres ainsi que le blocage des fibres sur les barres d'armature. Ce risque de blocage était accru avec un φ/φ_{max} plus élevé des mélanges F-A en raison de l'interaction entre les particules solides et les barres d'armature.

De plus, l'augmentation du rapport φ/φ_{max} du système F-A et des propriétés rhéologiques du mortier a réduit l'effet négatif de la distance d'écoulement et de la paroi de coffrage sur la distribution des fibres, mais, il a augmenté l'effet négatif de la présence de barres d'armature sur la distribution homogène des fibres. De même, un φ/φ_{max} plus élevé de F-A a conduit à des effets plus négatifs des barres de renfort sur l'orientation souhaitée des fibres. Cependant, l'orientation des fibres des

mélanges BAP-F proportionnelle à la viscosité plastique élevée du mortier et φ/φ_{max} de F-A étaient moins affectées par la distance d'écoulement.

Dans la perspective de travaux futurs, la corrélation entre les performances homogènes du BAP-F à l'état frais et les performances mécaniques des mélanges étudiés à l'état durci doit être évaluée. Par conséquent, différents échantillons doivent être prélevés à différentes distances du point de coulée pour les tests de flexion et de module d'âge. Ensuite, une corrélation peut être établie entre la performance du béton à l'état frais, la distribution et l'orientation des fibres, ainsi que la performance mécanique du BAP-F. De plus, il est fortement recommandé de modifier les modèles de prédiction existants ou de proposer de nouveaux modèles pour les mélanges BAP-F à base de fibres synthétiques de différentes tailles et rigidités.